T 285

# STUDIES ON THE DEVELOPMENT OF NANOCATALYSIS FOR SOME SELECTED ORGANIC TRANSFORMATIONS

A thesis submitted to Tezpur University
in partial fulfillment of the requirement
for the award of the degree of
*Doctor of Philosophy*

By

*VIJAY KUMAR DAS*

*Registration No. 015 of 2012*

School of Sciences
Department of Chemical Sciences
Tezpur University
Napaam, Tezpur - 784028
Assam, India
July, 2013

# DEDICATED TO

# MAA & PAPA

# WITH

# DEFERENCE & WORSHIP

# CONTENTS

# Abstract

*Background*

In the wake of increasing awareness in environmentally benign techniques during the past few decades, organic synthesis (for example; Carbon-carbon, carbon-heteroatom bond forming reactions, functional group transformations etc.) through nanocatalysis has received tremendous interests. Synthetic chemists aspire both to develop novel chemical reactions, reagents/catalysts/additives and to improve reaction conditions to maximize resource efficiency, energy efficiency, product selectivity, operational simplicity, and environmental health and safety. C-C and C-Heteroatom bond forming reactions are the central part of many chemical syntheses, and innovations in these types of reactions will profoundly improve overall synthetic efficiency over existing methods. Historically, nucleophilic additions, substitutions, and Friedel-Crafts-type reactions are the central methods of connecting two simpler molecules to generate a more complex one via the formation of a C-C bond in acyclic structures. The development in the domain of organic syntheses catalyzed by transition metals has increased the efficiency of C-C bond formations in modern organic chemistry and extended their scopes tremendously. However, since state-of-the-art C-C bond forming reactions must use prefunctionalized starting materials, transition metal catalyzed C-H bond activation and subsequent C-C bond formations have attracted much interests in recent years. The transition metal-catalyzed C-C bond forming reaction by the cross coupling of organic substrates is another well known domain in organic synthesis.

The nanoparticles have attracted a great deal of attention in the last 10 years; their preparation, structure determination, modification and applications are topics of current interest. Nanoparticles are defined as having 1-50 nm diameters at least in one

dimension, a size range where particles can show size dependent properties. The smaller the cluster of atoms, the higher the percentage of atoms is on the surface, rendering nanoparticles very interesting in catalysis. Thus, a nanoparticles of 10 nm diameter has about 10% of its atoms in the surface, but one of 1 nm has 100%. In recent times, interest in nanoparticle-catalysis has increased considerably because of its improved efficiency under mild and environmentally benign conditions in the context of Green Chemistry.

The emerging importance of nanoparticles in life processes as well as in other catalytic reactions has been emphasized in the literature. Nano-catalysis can be considered as a bridge between homogeneous and heterogeneous catalysis and is the central field of nanoscience and nanotechnology. Nanoscale supports to create catalysts with larger surface areas along with more edges and corners which can lead to higher performance of the catalyst. Other parameters (e.g. oxygen mobility, etc.) might play a key role in enhancing catalytic activity. Because of nano-size, i.e. high surface area, the contact between reactants and catalyst increases dramatically and they can operate in the same manner as homogeneous catalysts (close to homogeneous catalysis), at the same time, due to their insolubility in the reaction solvent, they can be separated out easily from the reaction mixture. Thus, Nano-materials can combine the advantages of both the systems, and can offer unique activity with high selectivity. Nanoparticles of transition metals have long been used as quasi-homogeneous catalysts in various types of chemical transformations such as C-C bond formation reactions, which include Suzuki, Heck, Sonogashira, Hiyama and Stille coupling reactions. These applications seem to be motivated by the intention to enhance the catalytic efficiency by virtue of large surface areas of the nanoparticles. However, a more intriguing aspect of the nanoparticle catalysis lies in the emergence

of novel catalytic activities and/or selectivities arising from their size specific electronics and geometric structures. Apart from the high surface area, the metal nanoparticles often have distinct optical, magnetic, thermal and chemical properties. In general, nanoparticles as a catalyst in organic synthesis have several advantages over homogeneous organic catalysts and hence the ultimate goal to work with nanoparticles is (i) their high catalytic activity, (ii) recoverability, (iii) simple product isolation, (iv) recyclability, (v) improved selectivity, (vi) criteria of evolution and (vii) role in green chemistry.

Thus, the heterogeneous solid catalysts have been recognized as robust alternatives to homogeneous organic catalyst.

*Scopes and Objectives of the Present Investigation*

Although various nanoparticles have several remarkable potential applications in the field of medicine and material science but only a few reports described its utilization as catalyst in organic transformations. Under the above background, the main objectives of the present investigation are as follows:

(i) The main objective is to search for applications of nanoparticles as catalysts in Carbon-Carbon, Carbon-Heteroatom and C-H bond forming reactions.

(ii) Whether nanocatalyst can catalyze the synthesis of complex fused systems, given that the ring systems are a feature of important compounds, including many of pharmaceutical interest?

(iii) To promote economical and environmentally friendly experimental procedures. By rethinking chemical design from the ground up, the green synthetic methodology has to be developed in new ways to manufacture products that fuel the economy and lifestyles, without the damages to the environment that have become all too evident in recent years.

(iv) To accomplish a comprehensive study of the scope and limitations of the synthesis of C-C, C-N, C-H, and C-O bonded compounds in the domain of nanocatalysis.

(v) To study and characterize the nano catalysts by spectroscopic and analytical techniques.

(vi) To study and characterize the prepared compounds by spectroscopic (high resolution $^1$H NMR and $^{13}$C NMR spectroscopy, Mass spectrometry, IR spectroscopy) methods and analytical methods (TGA, melting point/boiling point determination, and elemental analysis etc.).

(vii) To evaluate and demonstrate the **'green-ness'** of the newly developed protocols by considering the green metrics.

(viii) To study the significance of these reactions as they relate to the literature and will provide mechanistic insight into newly discovered and previously known organic reactions.

(ix) To study the stability of nanoparticles under the reaction condition.

(x) To study the recyclability of nanocatalysts and to search for methods to regain the activity of nanocatalysts in the case of decreasing activity in subsequent recycling.

(xi) To address the issues which arise during the investigation.

*Contents and Layout of the thesis*

The thesis entitled "**Studies On The Development Of Nanocatalysis For Some Selected Organic Transformation**" comprises of seven chapters. Chapter 1 deals with the general introduction of C-C and C-Heteroatom bonded organic compounds along with their syntheses. A brief review on nanoparticles, their importance, and history, general techniques for preparation, characterization,

properties and applications are described in this chapter. A brief literature survey on the various reactions catalyzed by nanoparticles has been incorporated in this chapter. This chapter also focuses the scopes and objectives in conjunction with the plans and methodologies of the present investigation.

Our experimental works start from chapter two and ends at chapter six. Chapter 2 has been divided into two sections (I and II). Section I updates a brief introduction on applications of nano-$Al_2O_3$ as well as $N$-bonded organic compounds (scheme 1). This section also reports the characterization and applications of nano-$Al_2O_3$. The nano-$Al_2O_3$ was characterized by several techniques such as SEM, EDX, XRD, TEM, SAED, FTIR spectroscopy and BET analyses. After its characterization, it has been used as a catalyst for the synthesis of $N$-bonded compounds.
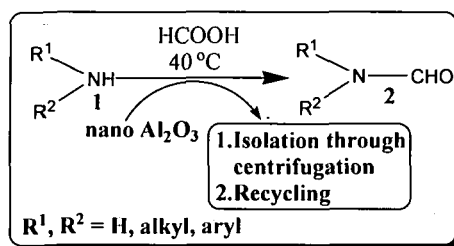


Scheme 1: $N$-Formylation of amines

The nano-$Al_2O_3$ has successfully played a great role as a catalyst in $N$-formylation of 1° amines, 2° amines (1) and indole derivatives. It also catalyzed the synthesis of acetamide derivatives under the optimized reaction condition. 36 examples of $N$-formylation reaction and 14 for acetamide synthesis catalyzed by nano-$Al_2O_3$ have been shown in this chapter. A mechanism has been proposed regarding the action of nano-$Al_2O_3$ in $N$-formylation reaction. Finally, the reusability study of nano-$Al_2O_3$ was performed and it was found that it remained active from fresh up to the 5$^{th}$ cycle.

Section II adumbrates the application of nano-$Al_2O_3$ as catalyst for the $N$-

formylation of complex bis-uracil derivatives (3) in good to high yield (scheme 2). 11 examples of different uracil derivatives are mentioned in this section. All the compounds in both the sections are characterized by their $R_f$ values, physical appearance, melting/boiling point, FTIR spectra, $^1H$ and $^{13}C$ NMR spectra, GC-MS and elemental analyses and confirmed by comparing these data with those reported ones. The required data and spectra have been given in this chapter for the new compounds. Herein, the recycling potential of nano-$Al_2O_3$ was also evaluated. In both the sections, the activities of reused catalyst after several runs were compared with the fresher one by SEM images.
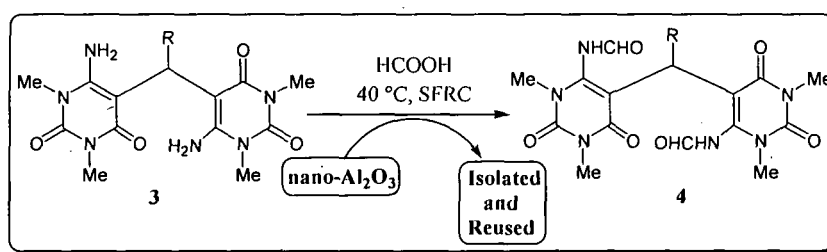


Scheme 2: $N,N$-diformylation of bis-uracil derivatives

In chapter 3, author presents the synthesis of nano-$Fe_2O_3$ and it is used as a catalyst for the oxidation of aldehydes (5) into corresponding carboxylic acid (6) (scheme 3). The full characterization of nano-$Fe_2O_3$ has been carried out by techniques as mentioned above. But it was observed that nano-$Fe_2O_3$ as such could not oxidize aldehydes efficiently and therefore, to enhance its catalytic activity bio-silica i.e., diatomaceous earth (DE) was used as a support. Bio-silica acted as a smart support by increasing the catalytic efficiency of nano-$Fe_2O_3$. Finally, nano-$Fe_2O_3$ supported on bio-silica exhibited fascinating catalysis for the oxidation of aldehydes. 25 examples for different aldehydes have been cited in this chapter which is catalyzed to corresponding carboxylic acids by bio-silica supported nano-$Fe_2O_3$.
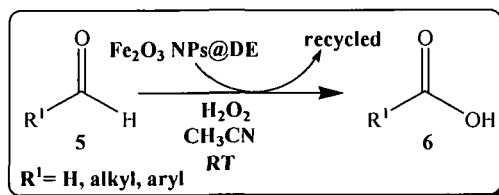
Scheme 3: Oxidation of aldehydes

All the compounds are known in literature and characterized by their $R_f$ values, physical appearance, melting/boiling point, FTIR spectra, $^1H$ and $^{13}C$ NMR spectra, GC-MS and elemental analyses. The formation of these compounds was confirmed by comparing these data with those reported ones. A Plausible mechanism has been suggested for the oxidation. In the present study, it is observed that bio-silica supported nano-$Fe_2O_3$ can be efficiently reused with a slight loss in its activity.

Chapter 4 is split into two sections (I and II). Section I describes nano-MgO catalyzed synthesis of amide derivatives (9) (scheme 4). 40 examples have been provided for nano-MgO catalyzed amide synthesis and a probable mechanism is also tailored in this chapter. The green-ness of the methodology was measured using green metrics by comparing with those previously reported.
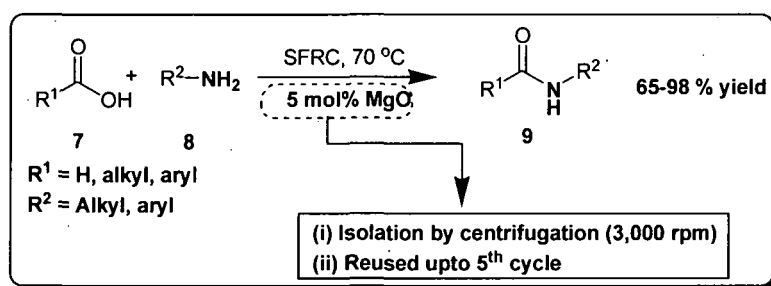


Scheme 4: Representative scheme for the synthesis of amides

Section II of chapter 4 outlines the efficient synthesis of amidine derivatives (12) catalyzed by nano-MgO (scheme 5). 10 different amidine derivatives have been synthesized which are known in the literature. The compounds are characterized by their $R_f$ values, physical appearance, melting/boiling point, FTIR spectra, $^1H$ and $^{13}C$ NMR spectra, GC-MS and elemental analyses and confirmed

by comparing these data with those reported ones. In both the sections, reusability test of nano-MgO is also experimented which showed that the catalyst remained active for several cycles in the reaction.
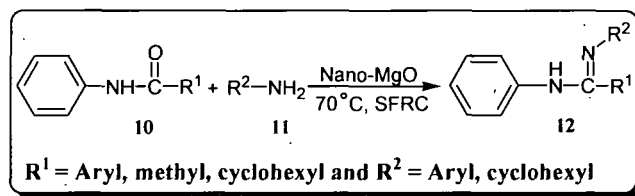


Scheme 5: Synthesis of amidine

Chapter 5 delineates nano-S catalyzed synthesis of amidoalkyl naphthol derivatives (16) (scheme 6). Nano-S has been prepared by our own greener method and its full characterization is also presented in this chapter. Nano-S catalyzes the synthesis of 20 numbers of amidoalkyl naphthol derivatives. All the compounds are characterized by their $R_f$ values, physical appearance, melting/boiling point, FTIR spectra, $^1H$ and $^{13}C$ NMR spectra, GC-MS and elemental analyses and confirmed by comparing these data with those reported ones. The required data and spectra have been provided in this chapter for the new compounds. The catalyst is reused up to $5^{th}$ cycles and after that its activity somewhat decreased. The slight loss in activity of the catalyst was regenerated and it demonstrated potential performance when it was reutilized.
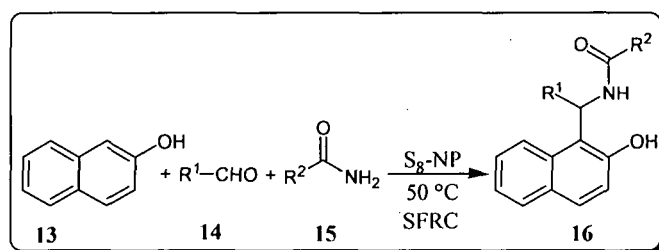


Scheme 6: Synthesis of 1-amidoalkyl-2-naphthols

Finally, the **green-ness** of the currently discovered methodology was measured by making use of green parameters called **green metrics**.

Chapter 6 enlightens the synthesis of uracil based compounds 6-Amino-1,3-dimethyl-5-indolyl-1$H$-pyrimidine-2,4-dione derivatives (19) catalyzed by highly proficient nano-Ag (scheme 7). The preparation of nano-Ag involves a very short extension of the previously reported technique. In this chapter, recyclability test of nano-Ag is demonstrated. It is found to be effective up to $3^{rd}$ cycle and after that its activity decreased. The newly synthesized uracil based compounds were fully characterized by their $R_f$ values, physical appearance, melting/boiling point, FTIR spectra, $^1$H and $^{13}$C NMR spectra, GC-MS and elemental analyses. The spectra and data have been supplied in this chapter.
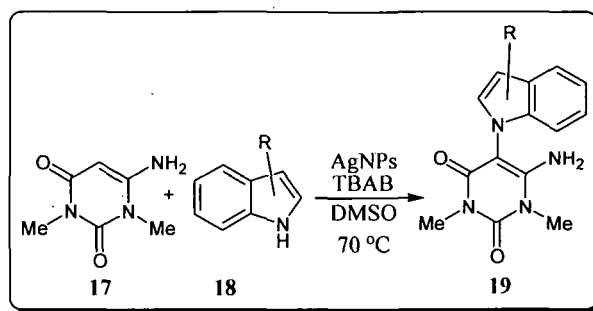


Scheme 7: Synthesis of uracil based compound

Chapter seven, the last chapter of the thesis encloses the concluding remarks, highlights of the findings and future scopes of the present investigation. The major achievements of the present investigation are as follows-

(i) A low cost and less toxic nanocatalyst (nano-$Al_2O_3$ and nano-MgO) was profitably utilized for the first time to industrially important $N$-formylation reactions and amide synthesis.

(ii) The synthesis of nano-S and nano-Ag include procedures based on green chemistry principle which are safe in handling and were successfully characterized by the analytical techniques.

(iii) The utilization of the bio-silica as a smart support for nano-$Fe_2O_3$ boosts up its catalytic efficiency dramatically.

(iv) The measurement of green-ness of the newly devised protocols using green

metrics will be a breakthrough in the avenue of organic synthesis.

**[x]**

# DECLARATION BY THE CANDIDATE

The thesis entitled **"Studies On The Development Of Nanocatalysis For Some Selected Organic Transformations"** is being submitted to the Tezpur University in **partial fulfillment for the award of the degree of Doctor of** Philosophy in Chemical Sciences is a record of bonafide research work accomplished by me under the supervision of Dr. Ashim Jyoti Thakur, Assoc. Prof. Dept. of Chemical Sciences, Tezpur University.

All helps from various sources have been duly acknowledged.

No part of thesis has been submitted elsewhere for award of any degree.

Date: 20/01/2014

Place: Tezpur

(Vijay Kumar Das)

Department of Chemical Sciences

Tezpur University

Napaam 784028

Assam, India

*Dr. Ashim Jyoti Thakur*
**Associate Professor**
Department of Chemical Sciences
Tezpur University
Tezpur 784 028, Assam, INDIA
*E-mail* : ashim@tezu.ernet.in & ajtthax@yahoo.com
Web: www.tezu.ernet.in
Ph : +91 (3712) 267173 (O)
        +91 9435181464 (Mob)
Fax: +91 (3712) 267005/6

30th July 2013

## CERTIFICATE OF THE SUPERVISOR

This is to certify that the thesis entitled, **"Studies On The Development Of Nanocatalysis For Some Selected Organic Transformations"** submitted to the School of Science, Tezpur University in part fulfillment for the award of the degree Doctor of Philosophy in Chemical Sciences (School of Science and Technology) is a record or research work carried out by Mr. Vijay Kumar Das under my supervision and guidance. He has complied with all the requirements as laid down in the regulations of Tezpur University for the award of Doctor of Philosophy in Chemical Sciences (School of Sciences) including course work.

All help received by him from various sources have been duly acknowledged.

No part of this thesis has been submitted elsewhere for award of any other degree or diploma of this or any other university/institution other than mentioned.

Date:

Place: Tezpur

(Dr. Ashim Jyoti Thakur)
Associate Professor
School of Sciences
Department of Chemical Sciences
Tezpur University
Napaam 784028, India

**[xii]**

## <u>Certificate from the External Examiner and ODEC</u>

This is to certify that the thesis entitled **"Studies On The Development Of Nanocatalysis For Some Selected Organic Transformations"** submitted by Mr. Vijay Kumar Das to Tezpur University in the Department of Chemical Sciences under the school of Sciences in partial fulfillment of requirement for the award of the degree of Doctor of Philosophy in Chemical Sciences has been examined by us on _____ and found to be satisfactory.

**Signature of:**

Principal Supervisor                                         External Examiner

Date: _____                                         Date:_____

# ACKNOWLEDGEMENTS

## List of Tables

# List of figures

[xix]

**List of schemes**

## Abbreviations used in the thesis

| | |
|---|---|
| SFRC | Solvent Free Reaction Condition |
| NPs | Nanoparticles |
| EM | Electron Microscope |
| TEM | Tunneling Electron Microscope |
| DNA | Dexoyribo Nucleic Acid |
| MRI | Magnetic Resonance Imaging |
| DMF | Di Methyl Formamide |
| UV-VIS | Ultra Violet Visible |
| PVP | Poly Vinyl Pyrrolidone |
| CTAB | Cetyl Trimethyl Ammonium Bromide |
| PAA | Poly Acrylic Acid |
| MORE | Microwave-assisted Organic Reaction Enhancement |
| NOSE | Nanoparticles-catalyzed Organic Synthesis Enhancement |
| CNF | Carbon Nano Fibers |
| PS-PDONPs | Polystyrene stabilized Palladium Nanoparticles |
| NMR | Nuclear Magnetic Resonace |
| IR | Infra Red |
| TGA | Thermo Gravimetric Analysis |
| FTIR | Fourier Transformed Infra Red |
| XRD | X-ray Diffraction |
| EDX | Energy Dispersive X-ray |
| XPS | X-ray Photoelectron Spectroscopy |
| SEM | Scanning Electron Microscope |
| BET | Brunauer–Emmett–Teller |
| SAED | Selected Area Electron Diffraction |
| JCPDS | Joint Committee on Powder Diffraction Standards |
| TON | Turn Over Number |
| TOF | Turn Over Frequency |
| MS | Mass Spectroscopy |
| TMS | Tetra Methyl Silane |
| TLC | Thin Layer Chromatography |

| | |
|---|---|
| FWHM | Full Width Half Maximum |
| DMSO | Dimethyl sulfoxide |
| GC-MS | Gas Chromatography Mass Spectrometry |
| RNA | Ribo Nucleic Acid |
| IONPs | Iron Oxide Nanoparticles |
| DE | Diatomaceous Earth |
| RT | Room Temperature |
| THF | Tetra Hydro Furan |
| LC-MS | Liquid Chromatography Mass Spectrometry |
| MWI | Microwave Irradiation |
| MCRs | Multi Component Reactions |
| HIV | Human Immuno Virus |
| TBAB | Tetra Butyl Ammonium Bromide |
| IBA | Diisopropylbenzylaminoboronic acid |
| CDI | Carbonyldiimidazole |

# Chapter 1

# Introduction
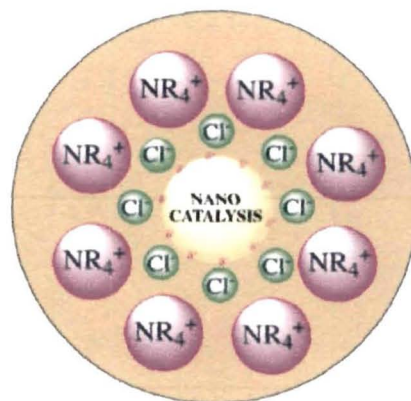
# 1. PREAMBLE

## *1.1 An overview of historical background and aspects of C-C and C-Heteroatom bond forming reaction*

The universal credence is that carbon compounds form the basis of all known life on Earth. Carbon-carbon bond formation represents the fundamental aspect of organic chemistry, a sub discipline of chemistry involving the study of structure, properties and reactions of carbon-based compounds. The term "organic", which dates back to the 1st century, was used to describe complex compounds that could only be synthesized by "life forces" using the classical elements viz., earth, water, air and fire.[1] Today, we know organic compounds to be primarily composed of C-C and C-H bonds. These types of bonds make up the skeletal backbone of the materials required to sustain life. Hence, development of reactions forming C-C and C-H bonds is essential for producing many of the pharmaceuticals, foods, dyes, polymers, and other materials needed in daily life.

Throughout the time, organic syntheses have been experiencing an explosive development with an incredible acceleration within the domain of C-C and C-Heteroatom bond forming reactions.[2] The main essence in this escalation is the desire to discover or to improve what has already been invented, to achieve the best result possible for improvements in daily life, or the discovery of new drugs to treat all kinds of diseases. Synthetic chemists aspire both to develop novel chemical reactions and to improve reaction conditions to maximize resource efficiency, energy efficiency, product selectivity, operational simplicity, and environmental health and safety. The innovations in the realm of C-C and C-Heteroatom bond forming reactions will profoundly improve overall synthetic efficiency over the existing methods. The skill to generate C-C bonds in a highly

selective manner has transfigured the pharmaceutical and agricultural industries as well as the field of material science.[3,4] Historically, nucleophilic additions, substitutions, and Friedel-Crafts-type reactions are the central methods of connecting two simpler molecules to generate a more complex one via the formation of a C-C bond in acyclic structures.[5] To meet this quest, the association of novel and green technology has to play an endemic role in the development of synthetic strategies. Although a number of methodologies based on classic organic reactions exist for the synthesis of C-C and C-Heteroatom containing compounds, they are commonly plagued by difficulties associated with the isolation of the products, low yields, poor selectivities and limited substrate scopes. These problems are further complicated by the trend in developing more cost effective and environmentally friendly alternatives. Thus, the development of more efficient, selective and cost effective methodologies for the synthesis of C-C and C-Heteroatom containing compounds continues to be significant yet daunting task for the modern synthetic organic chemist. In this regard, the advent of transition metal-catalyzed transformations in C-H bonds has enabled the efficient formation of a wide range of C-C and C-Heteroatom bonds from simple C-H bonds.[6] Whilst these processes embody a chemical ideal from the standpoint of atom economy and synthetic efficiency, the ubiquitous nature of C-H bonds and their relative strength[7] pose a significant challenge for selectivity and reactivity that has been the focus of research efforts over the past decade. Another breakthrough for the conversion of C-H bonds into C-C and C-Heteroatom bonds is fascinated by metallic nanoparticles catalysis which is the heart of modern organic synthesis and fine chemical industries.[8] In recent times, interest in nanoparticle-catalysis i.e., "nanocatalysis" for the synthesis of C-C and C-

Heteroatom containing units has increased considerably because of its improved efficiency under mild and environmentally benign conditions in today's context of Green Chemistry.[9]

## 1.2 Development of environmentally benign techniques

### 1.2.1 Concept of green chemistry

Chemistry brought about the revolution in the field of Science and Technology till about the middle of twentieth century in which drugs were discovered. In keeping with pace of demand, the world food supply also increased enormously due to the discovery of improved hybrid varieties, improved methods of farming, better seeds and use of insecticides, herbicides and fertilizers. The quality of life on earth became much better due to the discovery of dyes, plastics, cosmetics and other materials of comfort. Soon, in the darker side, the ill effects of chemistry also became pronounced, main among them being the pollution of land, water and atmosphere. This is caused mainly due to the effects of different by-products of chemical industries, which are being discharged into the air, rivers/oceans and the land. The hazardous wastes released add to the problem. The use of toxic reactants and reagents make the situation worse. The pollution reached such levels that different governments have to make laws to minimize it. This marked the beginning of *Green Chemistry* by the middle of 20th century. Broadly, green chemistry[10] is defined as environmentally benign chemical synthesis. The synthetic schemes are designed in such a way that there is least pollution to the environment. As on today, maximum pollution to the environment is caused by the numerous chemical industries. On the other hand, the cost involved in disposal of the waste product is also enormous. Therefore, attempts have been made to design synthesis for manufacturing processes in such

a way that the wastes generated are minimum, either they have no effects on the environment or their disposal is convenient. For carrying out reactions it is necessary that the starting materials, solvents and catalysts should be very carefully chosen. For example, the use of benzene as a solvent must be avoided at any cost since it is carcinogenic in nature. If possible, it is the best to carry out reactions in the aqueous phase. With this view in mind, synthetic methods should be designed in such a way that the starting materials are consumed to the maximum extent in the final product (concept of atom economy). The reactions are also not expected to generate any toxic by-products.

### 1.2.2 Advantage of solvent free reaction condition (SFRC)

Due to the growing concern for the influence of the organic solvents on the environment as well as on human body, organic reactions without the use of conventional organic solvents have attracted the attention of synthetic organic chemists.[11] Although a number of modern solvents, such as fluorous media, ionic liquids and water have been extensively studied recently, not using a solvent at all is definitely the best option. Development of **solvent-free reaction condition (SFRC)** is thus gaining prominence.[12] A solvent-free or solvent less or solid state reaction may be carried out using the reactants alone or incorporating them in clays, zeolites, silica, alumina or other matrices. Thermal process or irradiation with UV, microwave or ultrasound can be employed to bring about the reaction. It reduces the use of organic solvents and minimizes the formation of other wastes. The reactions occur under mild conditions and usually require easier workup procedures and simpler equipments. Moreover, it may allow access to compounds that require harsh reaction conditions under traditional approaches or when the yields are too low to be of practical convenience. Because of economy

and pollution, solvent-free reactions are of great interest in order to modernize classical procedures making them cleaner, safer, easy to perform and saving in labor. These would be especially important and significant during industrial production. Often, the products of solid state reactions turn out to be different from those obtained in solution phase reactions. This is because of specific spatial orientation or packing of the reacting molecules in the crystalline state. This is true not only of the crystals of single compounds, but also of co-crystallized solids of two or even more reactant molecules. The host-guest interaction complexes obtained by simply mixing the components intimately also adopt ordered structure. The orientational requirements of the substrate molecules in the crystalline state have provided excellent opportunities to achieve high degree of stereo selectivity in the products. This has made it possible to synthesize chiral molecules from prochiral ones either by complexation with chiral hosts or formation of intermediates with chiral partners. Therefore, the following benefits could be mentioned for SFRC:

(i) Avoidance of large volumes of solvent reduces emission and needs for distillation

(ii) Simple work-up, by extraction or distillation

(iii) The absence of solvents facilitates scale-up

(iv) Reactions are often cleaner, faster, and higher yielding

(v) Recyclable solid supports can be used instead of polluting mineral acids

(vi) Safety is enhanced by reducing risks of overpressure and explosions

*1.3  Nanoparticles- "The call for a century"*

In the esteemed wake of increasing awareness on the theme of investigation of science, nanotechnology is architecturing the synthesis and application of

interesting nanomaterials[13] and has mounted to a sort of scientific rumor that is being spread from culture to culture across the globe. It is vaguely described in most circles; the average conversation concerning nanotechnology dwell on intangibles from innovative dreams to doomsday projections of tiny machines turning the entire world to a puddle of goo. In fact, nanoscience is simply the study of matter at the length scale of one billionth of a meter ($10^{-9}$ m). To play with these materials, is inherently complicated due to the small size of the particles and high reactivity that arises from their high surface area and unusual morphologies. Undaunted by this involvedness, exploration and creation of nano-sized structures is the result of researchers' never ending inquisitiveness and constant probing of their universe to new limits. This inventive desire is epitomized by a challenge given to the scientific community by the brilliant physicist '**Richard Feynman**' who in 1959 charged scientists to find the means to write the encyclopedia on the head of a '**Pin**'.[14] The hype for this area of science is not unfounded. Elements and compounds that researchers had previously probed took on new exciting properties when broken down to the physical dimensions of the nano length scale.

The practice of utilizing 0-dimensional (0-D, nanoparticles), 1-D (nanowires, nanotubes, etc.), and 2-D (thin film, graphene, etc.) nanoscale materials in our real life, for instance the electric, photonic, catalytic, thermoelectric, magnetic, and plasmonic applications, have attracted enormous interests from both the academia and industries.[15] The new nano-sized products garnered exponentially higher reactivities as a large portion of the atoms composing the material reside exposed on the surface of the sample. New features of materials were discovered that could not be expressed by a few atoms or the infinite model of solid state

physics, but exist only in this new area in-between at compositions of hundreds to thousands of atoms. Most interestingly, the properties and chemistry of the nano-materials were found to change as the size of the sample was changed, leading to adjustable features.[16]

Metal nanoparticles have received an immense consideration due to their promising and diverse applications ranging from their large surface area, magnetic, thermal and chemical properties. Nanoparticles are the intermediates between the bulk and atomic forms of such materials and thus expected to exhibit novel electronic and optical properties that differentiate them from their bulk and atomic counterparts. Moreover, when the lithography-based "top-down" approach has gradually reached its limit in creating patterns in the deep nanometer regime, the "bottom-up" approach, with which material structures are hierarchically assembled from individual nanoscale building blocks, can circumvent the restrictions of lithography and lead to the formation of functional nanosystems with molecular precision. Up to now, 0-Dimensional nanoparticles (NPs), including metallic, metal oxide, semiconducting, and rare-earth-containing NPs are considered as the most potential nanoscale materials to be incorporated in real products, due to the easiness of preparation, mass production and processing, as well as well-established property database.[17]

To deal with the detail study of nanoparticles in general and metal nanoparticles in particular is made possible only by the use of the latest technological inventions in instrumental techniques. High resolution electron microscopy (HR-TEM, SEM, STM and AFM) allows scientists in this field to explore the structure, size, and shape of the nanosized objects, with the latest instruments being able to resolve individual atoms and give information on the

atomic structure of the crystals. Even more impressive are spectroscopic investigations that can be used in situ in the electron microscope to provide insight into the elemental composition and even chemical nature of the atoms within the particles themselves.

With these tools, it becomes effortless for the scientists to understand formation mechanism, like, how synthetic conditions affect the growth of NPs, so that it may be possible to obtain more elaborate control over the sizes, morphologies, or structures of the NPs. For now, the understanding of the synthesis is far from the capability to explain the evolution pathways that a precursor compound may take to form metal atoms, nuclei, and then well-defined NPs at the atomic level. Thus, at the existing stage, compared with the development of classical and quantum physics, the synthesis of metal NPs remains an art rather than a science considering the limited generally accepted fundamental knowledge we have on the growth mechanism of NPs. As a result, intensive efforts have been devoted to the exploration of how NPs evolve from atoms to nanoscale particles.

Scrounging the classical crystallization theory developed for bulk materials, the growth of fine metal NPs can be expressed in a typical process with three distinct stages: (a) **nucleation**, (b) **nuclei into seeds**, and (c) **growth of seeds into NPs**.[18] Owing to the small size of the nuclei as well as the difficulty of capturing them, only seeds and well developed NPs can be observed with electron microscope (EM). Very recently, with the development of technologies in in-situ observations in TEM, special TEM sample cells can be designed to observe objects in solution. In this way, the formation of noble metal NPs in solution can be directly visualized under TEM, which is one of the most

important advancements in the study of NPs.[19] Yet a long way to go before a systematic theory can be developed as a guideline for the synthesis of NPs.

Nanoparticles are used or being evaluated for use in many fields. Some of the uses of nanoparticles in biology and medicine include; creating fluorescent biological labels for important biological markers and molecules in research and diagnosis of diseases, drug delivery systems, gene delivery systems in gene therapy, for biological detection of disease causing organisms and diagnosis, detection of proteins, isolation and purification of biological molecules and cells in research, probing of DNA structure, genetic and tissue engineering, destruction of tumours with drugs or heat, in MRI studies and in pharmacokinetic studies. The 'nano' dimensionality is not only confined to engineered materials or technology; nature also creates NPs or nanostructures which are present as functional components in an organism; either in the form of enzymes which catalyze most of the biological reactions or as ribosomes which act as the sites for protein synthesis.[20]

### 1.4 Synthesis of metal nanoparticles

In the current hour of interest, extensive research has been carried out where the first critical step is the synthesis of metal nanoparticles with controlled dimensions. For instance, the Brust methods[21] have been successfully used to synthesize metal nanoparticles with varied size and high monodispersity. Thermolytic reduction of ruthenium and platinum salts in propanediol solution has also been used to produce the corresponding metal nanoparticles with high monodispersity.[22] Dimethylformamide (DMF), as both a solvent and reducing agent, has also been used to prepare silver and platinum nanoparticles when heated to high temperatures.[23] In these endeavors, to synthesize metal

nanoparticles, the nanoparticles are found to exhibit strong size-dependent physical properties due to the quantum confinement effects. For example, gold nanoparticles, when they are smaller than 2 nm in diameter, the nanoparticles exhibit discrete energy levels[24] and when the diameter of the gold nanoparticles is larger than 3 nm, UV-VIS spectroscopic measurements exhibit a plasmon absorption peak around 510 nm[25] which may shift to a different wavelength position depending on the exact size of nanoparticles.

At present period of time, two classes of noble metal NPs have been widely studied, (a) mono-metallic NPs such as Pt, Pd, Ag, Au, Rh, etc., and (b) multi-metallic NPs including alloy NPs such as Pt-Pd, Pt-Ru, Pt-Au, and Pt-Ni, etc., and heterogeneously structured NPs such as core-shell and dumbbell structures.

### 1.4.1 Synthesis of monometallic nanoparticles

The synthesis of mono-metallic NPs usually begins with a precursor containing the metal species, commonly a salt, or an organometallic precursor dissolved in a solvent. If salt precursor is used, metal atoms are commonly extracted by using reducing agent. Commonly used reducing agents are sodium borohydride ($NaBH_4$), hydrazine ($N_2H_4$), hydrogen ($H_2$), and carbon monoxide (CO), which are strong reductants, or polyol, ascorbic acid, citric acid, polyvinylpyrrolidone (PVP), etc., which are weak reductants, depending on the activity of the precursors, nature of the solvent, and the expected properties of the NPs.[26] While if organometallic precursor is used, the reaction is usually conducted in organic solvent at elevated temperature to extract the metal atoms by thermal decomposition.[24] In addition, stabilizing agent is also necessary in a typical synthesis if one expects to avoid aggregation and obtain NPs well dispersed in reaction solution. Commonly used stabilizing agents are some

charged small molecules such as halides (KBr, NaI), citric acid, phosphine or polarized long-carbon-chain molecules and polymeric molecules such as cetyltrimethylammonium bromide (CTAB), alkanethiol, oleic acid, PVP, polyacrylic acid (PAA).[27]

Two mechanisms are commonly accepted on how metal species form nuclei and grow into NPs. It used to be assumed that metal ions exist as monomeric units through complexation with anions, ligands, or solvent molecules and metal atoms are then reduced from the complex and aggregated to form nuclei.[28] Basically, in this theory, metal atoms are reduced first and then incorporated into the nuclei, which we called a "reduction-incorporation" mechanism. Later on, another pathway was found when studying the nucleation process of Ag NPs with $AgNO_3$ as precursor in aqueous solution.[29] It was confirmed with mass spectrometry (MS) that $[Ag_3(NO_3)_2]^+$ is the stable intermediate species towards nucleation, which means that Ag species are not in the atomic state before forming the nuclei. It was also discovered by simulation that in the synthesis of Pt NPs, the energy barrier is lower if Pt complexes (with water molecule and the anions) adsorb onto the Pt cluster first and then get reduced to zero valence directly on the surface, which we can call an "incorporation-reduction" mechanism.[30] In the synthesis, mechanisms vary from case by case, depending on the material system and the synthetic condition. So far, the two mechanisms can explain most of the phenomena, so they are both accepted by the academia.

### 1.4.2 Synthesis of multi-metallic nanoparticles

To triumph over the drawbacks of certain elements or incorporate more functionalities into the NPs, two or more elements can be used to synthesize multi-metallic NPs. The more elements it contains, the more functionalities the

NPs obtain, but the more complicate the system will be in terms of synthesis and analysis. Generally, this type of NPs can be divided into two groups: alloy NPs, and hierarchically-structured NPs. For bimetallic alloy NPs, the synthesis is more complicated due to the different natures or properties of individual components. They can be synthesized either by co-reduction of both precursor salts, or reduction of one precursor salt followed by the thermal decomposition of the other precursor and then annealed at elevated temperature in order for two species to fully mix and achieve a high alloying degree.[31] For some particular applications, such as magnetism, it requires chemically ordered lattice to achieve expected properties, which requires a further step of post-annealing to obtain chemically ordered crystalline structures.

For bimetallic NPs with heterogeneous structures, the driving force of synthesizing these structures is that the properties can be appropriately predicted and easily tuned by manipulating the individual component as long as each component is well studied. But the synthesis is even more complicated due to the fact that they are usually synthesized with a two-step approach.[32] Generally, depending on how the second component is incorporated, the final morphologies of the bimetallic NPs include: core@shell structures, dumbbell structures, etc.[33] For the core@shell NPs, the synthesis attracts the most interests because there are more parameters or factors that can be tuned. Depending on how the shell material is formed, enormous work has been done to obtain core@shell NPs with fully covering shell with thickness elaborated to the atomic level, or partially covering shell which forms only on certain facets or locations of the core particle.[34] For example, Ag and Au receive wide interests due to their superior plasmonic responses. Large amount of works have been done to synthesize

Ag@Au or Au@Ag core@shell NPs, firstly, to take advantage of the well-established surface chemistry of the shell material, and secondly, to retain the physical property of the core material.[35] However, it is quite possible that the core@shell NPs can show distinctly different, sometimes dramatically enhanced behavior compared with individual materials because of the change of crystalline structure, interaction of electronic structure, or the change of lattice induced by the strain at the interface.

### 1.5 Nano-catalysis- a vital area of modern science

It has been corroborated that for catalytic materials, the catalytic activity depends strongly on the atomic arrangement on the exposed facets because the atomic arrangement affects the adsorption of reacting molecules.[36] Besides, it has also been reported that the atoms at the corners and edges show higher catalytic activity because atoms at these locations, may possess more dangling bond which make them more active in binding with reacting molecules. For NPs which have high surface-to-volume ratio, both factors, the atomic arrangement on the facets, and the ratio of atoms at corners and edges, depend on the morphology. For instance, for the tetrahedrons, cuboctahedrons, and cubes of 5 nm in size, the ratios of atoms located at corners or edges are 35%, 13%, and 6%, respectively. As a result, synthesizing NPs with uniform morphology is of great interest to many chemists.

Well, nanoparticles can be defined as particles with 1-50 nm diameters at least in one dimension, a size range where it can show size dependent properties. Smaller the cluster of atoms, the higher the percentage of atoms is on the surface, rendering nanoparticles very interesting in catalysis. Hence, nanoparticles of 10 nm diameter have about 10% of its atoms in the surface, but one of 1 nm has

100%.[37] The interest in nanoparticle-catalysis i.e., nano-catalysis has grown significantly because of its improved efficiency under mild and environmentally benign conditions along the line of Green Chemistry. The term 'nano-catalysis' can be considered as a bridge between homogeneous and heterogeneous catalysis. On account of nano-size, i.e. high surface area, the contact between reactants and catalyst increases vividly and they can operate in the same manner as homogeneous catalysts (close to homogeneous catalysis). Additionally, because of their insolubility in the reaction solvent, the nanocatalysts can be separated out easily from the reaction mixture. Thus, nano-catalysis can unite the assistance of both the systems, and can offer unique activity with high selectivity.[38] Metal nanoparticles have long been used as quasi-homogeneous catalysts[39] in a variety of chemical transformations such as C-C bond formation reactions, which include Suzuki, Heck, Sonogashira, Hiyama and Stille coupling reactions.[40] The stated applications bestow the impression to be motivated by the intention to enhance the catalytic efficiency by virtue of large surface areas of the nanoparticles. Nevertheless, a more fascinating aspect of the nanoparticle catalysis lies in the emergence of novel catalytic activities and/or selectivities arising from their size specific electronics and geometric structures. Nano-catalysis in organic syntheses has several advantages over homogeneous organic catalysts, such as: (i) Easy recovery of the catalyst, (ii) Simple product isolation and (iii) Recyclability. Thus, the heterogeneous solid catalysts (nanocatalysts) have been recognized as robust alternatives to homogeneous organic catalyst.[41]

The exercise of nanoparticles as catalysts in organic synthesis has by now been highlighted in the literature and it is not a novel protocol. However, in order to study Nanoparticles-catalyzed Organic Synthesis Enhancement

comprehensively and systematically, akin to "**MORE**" (Microwave-assisted Organic Reaction Enhancement) chemistry, we believe that a separate domain is obligatory by looking at the number of increasing publications in this area, we are confident that in the forthcoming years. Hence, we have proposed the term "**NOSE**" (Nanoparticles-catalyzed Organic Synthesis Enhancement).[42] This will help the researchers all over the world to study these and related issues under one umbrella, i.e. "**NOSE**" chemistry.

### 1.6   A review of literature for the nano-catalysis in organic synthesis

The nano-catalysis has emerged as a dynamic and burgeoning area in the field of organic synthesis.[43] Of particular interest is the development of allowing methodologies to efficiently build up complex molecules using nano-catalysis. Recently, SciFinder explored an exponential growth of literature reported on nano-catalysis in organic synthesis during the past decade. This quickly growing research theme has been built upon productive multidisciplinary collaborations between scientists in nanosciences and organic chemistry as well as the remarkable catalytic activities and selectivities of nanometric materials. Besides, even if extensively utilized homogeneous catalysts continue as synthetic chemists' most powerful resources, but then heterogeneous nanoparticle catalysis features the opportunity for catalyst recycling, continuous processing, and ease of separation, thereby offering green and cost-effective options.[44] Notwithstanding the aforementioned promising attributes, nanocatalysts have not yet been established wide applications in the synthesis of complex molecule,[45] with most applications thus far limited to cross-couplings[46] and oxidations/reductions.[47] Thus, in this standpoint, we are outlining some of the selected examples employing nanoparticles as catalysts to create new-fangled chemical bonds (C-C

and C-Heteroatom) along with the emphasis on applications and opportunities in complex molecule synthesis.

### 1.6.1 Fe₃O₄@silica sulfuric acid nanoparticles catalyzed efficient solvent-free synthesis of indazolo[2,1-b]phthalazine-triones and pyrazolo[1,2-b]phthalazine-diones

Of late, magnetically separable and recyclable silica-coated magnetite nanoparticles introduces an efficient solid acid catalyst for the one-pot three-components condensation reaction of aromatic aldehydes 1, cyclic 2 or acyclic 1,3-diketones 3 and phthalhydrazide 4 (scheme 1).[48] Easy reaction conditions, high catalytic activity, reusability, and simple magnetically work-up, makes this protocol an attractive alternative for the economic synthesis of indazolo[2,1-b]phthalazinetriones 5 and pyrazolo[1,2-b]phthalazine-diones 6.
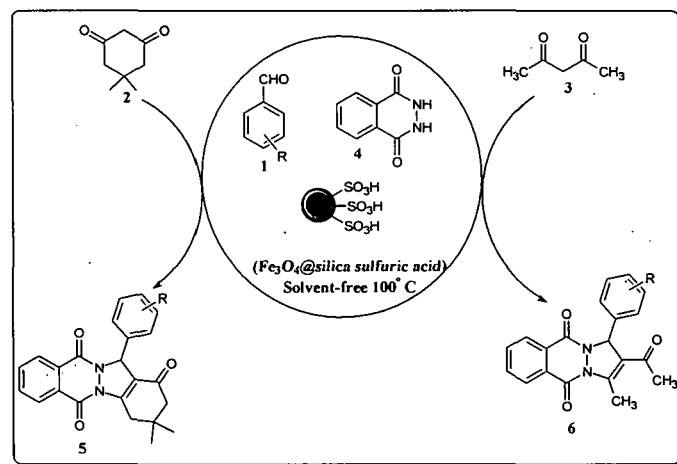


Scheme 1: Fe₃O₄@silica sulfuric acid catalyzed synthesis of indazolo[2,1-b]phthalazine-triones and pyrazolo[1,2-b]phthalazine-diones

### 1.6.2 Nanosized ruthenium particles decorated carbon nanofibers as active catalysts for the oxidation of p-cymene by molecular oxygen

Makgwane et al., has developed highly dispersed, nanosized ruthenium (Ru) particles anchored on carbon nanofibers (CNFs) with varying Ru loadings (1-7

wt%) demonstrated efficient catalytic activity in the aerobic oxidation of *p*-cymene 7 using molecular oxygen (scheme 2).[49] The action of the Ru catalysts was effected by the structural properties that resulted from the different metal loadings and by various reaction variables, such as the temperature, the amount of catalyst and the type of radical-initiator substrate. Under the standard reaction conditions, the 3% Ru/CNF catalyst exhibited excellent performance with a selectivity of 42% toward primary cymene hydroperoxide 8 and 33% towards tertiary cymene hydroperoxide 9 at 55% *p*-cymene conversion achieved within 5 h at 90 °C. The catalyst was reusable for five consecutive reaction cycles without appreciable loss of activity.
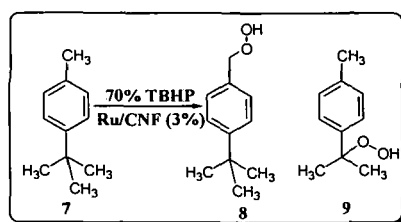


Scheme 2: Ru/CNF catalyzed oxidation of *p*-cymene by molecular oxygen

### 1.6.3 NiO nanoparticles catalyzed multicomponent one-pot synthesis of novel spiro and condensed Indole derivatives

Sachdeva and co-workers presented an proficient catalytic protocol for the synthesis of novel spiro[indoline-3,4′-pyrano[2,3-*c*]thiazole]carbonitriles 13 and condensed thiazolo[5″,4″:5′,6′]pyrano[4′, 3′:3,4]furo[2,3-*b*]indole derivatives 14 in a one-pot three-component approach involving substituted 1*H*-indole-2,3-diones 10, activated methylene reagent 11, and 2-thioxo-4-thiazolidinone 12 catalyzed by NiO nanoparticles (scheme 3) under conventional heating and microwave irradiation.[50] The synthesis of novel spiro and condensed indole derivatives was effected by Knoevenagel condensation followed by Michael addition. The operational simplicity, high yield of the products, and easy

handling of the catalyst are the beneficial aspects of this methodology. After

reaction course, NiO nanoparticles can be recycled and reused without any

apparent loss of activity.
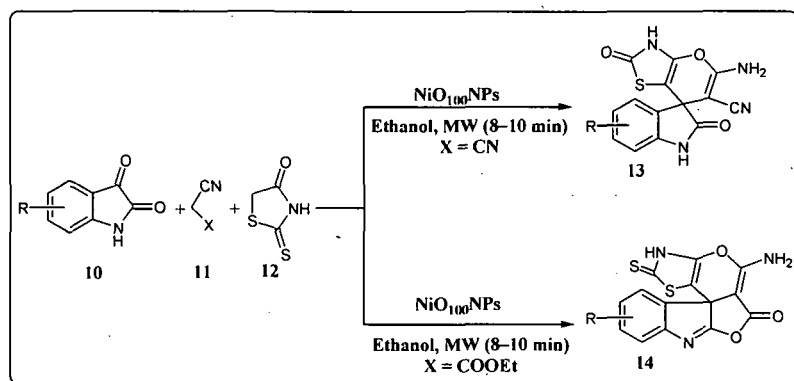


Scheme 3: Synthesis of spiro and condensed Indole derivatives catalyzed by NiO

NPs

*1.6.4 CuI nanoparticles as a reusable heterogeneous catalyst for the one-pot*

*synthesis of N-cyclohexyl-3-aryl-quinoxaline-2-amines under mild conditions*

Very recently, CuI nanoparticles as an expedient and recyclable catalyst was

reported for the synthesis of *N*-cyclohexyl-3-aryl-quinoxaline-2-amines **18** in

ethanol (scheme 4) via a multi-component reaction amongst *o*-phenylene diamine

**15**, aryl aldehydes **16** and cyclohexyl isonitrile **17**.[51] The catalyst could be

recycled and reused for several times without noticeably decreasing the catalytic

activity.
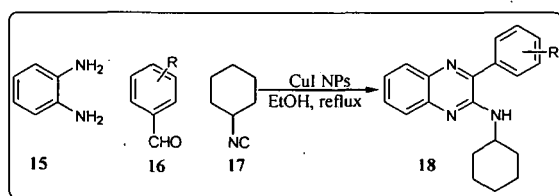


Scheme 4: Synthesis of *N*-cyclohexyl-3-arylquinoxaline-2-amines catalyzed by

CuI NPs

## 1.6.5 One-pot Synthesis of Dibenzyls and 3-Arylpropionic Acids Catalyzed by Linear Polystyrene-Stabilized Palladium Oxide Nanoparticles in Water

Ohtaka and his research team described linear, polystyrene-stabilized PdO nanoparticles (PS-PDONPs) as an active catalyst for one-pot, multistep reactions in water (scheme 5).[52] The one-pot synthesis of dibenzyl **21** by sequential Suzuki coupling of $\beta$-bromostyrene **19** with arylboronic acid **20** and subsequent hydrogenation was achieved. The same catalyst was also utilized for the synthesis of 3-arylpropionic acid **24** from aryl iodide **22** and propionic acid **23**.
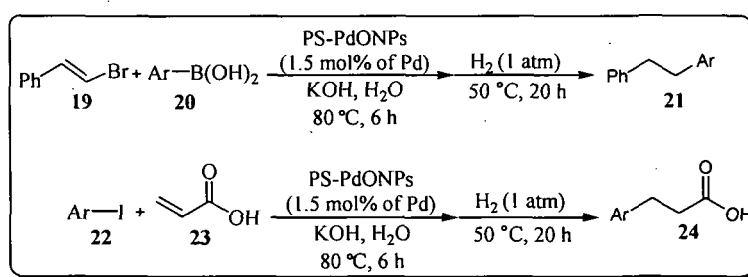


Scheme 5: Polystyrene-stabilized palladium oxide nanoparticles catalyzed synthesis of dibenzyls and 3-arylpropionic acids in water

## 1.6.6 ZnO nanoparticles as an efficient and reusable catalyst for the synthesis of quinoxaline under solvent free condition

More recently, Sadeghi et al., has reported that 1,2-Diketones **25** when reacted in one-pot with 1,2-diamines **26** at room temperature with ZnO nanoparticles as a catalyst produced quinoxaline (scheme 6) in high yields.[53]
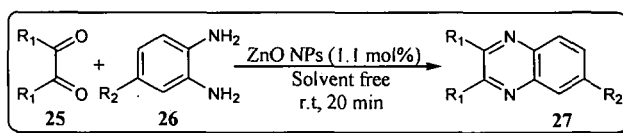


Scheme 6: ZnO nanoparticles catalyzed synthesis of quinoxaline under solvent free condition

## 1.6.7 Facile synthesis of palladium nanoparticles encapsulated in amine-functionalized mesoporous metal-organic frameworks and their catalytic

*activity for dehalogenation of aryl chlorides*

Huang *et al.*, discovered a facile synthetic route for the synthesis of Pd nanoparticles encapsulated in amine-functionalized mesoporous metal-organic frameworks MIL-101(Cr)-NH$_2$ (part of the amine groups shown) under mild conditions.[54] The well-dispersed Pd nanoparticles confined in mesoporous cages revealed high catalytic activity for the dehalogenation of aryl chlorides 28 in water under mild conditions (scheme 7) to produce 29. The catalyst was easily recoverable and reused several times.
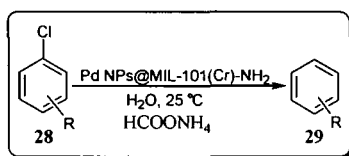


Scheme 7: Pd NPs encapsulated in amine-functionalized mesoporous metal-organic frameworks catalyzed dehalogenation of aryl chlorides in water

### 1.6.8 Magnetic nanoparticles catalyzed synthesis of diverse N-Heterocycles

Kidwai and his group synthesized a large library of diversified compounds pyrano[2,3-*d*]pyrimidines 33, pyrido[2,3-*d*]pyrimidines 35 and a variety of spirooxindoles through a very efficient, economical and environmentally benign process utilizing magnetic Fe$_3$O$_4$ nanoparticles as catalyst (scheme 8).[55] The catalyst is magnetically separable and reusable without much loss in its activity is an additional ecofriendly attribute of this catalytic system. The synthesized novel compounds could be further explored for their pharmaceutical application. Moreover, column chromatography and recrystallization of the products is not required as the crude products are already highly pure and hence can be used for target oriented synthesis on a wide scale.
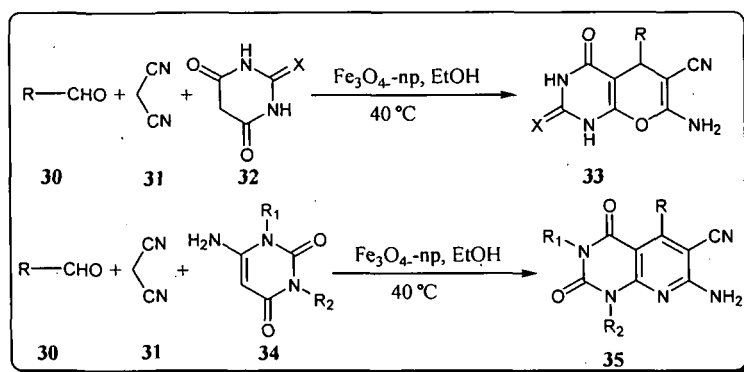
Scheme 8: Synthesis of various pyrano[2,3-*d*]pyrimidine and pyrido[2,3-*d*]pyrimidine derivatives at 40 °C with Fe₃O₄-nanoparticles as catalyst

### 1.6.9 ZnO nanoparticles catalyzed synthesis of 4H-Chromenes in aqueous medium via one-pot three component reactions : A Greener "NOSE" Approach

Ghosh *et al.*, enlightened the synthesis of 4*H*-chromenes **39** in water under thermal condition by one-pot three component reaction mediated by ZnO nanoparticles (scheme 9).[56] The highly product-selective three component electrophilic reaction of 2-hydroxybenzaldehyde **36** with an active methylene compound **37** and another carbon-based varied nature of nucleophile **38** has been developed by a reversible alkylation procedure using greener "NOSE" approach. The catalyst can be efficiently recycled up to the sixth run.
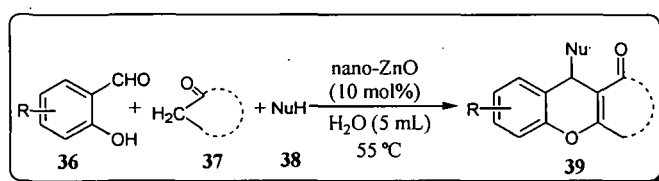


Scheme 9: Nano-ZnO catalyzed synthesis of 4*H*-Chromenes

### 1.6.10 A novel approach to bis(indolyl)methanes using nickel nanoparticles

It has been recently established that nano-sized nickel as a catalyst is developed for the electrophilic substitution reactions of indole **40** with various aromatic aldehydes **41** under solvent-free conditions to afford the corresponding bis(indolyl)methanes **42** in high yields (scheme 10).[57] The described method has

**Page | 21**

promising features, such as no hazardous organic solvents or catalysts, short reaction time, high product yields, simple work-up procedure, reusable catalyst and easy product separation without further purification with column chromatography.
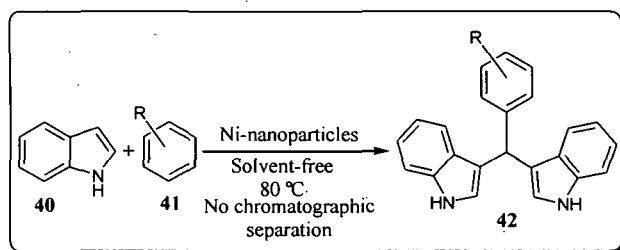


Scheme 10: Nano-Ni catalyzed synthesis of bis(indolyl)methanes

## 1.6.11 Synthesis of indolizines and heterocyclic chalcones catalyzed by supported copper nanoparticles

Albaladejo and co-workers have probed that copper nanoparticles supported on multi-walled carbon nano tubes worked smoothly as a catalyst for the synthesis indolizines **46** via multi component reaction of aldehydes **43**, amine **44** and an alkyne **45** (scheme 11). On the other hand, when aldehydes **43** and an alkyne **45** reacted together it produced heterocyclic chalcones **47** in good to high yields (scheme 11).[58]
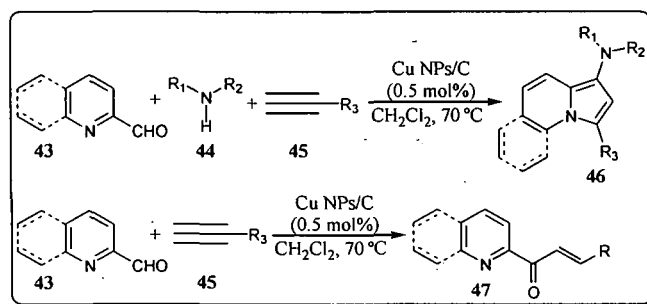


Scheme 11: Copper nanoparticles supported on multi-walled carbon nanotube catalyzed synthesis of indolizines and heterocyclic chalcones

## 1.6.12 Total synthesis of (±)-sorocenol b employing nanoparticle catalysis

Cong *et al.*, presented an outstanding work for the total synthesis of (±)-sorocenol B **50** which was accomplished by silver nanoparticle (AgNP)-catalyzed Diels-Alder cycloaddition and late-stage Pd(II)-catalyzed oxidative cyclization (scheme 12).[59] The synthetic natural product exhibited low micromolar cytotoxic activity against a number of human cancer cell lines.
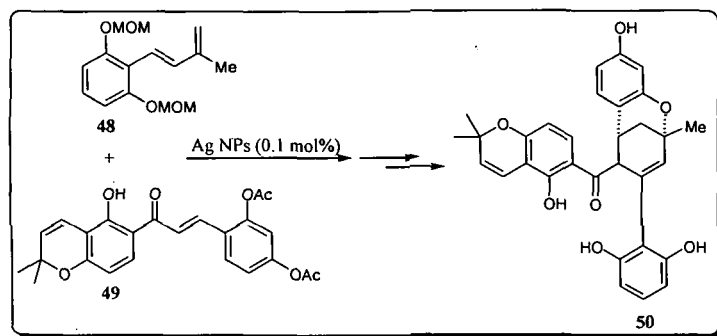


Scheme 12: AgNPs catalyzed total synthesis of (±)-sorocenol

### 1.6.13 Zinc Oxide nanoparticles catalyzed synthesis of bis-isoquinolinones

Krishnakumar and his research group reported the synthesis of diversified bis-isoquinolinones **55** in two steps, utilizing homophthalic acid **51** and various acid chlorides **52** providing 3-substituted isocoumarins **53** in the first step which on further condensation with 1,7-heptadiamine **54** involving C-N bond formation from the lactone (scheme 13) in the presence of zinc oxide nanoparticles (10 mol%).[60]
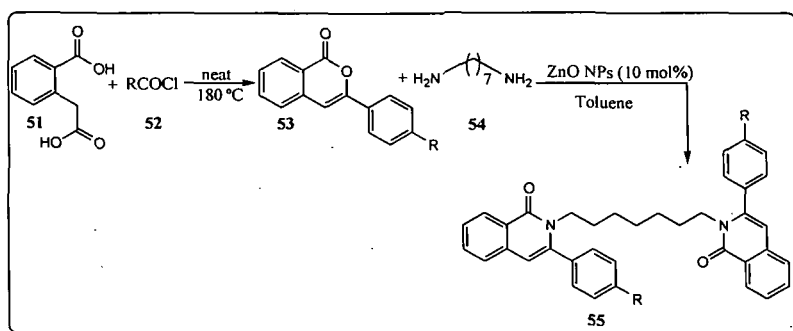


Scheme 13: Synthesis of substituted bis-isoquinolinones by nano-ZnO

*1.6.14 Polymer-incarcerated Au-Pd nanoclusters with boron on carbon as catalyst for the aerobic oxidation-Michael addition of 1,3-dicarbonyl compounds to allylic alcohols*

Yoo *et al.*, demonstrated a tandem aerobic oxidation-Michael addition process involving oxidation of allylic alcohol **57** followed by 1,4-addition of 1,3-dicarbonyl derivative **56** to Michael acceptor **58** catalyzed by polymer-incarcerated Au-Pd nanoclusters with boron on carbon (scheme 14).[61] It has been found that bimetallic Au-Pd nanoclusters particularly effective for the aerobic oxidation of allylic alcohols under base and water-free conditions.
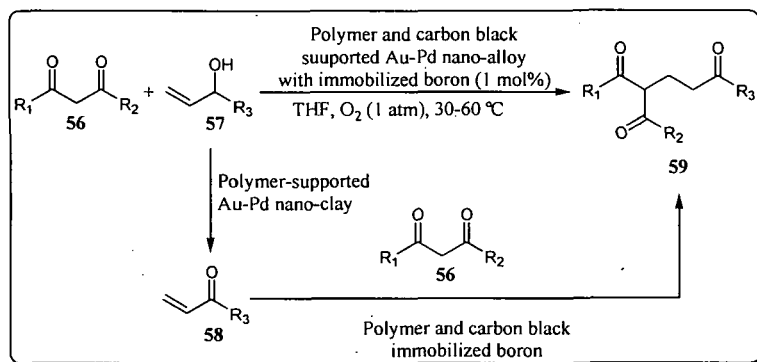


Scheme 14: Bimetallic Au-Pd nanoclusters catalyzed tandem aerobic oxidation-Michael addition process

*1.6.15 Cu-nanoparticles-catalyzed Mannich reaction*

Kidwai *et al.*, has reported that recyclable heterogeneous Cu-nanoparticles efficiently catalyzed one-pot three-component Mannich reaction at room temperature and afforded various β-amino carbonyl compounds **63** in good to excellent yields.
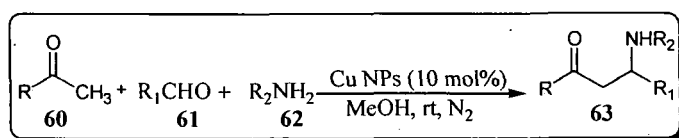


Scheme 15: Cu NPs catalyzed Mannich reaction

## 1.7 Scopes and Objectives of the Present Investigation

Although various nanoparticles have several remarkable potential applications in the field of medicine and material science but only a few reports described its utilization as catalyst in organic transformations. Under the above background, the main objectives of the present investigation are as follows:

(i) The main objective is to search for applications of nanoparticles as catalysts in Carbon-Carbon, Carbon–Heteroatom and C-H bond forming reactions.

(ii) Whether nanocatalyst can catalyze the synthesis of complex fused systems, given that the ring systems are a feature of important compounds, including many of pharmaceutical interest?

(iii) To promote economical and environmentally friendly experimental procedures. By rethinking chemical design from the ground up, the green synthetic methodology has to be developed in new ways to manufacture products that fuel the economy and lifestyles, without the damages to the environment that have become all too evident in recent years. Yes, we are talking about greener nanocatalysts.

(iv) To accomplish a comprehensive study of the scope and limitations of the synthesis of C-C, C-N, C-H, and C-O bonded compounds in the domain of nanocatalysis.

(v) To study and characterize the nano catalysts by spectroscopic and analytical techniques.

(vi) To study and characterize the prepared compounds by spectroscopic (high resolution $^1H$ NMR and $^{13}C$ NMR spectroscopy, Mass spectrometry, IR spectroscopy) methods and analytical methods (TGA, melting point/boiling point determination, and elemental analysis etc.).

(vii) To evaluate and demonstrate the 'green-ness' of the newly developed protocols by considering the green metrics.

(viii) To study the significance of these reactions as they relate to the literature and will provide mechanistic insight into newly discovered and previously known organic reactions.

(ix) To study the stability of nanoparticles under the reaction condition.

(x) To study the recyclability of nanocatalysts and to search for methods to regain the activity of nanocatalysts in the case of decreasing activity in subsequent recycling.

(xi) To address the issues which arise during the investigation.

### 1.8 Plan of Works

To fulfill the above objectives, the following plan of works has been formulated:

(i) A state of the art literature survey on the field of nanoparticles and their catalytic applications would be conducted.

(ii) The nanoparticles would be either synthesized by standard procedure or purchased or a new technique will be devised for its preparation.

(iii) The synthesized or purchased metal nanoparticles would be characterized by different analytical and spectroscopic techniques such as UV-VIS spectroscopy, FTIR spectroscopy, TGA, XRD, EDX, XPS, SEM and TEM etc.

(iv) The catalytic performance of the characterized metal nanoparticles would be investigated in some selected organic transformations e.g. N-formylation reactions, oxidation of aldehydic motif, syntheses of amide etc.

(v) The desired products obtained after reaction and purification would be fully analyzed and characterized by spectroscopic and analytical means.

(vi) The change in morphology of the nanocatalysts before and after reaction as well as after recycling would be inspected.

(vii) Finally to compare the 'green-ness' of the newly discovered protocols with the previously reported in terms of green metrics.

**References:**

1. Kinne-Saffran, E., & Kinne, R.K.H. *Am. J. Nephrol.* **19**, 290--294, 1999.

2. Beccalli, E.M., et al. *Chem. Rev.* **107**, 5318--5365, 2007.

3. For recent reviews on the impact of catalysis in the pharmaceutical industry, see: (a) Magano, J., & Dunetz, J.R. *Chem. Rev.* **111**, 2177--2250, 2011; (b) Busacca, C.A., et al. *Adv. Synth. Catal.* **353**, 1825--1864, 2011.

4. For a recent review on the application of cross-coupling in the synthesis of functional materials, see: Carsten, B. et al. *Chem. Rev.* **111**, 1493--1528, 2011.

5. (a) March, J. *Advanced Organic Chemistry: Reactions, mechanisms and structure*, 3$^{rd}$ ed., John Wiley & Sons, New York, 1985; (b) March, J. *Advanced Organic Chemistry: Reactions, mechanisms and structure*, 4$^{th}$ ed., Wiley, New York, 1992; (c) Wilkinson, M.C. *Org. Lett.* **13**, 2232--2235, 2011.

6. (a) Dyker, G. *Handbook of C-H Transformations*; Ed.; Wiley-VCH: Weinheim, 2005; (b) Li, H., et al. *Cat. Sci. Technol.* **1**, 191--206, 2011; (c) Wasa, M., et al. *Isr. J. Chem.* **50**, 605--616, 2010; (d) Lyons, T.W., & Sanford, M.S. *Chem. Rev.* **110**, 1147--1169, 2010; (e) Jazzar, R., et al. *Chem. Eur. J.* **16**, 2654--2672, 2010; (f) Giri, R., et al. *Chem. Soc. Rev.* **38**, 3242--3272, 2009; (g) Chen, X., et al. *Angew. Chem. Int. Ed.* **48**, 5094--5115, 2009; (h) Seregin, I.V., & Gevorgyan, V. *Chem. Soc. Rev.* **36**, 1173--1193, 2007.

7. Luo, Y.R. *Handbook of Bond Dissociation Energies in Organic Compounds*, CRC Press: Boca Raton, FL, 2003.

8. (a) Dhakshinamoorthy, A., & Garcia, H. *Chem. Soc. Rev.* **41**, 5262--5284, 2012; (b) Crooks, R. M., et al. *Acc. Chem. Res.* **34**, 181--190, 2001.

9. (a) Polshettiwar, V., & Varma, R.S. *Green Chem.* **12**, 743--54, 2010; (b) Polshettiwar, V., et al. *Chem. Commun.* **47**, 6318--6320, 2008; (c) Min Han, Y., et al. *Chin. J. Org. Chem.* **33**, 492--503, 2013; (c) Nasir, R.B., & Varma, R.S. *Chem. Commun.* **48**, 2582--2584, 2012; (d) Huang, Y. et al. *Journal of Catalysis* **292**, 111--117, 2012.

10. Anastas T.P. & Warner C.J. *Green Chemistry: Theory and Practice,* Oxford Publication, New York, 1998.

11. Talea, R.H., et al. *Eur. Chem. Bull.* **2**, 279--282, 2013.

12. Kaicharla, T. et al. *Green Chem.* **15**, 1608--1614, 2013.

13. (a) Seil, J.T., & Webster, T.J. *Int. J. Nanomedicine* **7**, 2767--2781, 2012; (b) Jin, R. *Nanotechnol. Rev.* **1**, 31--56, 2012; (c) Mahmoudi, M. *Chem. Rev.* **112**, 2323--2338, 2012; (d) Aragay, G., et al. *Chem. Rev.* **112**, 5317--5338, 2012.

14. Feynman, R.P. *Engineering and Science* **23**, 22--36, 1960.

15. (a) Talapin, D. V., et al. *Nature* **461**, 964--967, 2009; (b) Bell, A.T. *Science* **299**, 1688--1691, 2003; (c) Hernandez, J., et al. *J. Phys. Chem. C* **111**, 14078--14083, 2007.

16. Klabunde, K.J. *Nanoscale Materials in Chemistry*, Wiley, Interscience, New York, NY 2001.

17. (a) Daniel, M.C., & Astruc, D. *Chem. Rev.* **104**, 293--346, 2004; (b) Yan, Z.G., & Yan, C.H. *J. Mater. Chem.* **18**, 5046--5059, 2008; (c) Niu, W., & Xu, G. *Nano Today* **6**, 265--285, 2011; (d) Mazumder, V., et al. *Adv. Funct. Mater.* **20**, 1224--1231, 2010.

18. Lamer, V.K., & Dinegar, R.H. *J. Am. Chem. Soc.* **72**, 4847--4854, 1950.

19. (a) Zheng, H., et al. *Science* **324**, 1309--1312, 2009; (b) Yuk, J., et al. *Science* **336**, 61--64, 2012.

20. Palashuddin, S.M., et. al. *Scientific reports* **2**, 1--5, 2012.

21. Brust, M., et al. *J. Chem. Soc., Chem. Commun.* **7**, 801--802, 1994.

22. Chakroune, N., et al. *Langmuir* **21**, 6788--6796, 2005.

23. (a) Sanchez-Iglesias, A., et al. *Adv. Mater.* **18**, 2529--2534, 2006; (b) Pastoriza-Santos, I., & Liz-Marzan, L.M. *Langmuir* **15**, 948--951, 1999.

24. (a) Negishi, Y., et al. *J. Am. Chem. Soc.* **127**, 5261--5270, 2005; (b) Lee, D., et al. *J. Am. Chem. Soc.* **126**, 6193--6199, 2004; (c) Hostetler, M.J., et al. *Langmuir* **14**, 17--30, 1998.

25. (a) Link, S. &. El-Sayed, M.A. *J. Phys. Chem. B* **103**, 4212--4217, 1999; (b) Alvarez, M.M., et al. *J. Phys. Chem. B* **101**, 3706--3712, 1997.

26. (a) Huang, X., et al. *Nature Nanotechnology* **6**, 28--32, 2011; (b) Huang, X., et al. *J. Am. Chem. Soc.* **133**, 4718--4721, 2011; (c) Ahmadi, T.S., et al. *Science* **272**, 1924--1925, 1996.

27. (a) Chen, M., et al. *Adv. Mater.* **24**, 862--879, 2012; (b) Huang, X., et al. *J. Am. Chem. Soc.* **131**, 13916--13917, 2009; (c) Brust, M., et al. *J. Chem. Soc., Chem. Commun.* **7**, 801--802, 1994; (d) Chen, Y.-H., et al. *J. Am. Chem. Soc.* **131**, 9114--9121, 2009; (e) Bigall, N.C., et al. *Nano Lett.* **8**, 4588--4592, 2008; (f) Xiong, Y., et al. *J. Am. Chem. Soc.* **129**, 3665--3675, 2007.

28. Xia, Y., et al. *Angew. Chem. Int. Ed.* **48**, 60--103, 2009.

29. Xiong, Y., et al. *Angew. Chem. Int. Ed.* **46**, 4917--4921, 2007.

30. Ciacchi, L.C., et al. *J. Phys. Chem. B* **107**, 1755--1764, 2003.

31. (a) Sun, S.H., et al. *J. Phys. Chem. B* **107**, 5419--5425, 2003; (b) Shevchenko, E.V., et al. *J. Am. Chem. Soc.* **125**, 9090--9101, 2003.

32. (a) Lim, B., et al. *Science* **324**, 1302--1305, 2009; (b) Habas, S.E., et al. *Nat. Mater.* **6**, 692--697, 2007.

33. Wang, C., et al. *Nano Lett.* **9**, 1493--1496, 2009.

34. (a) Zeng, J., et al. *Angew. Chem. Int. Ed.* **51**, 2354--2358, 2012; (b) Zhang, J.L., et al. *J. Am. Chem. Soc.* **127**, 12480--12481, 2005.

35. Cao, Y.W., et al. *J. Am. Chem. Soc.* **123**, 7961--7962, 2001.

36. Huang, C.C., et al. *Langmuir* **20**, 6089--6092, 2004.

37. (a) Braunstein, P., Oro, L., & Raithby, P.R. In *Metal Clusters in Chemistry*, Wiley-VCH: Weinheim, Germany, 1998; (b) Fendler, J.H. In *Nanoparticles and Nanostructured Films. Preparation, Characterization and Applications*, Wiley-VCH: Weinheim, Germany, 1998; (c) Klabunde, K.J., & Mohs, C. *Nanoparticles and Nanostructural Materials.* In *Chemistry of Advanced Materials, An Overview*, Interrante, L.V. et al. eds., Wiley-VCH, New York, 1998, 271-327; (d) Rao, C.N.R., et al. *Chem. Soc. Rev.* **29**, 27--35, 2000; (e) Roucoux, A., et al. *Chem. Rev.* **102**, 3757--3778, 2002.

38. (a) Astruc, D. *Inorg. Chem.* **46**, 1884--1894, 2007; (b) Astruc, D., et al. *Angew. Chem. Int. Ed.* **44**, 7852--7872, 2005; (c) Polshettiwar, V, et al. *Chem. Commun.* **35**, 1837--1839, 2009.

39. (a) Lewis, L.N. *Chem. Rev.* **93**, 2693--2730, 1993; (b) Aiken, J.D., & Finke, R.G. *J. Mol. Catal. A* **145**, 1--44, 1999.

40. (a) Suzuki, A. *J. Organomet. Chem.* **576**, 147--168, 1999; (b) Moreno-Manas, M., & Pleixats, R. *Acc. Chem. Res.* **36**, 638--643, 2003; (c) Hiyama, T. *J. Organomet. Chem.* **653**, 58--61, 2002; (d) Espinet, P., & Echavarren, A.M. *Angew. Chem. Int. Ed.* **43**, 4704--4734, 2004.

41. Churruca, F., et al. *Tetrahedron Lett.* **47**, 3233--3237, 2006.

42. (a) Das, V.K., et al. *Green Chem.* **14**, 847--854, 2012; (b) Das, V.K., et al. *Appl. Catal. A: Gen.* **456**, 118--125, 2013; (c) Das, V.K., et al. *J. Org. Chem.* **78**, 3361--3366, 2013; (d) Das, V.K., & Thakur, A.J. *ISRN Organic Chemistry* 1--6, 2013; (e) Das, V.K., & Thakur, A.J. *Tetrahedron Lett.* **54**, 4164--4166, 2013.

43. (a) Astruc, D. *Nanoparticles and Catalysis.* Wiley-VCH; Weinheim: 2007; (b) Corma A., & Garcia H. *Chem. Soc. Rev.* **37**, 2096--2126, 2008; (c) Della P.C., et al. *Chem. Soc. Rev.* **37**, 2077--2095, 2008; (d) Shiju, N.R., & Guliants, V.V. *Appl. Catal. A-Gen.* **356**, 1--17, 2009.

44. Astruc, D., et al. *Angew. Chem. Int. Ed.* **44**, 7852--7872, 2005.

45. (a) Patil, N.T. *ChemCatChem.* **3**, 1121--1125, 2011; (b) Myers, V.S., et al. *Chem. Sci.* **2**, 1632--1646, 2011.

46. Moreno-Manas, M., & Pleixats, R. *Acc. Chem. Res.* **36**, 638--643, 2003.

47. Roucoux, A., et al. *Chem. Rev.* **102**, 3757--3778, 2002.

48. Kiasat, A.R., & Davarpanah, J. *J. Mol. Catal. A: Chem.* **373**, 46--54, 2013.

49. Makgwane, P.R., & Ray, S.S. *J. Mol. Catal. A: Chem.* **373**, 1--11, 2013.

50. Sachdeva, H., et al. *Journal of Chemistry,* 1--10, 2013.

51. Safaei-Ghomi, J., et al. *JNS* **2**, 79--83, 2012.

52. Ohtaka, A., et al. *Asian Journal of Organic Chemistry,* **2**, 399--402, 2013.

53. Sadeghi, B., & Karimi, F. *Iranian Journal of Catalysis,* **3**, 1--7, 2013.

54. Huang, Y., et al. *Journal of Catalysis,* **292**, 111--117, 2012.

55. Kidwai, M. *Mol. Divers.* **16**, 121--128, 2012.

56. Ghosh, P.P., & Das, A.R. *J. Org. Chem.* **78**, 6170--6181, 2013.

57. Olyaei, A. et al. *J. Serb. Chem. Soc.* **78**, 463--468, 2013.

58. Albaladejo, M.J. *Chem. Eur. J.* **19**, 5242--5245, 2013.

59. Cong, H. & Porco, J.H. *Org. Lett.* **14**, 2516--2519, 2012.

60. Krishnakumar, V. et al. *The Scientific World Journal* 1--7, 2012.

61. Yoo, W.J. et al. *J. Am. Chem. Soc.* 133, 3095--3103, 2011.

# Chapter 2

## Sections I & II

# Section I

# Nano rod shaped and reusable basic Al$_2$O$_3$ catalyst for *N*-formylation of amines under solvent free condition: A novel, practical and convenient 'NOSE' approach



HCOOH

Solvent free condition
40 °C

1. Isolation through centrifugation
2. Recycling

50 nm
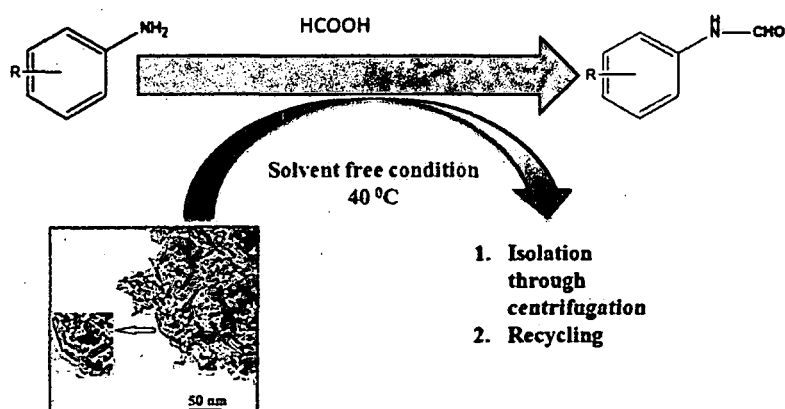
# Section I

# Nano rod shaped and reusable basic $Al_2O_3$ catalyst for *N*-formylation of amines under solvent free condition: A novel, practical and convenient 'NOSE' approach

## *2.I.1 Introduction*

In the wake of increasing awareness in environmentally benign techniques during the past few years, organic synthesis under solvent free condition has gained much popularity.[1] In this regard, the synthesis of N-bonded compounds has received considerable attention from the sight of green chemistry.[2] There is a growing appreciation for *N*-formylation of primary or secondary amines into formamides which is a common methodology in synthetic organic chemistry. The reaction product, formamides serve either as a polar solvent or as an important intermediate in several organic transformations since their skeletons exist in pharmaceutically valuable compounds such as fluoroquinolines,[3] imidazoles,[4] 1,2-dihydro quinolines,[5] nitrogen-bridged heterocycles,[6] oxazolidinones[7] and cancer chemotherapeutic agents.[8] They have also found significant applications as Lewis base catalysts in various organic transformations,[9] synthesis of formamidines,[10] isocyanides[11] and as *N*-formylating agent in histone proteins as a secondary modification arising from oxidative DNA damage.[12]

The literature is enumerated with several strategies[13] prescribed for *N*-formylation of amines. Regardless of the existing methodologies, most of them suffer from different drawbacks such as thermal instability, sensitivity to moisture, application of toxic and expensive formylating agents and catalysts,

poor atom economy, high temperature, prolonged reaction time, harsh reaction condition, formation of undesirable byproducts, low yields, leading to diformylation and/or lack of regioselectivity and tedious work up. Therefore, the synthesis of formamides still remains as an active research area in terms of operational simplicity and economic viability. In the recent years, formic acid[14] has been continually accepted as a potent formylating agent owing to its less toxicity, inexpensivity and easy practical applicability.

With the nanotechnology now available to the scientists, of late, Somorjai *et al* emphasizes that catalysis by transition metal nanoparticles is the central field of nanoscience and nanotechnology, [15] which are the frontiers between homogeneous and heterogeneous catalysis. [16] The growing interest on the catalytic properties of transition metal nanoparticles is due to their large surface area, distinct electronic, optical, magnetic, thermal and chemical properties.[17] The ultimate goal to work with nanoparticles is their high catalytic activity, recoverability, improved selectivity, criteria of evolution and role in green chemistry. [18] Hence, organic synthesis catalyzed by metal/metal oxide nanoparticles[19] has received tremendous importance in recent decades.

To cater the burgeoning·needs and aspirations, we have been focusing in the development of a protocol named 'NOSE'[20] (Nanoparticles-catalyzed Organic Synthesis Enhancement) chemistry in our laboratory. Nanoscale supports to create catalysts with larger surface area along with more edges and corners, which can lead to higher performance of the catalyst. Other parameters (e.g. oxygen mobility, etc.) might also play key role for enhancing catalytic activity. There are few reports that describe *N*-formylation of amines using nanoparticles. Preedasuriyachai and co-workers[21] have presented nanogold

catalyzed *N*-formylation of amines under aerobic conditions with MeOH or formalin. However, in terms of disadvantage, nanogold itself is very expensive. To the best of our knowledge, *N*-formylation of amine catalyzed by basic nano crystalline $Al_2O_3$ has not been reported. Very recently, a research group has reported the nanocrystalline $Al_2O_3$ catalyzed one-pot synthesis of poly-substituted quinolines.[22] There is an extensive study on the preparation and properties of $Al_2O_3$ nanomaterial.[23] The advantages[24] of using basic nano-$Al_2O_3$ is in terms of its crystalline size and shape, abrasive and insulating properties, less toxicity, large surface area and their basic surface characteristics, high resistant towards bases and acids, compatibility to very high temperature applications and has excellent wear resistance. Therefore, in this paper, we wish to focus on an effective, convenient and practical procedure employing nano rod-shaped basic $Al_2O_3$ (specific surface area approximately 185.6 $m^2g^{-1}$ and a crystalline size of approximately 38 nm) to catalyze *N*-formylation of 1° and 2° amines efficiently as a part of our 'NOSE' chemistry (Scheme 1) programme.
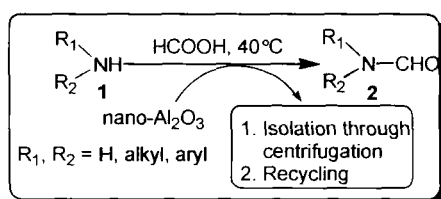


Scheme 1: *N*-Formylation of amines

## 2.1.2 Results and Discussion

### 2.1.2.1 Characterization of the pure nano-Al₂O₃

The SEM image of pure nano-$Al_2O_3$ sample has shown agglomeration of particles [figure 1 (a)]. The BET surface area of nano-$Al_2O_3$ was found to be 185.6 $m^2g^{-1}$ and the total pore volume was 0.9 $mLg^{-1}$. EDX analyses of pure nano-$Al_2O_3$ [figure 1 (b)] showed that the weight% of O and Al was 70.41 and

29.59 and atomic% was 80.05 and 19.95 respectively, as expected. Since the ratio of O to Al in the sample is 2:3, thus, it is obvious that percentage of O is higher with respect to Al. Thus, the EDX suggests the presence of only O and Al in the nano-$Al_2O_3$ sample.
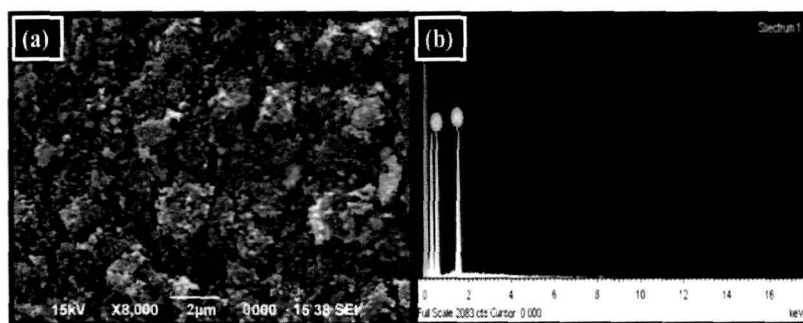


Figure 1. (a) SEM image and (b) EDX of pure nano-$Al_2O_3$

The XRD pattern of pure nano- $Al_2O_3$ (figure 2) shows that the peak of the sample corresponds to those of γ-alumina. [25] The crystalline sizes were determined by using Scherrer equation and choosing the two highest peaks (4 0 0) and (1 0 0) from XRD pattern. The crystalline sizes were found to lie between 39.7 and 37.4 nm. The average particle diameter calculated was 8.12 nm ($S_{BET}$ =185.6 $m^2g^{-1}$ and ρ =3.98 $gcm^{-3}$).
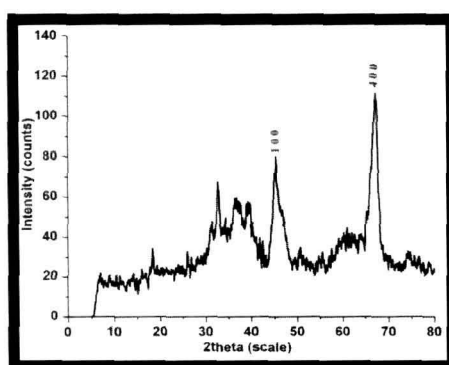


Figure 2. XRD pattern of pure nano-$Al_2O_3$

Figures 3(a) and (b) show the TEM images of nano-$Al_2O_3$. The nano rod-shape of the sample can be seen from these micrographs. The average length of the nano-$Al_2O_3$ from TEM image was found to be 25.5 nm and its average

**Page | 37**

diameter was 7.18 nm. It can also be seen that some agglomeration was present

and this was attributed to the large surface area of these nano rod-shaped $Al_2O_3$.
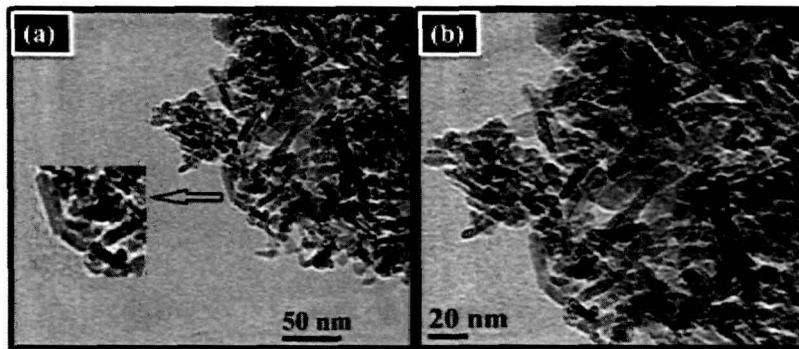


Figure 3. TEM images of nano rod-shaped $Al_2O_3$ at (a) 50 nm scale and (b) 20

nm scale

Typical SAED pattern of the $Al_2O_3$ nano rod generated as an inset is shown

in figure 4 (a). It showed that the nano rods were well-crystallined. The SAED

patterns were calculated and identified using JCPDS data card 10-425,

indicating that these rings corresponded to the diffraction planes of $\gamma$-$Al_2O_3$. No

un-assigned rings were left in the SAED patterns, eliminating the possibility of

formation of other types of metastable phases like $\delta$-$Al_2O_3$, $\theta$-$Al_2O_3$, etc. The

FTIR spectrum of pure nano-$Al_2O_3$ is shown in figure 4 (b). The peak at 3500

$cm^{-1}$ is attributed to the atmospheric water vapour or Al-OH in alumina.[26]
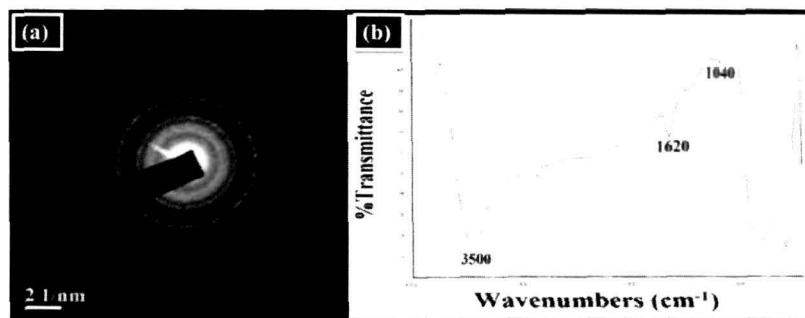


Figure 4. (a) Corresponding size distribution with inset showing SAED patterns

and (b) FTIR spectrum of pure nano-$Al_2O_3$

An absorption band at ca. 1620 $cm^{-1}$ is characteristic of alumina which is in

accordance with the literature.[27] The peak at 1040 cm^{-1} corresponds to the Al-O stretching vibration.[28]

### 2.1.2.2 Optimization of the reaction condition for N-formylation reaction

After the characterization of the nano-$Al_2O_3$, in order to optimize the reaction condition, a control experiment[14b] was carried out by taking formic acid (98%, 0.11 mL, 3 mmol) and aniline (0.09 mL, 1 mmol) as a model substrate by stirring at room temperature without using any catalyst and solvent (Table 1, entry 1). Under this condition, the reaction did not proceed and starting materials remained intact. Then we poured acetonitrile (5 mL) and continued stirring for 18 h and isolated the product in 5% yield (Table 1, entry 2). In order to improve the yield, we searched for the best experimental condition below 70 °C. By keeping this in mind, we performed the reactions at 40 °C in acetonitrile and also by stirring under solvent free condition (Table 1, entry 3). Interestingly, the reaction proceeded faster under solvent free condition providing 28% yield (Table 1, entry 4). We also conducted the reaction at 70 °C under solvent free condition and isolated 42% yield (Table 1, entry 5). Unsatisfied with these results, we felt the necessity of using a catalyst to increase the yield. Therefore, we surveyed some Lewis acid and base catalysts and out of them, we found dramatic increment in reaction rate and yield when we used nano basic $Al_2O_3$ (5 mol%) at 40 °C (Table 1, entry 15). We also attempted to compare the catalytic action of bulk basic and acidic $Al_2O_3$ with nano basic $Al_2O_3$ for N-formylation of aniline and we found excellent yield associated with lesser reaction time and low catalyst loading in case of nano-$Al_2O_3$ catalysis. We also tested the influence of solvents on reaction rate and yield by screening several solvents at 40 °C in the presence of $Al_2O_3$

nanoparticles and found that formamide formation took place faster in solvent free condition than in the presence of solvent (Table 1, entries 17-24). The turn over number (TON) was also calculated for each catalyst under different

**Table 1.** Optimization of the reaction conditions[a] for the *N*-formylation of aniline
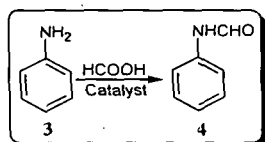


Scheme 2: *N*-Formylation of aniline (model reaction)

| Entry | Catalyst | Solvent | Temp. (°C) | Time (h) | Yield (%)[b] | TON | TOF (h$^{-1}$) |
|---|---|---|---|---|---|---|---|
| 1 | None | None | rt | 9 | NR[c] | 0 | 0 |
| 2 | None | MeCN | rt | 18 | 5% | 0 | 0 |
| 3 | None | MeCN | 40 | 15 | 12 | 0 | 0 |
| 4 | None | None | 40 | 10 | 28 | 0 | 0 |
| 5 | None | None | 70 | 7 | 42 | 0 | 0 |
| 6[d] | H$_3$BO$_3$ | None | 40 | 8 | 39 | 15.6 | 1.95 |
| 7[d] | Imidazole | None | 40 | 9 | NR[c] | 0 | 0 |
| 8[e] | Et$_3$N | None | 40 | 9 | NR[c] | 0 | 0 |
| 9[d] | PPh$_3$ | None | 40 | 10 | 50 | 20 | 2 |
| 10[e] | Pyridine | None | 40 | 9 | NR[c] | 0 | 0 |
| 11[d] | TiO$_2$ | None | 40 | 7 | 5 | 2 | 0.285 |
| 12[d] | Bulk basic Al$_2$O$_3$ | None | 40 | 7 | 64 | 25.6 | 3.65 |
| 13[e] | Bulk basic Al$_2$O$_3$ | None | 40 | 3 | 78 | 6.24 | 2.08 |
| 14[d] | Bulk acidic Al$_2$O$_3$ | None | 40 | 7 | 35 | 14 | 7 |
| 15[f,g] | Nano basic Al$_2$O$_3$ | None | 40 | 0.083 | <98 | 78.4 | 944.57 |
| 16[f,g] | Nano basic Al$_2$O$_3$ | None | 70 | 1 | 75 | 60 | 60 |
| 17[f,g] | Nano basic Al$_2$O$_3$ | MeCN | 40 | 8 | 25- | 20 | 2.5 |
| 18[f,g] | Nano basic Al$_2$O$_3$ | THF | 40 | 9 | 29 | 23.2 | 2.57 |
| 19[f,g] | Nano basic Al$_2$O$_3$ | MeOH | 40 | 4 | 68 | 54.4 | 13.6 |
| 20[f,g] | Nano basic Al$_2$O$_3$ | EtOH | 40 | 4 | 60 | 48 | 12 |
| 21[f,g] | Nano basic Al$_2$O$_3$ | DMF | 40 | 3 | 73 | 58.4 | 19.46 |
| 22[f,g] | Nano basic Al$_2$O$_3$ | Toluene | 40 | 6 | 58 | 46.4 | 7.73 |
| 23[f,g] | Nano basic Al$_2$O$_3$ | DMSO | 40 | 6 | NR[c] | 0 | 0 |
| 24[f,g] | Nano basic Al$_2$O$_3$ | H$_2$O | 40 | 6 | NR[c] | 0 | 0 |

[a] Reaction conditions: Aniline (0.09 mL, 1 mmol), formic acid (0.11 mL, 3 mmol), solvent free or solvent (5 mL), aerobic condition, [b] Isolated yields, [c] No reaction was observed, [d] 10 mol% catalyst was used, [e] 50 mol% catalyst was used. [f](15-24) 5 mol% catalyst was used, [g] Particle size (37.4-39.7 nm)

conditions (Table 1) and it is shown graphically in figure 5. From this graph, it can be seen that the TON is the highest when nano-$Al_2O_3$ was used under solvent free condition at 40 °C. The table 1 also displayed the turn over frequency (TOF) which was also maximum in case of nano rod-shaped $Al_2O_3$ as catalyst under solvent free condition at 40 °C.
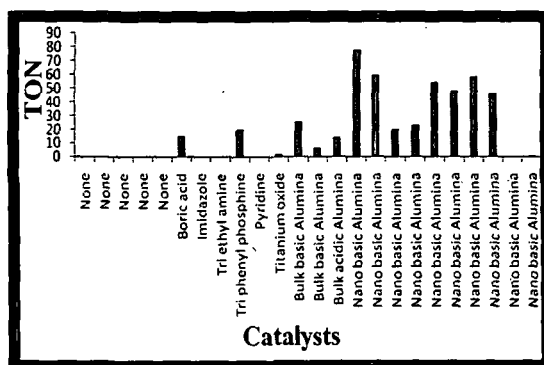


Figure 5. TON of several catalysts from Table 1

These comparative studies led us to undertake the reaction under solvent free condition because the reaction was sluggish and provided poor yield in the presence of solvent. The reactions were found to be mildly exothermic which required initial cooling using ice bath while formic acid was added to the reaction mixture containing alkyl/aryl amine and $Al_2O_3$ nano rod. Subsequently, the reaction was allowed to come to ambient temperature.

Triggered by these interesting results, we proceeded to repeat the model reaction with different quantities of formic acid and catalyst loading. As indicated in table 2, by increasing the quantity of formic acid from 1.0 to 3.0 equiv. and increasing the catalyst loading from 1 mol% to 5 mol%, the yield was clearly improved along with the reduction of reaction time. Further increasing of the catalyst loading to 15 mol% and decreasing the quantity of formic acid to 1.0 equiv. led to lower yield.

**Table 2.** Optimization of catalyst loading and amount of formic acid[a]

| Entry | Formic acid (equiv.) | Catalyst loading (mol%) | Time (min) | Yield (%)[b] |
|---|---|---|---|---|
| 1 | 1.0 | 1 | 50 | 60 |
| 2 | 1.0 | 3 | 30 | 78 |
| 2 | 1.0 | 5 | 30 | 80 |
| 3 | 1.0 | 10 | 80 | 70 |
| 4 | 1.0 | 15 | 130 | 61 |
| 5 | 2.0 | 5 | 20 | 85 |
| 5 | 3.0 | 5 | 5 | <98 |
| 6 | 3.0 | 10 | 10 | 80 |

[a] Reaction was performed at 40 °C under solvent free and aerobic condition using nano basic $Al_2O_3$, [b] Isolated yield

Realising this enhancement of $N$-formylation reaction by nano-$Al_2O_3$, our 'NOSE' chemistry approach was extended to other nanocatalysts considering the same model reaction. All these nanocatalysts were purchased from Sigma Aldrich and were used without further purifications. The results are summarised in table 3. From table 3, it is evident that using 5 mol% catalyst loading, only basic $Al_2O_3$ nano rod showed better catalytic performance at 40 °C (Table 3, entry 7). But, the other mentioned nanocatalysts provided comparatively poorer yield either at 40 °C or at 70 °C (Table 3, entries 1-6).

**Table 3.** Optimization with nanocatalysts

| Entry | Nanocatalyst[a] | Temp. (°C) | Time (min) | Yield (%)[b] |
|---|---|---|---|---|
| 1 | $\alpha$-$Fe_2O_3$ (19 nm) | 40, 70 | 180 | 44, 60 |
| 2 | $\gamma$-$Fe_2O_3$ (8 nm) | 40, 70 | 100 | 50, 35 |
| 3 | $Fe_2O_3$ (12 nm) | 40, 70 | 90 | 40, 60 |
| 4 | $Fe_3O_4$ (<50 nm) | 40, 70 | 60 | 70, 55 |
| 5 | FeO(OH) (20-40 nm) | 40, 70 | 80 | 74, 36 |
| 6 | $TiO_2$ (<80 nm) | 40, 70 | 300 | trace |
| 6 | MgO (<50 nm) | 40, 70 | 60 | 77, 68 |
| 7 | Nano basic $Al_2O_3$ (37.4-39.7 nm) | 40, 70 | 5, 60 | >98, 75 |

[a] 5 mol% of catalyst was used, [b] Isolated yield.

### 2.1.2.3 Nano-$Al_2O_3$ catalyzed N-formylation of 1° and 2° amines

With this convenient experimental reaction condition in hand, we next assessed the generality for various aromatic and aliphatic 1° and 2° amines under the standardized condition and the results are summarized in table 4. Nano-$Al_2O_3$ is found to be highly effective in formylating both electron-rich and electron-poor anilines in excellent yields (Table 4, entries 1-10). Hosseini et al., recently reported that ZnO catalyzed N-formylation of p-nitroaniline providing 77% yield.[13k] However, Choi and co-workers' procedure[14d] failed to give the product when p-nitroaniline was treated with formic acid in toluene with Dean-Stark trap. But, in our protocol using $Al_2O_3$ nano rod, the yield is comparatively enhanced (Table 4, entry 6). Phenyl hydrazine also reacted efficiently affording the product (Table 4, entry 11). The reaction of p-phenylene diamine proceeded with slower rate producing the expected N-formylation product in 85% (Table 4, entry 12) yield. But when o-phenylene diamine was reacted, it underwent cyclization to give benzimidazole[29] as the product (Table 4, entry 13). The formylation of diphenyl amine proceeded with faster rate yielding 97% (Table 4, entry 14) of the product. The N-formylation of amino acid derivatives was readily achieved using our protocol in very high yields (Table 4, entries 15 and 16), which was not found in the previous report.[30] In the course of our studies, the transformation of benzamide and acryl amide into the corresponding N-formylation products was also investigated. Both furnished slightly lower yields (70% in 3 and 4 h respectively). It might be due to the withdrawing of lone pair of electrons over N- atom towards the carbonyl group making N-atom electron deficient for the nucleophilic attack. The reaction of benzyl amine and imidazole under the present reaction condition also furnished N-formylation products in satisfactory yields (Table 4, entries 17 and 18).

**Table 4.** Nano rod-shaped basic $Al_2O_3$ catalyzed $N$-formylation of 1° and 2° amines

| Entry | Amine 1 | Time (min) | Yield (%)$^{a,b}$ |
|---|---|---|---|
| 1 | $C_6H_5NH_2$ | 5 | <98 |
| 2 | $4\text{-}ClC_6H_4NH_2$ | 10 | 93 |
| 3 | $2\text{-}ClC_6H_4NH_2$ | 10 | 90 |
| 4 | $2\text{-}NO_2C_6H_4NH_2$ | 15 | 90 |
| 5 | $3\text{-}NO_2C_6H_4NH_2$ | 10 | 93 |
| 6 | $4\text{-}NO_2C_6H_4NH_2$ | 10 | 90 |
| 7 | $4\text{-}MeOC_6H_4NH_2$ | 20 | 95 |
| 8 | $2\text{-}MeC_6H_4NH_2$ | 15 | 92 |
| 9 | $4\text{-}HOC_6H_4NH_2$ | 25 | 90 |
| 10 | $4\text{-}COOHC_6H_4NH_2$ | 30 | 92 |
| 11 | $C_6H_5NHNH_2$ | 45 | 90 |
| $12^c$ | $4\text{-}NH_2C_6H_4NH_2$ | 260 | 85 |
| $13^{c,d}$ | $2\text{-}NH_2C_6H_4NH_2$ | 300 | 85 |
| 14 | $(C_6H_5)_2NH$ | 12 | 97 |
| 15 | $NH_2CH_2COOH$ | 30 | 98 |
| 16 | $CH_3CH(Me)CH(NH_2)COOH$ | 30 | 98 |
| 17 | $C_6H_5CH_2NH_2$ | 30 | 93 |
| 18 | Imidazole | 90 | 85 |
| $19^c$ | Piperazine | 50 | 95 |
| $20^c$ | $NH_2(CH_2)_2NH_2$ | 15 | 95 |
| 21 | Pyrrolidine | 55 | 63 |
| 22 | $CH_3NH_2$ | 10 | 98 |
| 23 | $(CH_3CHCH_3)_2NH$ | 240 | 43 |
| 24 | $C_6H_5OH$ | ---- | $NR^e$ |
| 25 | $C_6H_5CH_2OH$ | ---- | $NR^e$ |
| 26 | $C_6H_5CHNOH$ | 300 | $f$ |
| 27 | $C_6H_5CHNNH_2$ | 300 | $f$ |
| 28 | $OHNH_2 \cdot HCl$ | ---- | $NR^e$ |
| 29 | $H_2NNH_2$ | ---- | $NR^e$ |

$^a$ Yields refer to the isolated pure products, $^b$ Products were characterised by IR and NMR ($^1H$ and $^{13}C$) spectroscopy, MS and also by comparing their melting points/boiling points with the authentic ones, $^c$ 6 mmol formic acid was used, $^d$ Benzimidazole was formed, $^e$ No reaction, $^f$ Mixture of unknown compounds

For aliphatic 1° and 2° amines, and diamines, the reaction showed good results towards the formation of $N$-formylation products under the present methodology (Table 4, entries 19-22). The $N$-formylation of sterically hindered diisopropyl amine could generate only 43% yield of the product even after

conducting the reaction for 6 h (Table 4, entry 23). In an attempt to transform phenol, benzyl alcohol, benzaldoxime, benzaldehyde hydrazone, hydroxyl amine and hydrazine hydrate into corresponding $N$-formylation products under our condition, the reactions failed even after stirring for 24 h and only starting material was recovered (Table 4, entries 24-29).

The transformation of anilines carrying different electron withdrawing and electron donating moieties into the corresponding $N$-formylation products proceeded smoothly under the present reaction condition that demonstrated the compatibility of those moieties towards the reaction condition. As a whole, the aryl and alkyl amines were converted into the desired formamides with high purities and yields and with no side product(s) formation.

Notably, previous report of $N$-formylation using KF-Al$_2$O$_3$,[31] is associated with some disadvantages, such as, (a) the system worked only for 2° amines and not for the 1° amines, (b) highly carcinogenic, chloroform was used, (c) KF-Al$_2$O$_3$ system was not recyclable, which is a set back from the aspect of economy and green chemistry. Similarly, Al$_2$O$_3$ supported formic acid[32] system also (a) took longer reaction time, (b) provided poor yield, and (c) loading of alumina as a support was quite higher.

### 2.1.2.4 Nano-Al$_2$O$_3$ catalyzed N-formylation of indole and its derivatives

In order to broaden the scope of using nano basic Al$_2$O$_3$ for $N$-formylation reactions, we next attempted the reaction using indole as a starting material. In this case, we could not obtain the expected product in good yield at 40 °C. Of particular significance is that by raising temperature to 70 °C, $N$-formylation product was obtained in excellent yield (Table 5, entry 1). Therefore, taking it to be standard reaction condition for indole, the generality of the reaction was

investigated for several indole derivatives and the results are presented in table 5. We were pleased to find that indoles substituted with electron donating groups at 2- and 3-positions underwent $N$-formylation reaction effectively akin to indole giving desired products in good to high yields (Table 5, entries 2 and 3). 6-bromo indole having an electron withdrawing moiety also provided high yield under the present reaction condition (Table 5, entry 4). Indole-3-acetonitrile also produced $N$-formylation product in high yield (Table 5, entry 5). Indole-3-acetic acid and Indole-3-butyric acid were also transformed into the corresponding $N$-formylation products with somewhat lower yields (Table 5, entries 6 and 7). It might be due to the steric crowding at 3-position.

**Table 5.** Nano-$Al_2O_3$ catalyzed $N$-formylation of indole and its derivatives[a]

| Entry | Substrate | Time (min) | Yield (%)[b,c] |
|-------|-----------|------------|----------------|
| 1 | Indole | 10 | 98 |
| 2 | 2-methyl indole | 45 | 92 |
| 3 | 3-methyl indole | 45 | 90 |
| 4 | 6-bromo indole | 30 | 90 |
| 5 | Indol-3-acetonitrile | 60 | 90 |
| 6 | Indol-3-acetic acid | 160 | 75 |
| 7 | Indol-3-buyric acid | 200 | 68 |

[a] Reaction condition: 1 mmol indole, 3 mmol formic acid, 70 °C, [b] Yields refer to the isolated pure products, [c] Products were characterised by IR and NMR ($^1$H and $^{13}$C) spectroscopy, MS and melting points.

## 2.1.2.5 Nano-Al₂O₃ catalyzed synthesis of acetamide

After gaining such versatile applications of nano basic $Al_2O_3$, we were curious to see what would happen if we replaced formic acid by acetic acid under the standard condition (Scheme 3).

$$R\text{---}NH_2 \xrightarrow[\text{70 °C}]{\begin{array}{c}\text{nano-}Al_2O_3\\ CH_3COOH\end{array}} R\text{---}\overset{H}{N}\text{---}COCH_3$$

$$\underset{5}{} \qquad\qquad \underset{6}{}$$

R = alkyl, aryl

Scheme 3: Synthesis of acetamide derivatives

With this notion in mind, we checked the reaction with aniline (10.7526

mmol, 1000 mg) and glacial acetic acid (10.7526 mmol, 0.61 mL) in the presence of nano-$Al_2O_3$ (5.0 mol%, 54.8 mg) and we observed the formation of acetamide with high yield without any side product (Table 6, entry 1). The experimental conditions and details are described in table 6.

In our studies, we found that both the aryl and alkyl amines underwent reaction with acetic acid in the presence of nano-$Al_2O_3$ forming acetamide derivatives efficiently. It is found that aryl amines substituted with electron withdrawing moieties produced significantly lower yield of products than those substituted with electron donating moieties (Table 6, entries 1-12).

**Table 6.** Nano-$Al_2O_3$ catalyzed synthesis of acetamide[a]

| Entry | R | Time (min) | Yield (%)[b,c] |
|-------|---|------------|----------------|
| 1 | $C_6H_5$ | 10 | 99 |
| 2 | $4\text{-}ClC_6H_4$ | 18 | 90 |
| 3 | $2\text{-}ClC_6H_4$ | 20 | 90 |
| 4 | $2\text{-}NO_2C_6H_4$ | 15 | 90 |
| 5 | $3\text{-}NO_2C_6H_4$ | 15 | 85 |
| 6 | $4\text{-}NO_2C_6H_4$ | 35 | 70 |
| 7 | $4\text{-}MeOC_6H_4$ | 20 | 95 |
| 8 | $2\text{-}MeC_6H_4$ | 15 | 92 |
| 9 | $4\text{-}HOC_6H_4$ | 45 | 80 |
| 10 | $4\text{-}COOHC_6H_4$ | 30 | 88 |
| 11 | $C_6H_5CH_2$ | 10 | 93 |
| 12 | $CH_3$ | 25 | 98 |
| 13[d] | $4\text{-}NH_2C_6H_4$ | 260 | Trace |
| 14[d] | $2\text{-}NH_2C_6H_4$ | 360 | 85[e] |

[a] Reaction condition: 1 mmol aryl/alkyl amines, 1 mmol acetic acid, 5 mol% nano basic $Al_2O_3$, 70 °C, [b] Yields refer to the isolated pure products, [c] Products were characterised by IR, NMR ($^1H$ and $^{13}C$), MS and melting points, [d] 2 mmol acetic acid was used. [e] Benzimidazole was formed

Under the present reaction condition, p-phenylene diamine showed trace yield (Table 6, entry 13) of product. However, with o-phenylene diamine, instead of furnishing amide, cyclization occurred and 2-methylbenzimidazole was obtained in good yield (Table 6, entry 14). Furthermore, the attempt to use cyano acetic acid and trifluoro acetic acid for the synthesis of expected products

failed under the present condition. Our studies revealed that the treatment of aniline with propionic acid and butanoic acid in the presence of nano basic $Al_2O_3$ produced the corresponding amides in moderate yields (45% and 50% respectively) upon heating at 70 °C for 15 h. However, dicarboxylic acids (such as adipic and malonic acid) and the long chain monocarboxylic acids (such as lauric and behenic acid) remained unreactive with aniline even after stirring at 80-100 °C for more than 24 h.

### 2.1.2.6 Plausible mechanism for the N-formylation of amines

To present a mechanistic rationale of this protocol, a plausible mechanism for N-formylation of amines catalyzed by nano basic $Al_2O_3$ is depicted in scheme 4. It has been proposed that the action of nano $Al_2O_3$ as Lewis base increases the electron density on carbon centre of formic acid, possibly via the formation of an intermediate I. This increase in electron density normally translates to enhanced nucleophilicity of the acceptor subunit. However, due to the counterintuitive consequence of the binding of a Lewis base, the electrophilic character of the acceptor in the reactive intermediate (I) is enhanced. Finally, elimination of water from (II) leads to the formation of N-formylation product.
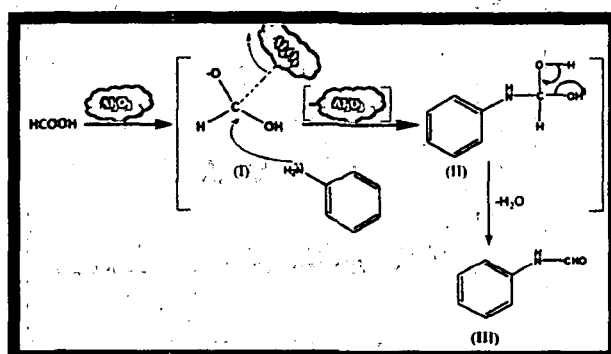


Scheme 4: Plausible mechanism for the N-formylation of amines

### 2.1.2.7 Investigation on recycling potential of nano-$Al_2O_3$

It is important to emphasize that catalyst recyclability is an essential aspect of the green chemistry. Therefore, the recycling potential of the nano-$Al_2O_3$ was also inspected during our studies of the model reaction (Scheme 2). It is our pleasure to mention that nano-$Al_2O_3$ is found to be equally effective from fresh up to the 5th cycle without significant loss of activity (Table 7). It could also be efficiently reused in the 6th cycle, however, after that the yield of the product started to decrease.

**Table 7.** Recycling potential of nano-$Al_2O_3$

| Number of cycles[a] | Fresh | Run 1 | Run 2 | Run 3 | Run 4 | Run 5 | Run 6 | Run 7 | Run 8 | Run 9 |
|---|---|---|---|---|---|---|---|---|---|---|
| Yield (%)[b] | 98 | 98 | 98 | 98 | 98 | 98 | 90 | 85 | 75 | 60 |
| Time (min.) | 5 | 5 | 5 | 5 | 5 | 5 | 25 | 40 | 60 | 180 |
| TON | 78.4 | 78.4 | 78.4 | 78.4 | 78.4 | 78.4 | 72 | 68 | 60 | 48 |

[a] Reaction condition: 3.225 mmol anilines 9.6774 mmol formic acid, 0.16129 mmol (5 mol%) nano basic $Al_2O_3$, 40 °C, [b] Yields refer to the isolated pure products.

The XRD pattern of the fresh nano-$Al_2O_3$ was compared with the recovered one after 5th cycle (figure 6). It was observed from the figure 6 that the intensity of the two highest peaks in fresh nano-$Al_2O_3$ decreased in the recycled one after 5th run and it might be due to the dislocation of the crystal planes which might
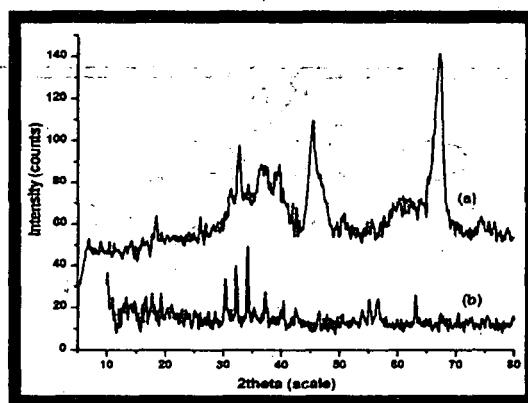


Figure 6. Comparison of XRD of (a) fresh and (b) the recovered nano-$Al_2O_3$ after 5th cycle

be the legitimate cause for the considerable lowering of yield of the *N*-formylation product in 6$^{th}$ run and so on.

SEM and TEM micrographs of recovered nano-$Al_2O_3$ after 5$^{th}$ run is shown in figure 7 (a) and 7 (b). High agglomeration of the nano-$Al_2O_3$ was observed, which might also play a role in reducing the yield and reaction rate. It is clear from table 7 that the TON of the catalyst is retained from fresh to the 5$^{th}$ cycle and then it starts declining.
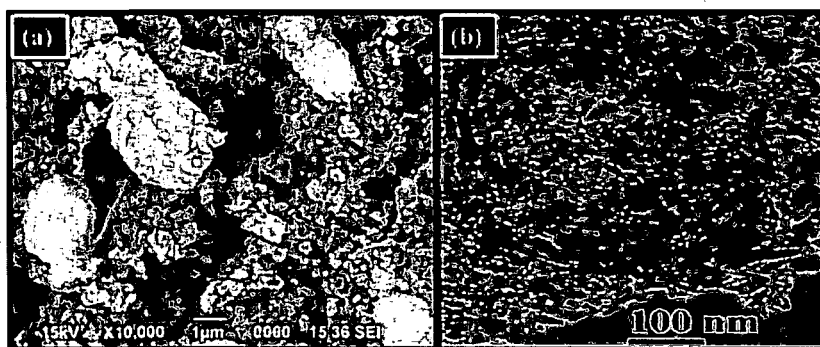


Figure 7. (a) SEM and (b) TEM image of recovered nano- $Al_2O_3$ after 5$^{th}$ cycle

The recyclability chart of catalytic potential of nano-$Al_2O_3$ is shown in figure 8. It is thus clear from figure 8 that the catalytic activity was maintained up to 5$^{th}$ run and after that it started decreasing considerably.
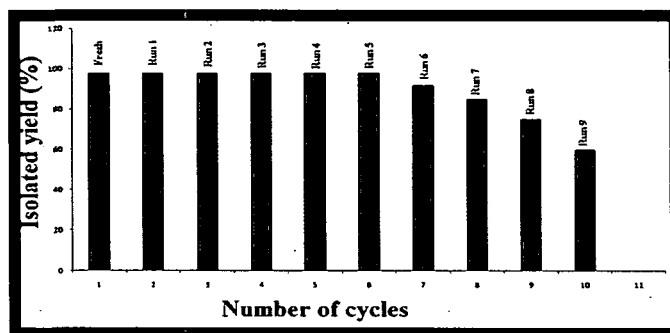


Figure 8. Catalyst recyclability chart

## 2.1.3 Conclusions

In conclusion, in a novel and convenient protocol we have shown that the *N*-formylation of amines occurs under solvent free condition using nano rod-

shaped basic $Al_2O_3$ as an efficient catalyst. The advantages offered by this method include (a) simple experimental procedure and reaction setup only at 40 °C/70 °C, (b) does not require any specialized equipment, (c) high yields of desired products, (d) proceeds under ambient conditions with diverse substrate compatibility, (e) good chemo selectivity, (f) suitable recyclability, (g) moisture stability of the catalyst, (g) cost effectiveness, and (h) environmentally benign along the line of green chemistry. The application of nano-$Al_2O_3$ in organic synthesis is not fully explored. Hence, as communicated here, we are optimistic that metal nanoparticles including $Al_2O_3$ nano rod would find increasing applications for new chemical transformations, including those which enable the synthesis of complex natural products and derivatives. Efforts are currently underway in our research group to apply 'NOSE' chemistry to the construction of other potentially valuable organic molecules like pyrimidine derivatives.

## *2.1.4 Experimental*

### *2.1.4.1 General Experimental Methods*

Rod-shaped nano $Al_2O_3$ (The average particle diameter 8.12 nm and average length 25.5 nm, $S_{BET}$ =185.6 $m^2g^{-1}$ and $\rho$ =3.98 $gcm^{-3}$, purity, 99.99%) were purchased from Sigma Aldrich and used as received. The chemicals and reagents were purchased from Sigma-Aldrich, Merck, M/S S. D. Fine Chemicals Pvt. Ltd. and Loba chemical, and used without further purification. Transmission electron microscopy was performed by (TEM) [CM12, PHILIPS] with energy dispersive spectroscopy (EDS) [OXFORD] and sample preparation facility. The surface morphology and EDX were studied using JEOL scanning electron microscope (model JSM-6390LV SEM). The XRD pattern was recorded with Rigaku X-ray diffractometer. Melting points were determined in

a Büchi 504 apparatus. IR spectra were recorded as KBr pallets in a Nicolet (Impact 410) FT-IR spectrophotometer. $^1H$ and $^{13}C$ NMR spectra were recorded in a 400 MHz NMR spectrophotometer (JEOL, JNM ECS) using tetramethylsilane (TMS) as the internal standard and coupling constants are expressed in Hertz. Elemental analyses were carried out in a Perkin–Elmer CHN analyser (2400 series II). Mass spectra were recorded with a Waters Q-TOF Premier and Aquity UPLC spectrometer. Visualization was accomplished with UV lamp or $I_2$ stain. Reactions were monitored by thin-layer chromatography using aluminium sheets with silica gel 60 $F_{254}$ (Merck).

### 2.1.4.2 General Procedure for the N-formylation of alky/aryl amines

In an oven dried round bottomed flask (50 mL) rod-shaped nano basic $Al_2O_3$ (5.0 mol%) were added and then alky/aryl amines (5.0 mmol) and formic acid (15.0 mmol) were added. The reaction was found to be mildly exothermic which required initial cooling on ice bath while formic acid was added to the reaction mixture containing alkyl/aryl amine and nano basic alumina. After that it was allowed to stir on a pre heated oil bath at 40 °C under aerobic condition till the required time (the progress of the reaction was judged by TLC). The reaction mixture was brought to room temperature after its completion and ethyl acetate (3x10 mL) was added to. Having done this, the reaction mixture was washed with water and brine, dried over $Na_2SO_4$, concentrated in a rotary evaporator and finally the crude product was charged to column chromatography (30% ethyl acetate: hexane as an eluent) for purification and wherever necessary the products were recrystallized from hot ethanol.

### 2.1.4.3 General Procedure for the N-formylation of indole

To a two neck round bottomed flask (50 mL) rod-shaped nano basic $Al_2O_3$

(5.0 mol%, 5.0 mg) were added and then indole (1.0 mmol, 117 mg) and formic acid (98%, 3.0 mmol, 0.11 mL) were added. After that it was allowed to stir on a pre heated oil bath at 70 °C till the required time (the progress of the reaction was judged by TLC). The reaction mixture was brought to room temperature after its completion and ethyl acetate (3x10 mL) was added to it. Having done this, the reaction mixture was washed with water and brine, dried over $Na_2SO_4$, concentrated in a rotary evaporator and finally the crude product was purified by column chromatography (30% ethyl acetate: hexane as an eluent).

### 2.I.4.4 General Procedure for the synthesis of acetamide

To a 50 mL round bottomed flask, nano alumina (5.0 mol%, 54.8 mg) were taken with aniline (10.7526 mmol, 1000 mg) and then acetic acid glacial (10.7526 mmol, 0.61 mL) was added to it. Then the reaction mixture was heated at 70 °C on a preheated oil bath till the product formation (monitored by TLC). The reaction mixture was brought to room temperature after its completion and ethyl acetate (3x10 mL) was added to. Having done this, the reaction mixture was washed with water and brine, dried over $Na_2SO_4$, concentrated in a rotary evaporator and finally subjected column chromatography (30% ethyl acetate: hexane as an eluent) for purification.

### 2.I.4.5 Recycling potential of rod-shaped nano alumina

After carrying out the experiment, ethyl acetate was poured and the reaction mixture was centrifuged to pellet out the nano $Al_2O_3$. The particles were then extracted by simple centrifugation (3,000-5,000 r.p.m) and washed with hot ethanol (3x10 mL) to remove all the organic impurities. Finally, it was decanted and dried in vacuo. The recovered nano alumina rod was used directly in the next cycle. The nano alumina rod was found to be effective equally up to the

fifth cycle and after that the yield of the product slightly decreased.

## 2.I.5 Several equations used

The crystallite sizes were calculated from the X-ray line broadening (figure 2) by applying full width half maximum (FWHM) of characteristic peaks (4 0 0) and (1 0 0) to the Scherrer equation.

$$D_{hkl} = \frac{0.9\lambda}{\beta \cos\theta} \quad\text{...............................................................................(i)}$$

The theoretical particle size was also calculated from the surface area assuming particles to be spherical. The equation for calculating the average particle diameter in nanometers is:

$$D_{BET} = \left(\frac{6000}{S_{BET} \times \rho}\right) \quad\text{..................................................................(ii)}$$

where $D_{BET}$ is the equivalent particle diameter in nanometers, $\rho$ is the density of the material in $gcm^{-3}$, and S is the specific surface area in $m^2 g^{-1}$ ($S_{BET} = 185.6$ $m^2 g^{-1}$ and $\rho = 3.98$ $gcm^{-3}$).

## 2.I.6 Physical and spectroscopic data of selected compounds

**N-(4-Formylamino-phenyl)-formamide (Table 4, entry 12)**
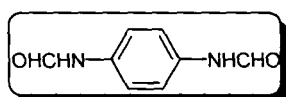


Light brown solid; $R_f = 0.30$ (30% AcOEt:hexane); mp 135-140 °C; $^1$H NMR (400 MHz, DMSO, TMS): δ 8.22 (s, 1H), 7.53 (d, $J = 2.76$, 2H, Ar-H), 7.13 (d, $J = 2.76$, 2H, Ar-H); $^{13}$C NMR (100 MHz, DMSO, TMS): δ 159.8, 134.8, 120.7, 120.1; IR (KBr pellets) $v_{max}$: 3380 cm$^{-1}$ (NH), 1710 cm$^{-1}$ (CO), 2790 cm$^{-1}$ (CH); m/z (GC-MS) 164.10 [M$^+$]; Anal. Calcd (%) for $C_8H_8N_2O_2$: C, 58.53; H, 4.91; N, 17.06. Found C, 58.12, H, 4.51, N, 16.66.

**N,N-Diphenyl-formamide (Table 4, entry 14)**
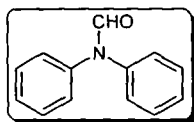
Yellow solid; $R_f$ = 0.76 (30% AcOEt:hexane); mp 68-73 °C; $^1$H NMR (400 MHz, CDCl$_3$, TMS): δ 8.69 (s, 1H), 7.16-7.7.39 (m, 10H, Ar-H); $^{13}$C NMR (100 MHz, DMSO, TMS): δ 161.8, 141.8, 139.7, 129.7, 129.2, 127.1, 126.9, 126.2, 125.1; IR (KBr pellets) $v_{max}$: 1700 cm$^{-1}$ (CO), 2820 cm$^{-1}$ (CH); m/z (GC-MS) 197.00 [M$^+$]; Anal. Calcd (%) for C$_{13}$H$_{11}$NO: C, 79.16; H, 5.62; N, 10.00. Found C, 78.75, H, 5.21, N, 9.60.

**Formylamino-acetic acid (Table 4, entry 15)**
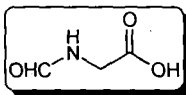


White solid; $R_f$ = 0.53 (30% AcOEt:hexane); mp 133-138 °C; $^1$H NMR (400 MHz, D$_2$O, TMS): δ 7.98 (s, 1H), 3.86 (s, 3H); $^{13}$C NMR (100 MHz, D$_2$O, TMS): δ 173.1, 164.6, 40.6; IR (KBr pellets) $v_{max}$: 3400 cm$^{-1}$ (NH), 1720 cm$^{-1}$ (CO); 1690 (CO), 2800 cm$^{-1}$ (CH); m/z (GC-MS) 103.03 [M$^+$]; Anal. Calcd (%) for C$_3$H$_5$NO$_3$: C, 34.96; H, 4.89; N, 13.59. Found C, 34.56, H, 4.48, N, 13.19.

**2-Formylamino-3-methyl-butyric acid (Table 4, entry 16)**
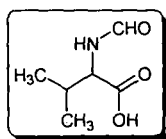


White solid; $R_f$ = 0.45 (30% AcOEt:hexane); mp 203-208 °C; $^1$H NMR (400 MHz, D$_2$O, TMS): δ 8.17 (s, 1H), 3.99 (d, $J$ = 5.04, 3H), 3.41 (d, $J$ = 5.04, 3H), 1.96-2.09 (m, 1H); $^{13}$C NMR (100 MHz, D$_2$O, TMS): δ 177.7, 169.6, 60.2, 29.7, 16.5, 16.4; IR (KBr pellets) $v_{max}$: 3410 cm$^{-1}$ (NH), 1725 cm$^{-1}$ (CO); 1685 (CO), 2810 cm$^{-1}$ (CH); m/z (GC-MS) 145.07 [M$^+$]; Anal. Calcd (%) for C$_6$H$_{11}$NO$_3$: C, 49.65; H, 7.64; N, 9.65. Found C, 49.23, H, 7.24, N, 9.25.

**Piperazine-1,4-dicarbaldehyde (Table 4, entry 21)**
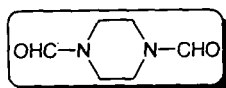


Light yellow tinted powder; $R_f = 0.43$ (30% AcOEt:hexane); mp 123-128 °C;

$^1H$ NMR (400 MHz, DMSO, TMS): δ 8.30 (s, 1H), 3.10 (s, 8H); $^{13}C$ NMR (100

MHz, DMSO, TMS): δ 167.9, 33.6; IR (KBr pellets) $v_{max}$: 1735 cm$^{-1}$ (CO);

2815 cm$^{-1}$ (CH); m/z (GC-MS) 142.03 [M$^+$]; Anal. Calcd (%) for $C_6H_{10}N_2O_2$:

C, 50.69; H, 7.09; N, 19.71. Found C, 50.29, H, 6.69, N, 19.31.

**N-(2-Formylamino-ethyl)-formamide (Table 4, entry 22)**
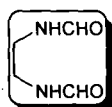


Off white powder; $R_f = 0.48$ (30% AcOEt:hexane); mp 110-115 °C; $^1H$ NMR

(400 MHz, DMSO, TMS): δ 8.14 (s, 1H), 3.42 (s, 4 H); $^{13}C$ NMR (100 MHz,

DMSO, TMS): δ 167.9, 35.5; IR (KBr pellets) $v_{max}$: 3435 cm$^{-1}$ (NH), 1715 cm$^{-1}$

(CO), 2825 cm$^{-1}$ (CH); m/z (GC-MS) 116.00 [M$^+$]; Anal. Calcd (%) for

$C_4H_8N_2O_2$ : C, 41.37; H, 6.94; N, 24.12. Found C, 40.97, H, 6.52, N, 23.71.

**N-Methyl-formamide (Table 4, entry 24)**
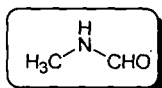


Light yellow slightly viscous liquid; $R_f = 0.84$ (30% AcOEt:hexane); $^1H$ NMR

(400 MHz, CDCl$_3$, TMS): δ 8.45 (br, 1H), 8.26 (s, 1H), 2.78 (d, $J$ = 11.44, 3H);

$^{13}C$ NMR (100 MHz, CDCl$_3$, TMS): δ 167.9, 24.6; IR (KBr pellets) $v_{max}$: 3455

cm$^{-1}$(NH), 1738 cm$^{-1}$ (CO), 2820 cm$^{-1}$ (CH); m/z (GC-MS) 59.05 [M$^+$]; Anal.

Calcd (%) for $C_2H_5NO$: C, 40.67; H, 8.53; N, 23.71. Found C, 40.23, H, 8.11,

N, 23.31.

**Indole-1-carbaldehyde (Table 5, entry 1)**
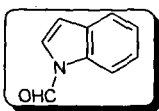
Off white powder; $R_f$ = 0.67 (30% AcOEt:hexane); mp 90-95 °C; $^1$H NMR (400 MHz, CDCl$_3$, TMS): δ 8.94 (s, 1H), 6.99-7.32 (m, 6H, Ar-H); $^{13}$C NMR (100 MHz, CDCl$_3$, TMS): δ 160.7, 137.0, 137.9, 127.9, 124.9, 124.7, 122.9, 122.7, 122.5, 120.3, 119.3, 119.2, 116.4, 111.7; IR (KBr pellets) $v_{max}$: 1727 cm$^{-1}$ (CO), 2822 cm$^{-1}$ (CH); m/z (GC-MS) 145.05 [M$^+$]; Anal. Calcd (%) for C$_9$H$_7$NO: C, 74.47; H, 4.86; N, 9.65. Found C, 74.07, H, 4.45, N, 9.25.

**(1-Formyl-1$H$-indol-3-yl)-acetonitrile (Table 5, entry 5)**
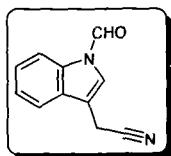


Brown oil; $R_f$ = 0.24 (30% AcOEt:hexane); $^1$H NMR (400 MHz, CDCl$_3$, TMS): δ 8.03 (s, 1H), 7.10-7.17 (m, 4H, Ar-H), 6.70 (s, 1H, Ar-H), 2.98 (s, 2H); $^{13}$C NMR (100 MHz, CDCl$_3$, TMS): δ 161.6, 136.4, 127.4, 122.0, 121.6, 119.3, 118.9, 115.4, 115.2, 111.2, 35.5; IR (KBr pellets) $v_{max}$: 1705 cm$^{-1}$ (CO), 2815 cm$^{-1}$ (CH), 2200 (CN); m/z (GC-MS) 184.06 [M$^+$]; Anal. Calcd (%) for C$_{11}$H$_8$N$_2$O: C, 71.73; H, 4.38; N, 15.21. Found C, 71.43, H, 3.98, N, 14.81.

**4-(1-Formyl-1$H$-indol-3-yl)-butyric acid (Table 5, entry 7)**
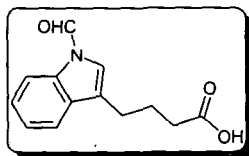


Light yellowish brown solid, $R_f$ = 0.20 (30% AcOEt:hexane); mp 111-116 °C; $^1$H NMR (400 MHz, CDCl$_3$, TMS): δ 9.3 (br, 1H), 9.0 (s, 1H), 7.11-7.59 (m, 4H, Ar-H), 6.97 (s, 1H, Ar-H), 2.81 (q, $J$ = 7.28, 2H), 2.42 (t, $J$ = 7.32, 2H), 2.06 (d, $J$ = 7.32, 2H); $^{13}$C NMR (100 MHz, CDCl$_3$, TMS): δ 180.0, 167.6,

136.4, 127.4, 122.0, 121.6, 119.3, 118.9, 115.4, 111.2, 33.6, 33.5, 25.1, 24.4; IR

(KBr pellets) $v_{max}$: 1720 cm$^{-1}$ (CO), 1685 cm$^{-1}$ (CO), 2807 cm$^{-1}$ (CH), 3420

(OH); m/z (GC-MS) 231.09 [M$^+$]; Anal. Calcd (%) for $C_{13}H_{13}NO_3$: C, 67.52; H,

5.67; N, 6.06. Found C, 67.12, H, 5.27, N, 5.66.

**N-(4-Chloro-phenyl)-acetamide (Table 6, entry 2)**
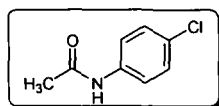


Off white crystalline needle; $R_f$ = 0.26 (30% AcOEt:hexane); mp 177-182 °C;

$^1$H NMR (400 MHz, CDCl$_3$, TMS): δ 7.45 (d, $J$ = 8.72,2H, Ar-H), 7.27 (d, $J$ =

8.72, 2H, Ar-H), 7.34 (br, 1H), 2.17 (s, 3H); $^{13}$C NMR (100 MHz, CDCl$_3$,

TMS): δ 168.4, 136.4, 129.3, 129.0, 121.1, 29.7, 24.6; IR (KBr pellets) $v_{max}$:

3406 cm$^{-1}$ (NH), 1702 cm$^{-1}$ (CO); m/z (GC-MS) 169.03 [M$^+$]; Anal. Calcd (%)

for $C_8H_8ClNO$: C, 56.65; H, 4.75; N, 8.26. Found C, 56.25, H, 4.35, N, 7.85.

**N-(4-Methoxy-phenyl)-acetamide (Table 6, entry 7)**
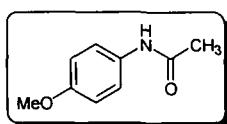


Light purple powder; $R_f$ = 0.32 (30% AcOEt:hexane); mp 134-139 °C; $^1$H NMR

(400 MHz, CDCl$_3$, TMS): δ 7.67 (br, 1H), 7.36 (d, $J$ = 7.80, 2H, Ar-H), 7.09 (d,

$J$ = 7.76, 2H), 2.29 (s, 3H), 2.12 (s, 3H); $^{13}$C NMR (100 MHz, CDCl$_3$, TMS): δ

168.5, 135.4, 133.9, 129.4, 120.1, 24.4, 20.8; IR (KBr pellets) $v_{max}$: 3378 cm$^{-1}$

(NH), 1674 cm$^{-1}$ (CO); m/z (GC-MS) 165.08 [M$^+$]; Anal. Calcd (%) for

$C_9H_{11}NO_2$: C, 65.44; H, 6.71; N, 8.48. Found C, 65.04, H, 6.31, N, 8.08.

**N-Methyl-acetamide (Table 6, entry 12)**
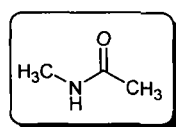
Colorless solid; $R_f$ = 0.38 (30% AcOEt:hexane); mp 134-139 °C; $^1$H NMR (400

MHz, CDCl$_3$, TMS): δ 5.52 (br, 1H), 2.82 (d, $J$ = 5.04, 3H), 2.04 (s, 3H); $^{13}$C

NMR (100 MHz, CDCl$_3$, TMS): δ 170.8, 26.4, 23.1; IR (KBr pellets) $v_{max}$: 3332

cm$^{-1}$ (NH), 1690 cm$^{-1}$ (CO); m/z (GC-MS) 73.05 [M$^+$]; Anal. Calcd (%) for

C$_3$H$_7$NO: C, 49.30; H, 9.65; N, 19.16. Found C, 48.90, H, 9.23, N, 18.86.

**References:**

1. (a) Martins, M.A.P., et al. *Chem. Rev.* **109**, 4140--4182, 2009; (b) Walsh, P.J. et al. *Chem. Rev.* **107**, 2503--2545, 2007; (c) Tanaka, K., & Toda, F. *Chem. Rev.* **100**, 1025--1074, 2000; (d) Nagendrappa, G. *Resonance* 7, 59--68, 2002.

2. (a) Shimizu, K., et al. *Chem. Eur. J.* **15**, 9977--9980, 2009; (b) Gunanathan, C., et al. *Science* **317**, 790--792, 2007; (c) Nordstrom, L.U., et al. *J. Am. Chem. Soc.* **130**, 17672--17673, 2008.

3. Jackson, A., & Meth-Cohn, O. *J. Chem. Soc., Chem. Commun.* **13**, 1319--1319, 1995.

4. Chen, B.-C., et al. *Tetrahedron Lett.* **41**, 5453--5456, 2000.

5. Kobayashi, K., et al. *Chem. Lett.* **24**, 575--576, 1995.

6. Kakehi, A., et al. *Bull. Chem. Soc. Jpn.* **68**, 3573--3580, 1995.

7. Lohray, B.B., et al. *Tetrahedron Lett.* **40**, 4855--4856, 1999.

8. Petit, G.R., et al. *J. Org. Chem.* **26**, 2563--2566, 1961.

9. (a) Kobayashi, S., & Nishio, K. *J. Org. Chem.* **59**, 6620--6628, 1994; (b) Kobayashi, S., et al. *Chem. Lett.* **25**, 407--408, 1996; (c) Iseki, K., et al. *Tetrahedron* **55**, 977--988, 1999; (d) Kizuka, H., & Elmaleh, D.R. *Nucl. Med. Biol.* **20**, 239--242, 1993; (e) Downie, I.M., et al. *Tetrahedron* **49**, 4015--4034, 1993; (g) Martinez, J., & Laur, J. *Synthesis*, 979--981, 1982.

10. Joulain, D. *Flavour Fragrance J.* **2**, 149--155, 1987.

11. Han, Y., & Cai, L. *Tetrahedron Lett.* **38**, 5423--5426, 1997.

12. (a) Waki, J., & Meienhofer, J. *J. Org. Chem.* **42**, 2019--2020, 1977; (b) Ugi, I. *Angew. Chem. Int. Ed. Engl.* **21**, 810--819, 1982; (c) Schollkopf, U. *Angew. Chem. Int. Ed. Engl.* **16**, 339--348, 1977.

13. (a) Jiang, T., et al. *Proc. Natl. Acad. Sci. U.S.A.* **104**, 60--65, 2007; (b) Das, B., et al. *Tetrahedron Lett.* **49**, 2225--2227, 2008; (c) Hill, D.R., et al. *Org. Lett.* **4**, 111--113, 2002; (d) Reddy, P.G., & Baskaran, S. *Tetrahedron Lett.* **43**, 1919--1922, 2002; (e) Reddy, P.G., et al. *Tetrahedron Lett.* **41**, 9149--9151, 2000; (f) Deutsch, J., et al. *Tetrahedron* **65**, 10365--10369, 2009; (g) Pratap, T.V., & Baskaran, S. *Tetrahedron Lett.* **42**, 1983--1985, 2001; (h) Kotha, S., et al. *Tetrahedron Lett.* **45**, 7589--7590, 2004; (i) Rahman, M., et al. *Tetrahedron Lett.* **51**, 2896--2899, 2010; (j) Saidi, O., et al. *Tetrahedron Lett.* **51**, 5804--5806, 2010; (k) Hosseini-Sarvari, M. & Sharghi, H. *J. Org. Chem.* **71**, 6652--6654, 2006.

14. (a) Kim, J.G., & Jang, D.K. *Synlett.* **14**, 2093--2096, 2010; (b) Kim, J.G., & Jang, D.K. *Synlett.* **8**, 1231--1234, 2010; (c) Chandra Shekhar, A., et al. *Tetrahedron Lett.* **50**, 7099--7101, 2009; (d) Jung, S.H., et al. *Bull. Korean Chem. Soc.* **23**, 149--150, 2002; (e) Reddy, M., et al. *Chin. J. Catal.* **31**, 518--520, 2010.

15. Grunes, J., & Somorjai, G.A. *Chem. Commun.* **18**, 2257--2260, 2003.

16. Astruc, D., et al. *Angew. Chem., Int. Ed.* **44**, 7852--7872, 2005.

17. (a) Reetz, M.T., & Lohmer, G. *Chem. Commun.* **16**, 1921--1922, 1996; (b) Reetz, M.T., & Westermann, E. *Angew. Chem., Int. Ed.* **39**, 165--168, 2000; (c) Ramarao, C., et al. *Chem. Commun.* **10**, 1132--1133, 2002.

18. (a) Gladysz, J.A. *Pure Appl. Chem.* **73**, 1319--1324, 2001; (b) Gladysz, J.A. *Chem. Rev.* **102**, 3215--3216, 2002.

19. Wang, S., et al. *Dalton Trans.* **43**, 9363--9373, 2009.

20. In analogy with MORE (microwave-induced organic reaction enhancement) chemistry, we have coined the term 'NOSE' chemistry.

21. Preedasuriyachai, P., et al. *Chem. Lett.* **39**, 1174--1176, 2010.

22. Sadjadi, S., et al. *Monatsh. Chem.* **140**, 1343--1347, 2009.

23. (a) Huang, C., et al. *Mater. Lett.* **59**, 3746--3749, 2005; (b) Zhang, Y., et al. *Chem. Phys. Lett.* **360**, 579--584, 2002.

24. Shojaie-Bahaabad, M., & Taheri-Nassaj, E. *Mater. Lett.* **62**, 3364--3366, 2008.

25. (a) Bhatnagar, A., et al. *Chem. Eng. J.* **163**, 317--323, 2010; (b) Tok, A.I.Y., et al. *J. Mater. Process. Technol.* **178**, 270--273, 2006; (c) Fletcher, D.A., et al. *J. Chem. Inf. Model.* **36**, 746--749, 1996.

26. Guo, Z., et al. *J. Mater. Chem.* **16**, 2800--2808, 2006.

27. Tsuchida, T. *Solid State Ionics* **63**, 464--470, 1993.

28. Zhareslu, M., et al. *J. Optoelectron. Adv. Mater.* **5**, 1411--1416, 2003.

29. Krishnakumar, B., & Swaminathan, M. *J. Mol. Catal. A: Chem.* **334**, 98--102, 2011.

30. Lei, M., et al. *Tetrahedron Lett.* **51**, 4186--4188, 2010.

31. Miharaa, M., et al. *Synthesis* **15**, 2317--2320, 2003.

32. Desai, B., et al. *Tetrahedron Lett.* **46**, 955--957, 2005.

# Section II

# Nano rod-shaped basic $Al_2O_3$ catalyzed *N,N*-diformylation of

# bis-uracil Derivatives: A greener 'NOSE' approach
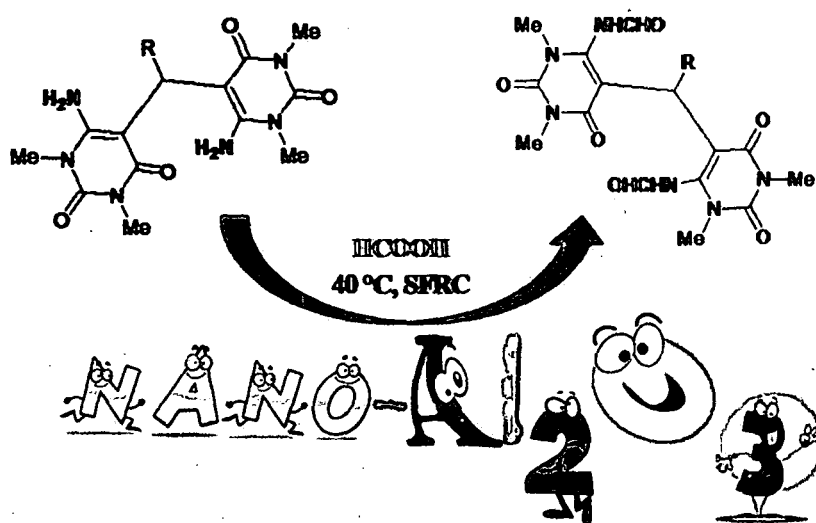
# Section II

## Nano rod-shaped basic $Al_2O_3$ catalyzed *N,N*-diformylation of bis-uracil Derivatives: A greener 'NOSE' approach

### *2.II.1 Introduction*

The exercise of metal/metal oxide nanoparticles as a frontier between the homogeneous and heterogeneous catalysis[1] in organic synthesis has invoked tremendous interests[2] in the recent times. The interesting features inherited with these small particle sizes are their large surface area along with more edges and corners, distinct electronic, optical, magnetic, thermal and chemical properties.[3] The crucial role of nanoparticles in organic transformations is their excellent catalytic activity, straightforward recoverability, better selectivity, criteria of evolution and their versatile role in green chemistry.[4] Thus, the domain of metal nanoparticle catalysis[5] should offer opportunities for mining new chemical reactions[6] which include the synthesis of biologically important and synthetically challenging natural products. In the context of green chemistry,[7] organic synthesis in solvent free reaction condition[8] has occupied a significant position in the recent years since solvent free reaction condition involves the best reaction medium with 'no medium'.[9]

One of the key motifs present in the biopolymer RNA[10] is uracil, a nucleobase of the pyrimidine family which participates in various functions in our life processes.[11] Uracil derivatives also have several potent medicinal properties such as bronchodilators and anticancer,[12] antiallergic,[13] antiviral,[14] antihypertensive and adenosine receptor antagonists.[15] Recently, our research group reported a greener protocol for the synthesis of bis-uracil derivatives.[16] Bis-uracil and their analogues have also been isolated from marine sea hare *Dolabella auricularia*.[17]

**Page | 63**

Some of the *N*-substituted bis-uracil analogues have been screened for bioactivities against several diseases.[18]

To explore the possible applications of the metal/metal oxide nanoparticles in organic synthesis, we have been focusing on the advancement of a protocol termed "**NOSE**" (Nanoparticles-catalyzed Organic Synthesis Enhancement)[19] chemistry in our laboratory. To the best of our knowledge, there has been no report on nano rod shaped $Al_2O_3$ catalyzed *N,N*-diformylation of bis-uracil derivatives. Recently, we reported *N*-formylation of amines catalyzed by nano-$Al_2O_3$ under solvent free reaction condition.[19a] This work inspired us to focus on nano-$Al_2O_3$ catalysis for the *N,N*-diformylation of bis-uracil analogous. Therefore, in this report we wish to account for the same (scheme 1).
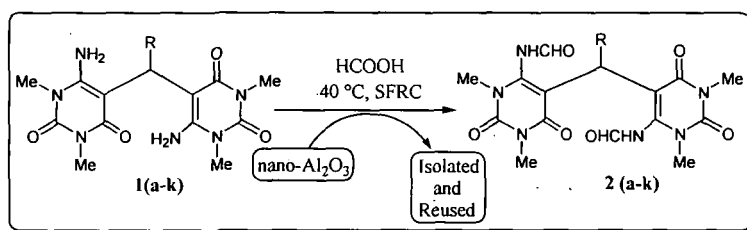


Scheme 1. *N,N*-diformylation of bis-uracil derivatives **1(a-k)**

Nano-$Al_2O_3$ draws our attention due to its crystalline size and shape, abrasive and insulating properties, less toxicity, large surface area, basic surface characteristics, high resistant towards bases and acids and excellent wear resistance.[20]

### 2.II.2. Results and Discussion

#### 2.II.2.1 Optimization of the reaction condition for N,N-diformylation reaction

With the previously reported catalyst characterizations in hand,[19(a)] to begin with, reaction of 6,6'-Diamino-1,1',3,3'-tetramethyl-5,5'-(benzylidene) bis[pyrimidine-2,4($1H$, $3H$)-dione][16] (**1a**, 1 mmol) with formic acid (6 mmol) was chosen as the model reaction (Scheme 2). The optimization of the various

**Page | 64**

parameters of this reaction is elaborated in Table 1. Initially, the reaction was carried out without using catalyst under solvent free reaction condition at 40 °C and 80 °C which did not yield any product (Table 1, entries 1 and 2).

**Table 1.** Optimization of the reaction conditions for the $N,N$-diformylation of **1a**
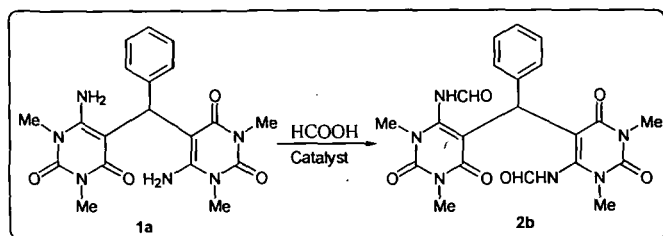


Scheme 2. Optimization of reaction condition

| Entry | Catalyst | Solvent | Temp. (°C) | Time (h) | Yield (%)[b] |
|-------|----------|---------|------------|----------|--------------|
| 1 | None | Solvent free | 40 | 9 | NR[c] |
| 2 | None | Solvent free | 80 | 9 | NR[c] |
| 3 | None | $H_2O$ | 40 | 12 | NR[c] |
| 4 | None | $CH_3CN$ | 40 | 12 | NR[c] |
| 5 | None | MeOH | 40 | 12 | NR[c] |
| 6 | None | EtOH | 40 | 12 | NR[c] |
| 7 | None | THF | 40 | 12 | NR[c] |
| 8 | None | Toluene | 40 | 12 | NR[c] |
| 9 | None | DMSO | 40 | 12 | NR[c] |
| 10 | None | Xylene | 40 | 12 | NR[c] |
| 11 | None | DMF | 40 | 12 | NR[c] |
| 12[d] | $K_2CO_3$ | Solvent free | 40 | 12 | NR[c] |
| 13[d] | $PPh_3$ | Solvent free | 40 | 12 | NR[c] |
| 14[d] | Imidazole | Solvent free | 40 | 10 | Trace |
| 15[d] | Nano-$Al_2O_3$[i] | Solvent free | 40 | 45 min | 70 |
| 16[d] | Nano-MgO[j] | Solvent free | 40 | 3 | 34 |
| 17[d] | Nano-$Fe_2O_3$[k] | Solvent free | 40 | 5 | 12 |
| 18[d] | Nano-$TiO_2$[l] | Solvent free | 40 | 4 | 8 |
| 19[d] | Nano-$Al_2O_3$[i] | Solvent free | 80 | 2 | 43 |
| 20[e] | Nano-$Al_2O_3$[i] | Solvent free | 40 | 3 | 25 |
| 21[f] | Nano-$Al_2O_3$[i] | Solvent free | 40 | 4 | 17 |
| 22[g] | Nano-$Al_2O_3$[i] | Solvent free | 40 | 6 | 8 |

[a] Reaction condition: Bis-uracil **1a** (1 mmol, 0.454 g), formic acid (6 mmol, 0.66 mL), solvent (5 mL). [b] Isolated yields. [c] No reaction was observed. [d] 7 mol% catalyst was used. [e] 5 mol% catalyst was used. [f] 3 mol% catalyst was used. [g] 10 mol% catalyst was used. [h] 1 mol% catalyst was used. [i] Particles size (17.4-16.4 nm). [j] Particles size (<50 nm). [k] Particles size (12 nm). [l] Particles size (<80 nm).

Various solvents were also tested under the mentioned condition but all failed

(Table 1, entries 3-11) to provide any product. These negative results suggested

us to look for an effective catalyst in the present study. Next, various Lewis acid-base catalysts (Table 1, entries 12-14) along with the nanocatalysts (Table 1, entries 15-18) were surveyed to observe the influence on rate and yield of $N,N$-diformylation of 1a which were not fruitful. Interestingly, nano rod shaped basic $Al_2O_3$ stood out as a choice of catalyst at 7 mol% loading (Table 1, entry 15) under solvent free reaction condition at 40 °C. During the course of our experiment, we observed that at higher temperature (Table 1, entry 19) and at lower/higher catalyst loading the yield of the products were poor (Table 1, entries 20-22). Thus, the yield of $N,N$-diformylation product of bis-uracil derivatives is highly dependent upon the temperature and catalyst loading.

### 2.II.2.2 Nano-Al$_2$O$_3$ catalyzed N,N-diformylation of bis-uracil derivatives

With this supportive optimized reaction condition in hand, a series of bis-uracil derivatives (entries 1-11) bearing different aliphatic, aromatic and heterocyclic moieties were examined to explore the scope and limitations of this reaction and the outcomes are presented in table 2.

**Table 2.** Nano-Al$_2$O$_3$ catalyzed $N,N$-diformylation of bis-uracil derivatives

| Entry | 'R' in 1 | Product 2 | Time (min) | Yield (%)$^{a,b}$ |
|-------|----------|-----------|------------|-------------------|
| 1 | $C_6H_5$ (1a) | 2a | 45 | 70 |
| 2 | $p$-OMeC$_6$H$_4$ (1b) | 2b | 60 | 68 |
| 3 | $p$-ClC$_6$H$_4$ (1c) | 2c | 75 | 58 |
| 4 | $p$-OHC$_6$H$_4$ (1d) | 2d | 90 | 55 |
| 5 | $p$-NO$_2$C$_6$H$_4$ (1e) | 2e | 90 | 52 |
| 6 | $p$-MeC$_6$H$_4$ (1f) | 2f | 70 | 60 |
| 7 | $o$-OHC$_6$H$_4$ (1g) | 2g | 100 | 52 |
| 8 | $m$-NO$_2$C$_6$H$_4$ (1h) | 2h | 90 | 65 |
| 9 | CH$_3$ (1i) | 2i | 100 | 52 |
| 10 | CH$_3$(CH$_2$)$_3$ (1j) | 2j | 120 | 44 |
| 11 | 2-furyl (1k) | 2k | 150 | 57 |

$^a$ 6 mmol of formic acid was used. $^b$ Isolated yield. $^c$ Products were characterized by IR and NMR ($^1$H and $^{13}$C) spectroscopy, MS and also by melting points.

It is clear from table 2 that bis-uracil derivatives carrying both electron donating and electron withdrawing groups in benzene ring underwent $N,N$-

diformylation reaction smoothly producing good yields (Table 2, entries 1-8). However, longer reaction times were required for bis-uracil derivatives substituted with furan and alkyl groups (Table 2, entries 9-11). It is worth mentioning that 6-amino-1,3-dimethyluracil when treated with formic acid under the current condition gave $N,N$-diformylation product in lower yield (26%, 9 h). The reactions were found to be clean and no side products were formed.

### 2.II.2.3 Investigation on recycling potential of nano-$Al_2O_3$

To test the recyclability (vide scheme 2) of nano-$Al_2O_3$, it was separated from the reaction mixture by adding ethyl acetate (10 mL), centrifuged at 3,000 r.p.m. to pellet out the catalyst. The separated particles were washed with hot ethanol (3x10 mL) to remove the organic impurities, decanted, dried in an oven at 80 °C for 6 h and reused for further reactions. The efficiency of the catalyst was found to be unaffected up to 4th run and after that its action started decreasing as shown in table 3. The TONs were also retained from fresh up to the 5$^{th}$ cycle and after that it decreased considerably.

**Table 3.** Recycling study of nano-$Al_2O_3$

| Entry | No. of cycles | Time (min) | Yield (%)$^b$ | TONs |
|-------|---------------|------------|---------------|------|
| 1 | Fresh | 45 | 70 | 88 |
| 2 | 1$^{st}$ run | 45 | 70 | 88 |
| 3 | 2$^{nd}$ run | 45 | 70 | 88 |
| 4 | 3$^{rd}$ run | 45 | 70 | 88 |
| 5 | 4$^{th}$ run | 45 | 70 | 88 |
| 6 | 5$^{th}$ run | 60 | 58 | 76 |
| 7 | 6$^{th}$ run | 180 | 40 | 70 |

$^a$ Reaction conditions: 2 mmol of **2b**, 12 mmol formic acid, 7 mol% nano basic $Al_2O_3$, 40 °C. $^b$ Yields refer to the isolated pure products.

The recovered catalyst was also investigated through powder XRD and it was compared with the fresh nano-$Al_2O_3$ [figure 1(a)]. In the powder XRD of the recovered catalyst after 6$^{th}$ run (figure 1), the intensity of the peaks (4 0 0) and (1 0 0) weakened and became broad. It might be due to the blockage of the pores of

the catalyst which caused a decrease in effective active sites and also by the

dislocation of the crystal planes after each run which in turn decreased the yield.

The SEM micrograph of the fresh nano-$Al_2O_3$ previously reported by us[19a] was

also compared with the recycled one [figure 1 (b)] under the present study. As

indicated in figure 2, the recycled nano-$Al_2O_3$ revealed the aggregation of the

particles [also see the TEM image of recycled nano-$Al_2O_3$, figure 7 (b) in chapter

2, section I, page no 50] responsible for reducing its surface area and hence,

deactivated the catalyst after $4^{th}$ run which caused the lower yield of product.
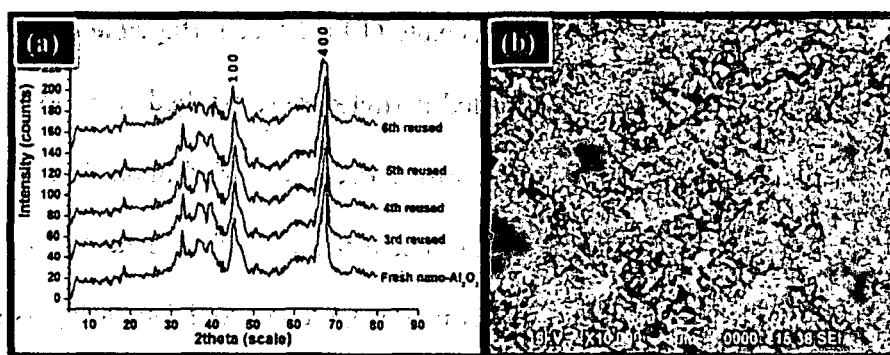


Figure 1. (a) Comparison of XRD of fresh nano-$Al_2O_3$ with the recovered ones

and (b) SEM image of recovered nano-$Al_2O_3$ after $4^{th}$ run

## 2.II.3 Conclusions

In conclusion, we have demonstrated a novel method for the N,N-

diformylation of bis-uracil derivatives in good yield under solvent free reaction

condition at 40 °C catalyzed by recyclable nano-$Al_2O_3$ rods. Nano-$Al_2O_3$

catalyzed organic transformations are less explored. We believe that this work

would find wide applications for new chemical transformations, including those

which enable the synthesis of complex natural products and derivatives.

## 2.II.4 Experimental

### 2.II.4.1 General Experimental Methods

Rod shaped nano-$Al_2O_3$ (The average particle diameter 8.12 nm and average

length 25.5 nm, $S_{BET}$ =185.6 $m^2g^{-1}$ and $\rho$ =3.98 $gcm^{-3}$, purity, 99.99%) were purchased from Sigma Aldrich and used as received. The chemicals and reagents were purchased from Sigma-Aldrich, Merck, M/S S. D. Fine Chemicals Pvt. Ltd. and Loba chemical, and used without further purification. The XRD pattern was recorded with Rigaku X-ray diffractometer. Melting points were determined in a Büchi 504 apparatus. IR spectra were recorded as KBr pallets in a Nicolet (Impact 410) FT-IR spectrophotometer. $^1H$ and $^{13}C$ NMR spectra were recorded in a 400 MHz NMR spectrophotometer (JEOL, JNM ECS) using tetramethylsilane (TMS) as the internal standard and coupling constants are expressed in Hertz. Elemental analyses were carried out in a Perkin–Elmer CHN analyser (2400 series II). Mass spectra were recorded with a Waters Q-TOF Premier and Aquity UPLC spectrometer. Visualization was accomplished with UV lamp or $I_2$ stain. Reactions were monitored by thin-layer chromatography using aluminium sheets with silica gel 60 $F_{254}$ (Merck).

### 2.II.4.2 General procedure for N,N-diformylation of bis-uracil derivatives

In a two neck round bottom flask (50 mL), nano rod shaped basic $Al_2O_3$ (7.0 mol%, 7.12 mg) were taken and then 1g (1.0 mmol, 414 mg) and formic acid (98%, 6.0 mmol, 0.23 mL) were added. After that it was allowed to stir on a pre heated oil bath at 40 °C till the required time (the progress of the reaction was judged by TLC). The reaction mixture was brought to room temperature after its completion and ethyl acetate (3x10 mL) was added and then centrifuged (3,000 r.p.m) to recover the nano catalyst. Having done this, the reaction mixture was washed with water and brine, dried over anhydrous $Na_2SO_4$, concentrated in a rotary evaporator and finally the crude product was purified by column chromatography (30% ethyl acetate: hexane as an eluent). The recovered catalyst

was washed with hot ethanol (3x10 mL) to remove the organic impurities, decanted, dried in an oven at 80 °C for 6 h and reused for evaluating the performances in the next run in the reaction as shown in scheme 2.

## 2.II.5 Physical and Spectroscopic Data of compounds

**6,6'-Diformamide-1,1',3,3'-tetramethyl-5,5'-(benzylidene)bis[pyrimidine-2,4(1H,3H)-dione] (Table 2, entry 1)**
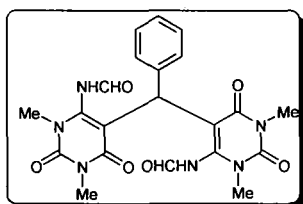


Pale yellow powder; $R_f$ = 0.42 (30% AcOEt:hexane); mp 252-254 °C; $^1$H NMR (400 MHz, CDCl₃, TMS): δ 3.19 (s, 3H, NCH₃), 3.31 (s, 3H, NCH₃), 3.47 (s, 3H, NCH₃), 3.54 (s, 3H, NCH₃), 4.95 (s, 1H, CH), 6.56 (br, s, 2H), 7.11-7.27 (m, 5 H, Ar-H), 8.67 (s, 2H, CHO); $^{13}$C NMR (100 MHz, CDCl₃, TMS): δ 27.8, 28.1, 28.8, 28.9, 35.4, 87.1, 88.3, 125.2, 126.3, 127.2, 137.5, 150.4, 153.1, 154.2, 162.8, 164.2, 170.1, 170.8; IR (KBr pellets) $v_{max}$ (cm$^{-1}$): 3450 (NH), 2830 (CH), 2810 (CH), 1710 (CO), 1680 (CO); m/z 454.16 [M$^+$]; Anal. Calcd (%) for C₂₁H₂₂N₆O₇: C, 55.50; H, 4.88; N, 18.49. Found C, 55.27, H, 4.50, N, 18.36.

**6,6'-Diformamide-1,1',3,3'-tetramethyl-5,5'-(4-methoxybenzylidene)bis-[pyrimidine-2,4 (1H,3H)-dione] (Table 2, entry 2)**
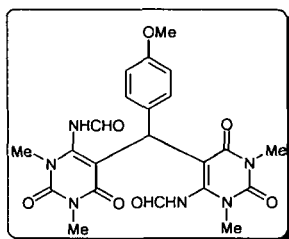


White solid; $R_f$ = 0.34 (30% AcOEt:hexane); mp 243–245 °C; $^1$H NMR (400 MHz, CDCl₃, TMS): δ 3.21 (s, 3H, NCH₃), 3.32 (s, 3H, NCH₃), 3.39 (s, 3H,

NCH₃), 3.43 (s, 3H, NCH₃), 3.49 (s, 3H, OCH₃), 4.48 (s, 1H, CH), 6.51 (br, s,

2H, NH), 7.18 (d, $J$ = 8.12 Hz, 2H, Ar-H), 7.21 (d, $J$ = 8.12 Hz, 2H, ArH), 9.51

(s, 1H, CHO), 9.13 (s, 1H, CHO); ¹³C NMR (100 MHz, CDCl₃, TMS): δ 29.1,

29.4, 29.6, 29.8, 32.8, 58.6, 87.1, 88.7, 114.2, 128.1, 130.3, 152.1, 154.6, 157.7,

158.7, 164.5, 166.1, 170.7; IR (KBr pellets) $v_{max}$ (cm⁻¹): 3394 (NH), 2953 (CH),

2822 (CH), 1725 (CO), 1679 (CO); m/z 484.17 [M⁺]; Anal. Calcd (%) for

C₂₂H₂₄N₆O₇: C, 54.54; H, 4.99; N, 17.35. Found C, 54.28, H, 4.71, N, 17.13.

**6,6'-Diformamide-1,1',3,3'-tetramethyl-5,5'-(4-chlorobenzylidene)bis-**

**[pyrimidine-2,4(1$H$, 3$H$)-dione] (Table 2, entry 3)**
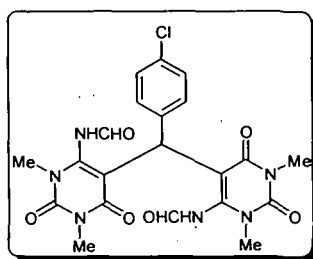


Off white solid; R$_f$ = 0.38 (30% AcOEt:hexane); mp 185-188 °C; ¹H NMR (400

MHz, DMSO, TMS): δ 3.25 (s, 3H, NCH₃), 3.31 (s, 3H, NCH₃), 3.48 (s, 6H,

NCH₃), 5.68 (s, 1H, CH), 7.48-7.68 (m, 4H, Ar-H), 8.35 (s, 2H, CHO); ¹³C NMR

(100 MHz, DMSO, TMS): δ 29.1, 29.3, 29.5, 29.7, 36.5, 88.3, 88.7, 127.8, 128.3,

131.5, 136.7, 151.2, 153.8, 155.4, 164.8, 165.7, 171.1; IR (KBr pellets) $v_{max}$ (cm⁻

¹): 3376 (NH), 2948 (CH), 2834 (CH), 1732 (CO), 1687 (CO); m/z 488.12 [M⁺];

Anal. Calcd (%) for C₂₁H₂₁ClN₆O₆: C, 51.59; H, 4.33; N, 17.19. Found C, 51.27,

H, 4.08, N, 16.87.

**6,6'-Diformamide-1,1',3,3'-tetramethyl-5,5'-(4-hydroxybenzylidene)bis-**

**[pyrimidine-2,4(1$H$, 3$H$)-dione] (Table 2, entry 4)**
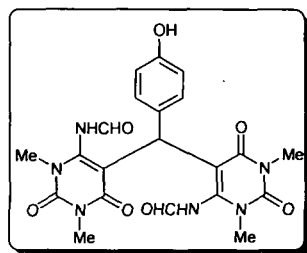
Light brown solid; $R_f$ = 0.24 (30% AcOEt:hexane); mp 217-218 °C; $^1H$ NMR

(400 MHz, DMSO, TMS): δ 2.97 (s, 3H, NCH₃), 3.03 (s, 3H, NCH₃), 3.07 (s,

3H, NCH₃), 3.22 (s, 3H, NCH₃), 4.88 (s, 1H, CH), 6.72 (br, 2H, NH), 7.81-8.02

(m, 4H, Ar-H), 8.87 (d, $J$ = 7.52 Hz, 2H, CHO) 10.21 (br, 1H, OH); $^{13}C$ NMR

(100 MHz, DMSO, TMS): δ 29.4, 29.6,34.8,114.7, 127.3, 127.7, 129.6, 151.7,

155.6, 168.9, 169.2, 170.6; IR (KBr pellets) $v_{max}$ (cm⁻¹): 3398 (NH), 1705 (CO),

2957 (CH), 2827 (CH), 1655 (CO); m/z 470.15 [M⁺]; Anal. Calcd (%) for

$C_{21}H_{22}N_6O_7$: C, 53.62; H, 4.71; N, 17.86. Found C, 53.28, H, 4.42, N, 17.54.

**6,6'-Diformamide-1,1',3,3'-tetramethyl-5,5'-(4-nitrobenzylidene)bis-**

**[pyrimidine-2,4(1$H$, 3$H$)-dione] (Table 2, entry 5)**
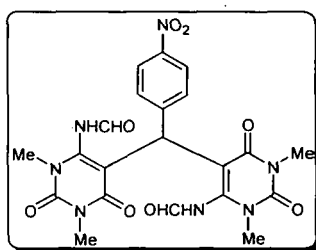


Light brown solid; $R_f$ = 0.29 (30% AcOEt:hexane); mp 205-208 °C; $^1H$ NMR

(400 MHz, CDCl₃, TMS): δ 3.33 (s, 3H, NCH₃), 3.41 (s, 3H, NCH₃), 3.43 (s, 3H,

NCH₃), 3.51 (s, 3H, NCH₃), 6.61 (br, s, 2H, NH), 8.02-8.31 (m, 4H, Ar-H), 9.45

(s, 2H, CHO); $^{13}C$ NMR (100 MHz, CDCl₃, TMS): δ 28.4, 29.5, 29.8, 30.2, 36.7,

87.6, 88.7, 122.8, 128.3, 141.5, 149.7, 152.1, 154.3, 156.3, 165.1, 167.2, 173.3,

173.7; IR (KBr pellets) $v_{max}$ (cm⁻¹): 3433 (NH), 2933 (CH), 2818 (CH), 1728

(CO), 1678 (CO); m/z 499.15 [M⁺]; Anal. Calcd (%) for $C_{21}H_{21}N_7O_8$: C, 50.50; H, 4.24; N, 19.63. Found C, 50.16, H, 3.91, N, 19.35.

**6,6'-Diformamide-1,1',3,3'-tetramethyl-5,5'-(4-methylbenzylidene)bis-[pyrimidine-2,4(1*H*,3*H*)-dione] (Table 2, entry 6)**
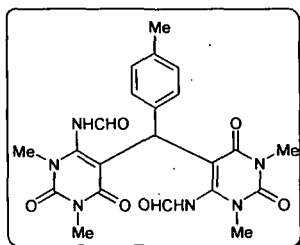


White solid; $R_f$ = 0.56 (30% AcOEt:hexane); mp 239-242 °C; ¹H NMR (400 MHz, CDCl₃, TMS): δ 2.23 (s, 3H, CH₃), 2.38 (s, 3H, NCH₃), 2.77 (s, 3H, NCH₃), 2.94 (s, 3H, NCH₃), 3.19 (s, 3H, NCH₃), 5.19 (s, 1H, CH), 6.39 (br, s, 2H, NH), 7.34 (d, 2H, $J$ = 8.35 Hz, Ar-H), 7.57 (d, 2H, $J$ = 8.35 Hz, Ar-H), 8.87 (s, 2H, CHO); ¹³C NMR (100 MHz, CDCl₃, TMS): δ 19.8, 27.3, 27.7, 29.1, 29.6, 35.8, 87.7, 88.5, 127.4, 129.0, 135.5, 136.8, 151.1, 153.4, 154.8, 162.8, 163.6, 169.1, 169.8; IR (KBr pellets) $v_{max}$ (cm⁻¹): 3441 (NH), 2928 (CH), 2870 (CH), 1713 (CO), 1632 (CO); m/z 468.18 [M⁺]; Anal. Calcd (%) for $C_{22}H_{24}N_6O_6$: C, 56.40; H, 5.16; N, 17.94. Found C, 56.13, H, 4.93, N, 17.73.

**6,6'-Diformamide-1,1',3,3'-tetramethyl-5,5'-(2-hydroxybenzylidene)bis-[pyrimidine-2,4(1*H*,3*H*)-dione] (Table 2, entry 7)**
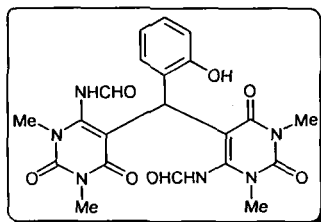


Off white powder; $R_f$ = 0.35 (30% AcOEt:hexane); mp 210-214 °C; ¹H NMR (400 MHz, CDCl₃, TMS): δ 3.11 (s, 3H, NCH₃), 3.35 (s, 3H, NCH₃), 3.50 (s, 3H,

NCH₃), 3.59 (s, 3H, NCH₃), 4.85 (s, 1H, CH), 5.77 (s, 1H, OH), 6.39 (br, s, 2H,

NH), 7.10-7.26 (m, 5H, Ar-H), 8.59 (s, 2H, CHO); $^{13}$C NMR (100 MHz, CDCl₃,

TMS): δ 27.6, 28.3, 29.3, 29.4, 30.1, 87.9, 93.4, 115.7, 123.5, 125.3, 128.0,

128.4, 150.5, 150.6, 151.4, 151.6, 154.4, 161.3, 164.2, 168.9; IR (KBr pellets)

$v_{max}$ (cm⁻¹): 3430 (NH), 2830 (CH), 2812 (CH), 1710 (CO), 1680 (CO); m/z

470.15 [M⁺]; Anal. Calcd (%) for $C_{21}H_{22}N_6O_7$: C, 53.62; H, 4.71; N, 17.86.

Found C, 53.31, H, 4.40, N, 17.52.

**6,6'-Diformamide-1,1',3,3'-tetramethyl-5,5'-(3-nitrobenzylidene)bis-**

**[pyrimidine-2,4(1H, 3H)-dione] (Table 2, entry 8)**
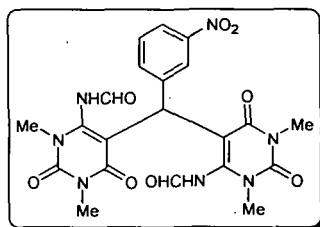


Pale brown solid; $R_f$ = 0.30 (30% AcOEt:hexane); mp 197-198 °C; $^{1}$H NMR (400

MHz, CDCl₃, TMS): δ 3.37 (s, 3H, NCH₃), 3.50 (s, 3H, NCH₃), 3.52 (s, 3H,

NCH₃), 3.55 (s, 3H, NCH₃), 4.88 (s, 1H, CH), 6.68 (br, s, 2H, NH), 7.37-7.83 (m,

4H, Ar-H), 8.35 (s, 2H, CHO); $^{13}$C NMR (100 MHz, CDCl₃, TMS): δ 28.8, 29.3,

29.8, 30.2, 35.6, 85.8, 87.3, 121.5, 122.3, 129.3, 134.2, 142.5, 148.8, 152.3,

154.3, 154.7, 164.7, 166.3, 169.3, 170.1; IR (KBr pellets) $v_{max}$ (cm⁻¹): 3414 (NH),

3095 (CH), 2902 (CH), 1713 (CO), 1696 (CO); m/z 499.15 [M⁺]; Anal. Calcd

(%) for $C_{21}H_{21}N_7O_8$: C, 50.50; H, 4.24; N, 19.63. Found C 50.28, H, 4.02, N,

19.38.

**6,6'-Diformamide-1,1',3,3'-tetramethyl-5,5'-(ethylidene)bis-[pyrimidine-**

**2,4(1H, 3H)-dione] (Table 2, entry 9)**
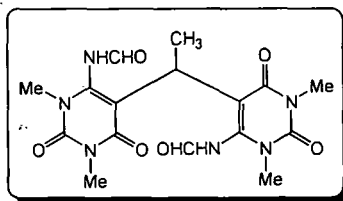
White solid; R$_f$ = 0.64 (30% AcOEt:hexane); mp 288-290 °C; $^1$H NMR (400

MHz, CDCl$_3$, TMS): δ 1.28 (d, $J$ = 6.83 Hz, 3H, CH$_3$), 2.71 (s, 3H, NCH$_3$), 2.86

(s, 3H, NCH$_3$), 2.88 (s, 3H, NCH$_3$), 2.92 (s, 3H, NCH$_3$), 3.77-4.13 (m, 1H, CH),

6.01 (br, s, 2H, NH), 8.15 (s, 2H, CHO); $^{13}$C NMR (100 MHz, CDCl$_3$, TMS): δ

12.4, 21.3, 28.1, 28.3, 29.3, 29.9, 88.5, 89.1, 148.0, 149.2, 152.2, 159.6, 161.3,

165.3, 167.6; IR (KBr pellets) ν$_{max}$ (cm$^{-1}$): 3409 (NH), 3041 (CH), 2989 (CH),

1705 (CO), 1688 (CO); m/z 392.14 [M$^+$]; Anal. Calcd (%) for C$_{16}$H$_{20}$N$_6$O$_6$: C,

48.98; H, 5.14; N, 21.42. Found C 48.63, H, 4.82, N, 21.08.

**6,6'-Diformamide-1,1',3,3'-tetramethyl-5,5'-(pentylidene)bis-[pyrimidine-
2,4(1$H$, 3$H$)-dione) (Table 2, entry 10)**
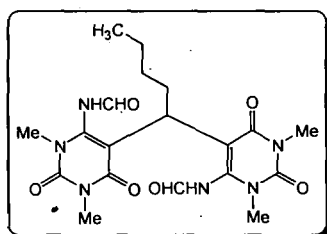


White solid; R$_f$ = 0.68 (30% AcOEt:hexane); mp 108-111 °C; $^1$H NMR (400

MHz, CDCl$_3$, TMS): δ 0.98-1.02 (m, 3H, CH$_3$), 1.38-1.42 (m, 4H, CH$_2$CH$_2$),

2.38-2.51 (m, 2H, CH$_2$), 3.37 (s, 3H, NCH$_3$), 3.42 (s, 3H, NCH$_3$), 3.47 (s, 3H,

NCH$_3$), 3.49 (s, 3H, NCH$_3$), 4.25-4.31 (m, 1H, CH), 6.69 (br, 2H, NH), 8.82 (s,

2H, CHO); $^{13}$C NMR (100 MHz, CDCl$_3$, TMS): δ 14.1, 22.7, 26.5, 27.1, 28.8,

29.2, 29.8, 30.8, 35.2, 88.7, 89.6, 151.2, 151.8, 152.3, 154.4, 164.4, 165.6, 170.7,

171.0; ν$_{max}$ (cm$^{-1}$): 3455 (NH), 3012 (CH), 2882 (CH), 1722 (CO), 1693 (CO);

m/z 434.19 [M$^+$]; Anal. Calcd (%) for $C_{19}H_{26}N_6O_6$: C, 52.53; H, 6.03; N, 19.34. Found C 52.24, H, 5.82, N, 19.11.

**6,6'-Diformamide-1,1',3,3'-tetramethyl-5,5'-(2-furyl)bis-[pyrimidine-2,4 (1*H*,3*H*)-dione] (Table 2, entry 11)**
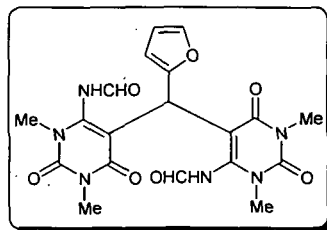


Yellow viscous oil; $R_f$ = 0.12 (30% AcOEt:hexane); $^1$H NMR (400 MHz, CDCl$_3$, TMS): δ 2.71 (s, 3H, NCH$_3$), 2.75 (s, 3H, NCH$_3$), 2.87 (s, 3H, NCH$_3$), 2.91 (s, 3H, NCH$_3$), 5.11 (s, 1H, CH), 5.88 (d, 1H, Furan-H), 6.18 (d, 1H, Furan-H), 6.27 (d, 1H, Furan-H), 6.55 (br, 2H, NH), 9.22 (s, 2H, CHO); $^{13}$C NMR (100 MHz, CDCl$_3$, TMS): δ 28.3, 28.5, 29.1, 30.2, 87.1, 105.2, 110.5, 141.3, 151.2, 152.6, 153.6, 164.4, 170.3; $v_{max}$ (cm$^{-1}$): 3348 (NH), 2974 (CH), 2862 (CH), 1996 (CO), 1636 (CO); m/z 444.14 [M$^+$]; Anal. Calcd (%) for $C_{19}H_{20}N_6O_7$: C, 51.35; H, 4.54; N, 18.91. Found C 51.12, H, 5.33, N, 18.68.

## References:

1. Astruc, D., et al. *Angew. Chem., Int. Ed.* **44**, 7852--7872, 2005.

2. Grunes, J., et al. *Chem. Commun.* **9**, 2257--2260, 2003.

3. (a) Rautio, J., et al. *Microchem. J.* **91**, 272--276, 2009; (b) Reetz, M.T., & Westermann, E. *Angew. Chem., Int. Ed.* **39**, 165--168, 2000; (c) Ramarao, C., et al. *Chem. Commun.* **10**, 1132--1133, 2002.

4. (a) Gladysz, J.A. *Pure Appl. Chem.* **73**, 1319--1324, 2001; (b) Gladysz, J.A. *Chem. Rev.* **102**, 3215--3216, 2002; (c) Pacchioni, G. *Surface Rev. Lett.* **7**, 277--306, 2000; (d) Cox, D.M., et al. *J. Phys. Chem.* **92**, 421--429, 1988; (e) Polshettiwar, V., & Varma, R.S. *Green Chem.* **12**, 743--754, 2010.

5. (a) Polshettiwar, V., et al. *ACS Nano* **3**, 728--736, 2009; (b) Polshettiwar, V., et al. *Chem. Commun.* **47**, 6318--6320, 2008; (c) Fihri, A., et al. *ChemSusChem* **5**, 1241--1248, 2012.

6. (a) Shimizu, K., et al. *Angew. Chem., Int. Ed.* **48**, 3982--3986, 2009; (b) Murugadoss, A., et al. *J. Mol. Catal. A* **304**, 153--158, 2009; (c) Witham, C.A., et al. *Nature Chemistry* **2**, 36--41, 2010.

7. Anastas, P.T., & Warner, J.C. *Green Chemistry: Theory and Practice*, Oxford Publication, New York, NY, USA, 1998.

8. (a) Martins, M.A.P., et al. *Chem. Rev.* **109**, 4140--4182, 2009; (b) Walsh, P.J., et al. *Chem. Rev.* **107**, 2503--2545, 2007; (c) Tanaka, K., & Toda, F. *Chem. Rev.* **100**, 1025--1074, 2000; (d) Nagendrappa, G. *Resonance* **7**, 59--68, 2002.

9. Tanaka, K. *Solvent-Free Organic Synthesis*, Wiley-VCH, Weinheim, Germany, 2009

10. (a) Fathalla, M., et al. *Chem. Soc. Rev.* **38**, 1608--1620, 2009; (b) Sivakova, S., & Rowan, S.J. *Chem. Soc. Rev.* **34**, 9--21, 2005; (c) Powner, M.W., et al.

*Nature* **459**, 239--242, 2009; (d) Pedersen, O.S., & Pedersen, E.B. *Antiviral Chem. Chemother.* **10**, 285--314, 1999.

11. Dinner, A.R., et al. *Nature* **413**, 752--755, 2001.

12. (a) Tucci, F.C., et al. *J. Med. Chem.* **47**, 3483--3486, 2004; (b) Sutherlin, D.P., et al. *J. Med. Chem.* **53**, 1086--1097, 2010.

13. (a) Manta, S., et al. *Bioorg. Chem.* **38**, 48--55, 2010; (b) Lundqvist, T., et al. *Nature* **447**, 817--822, 2007.

14. (a) Parker, J.B., et al. *Nature* **449**, 433--437, 2007; (b) Okamoto, A. *Org. Biomol. Chem.* **7**, 21--26, 2009.

15. (a) Samanta, A., et al. *J. Med. Chem.* **52**, 932--942, 2009.; (b) Rico-Gomez, R., et al. *Carbohydr. Res.* **343**, 855--864, 2008.

16. Das, S., & Thakur, A.J. *Eur. J. Org. Chem.* **12**, 2301--2308, 2011.

17. Blunt, J.W., et al. *Nat. Prod. Rep.* **26**, 170--224, 2008.

18. Semenov, V.E., et al. *Mendeleev Commun.* **11**, 96--97, 2001.

19. (a) Das, V.K., et al. *Green Chem.* **14**, 847--854, 2012; (b) Das, V.K., et al. *Appl. Catal. A* **456**, 118--125, 2013; (c) Das, V.K., et al. *J. Org. Chem.* **78**, 3361--3366, 2013; (d) Das, V.K., & Thakur, A.J. *Tetrahedron Lett.* **54**, 4164--4166, 2013.

20. (a) Shojaie-Bahaabad, M., & Taheri-Nassaj, E. *Mater. Lett.* **62**, 3364--3366, 2008; (b) Huang, C., et al. *Mater. Lett.* **59**, 3746--3749, 2005; (c) Zhang, Y., et al. *Chem. Phys. Lett.* **360**, 579--584, 2002.

that DE played the role of support which enhanced the catalytic activity of $Fe_2O_3$ NPs.

**Table 2.** Optimization of reaction condition[a] with DE supported IONPs

| Entry | Supported IONPs catalysts | Time (min) | Yield (%)[b] |
|---|---|---|---|
| 1 | $\alpha$-$Fe_2O_3$NPs@DE (19 nm) | 90 | 80 |
| 2 | $\gamma$- $Fe_2O_3$NPs@DE (8 nm) | 60 | 85 |
| 3 | $Fe_2O_3$NPs@DE (12 nm) | 25 | 94 |
| 4 | $Fe_3O_4$NPs@DE (< 50 nm) | 85 | 80 |
| 5 | FeO(OH)NPs@DE (<40nm) | 120 | 75 |

[a] Reaction condition: **3** (5 mmol, 755 mg), 30% $H_2O_2$ (5 mmol, 0.15 mL), DE supported IONPs (3 mol%,0.18 mmol, 12 mg) $CH_3CN$ (3 mL), RT, [b] isolated yield.

The smartness of DE as support was evident by the diminution of the clinging of $Fe_2O_3$ NPs to the magnetic needle while stirring. This modification brought about the appropriate dispersion of $Fe_2O_3$ NPs into the reaction media which increased the yield and decreased the scavenging time. The low catalyst loading is a key point in the realm of green chemistry; therefore, we studied the model reaction at different $Fe_2O_3$NPs@DE loading (Table 3) to understand its role in the oxidation of **3**.

**Table 3.** Optimization of catalyst loading [a]

| Entry | Mol% of catalyst | Time (min) | Yield (%)[b] |
|---|---|---|---|
| 1 | 1 | 80 | 78 |
| 2 | 2 | 50 | 85 |
| 3 | 3 | 25 | 94 |
| 4 | 5 | 45 | 80 |
| 5 | 7 | 50 | 75 |
| 6 | 10 | 50 | 60 |

[a] Reaction condition: **3** (5 mmol, 755 mg), 30% $H_2O_2$ (5 mmol, 0.15 mL), [b] isolated yield.

The significant increase in formation of **4** was found using 3 mol% of $Fe_2O_3$NPs@DE which gave 94% yield (Table 3, entry 6). The results of catalyst loading are depicted in figure 1 (Table 3, entries 1-5). The profile of the curve

condition but these too could not improve the yield (Table 1, entries 6-10). The ultimate difficulty to work with IONPs is that they clinged to the magnetic needle for which they did not undergo proper dispersion into the reaction media causing lower yield. Facing this practical difficulty we thought to perform the experiment using bulk iron containing catalysts for comparing the catalytic activity and resolving the clinging problem. With this notion in mind we inspected a series of bulk iron containing catalysts (10 mol %) in various solvents but none of them showed better performance in terms of yields and reaction time (Table 1, entries 11-18) than the IONPs. We also examined $Fe_2O_3$ NPs in various solvents to observe the effect on yield and rate of product formation but no further improvement was seen (Table 1, entries 19-21). Thus, we noted that the reaction was influenced to a considerable extent by the solvent utilized; $CH_3CN$, in particular, was found to be more favorable solvent than others.

Overall, our data showed that $Fe_2O_3$ NPs was comparatively little bit more efficient in promoting this reaction as compared with others. These outcomes led us to opt for supported IONPs for the model reaction. Recently, Zhang et al reported diatomite supported Pd NPs as catalyst for Heck and Suzuki Reactions.[28] Therefore, assuming DE to be an smart support for IONPs, we prepared five sets of DE supported IONPs and investigated their role in the optimization of model reaction at 3 mol% catalyst loading in acetonitrile at room temperature. As indicated in table 2, $Fe_2O_3NPs@DE$ stood out the choice of catalyst in $CH_3CN$ with much better improved yield of the product (4) and shorter reaction time at room temperature (Table 2, entry 3). It is important to mention that when the oxidation of 3 was carried out using only DE (10 mol%) as catalyst, it could not give 4 even after stirring for 16 h. Thus, it was revealed

in presence of acetonitrile at RT and also at 70 °C which produced very less yield

(Table 1, entries 3 and 4). Unsatisfied with these results, the need for a catalyst

was realised. With this idea we started the model reaction under the same reaction

condition with 3 mol% of $Fe_2O_3$ NPs (maghemite form) which was synthesized

according to a report in the literature[27] and it gave a yield of 68% (Table 1, entry

5). We also tested the influence of $\alpha$-$Fe_2O_3$ NPs, $\gamma$-$Fe_2O_3$ NPs, FeO(OH) NPs and

$Fe_3O_4$ NPs (procured from Sigma Aldrich) for the model reaction under the same

**Table 1.** Optimization of reaction condition[a]
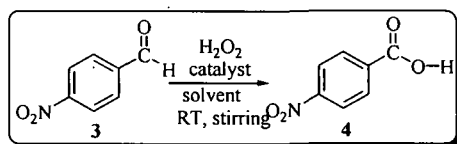


Scheme 2: Model reaction

| Entry | Catalysts | Solvent | Temp. (°C) | Time (h) | Yield(%)[b] |
|-------|-----------|---------|------------|----------|-------------|
| 1 | None | $CH_3CN$ | RT | 12 | [c] |
| 2* | None | None | RT | 2 | trace |
| 3 | None | $CH_3CN$ | RT | 10 | 17 |
| 4 | None | $CH_3CN$ | 70 | 9 | 31 |
| 5[d] | $Fe_2O_3$ NPs (12 nm) | $CH_3CN$ | RT | 3 | 68 |
| 6[d] | $\alpha$-$Fe_2O_3$ NPs (19 nm) | MeOH | RT | 7 | 40 |
| 7[e] | $\alpha$-$Fe_2O_3$ NPs (19 nm) | $CH_3CN$ | RT | 7 | 45 |
| 8[d] | $\gamma$- $Fe_2O_3$ NPs (8 nm) | $CH_3CN$ | RT | 7 | 48 |
| 9[e] | $Fe_3O_4$ NPs (< 50 nm) | $CH_3CN$ | RT | 5 | 50 |
| 10[f] | FeO(OH) NPs (<40 nm) | $CH_3CN$ | RT | 7 | 45 |
| 11[e] | $FeCl_3$ (anhydrous) | $CH_3CN$ | RT/reflux | 12 | trace |
| 12[e] | $FeCl_3 \cdot 6H_2O$ | $H_2O$ | RT/70 | 15 | trace |
| 13[e] | $FeSO_4 \cdot 7H_2O$ | $H_2O$ | RT/70 | 15 | trace |
| 14[e] | FeS | MeOH | RT | 18 | trace |
| 15[e] | $Fe_2O_3$ | THF | RT | 20 | 12 |
| 16[e] | $Fe_2O_3$ | neat | 70 | 24 | trace |
| 17[e] | $Fe_2O_3$ | $CH_3CN$ | 70 | 18 | 18 |
| 18[e] | $Fe_2O_3$ | $CH_3CN$ | RT | 12 | 43 |
| 19[f] | $Fe_2O_3$ NPs (12 nm) | $CH_3OH$ | RT | 5 | 44 |
| 20[f] | $Fe_2O_3$ NPs (12 nm) | THF | RT | 6 | 50 |
| 21[f] | $Fe_2O_3$ NPs (12 nm) | DMSO | RT | 5 | 52 |

[a] Reaction condition: 3 (5 mmol, 755 mg), 30% $H_2O_2$ (5 mmol, 0.15 mL), solvent (3 mL), [b] isolated yield, [c] no reaction, [d] 7 mol% of catalyst was used, [e] 10 mol% of catalyst was used, [f] 15 mol% of catalyst was used, * Grinded using mortar and pestle.

Therefore, economical, efficient, mild, practical, convenient, catalytic and benign alternative practice is still in demand for the oxidation of aldehydes to corresponding carboxylic acids.

To develop the domain of nanocatalysis underneath single scabbard, our effort for the advancement of a protocol called 'NOSE' (Nanoparticles-catalyzed Organic Synthesis Enhancement) chemistry[26] is in progress in our laboratory. Therefore, in this paper, we wish to report a green oxidation method involving bio-silica supported $Fe_2O_3$ NPs catalyzed oxidation of aldehydes into the corresponding carboxylic acid by stirring at room temperature (RT) using environmentally benign $H_2O_2$ as a sole oxidant in acetonitrile under aerobic condition (scheme 1).
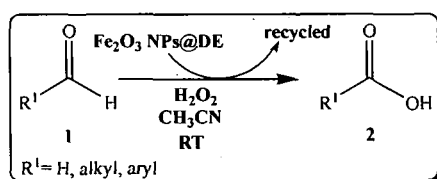


Scheme 1: Oxidation of aldehydes

### 3.2 Results and Discussion

### 3.2.1 Optimization of the reaction condition for the oxidation of aldehyde

In order to search for the best operative experimental conditions for the oxidation of aldehydes into corresponding carboxylic acids, a control experiment was performed by considering the model reaction (scheme 2) of 3 (5 mmol, 755 mg) in acetonitrile in air under stirring condition to check up to what extent it can yield product. But unfortunately it could not give any product upon stirring for 12 h (Table 1, entry 1). We then used 30% $H_2O_2$ (5 mmol, 0.15 mL) in absence of solvent and grinded with mortar-pestle which was also not fruitful (Table 1, entry 2). This mixture was then transferred to a round bottom flask (50 mL) and stirred

of 87-91% $SiO_2$, with significant quantities of $Al_2O_3$ and $Fe_2O_3$.[12] Due to its porous structure, high silica content, low density, low conductivity coefficient, etc.,[13] it has widely been applied as filter aid,[14] adsorbent,[15] insulating material,[16] catalyst support or carrier[17] and natural insecticide or grain protectant.[18] It is noted that DE has excellent absorption power because of its macroporous structure.[19]

Oxidation of aldehydes to the corresponding carboxylic acid using oxidizing agent is a fundamental reaction in organic synthesis.[20] Hence, from the ecological sight, using clean, cheap and less toxic oxidant such as hydrogen peroxide[21] towards green oxidations of aldehydes is of great significance. $H_2O_2$ is an ideal waste-avoiding oxidant, since water is the only by-product, and is very attractive as an oxidant for liquid-phase reactions because of its solubility in water and many organic solvents. In the recent years, a range of methodologies using $H_2O_2$ as an oxidant under harsh basic conditions[22] or in combination with other reagents and transition metals have been stated in the literature.[23] A few of the pioneer works in the green oxidation of aldehydes to carboxylic acids have been explored in the literature.[24] Very recently, our group also reported the oxidation of aldehydes into the corresponding carboxylic acid in the presence of aqueous $H_2O_2$ catalyzed by $VO(acac)_2$.[25] Despite the existing tactics, most of them endure different shortcomings such as production of abundant amounts of undesirable wastes, poor atom economy, high temperatures, prolonged reaction times, harsh reaction conditions, requirement of strong acidic conditions, and stoichiometric or super stoichiometric amounts of costly or hazardous oxidants, utilization of toxic and heavy metals, longer reaction times high cost, and lower yields of the desired products, formation of unwanted by-products, and tedious work up.

# Greener oxidation of aldehydes over bio-silica supported Fe₂O₃ nanoparticles: A convenient 'NOSE' approach

## 3.1 Introduction

In the recent period, metal oxide nanoparticles have attracted increasing interests for their applications such as cellular delivery carriers,[1] magnetic storage media[2] and MRI contrast agents.[3] The nanoparticles show features contradictory to the bulk metal due to quantum size effects, including novel electronic, optical and chemical behaviour.[4] The tuning in the properties may be achieved via control of shape, size, inter-particle spacing and dielectric environment, and methods to vary these parameters have been developed.[5] The metal oxide nanocatalysis are considered as a bridge between homogeneous and heterogeneous catalysis because of their growing interest on the catalytic properties.[6] Hence, the field of metal oxide nanocatalysis should recommend prospects for mining new chemical reactions.[7] Consequently, it is noteworthy that the combination of safe supported-catalysis with the use of solvent-free technique represents a suitable way towards the so-called "ideal synthesis".[8] Over the past few years, iron oxide nanoparticles (IONPs) have found tremendous attentions due to their high magnetic moment, low toxicity and ease of synthesis.[9] IONPs have also been applied in drug and gene delivery systems, separation and purification technology, magnetic resonance imaging and hyperthermia.[10] They have also found significant importance in the extraction of heavy metal ions and in the treatment of cancer cells through the application of external magnetic fields.[11]

Diatomaceous earth (DE) or diatomite also called bio-silica, typically consists

# Chapter 3

**Greener oxidation of aldehydes over bio-silica supported**

**Fe$_2$O$_3$ nanoparticles: A convenient 'NOSE' approach**
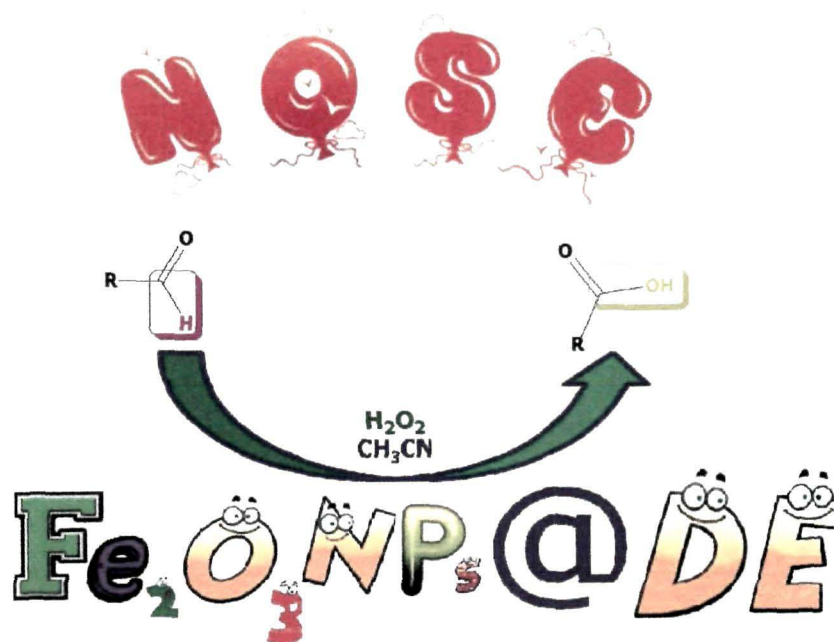
# Chapter 3

indicates that catalytic activity of Fe$_2$O$_3$NPs@DE increased from 1 to 2 mol%, it attains the maximum activity at 3 mol% and after that it starts decreasing. The decrease in yield with increasing catalyst loading may be attributed to the reduction in the surface area due to the aggregation of the particles. The decrease in the yield of **4** with increase in the catalyst loading might be due to the aggregation of Fe$_2$O$_3$ NPs in CH$_3$CN which in turn reduced its surface area. It was also observed that the addition of hydrogen peroxide in one portion gave a poor yield of the desired product while its drop wise addition gave the maximum yield of the product in a shorter reaction time.
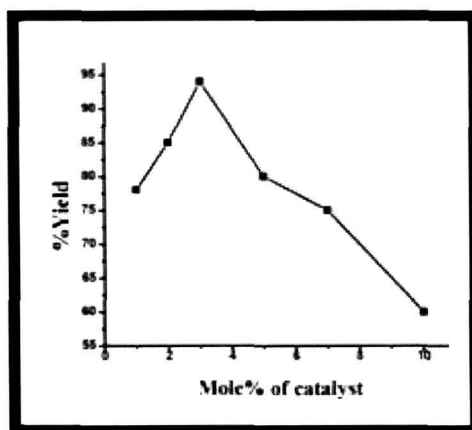


Figure 1. Graph of isolated yield of **3** versus mol% of IONPs@DE

### 3.2.2 Characterization of Fe$_2$O$_3$NPs@DE

EDX analyses of Fe$_2$O$_3$NPs@DE [Fig. 2(a)] showed that the weight% of O, Al, Si and Fe was 55.88, 0.88, 35.85 and 4.89 and atomic% was 69.89, 0.23,
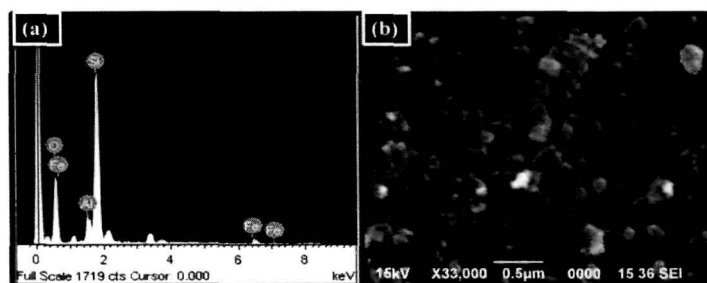


Figure 2. (a) EDX analysis of Fe$_2$O$_3$NPs@DE, (b) SEM image of Fe$_2$O$_3$NPs@DE

25.52 and 3.46 respectively. The SEM image of $Fe_2O_3NPs@DE$ [Fig. 2(b)] explained that the material has relatively uniform morphology and particle size distribution. In addition, some particle clusters may be observed due to the magnetic interaction between the particles.

Transmission electron microscopy (TEM) analysis of $Fe_2O_3NPs@DE$ [Fig. 3(a)] displayed the particles with an average diameter of $12\pm3$ nm (modeled as spheres). Figure 3(b) unveiled several diffraction rings which were the sum of diffraction patterns of different $Fe_2O_3$ NPs and DE as shown in the SAED [Fig. 3(c)] pattern and the great majority of the particles have sizes between 7 to 10 nm in diameter.
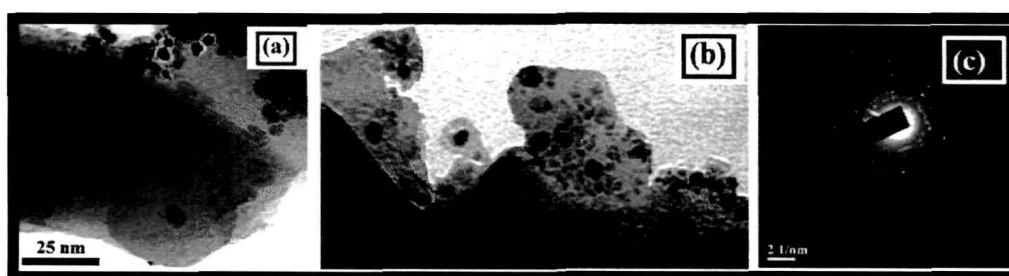


Figure 3. (a) and (b) TEM micrographs of $Fe_2O_3NPs@DE$, (c) SAED pattern of $Fe_2O_3NPs@DE$

The powder X-ray diffraction pattern of $Fe_2O_3NPs$, DE and $Fe_2O_3NPs@DE$ is are assembled in figure 4. $Fe_2O_3NPs$ produced peaks corresponding to (0 1 2), (1 0 4), (1 1 0), (0 2 4) and (1 1 6) planes with their relative intensities 24.044°, 33.063°, 35.581°, 49.389° and 53.960 respectively. It also gave a clear indication of the rhombohedral system with rhomb-centered lattice sites having lattice constant 0.5023 nm (JCPDS data card no: 89-8104). The crystalline sizes $Fe_2O_3NPs$ were determined by using Scherrer equation by considering the three intense peaks (0 1 2), (1 0 4) and (1 1 0) from XRD pattern. The crystalline sizes were found to be 19.7 nm calculated from the X-ray line broadening by applying

full width half maximum (FWHM) of characteristic peaks (0 1 2), (1 0 4) and (1 1 0) to the Scherrer equation. The X-ray diffraction pattern of DE revealed the lines (1 0 0), (1 0 1), (1 1 0), (1 0 2), (2 0 0), (2 0 1) and (1 1 2) with their relative intensities 20.810, 26.594, 36.577, 39.313, 42.361, 45.657 and 50.104 respectively. The DE is hexagonal system having primitive lattice sites with a lattice constant 0.4996 nm (JCPDS data card no: 89-8949). The XRD of $Fe_2O_3NPs@DE$ showed some significant changes. The intensities of the planes (0 1 2), (1 0 4), (1 1 0), (0 2 4) and (1 1 6) of $Fe_2O_3NPs$ diminished when it was entrapped into the pores of DE which clarified the strong covalent interaction between them. The intensities of (1 0 0), (1 0 1), (1 1 0), (1 0 2), (2 0 0), (2 0 1) and (1 1 2) planes of DE also got decreased during the course of strong interactions. Thus, it was found that DE performed as a smart support for holding $Fe_2O_3NPs$ tightly in its pores.
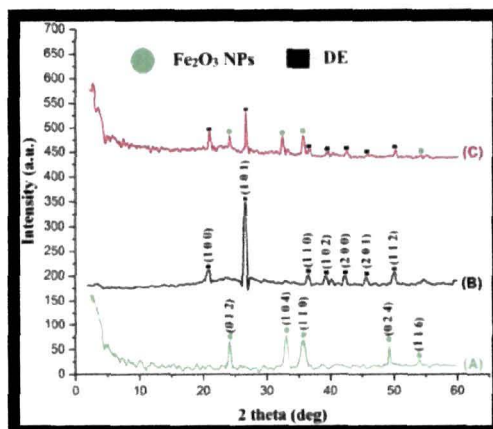


Figure 4. Powder X-ray diffraction pattern of (A) $Fe_2O_3NPs$, (B) DE and (C) $Fe_2O_3NPs@DE$

Furthermore, the strong interaction was supported by Fourier transform infrared (FTIR) spectroscopy analysis used for the observation of changes occurred before and after loading $Fe_2O_3NPs$ on the surface of DE and these modifications are collected in figure 5. $Fe_2O_3NPs$ presented two absorption bands

at 400 and 600 cm$^{-1}$ which were assigned to the Fe-O stretching modes.[29] The weak band at 1640 cm$^{-1}$ was due to the stretching frequency of carbonyl group of stearic acid. The characteristic bands ranging from 1400 and 400 cm$^{-1}$ were due to silicates structure.[30] The wide band centered at ca. 1090 cm$^{-1}$ might be due to Si–O–Si in-plane vibration (asymmetric stretching). Similar observations could be seen at ca. 795 cm$^{-1}$, which was also a feature of silica. Again, the weak absorption peak at 616 cm$^{-1}$ was possibly attributed to Si–O deformation. An absorption band at ca. 1620 cm$^{-1}$ is characteristic of Al-O stretching ~~which was~~ according to the literature.[31]
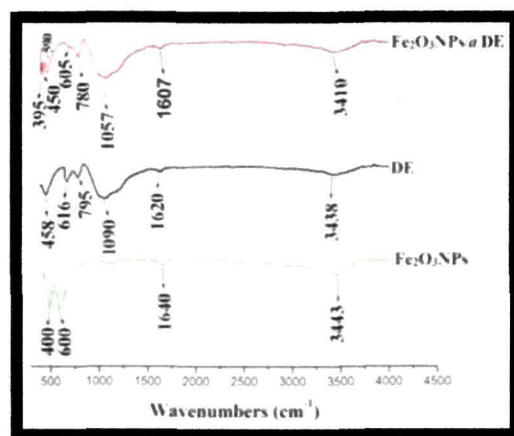


**Figure 5.** FTIR spectra of Fe$_2$O$_3$NPs, DE and Fe$_2$O$_3$NPs@DE

Some significant changes were observed in the IR bands of Fe$_2$O$_3$NPs when supported on bio-silica. The shifting in the values of IR stretching bands of both DE and Fe$_2$O$_3$NPs and weakening in their intensities represented that the strong covalent interaction hold between them making DE a smart support.

### 3.2.3 Fe$_2$O$_3$NPs@DE catalyzed oxidation of aldehydes

With this encouraging experimental condition and catalyst characterization in hand, we next assessed the generality for various aromatic and aliphatic aldehydes under the standardized conditions and the results are summarized in Table 4. As stated in table 4 the benzene substituted with both electron donating

and withdrawing groups were oxidized efficiently (Table 1, entries 1-14).

Table 4. $Fe_2O_3NPs@DE$ catalyzed oxidation of aldehydes

| Entry | $R^1$ | Time (min) | Yield (%)[a,b] | Melting point (°C) | TON |
|---|---|---|---|---|---|
| 1 | $C_6H_5$ | 10 | 98 | 118.5-119.8 | 65.3 |
| 2 | $2\text{-}ClC_6H_4$ | 18 | 96 | 139.3-140.6 | 64.0 |
| 3 | $3\text{-}ClC_6H_4$ | 20 | 94 | 154.2-157.3 | 62.6 |
| 4 | $4\text{-}ClC_6H_4$ | 15 | 96 | 241.2-242.4 | 64.0 |
| 5 | $2\text{-}NO_2C_6H_4$ | 45 | 90 | 147.5-148.2 | 60.0 |
| 6 | $3\text{-}NO_2C_6H_4$ | 55 | 90 | 139.0-140.4 | 60.0 |
| 7 | $4\text{-}NO_2C_6H_4$ | 25 | 94 | 235.4-236.8 | 62.6 |
| 8 | $2\text{-}OHC_6H_4$ | 35 | 90 | 156.2-158.0 | 60.0 |
| 9 | $4\text{-}OHC_6H_4$ | 25 | 90 | 214.3-217.5 | 60.0 |
| 10 | $4\text{-}NH_2C_6H_4$ | 25 | 92 | 187.4-188.9 | 61.3 |
| 11 | $2\text{-}OCH_3C_6H_4$ | 25 | 94 | 98.7-100.7 | 64.0 |
| 12 | $4\text{-}OCH_3C_6H_4$ | 25 | 97 | 182.1-185.3 | 64.0 |
| 13 | $2\text{-}CH_3C_6H_4$ | 25 | 96 | 104.3-105.2 | 64.0 |
| 14 | $4\text{-}CH_3C_6H_4$ | 25 | 96 | 179.0-182.5 | 64.3 |
| 15 | $C_6H_5CH{=}CH$ | 45 | 95 | 131.5-133.2 | 63.3 |
| 16[c] | $CHOC_6H_4$ | 55 | 96 | 298.7-299.8 | 64.0 |
| 17 | Thiophen | 80 | 92 | 127.2-130.7 | 61.3 |
| 18 | Furan | 70 | 94 | 126.1-129.3 | 62.6 |
| 19[d] | $CH_3$ | 10 | 98 | 117.8-119.0 | 65.3 |
| 20 | $CH_3CH_2$ | 22 | 94 | [e] | 62.6 |
| 21 | $CH_3CH_2CH_2$ | 30 | 90 | [e] | 60.0 |
| 22 | $CH_3(CH_2)_3$ | 50 | 90 | [e] | 60.0 |
| 23[d] | H | 50 | 85 | 99.1-100.8 | 56.6 |
| 24 | $C_6H_{11}$ | 50 | 96 | 30.0-32.8 | 64.0 |
| 25 | $C_6H_5CH_2$ | 50 | 93 | 76.3-77.2 | 62.0 |

[a] Yields refer to the isolated pure products, [b] Products were characterised by IR and NMR ($^1H$ and $^{13}C$) spectroscopy, MS and also by comparing their melting points and boiling points with the authentic ones, [c] 2 eqv. of 30% $H_2O_2$ were used, [d] Liquid compound, [e] Colourless oil.

Several reports[32] presented the low yield and difficulty in oxidizing 4-methoxy benzaldehyde, but $Fe_2O_3NPs@DE$ made this oxidation faster with excellent yield (Table 4, entry 12). Trans-cinnamaldehyde was also oxidized smoothly furnishing excellent yield (Table 4, entry 15). Terephthaldehyde, furan-2-carbaldehyde and thiophene-2-carbaldehyde were also oxidized to the corresponding carboxylic acids with elevated yields (Table 4, entries 16-18). The potential scope of this method was evident when the protocl was extended to simple aliphatic aldehydes (Table 4, entries 19-22). In most cases, the oxidation

proceeds with high efficiency and yields of greater than 90% were obtained. While affording clean reactions, smaller aliphatic aldehyde (Table 4, entry 23) provided slightly lower yield but cyclic aldehyde gave higher yield (Table 4, entry 24). The oxidation of phenyl-acetaldehyde also took place readily giving 96% yield (Table 4, entry 25). The oxidation of aldehydes carrying different electron withdrawing and electron-donating moieties into the corresponding carboxylic acids proceeded smoothly under the current reaction conditions, which demonstrated the compatibility of those moieties towards the reaction conditions. As a whole, the aryl and alkyl aldehydes were converted into the desired carboxylic acids with high purities and yields and with no side product(s) formation.

### 3.2.4 Plausible mechanism of oxidation of aldehyde

To rationalize the oxidation product, a tentative mechanism has been proposed (scheme 3). It has been hypothesized that the complexation of $Fe_2O_3NPs@DE$ to the aldehyde (I) makes the carbonyl carbon highly electron deficient to which when $H_2O_2$ is added dropwise, it forms a hydroperoxo species as an intermediate (II). Finally, elimination of water from (II) leads to the formation of carboxylic acid (III).
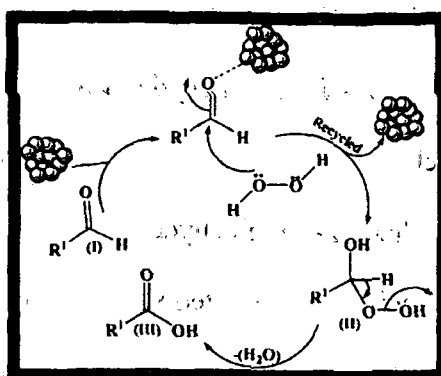


, Scheme 3: Plausible mechanism of oxidation of aldehydes.

### 3.2.5 Investigation on recycling potential of $Fe_2O_3NPs@DE$

The catalyst recyclability is an indispensable theme in the zone of green chemistry. Therefore, to examine the feasibility of recycling of $Fe_2O_3NPs@DE$, the oxidation of 4-methoxy benzaldehyde was carried out (scheme 4) as a test reaction. The reaction mixture was centrifuged (3,500 rpm) to pellet out the $Fe_2O_3NPs@DE$ after its completion. The extracted particles were washed with hot ethanol (5x10 mL) to remove all the organic impurities. Finally, it was decanted and dried in an oven at 80 °C for 7 h. Then the catalyst was reused for evaluating the performances in the next run in the reaction as shown in scheme 4.

**Table 5.** Reusability of $Fe_2O_3NPs@DE$ on the yield of 4-methoxybenzoic acid 6
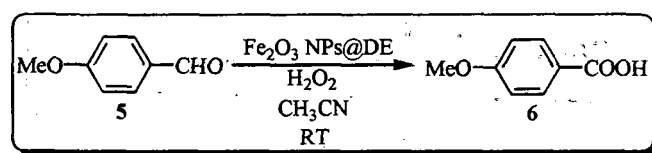


Scheme 4: Catalyst recyclability test

| Number of cycles[a] | Fresh | 1st run | 2nd run | 3rd run | 4th run | 5th run | 6th run | 7th run |
|---|---|---|---|---|---|---|---|---|
| Yield (%)[b] | 97 | 97 | 97 | 97 | 97 | 94 | 90 | 84 |
| Time (min) | 25 | 25 | 25 | 25 | 35 | 50 | 70 | 85 |
| TON | 53.8 | 53.8 | 53.8 | 53.8 | 53.8 | 52.2 | 50.0 | 46.6 |

[a] Reaction condition: 4-methoxybenzaldehyde (5 mmol, 680 mg), $H_2O_2$ (5 mmol, 0.15 mL), $Fe_2O_3NPs@DE$ (3 mol%, 0.18 mmol, 12 mg), [b] Yields refer to the isolated pure 4-methoxy benzoic acid

It is noteworthy to mention that $Fe_2O_3NPs@DE$ is equally effective from fresh up to the 3rd cycle, a bit longer time was required in the 4th cycle to achieve the similar result and after that the yield of 4-methoxybenzoic acid slightly decreased (Table 5).

To demonstrate the marginal loss of activity of $Fe_2O_3NPs@DE$ after 5th run, we performed the comparative study from XRD pattern of fresh and reused $Fe_2O_3NPs@DE$ (figure 6). The XRD pattern for fresh and reused $Fe_2O_3NPs@DE$

**Page | 91**

could not show important changes. However, the intensity of (0 1 2) peak of

Fe$_2$O$_3$NPs slightly diminished after 3$^{rd}$ and 5$^{th}$ run. The lowering in yield of 4-

methoxybenzoic acid might be due to the blockage of the active sites of the

catalyst after 5$^{th}$ run.
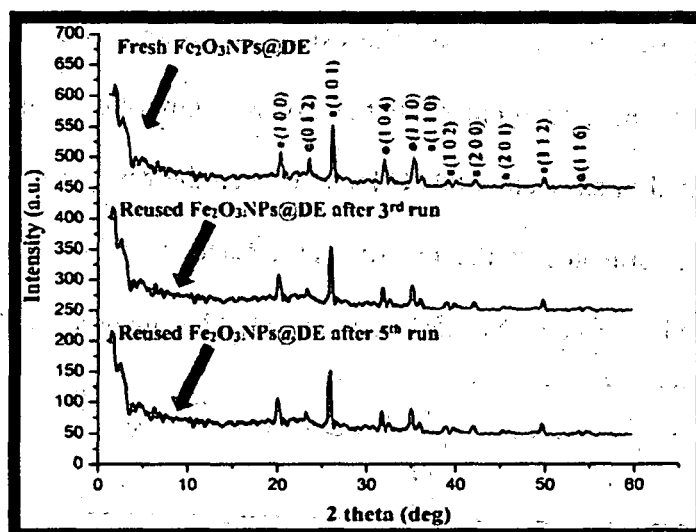


Figure 6. XRD pattern of fresh and reused Fe$_2$O$_3$NPs@DE after 3$^{rd}$ and 5$^{th}$ runs

The TEM micrographs (figure 7) of Fe$_2$O$_3$NPs@DE after 3$^{rd}$ and 5$^{th}$ cycles

showed the agglomeration of the Fe$_2$O$_3$NPs which might play a key role in the

loss of its activity and lower yield of product after 5$^{th}$ run.
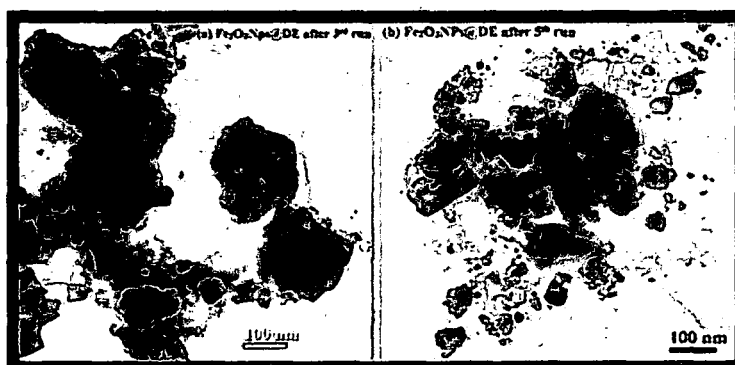


Figure 7. TEM micrographs of Fe$_2$O$_3$NPs@DE (a) after 3$^{rd}$ run and (b) after 5$^{th}$

run

Further to confirm the loss in activity of Fe$_2$O$_3$NPs@DE after 4$^{th}$ run, leaching

study was performed using atomic absorption spectrophotometer (Lab India AA 7000). It was found that only 0.007% of iron got leached from DE after $4^{th}$ run which might have slightly deactivated the catalysis of $Fe_2O_3NPs@DE$ in the present reaction.

### 3.2.6 Measurement and comparisons of green-ness of the present protocol with some reported methods

In the present work, the "green-ness" of our protocol was measured using several parameters of green chemistry. The assessment of "green-ness" is shown in table 6. The superiority of our protocol could be evident amongst the reported ones. As indicated in the table 6, the waste produced is the least in the present methodology and $Fe_2O_3NPs@DE$ is found to be much cleaner and more competent than the others. Moreover, the issues like solvent reusability and catalyst recyclability are neglected by $E$-factor which absolutely raises the accuracy.

Table 6. A comparision of "green-ness" among the catalysts/reagents in the oxidation of 4-methoxybenzaldehyde

| Catalysts/reagents | $E$-factor[a] | Mass intensity | Atom Economy (%) | Atom Efficiency (%) | Yield (%)[b] |
|---|---|---|---|---|---|
| $SeO_2$ | 20.9 | 22.0 | 89.4 | 41.1 | 46[32(a)] |
| $H_2O_2/[CH_3(nC_8H_{17})_3]HSO_4$ | 15.4 | 16.4 | 89.4 | 8.04 | 9[24(a)] |
| Oxone | 312 | 316 | 52.7 | 16.3 | 31[32(b)] |
| $Bi_2O_3$ | 5.9 | 7.0 | 67.2 | 86.7 | 97[32(c)] |
| $H_2O_2/HCl$ and $H_2NOH.HCl$ | 7.5 | 8.5 | 55.1 | 53.3 | 93[32(d)] |
| $Fe_2O_3NPs@DE$ | 3.3 | 4.3 | 89.4 | 86.7 | 97[our work] |

[a] $E$-factor shown does not account for the waste produced in the synthesis of reagents/ catalysts, [b] yield refer to the isolated pure 4-methoxybenzoic acid

### 3.3 Conclusion

In conclusion, in the convenient 'NOSE' chemistry approach, we demonstrate

a novel $Fe_2O_3NPs@DE$ catalyst for the green oxidation of aldehydes. DE acts as a smart support for $Fe_2O_3NPs$ and enhances its oxidative catalytic action. The method offers several advantages including excellent yields of the products, safe handling, experimental simplicity and "green-ness" which make it a useful, attractive and benign alternative over the existing methodologies. $Fe_2O_3NPs@DE$ works efficiently at room temperature without using any additive or ligands.

## 3.4 Experimental

### 3.4.1 General Experimental Methods

The chemicals and reagents were purchased from Sigma-Aldrich, Merck, M/S S. D. Fine Chemicals Pvt. Ltd. and Loba chemical, and used without further purification. Transmission electron microscopy was performed by (TEM) [CM12, PHILIPS] with energy dispersive spectroscopy (EDS) [OXFORD] and sample preparation facility. The surface morphology and EDX were studied using JEOL scanning electron microscope (model JSM-6390LV SEM). The XRD pattern was recorded with Rigaku X-ray diffractometer. Melting points were determined in a Büchi 504 apparatus. IR spectra were recorded as KBr pallets in a Nicolet (Impact 410) FT-IR spectrophotometer. $^1H$ and $^{13}C$ NMR spectra were recorded in a 400 MHz NMR spectrophotometer (JEOL, JNM ECS) using tetramethylsilane (TMS) as the internal standard and coupling constants are expressed in Hertz. Elemental analyses were carried out in a Perkin–Elmer CHN analyser (2400 series II). Mass spectra were recorded with a Waters Q-TOF Premier and Aquity UPLC spectrometer. Visualization was accomplished with UV lamp or $I_2$ stain. Reactions were monitored by thin-layer chromatography using aluminium sheets with silica gel 60 $F_{254}$ (Merck).

### 3.4.2 Typical procedure for the preparation of diatomite supported $Fe_2O_3$ NPs

In a two necked round bottomed flask (250 mL), Fe$_2$O$_3$ NPs (700 mg) and diatomite (1400 mg) were taken followed by the addition of THF (30 mL). The mixture was mechanically stirred at 60 °C for about 3 h to get a single phase. After the completion, THF was concentrated using rotary evaporator and finally dried in an oven at 80 °C for 6 h.

### 3.4.3 General procedure for the oxidation of aldehydes

In an oven dried round bottomed flask (50 mL) Fe$_2$O$_3$NPs@DE (3.0 mol%) was put in distilled CH$_3$CN (3 mL) and then alky/aryl aldehyde (1.0 mmol) was added. After that it was allowed to stir at room temperature under aerobic condition with the drop wise addition of H$_2$O$_2$ (1 mmol) till the required time (the progress of the reaction was judged by TLC). After the completion, CH$_3$CN was removed using rotary evaporator and ethyl acetate (3x10 mL) was added to it. Then the reaction mixture was centrifuged at 3,500 rpm to recover Fe$_2$O$_3$NPs@DE. Having done this, the reaction mixture was washed with water and brine, dried over anhydrous Na$_2$SO$_4$, concentrated in a rotary evaporator and finally the crude product was charged to column chromatography (30% ethyl acetate: hexane as an eluent) for purification and wherever necessary the products were recrystallized from hot ethanol.

The recovered catalyst was washed with hot ethanol (5x10 mL) to remove all the organic impurities. Finally, it was decanted and dried in an oven at 80 °C for 7 h. Then the catalyst was reused for evaluating the performances in the next run in the reaction.

## 3.5 Calculation for Turn Over Number (TON) for Fe$_2$O$_3$NPs@DE in scheme 4

| Entry | Input | mmol |
|-------|-------|------|
| 1 | 4-methoxy benzaldehyde | 5 |
| 2 | 30% H$_2$O$_2$ | 5 |
| 3 | Fe$_2$O$_3$NPs@DE | 0.18 (3 mol%) |

$$\text{TON from fresh upto 4th run} = \frac{(5+5)}{(0.18)} \times (0.97) = 53.8$$

$$\text{TON in 5th run} = \frac{(5+5)}{(0.18)} \times (0.94) = 52.2$$

$$\text{TON in 6th run} = \frac{(5+5)}{(0.18)} \times (0.90) = 50.0$$

$$\text{TON in 7th run} = \frac{(5+5)}{(0.18)} \times (0.84) = 46.6$$

## 3.6 Calculation of Green metrics

### 3.6.1 Calculation of green metrics for the oxidation of 4-methoxy benzaldehyde using SeO$_2$[32(a)]
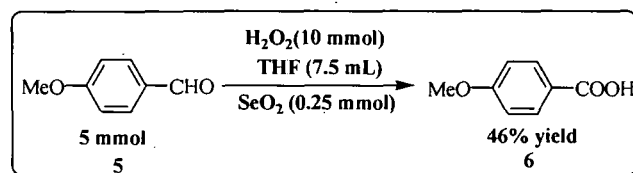


Scheme 5: Oxidation of 4-methoxy benzaldehyde using SeO$_2$

| Entry | Input | | Output | |
|-------|-------|------|--------|------|
| 1 | 4-methoxy benzaldehyde | 680 mg | 6 | 349.6 mg |
| 2 | 30% H$_2$O$_2$ | 340 mg | SeO$_2$ | 28 mg |
| 3 | THF | 6669 mg | | |
| | Total | 7686 mg | Total | 377.6 mg |

$$E - Factor = \frac{(7686 - 377.6)}{(349.6)} = 20.9$$

$$\text{Mass intensity} = \frac{(680 + 340 + 6669 + 28)}{(349.6)} = 22.0$$

$$\text{Atom economy} = \frac{(152)}{(136+34)} \times 100 = 89.4\%$$

$$\text{Atom efficiency} = 89.4\% \times 46\% = 41.1\%$$

### 3.6.2 Calculation of green metrics for the oxidation of 4-methoxy benzaldehyde using $H_2O_2/[CH_3(n\text{-}C_8H_{17})_3]HSO_4$[24(a)]
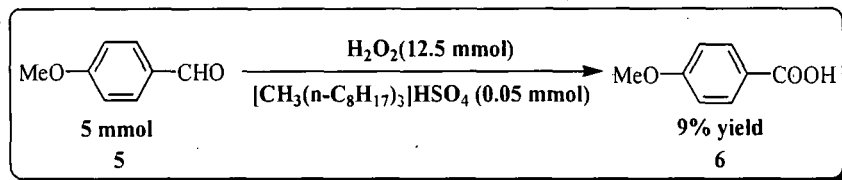


Scheme 6: Oxidation of 4-methoxy benzaldehyde using $H_2O_2/[CH_3(n\text{-}C_8H_{17})_3]HSO_4$

| Entry | Input | | Output | |
|---|---|---|---|---|
| 1 | 4-methoxy benzaldehyde | 680 mg | 6 | 68.4 mg |
| 2 | 30% $H_2O_2$ | 425 mg | | |
| 3 | $CH_3(n\text{-}C_8H_{17})_3]HSO_4$ | 23 mg | | |
| | Total | 1128 mg | Total | 68.4 mg |

$$E - \text{Factor} = \frac{(1128-68.4)}{(68.4)} = 15.4$$

$$\text{Mass intensity} = \frac{(1128)}{(68.4)} = 16.4$$

$$\text{Atom economy} = \frac{(152)}{(136+34)} \times 100 = 89.4\%$$

$$\text{Atom efficiency} = 89.4\% \times 9\% = 8.04\%$$

### 3.6.3 Calculation of green metrics for the oxidation of 4-methoxy benzaldehyde using Oxone[32(b)]
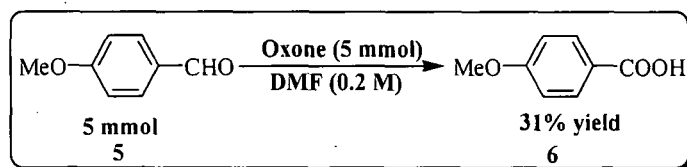


Scheme 7: Oxidation of 4-methoxy benzaldehyde using Oxone

| Entry | Input | | Output | |
|-------|-------|------|--------|------|
| 1 | 4-methoxy benzaldehyde | 680 mg | **6** | 235.6 mg |
| 2 | Oxone | 760 mg | | |
| 3 | DMF | 73050 mg | | |
| | Total | 74490 mg | Total | 235.6 mg |

$$E - \text{Factor} = \frac{(74490 - 235.6)}{(235.6)} = 315$$

$$\text{Mass intensity} = \frac{(74490)}{(235.6)} = 316$$

$$\text{Atom economy} = \frac{(152)}{(136 + 152)} \times 100 = 52.7\%$$

$$\text{Atom efficiency} = 52.7\% \times 31\% = 16.3\%$$

### 3.6.4 Calculation of green metrics for the oxidation of 4-methoxy benzaldehyde using $Bi_2O_3$[32(c)]
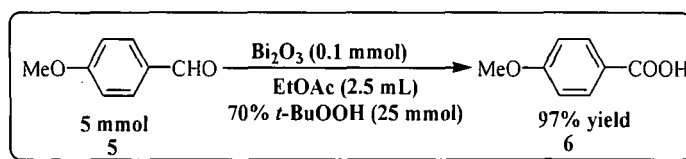


Scheme 8: Oxidation of 4-methoxy benzaldehyde using $Bi_2O_3$

| Entry | Input | | Output | |
|-------|-------|------|--------|------|
| 1 | 4-methoxy benzaldehyde | 680 mg | **6** | 737.2 mg |
| 2 | 70% *t*-BuOOH | 2250 mg | $Bi_2O_3$ | 46.6 mg |
| 3 | EtOAc | 2242 mg | | |
| | Total | 5172 mg | Total | 783.8 mg |

$$E - \text{Factor} = \frac{(5172 - 783.8)}{(737.2)} = 5.9$$

$$\text{Mass intensity} = \frac{(5172 + 46.6)}{(737.2)} = 7.0$$

$$\text{Atom economy} = \frac{(152)}{(136 + 90)} \times 100 = 67.2\%$$

$$\text{Atom efficiency} = 67.2\% \times 97\% = 65.2\%$$

### 3.6.5 Calculation of green metrics for the oxidation of 4-methoxy benzaldehyde using $H_2O_2/HCl$ and $H_2NOH\cdot HCl^{32(d)}$.
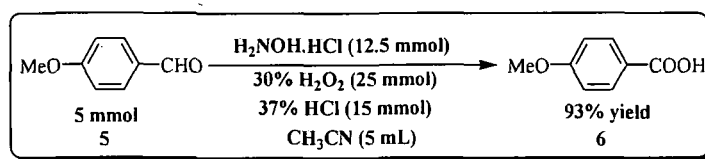


**Scheme 9:** Oxidation of 4-methoxy benzaldehyde using $H_2O_2/HCl$ and

$H_2NOH\cdot HCl$

| Entry | Input | | Output | |
|-------|-------|------|--------|--------|
| 1 | 4-methoxy benzaldehyde | 680 mg | **6** | 707 mg |
| 2 | $H_2O_2$ | 850 mg | | |
| 3 | $H_2NOH\cdot HCl$ | 863 mg | | |
| 4 | HCl | 548 mg | | |
| 5 | $CH_3CN$ | 3930 mg | | |
| | Total | 6020 mg | Total | 707 mg |

$$E - \text{Factor} = \frac{(6020 - 707)}{(707)} = 7.5$$

$$\text{Mass intensity} = \frac{(6020)}{(707)} = 8.5$$

$$\text{Atom economy} = \frac{(152)}{(136 + 34 + 69 + 36.5)} \times 100 = 55.1\%$$

$$\text{Atom efficiency} = 55.1\% \times 93\% = 51.3\%$$

### 3.6.6 Calculation of green metrics for the oxidation of 4-methoxy benzaldehyde using $Fe_2O_3NPs@DE^{Our\ work}$
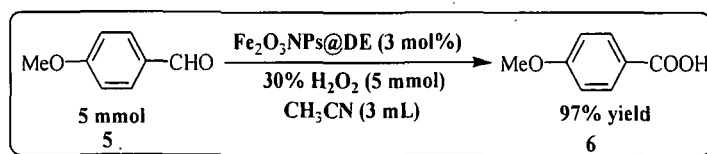


**Scheme 10:** Oxidation of 4-methoxy benzaldehyde using $Fe_2O_3NPs@DE$

| Entry | Input | | Output | |
|-------|-------|------|--------|------|
| 1 | 4-methoxy benzaldehyde | 680 mg | **6** | 737.2 mg |
| 2 | $H_2O_2$ | 170 mg | $Fe_2O_3NPs@DE$ | 12 mg |
| 3 | $CH_3CN$ | 2358 mg | | |
| | Total | 3208 mg | Total | 749.2 mg |

$$E - \text{Factor} = \frac{(3208 - 749.2)}{(737.2)} = 3.3$$

$$\text{Mass intensity} = \frac{(3208 + 12)}{(737.2)} = 4.3$$

$$\text{Atom economy} = \frac{(152)}{(136 + 34)} \times 100 = 89.4\%$$

$$\text{Atom efficiency} = 89.4\% \times 97\% = 86.7\%$$

## 3.7 Physical and spectroscopic data for all carboxylic acids

**Benzoic acid (Table 4, entry 1)**
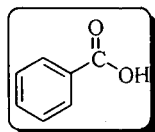


White solid; $R_f$ = 0.36 (20% AcOEt:hexane); mp 118.5-119.8 °C; $^1$H NMR (400 MHz, $CD_3OD$, TMS): δ 8.00-7.40 (m, 5H, Ar-H), 4.93 (br, s, 1H, OH); $^{13}$C NMR (100 MHz, $CD_3OD$, TMS): δ 168.5, 312.7, 130.5, 129.3, 128.1; IR (KBr pellets) $v_{max}$: 2661 cm$^{-1}$ (OH), 1684 cm$^{-1}$ (CO); m/z (LC-MS) 122.04 [M$^+$].

**2-Chloro-benzoic acid (Table 4, entry 2)**
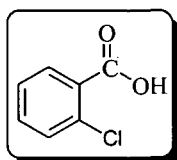


White solid; $R_f$ = 0.32 (20% AcOEt:hexane); mp 139.3-140.6 °C; $^1$H NMR (400 MHz, $CD_3OD$, TMS): δ 7.84 (d, $J$ = 6.88 Hz, 2H, Ar-H), 7.51-7.47 (m, 2H, Ar-H) 4.81 (br, s, 1H, OH); $^{13}$C NMR (100 MHz, $CD_3OD$, TMS): δ 167.1, 132.3,

132.4, 130.6, 130.1, 126.7; IR (KBr pellets) $v_{max}$: 2722 cm$^{-1}$ (OH), 1688 cm$^{-1}$

(CO); m/z (LC-MS) 156.00 [M$^+$].

**3-Chloro-benzoic acid (Table 4, entry 3)**
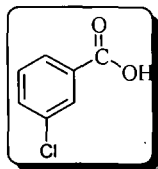


White solid; $R_f$ = 0.34 (20% AcOEt:hexane); mp 154.2-157.3 °C; $^1$H NMR (400

MHz, CD$_3$OD, TMS): δ 7.89 (d, $J$ = 6.88 Hz, 2H, Ar-H), 7.58-7.51 (m, 2H, Ar-

H) 4.85 (br, s, 1H, OH); $^{13}$C NMR (100 MHz, CD$_3$OD, TMS): δ 166.4, 133.1,

132.9, 131.1, 129.8, 127.2; IR (KBr pellets) $v_{max}$: 2776 cm$^{-1}$ (OH), 1682 cm$^{-1}$

(CO); m/z (LC-MS) 156.00 [M$^+$].

**4-Chloro-benzoic acid (Table 4, entry 4)**
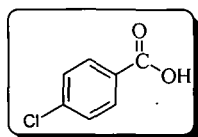


White solid; $R_f$ = 0.32 (20% AcOEt:hexane); mp 241.2-242 °C; $^1$H NMR (400

MHz, CD$_3$OD, TMS): δ 7.83 (d, $J$ = 6.88 Hz, 2H, Ar-H), 7.48-7.46 (m, 2H, Ar-

H) 4.89 (br, s, 1H, OH); $^{13}$C NMR (100 MHz, CD$_3$OD, TMS): δ 167.6, 132.8,

132.2, 130.9, 130.6, 126.5; IR (KBr pellets) $v_{max}$: 2784 cm$^{-1}$ (OH), 1690 cm$^{-1}$

(CO); m/z (LC-MS) 156.00 [M$^+$].

**2-Nitro-benzoic acid (Table 4, entry 5)**
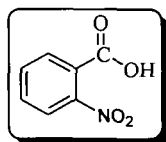


Yellow solid; $R_f$ = 0.30 (20% AcOEt:hexane); mp 147.5-148.2 °C; $^1$H NMR (400

MHz, CD$_3$OD, TMS): δ 8.71-7.73 (m, 4H, Ar-H), 4.90 (br, s, 1H, OH); $^{13}$C NMR

(100 MHz, CD$_3$OD, TMS): δ 166.9, 148.8, 135.4, 132.9, 130.2, 127.3, 123.5; IR

(KBr pellets) $v_{max}$: 2804 cm$^{-1}$ (OH), 1694 cm$^{-1}$ (CO); m/z (LC-MS) 167.02 [M$^+$];

Anal. Calcd (%) for C$_7$H$_5$NO$_4$: C, 50.31; H, 3.02; N, 8.38; Found C, 52.91, H,

2.62, N, 7.98.

### 3-Nitro-benzoic acid (Table 4, entry 6)
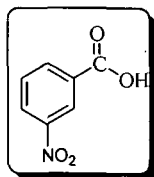


Pale yellow solid; R$_f$ = 0.34 (20% AcOEt:hexane); mp 139.0-140.4 °C; $^1$H NMR

(400 MHz, CD$_3$OD, TMS): δ 8.74-7.76 (m, 4H, Ar-H), 4.96 (br, s, 1H, OH); $^{13}$C

NMR (100 MHz, CD$_3$OD, TMS): δ 166.3, 148.5, 135.1, 132.7, 129.9, 127.0,

123.3; IR (KBr pellets) $v_{max}$: 2848 cm$^{-1}$ (OH), 1691 cm$^{-1}$ (CO); m/z (LC-MS)

167.02 [M$^+$]; Anal. Calcd (%) for C$_7$H$_5$NO$_4$: C, 50.31; H, 3.02; N, 8.38; Found C,

52.91, H, 2.62, N, 7.98.

### 4-Nitro-benzoic acid (Table 4, entry 7)
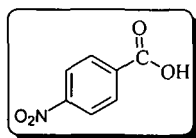


Light yellow solid; R$_f$ = 0.31 (20% AcOEt:hexane); mp 235.4-236.8°C; $^1$H NMR

(400 MHz, CD$_3$OD, TMS): δ 8.78-7.74 (m, 4H, Ar-H), 4.92 (br, s, 1H, OH); $^{13}$C

NMR (100 MHz, CD$_3$OD, TMS): δ 166.0, 148.3, 135.0, 132.5, 129.7, 126.9,

123.9; IR (KBr pellets) $v_{max}$: 2866 cm$^{-1}$ (OH), 1698 cm$^{-1}$ (CO); m/z (LC-MS)

167.02 [M$^+$]; Anal. Calcd (%) for C$_7$H$_5$NO$_4$: C, 50.31; H, 3.02; N, 8.38; Found C,

52.91, H, 2.62, N, 7.98.

### 2-Hydroxy-benzoic acid (Table 4, entry 8)
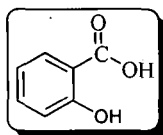
Colorless solid; $R_f = 0.27$ (20% AcOEt:hexane); mp 156.2-158.0 °C; $^1$H NMR (400 MHz, CD$_3$OD, TMS): δ 10.18 (br, s, 1H, OH ), 8.00-7.62 (m, 4H, Ar-H), 4.92 (br, s, 1H, OH); $^{13}$C NMR (100 MHz, CD$_3$OD, TMS): δ 169.1, 134.0, 131.1, 130.4, 129.7; IR (KBr pellets) $v_{max}$: 2896 cm$^{-1}$ (OH), 1708 cm$^{-1}$ (CO); m/z (LC-MS) 138.03 [M$^+$].

### 4-Hydroxy-benzoic acid (Table 4, entry 9)
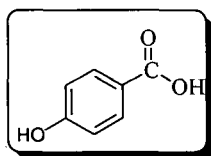


White solid; $R_f = 0.24$ (20% AcOEt:hexane); mp 214.3-217.5 °C; $^1$H NMR (400 MHz, CD$_3$OD, TMS): δ 10.23 (br, s, 1H, OH ), 8.10-7.42 (m, 4H, Ar-H), 4.98 (br, s, 1H, OH); $^{13}$C NMR (100 MHz, CD$_3$OD, TMS): δ 169.6, 134.2, 131.3, 130.0, 129.2; IR (KBr pellets) $v_{max}$: 2921 cm$^{-1}$ (OH), 1727 cm$^{-1}$ (CO); m/z (LC-MS) 138.03 [M$^+$].

### 4-Amino-benzoic acid (Table 4, entry 10)
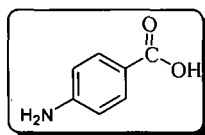


Grayish white solid; $R_f = 0.36$ (20% AcOEt:hexane); mp 187.4-188.9 °C; $^1$H NMR 400 MHz, CD$_3$OD, TMS): δ 8.85-7.78 (m, 4H, Ar-H), 5.69 (br, s, 1H, OH), 4.62 (br, s, 1H, NH); $^{13}$C NMR (100 MHz, CD$_3$OD, TMS): δ 169.3, 148.6, 136.6, 133.2, 129.9, 127.9, 124.3; IR (KBr pellets) $v_{max}$: 2578 cm$^{-1}$ (OH), 1696 cm$^{-1}$ (CO); m/z (LC-MS) 137.05 [M$^+$]; Anal. Calcd (%) for C$_7$H$_7$NO$_2$: C, 61.31; H, 5.14; N, 10.21; Found C, 60.91, H, 4.74; N, 9.81.

**2-Methoxy-benzoic acid (Table 4, entry 11)**
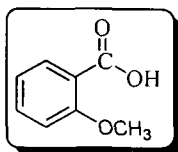


Pale yellow solid; $R_f$ = 0.35 (20% AcOEt:hexane); mp 98.7-100.7 °C; $^1$H NMR (400 MHz, CDCl$_3$, TMS): δ 10.51 (br, s, 1H, OH), 7.31 (d, $J$=7.80 Hz, 2H, Ar-H), 7.03 (d, $J$=7.80 Hz, 2H), 3.31 (s, 3H, OCH$_3$); $^{13}$C NMR (100 MHz, CDCl$_3$, TMS): δ 172.3, 168.1, 135.2, 133.4, 129.3, 56.5; IR (KBr pellets) $v_{max}$: 2556 cm$^{-1}$ (OH), 1686 cm$^{-1}$ (CO); m/z (LC-MS) 152.05 [M$^+$].

**4-Methoxy-benzoic acid (Table 4, entry 12)**
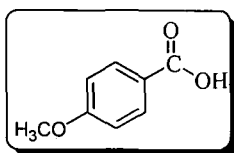


Pale crimson solid; $R_f$ = 0.33 (20% AcOEt:hexane); mp 182.1-185.3 °C; $^1$H NMR (400 MHz, CDCl$_3$, TMS): δ 10.59 (br, s, 1H, OH), 7.36 (d, $J$=7.80 Hz, 2H, Ar-H), 7.09 (d, $J$=7.80 Hz, 2H), 3.39 (s, 3H, OCH$_3$); $^{13}$C NMR (100 MHz, CDCl$_3$, TMS): δ 172.0, 168.5, 135.4, 133.9, 129.4, 56.1; IR (KBr pellets) $v_{max}$: 2575 cm$^{-1}$ (OH), 1697 cm$^{-1}$ (CO); m/z (LC-MS) 152.05 [M$^+$].

**2-Methyl-benzoic acid (Table 4, entry 13)**
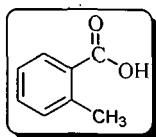


White solid; $R_f$ = 0.39 (20% AcOEt:hexane); mp 104.3-105.2 °C; $^1$H NMR (400 MHz, CDCl$_3$, TMS): δ 10.48 (br, s, 1H, OH), 7.43 (d, $J$=7.80 Hz, 2H, Ar-H), 7.12 (d, $J$=7.80 Hz, 2H), 2.35 (s, 3H, CH$_3$); $^{13}$C NMR (100 MHz, CDCl$_3$, TMS): δ 171.4, 167.8, 134.6, 132.4, 128.0, 19.8; IR (KBr pellets) $v_{max}$: 2732 cm$^{-1}$

(OH), 1715 cm$^{-1}$ (CO); m/z (LC-MS) 136.05 [M$^+$].

**4-Methyl-benzoic acid (Table 4, entry 14)**
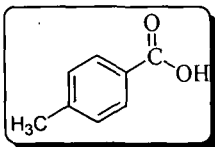
White solid; R$_f$ = 0.36 (20% AcOEt:hexane); mp 179.0-182.5 °C; $^1$H NMR (400

MHz, CDCl$_3$, TMS): δ 10.43 (br, s, 1H, OH), 7.48 (d, J=7.80 Hz, 2H, Ar-H),

7.18 (d, J=7.80 Hz, 2H), 2.29 (s, 3H, CH$_3$); $^{13}$C NMR (100 MHz, CDCl$_3$, TMS):

δ 171.8, 167.6, 134.8, 132.7, 128.2, 21.3; IR (KBr pellets) v$_{max}$: 2738 cm$^{-1}$ (OH),

1720 cm$^{-1}$ (CO); m/z (LC-MS) 136.05 [M$^+$].

**3-Phenyl-acrylic acid (Table 4, entry 15)**
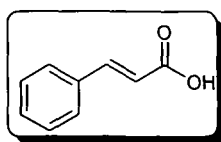
White solid; R$_f$ = 0.21 (20% AcOEt:hexane); mp 131.5-133.2 °C; $^1$H NMR (400

MHz, CD$_3$OD, TMS): δ 7.48-7.29 (m, 5H, Ar-H), 6.41 (d, J = 7.21 Hz, 1H, CH),

6.37 (d, J = 7.21 Hz, 1H, CH), 4.80 (br, s, 1H, OH); $^{13}$C NMR (100 MHz, CDCl$_3$,

TMS): δ 169.1, 144.9, 134.5, 130.0, 128.6, 128.1, 127.8, 118.0; IR (KBr pellets)

v$_{max}$: 2869 cm$^{-1}$ (OH), 1727 cm$^{-1}$ (CO); m/z (LC-MS) 136.05 [M$^+$].

**Terephthalic acid (Table 4, entry 16)**
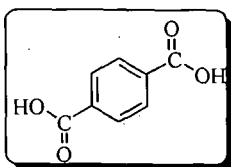
White solid; R$_f$ = 0.25 (20% AcOEt:hexane); mp 298.7-299.8 °C; $^1$H NMR (400

MHz, CD$_3$OD, TMS): δ 7.45 (d, J = 8.75 Hz, 2H, Ar-H), 7.27 (d, J = 8.75 Hz,

2H, Ar-H), 5.36 (br, s, 1H, OH); $^{13}$C NMR (100 MHz, CDCl$_3$, TMS): δ 170.2,

135.7, 130.5; IR (KBr pellets) $v_{max}$: 3123 cm$^{-1}$ (OH), 1725 cm$^{-1}$ (CO); m/z (LC-MS) 166.03 [M$^+$].

**Thiophene-2-carboxylic acid (Table 4, entry 17)**
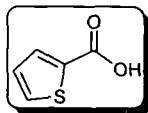


Light brown solid; $R_f$= 0.42 (20% AcOEt:hexane); mp 127.2-130.7 °C; $^1$H NMR (400 MHz, CD$_3$OD, TMS): δ 7.74-7.10 (m, 3H, Ar-H), 4.82 (br, s, 1H, OH); $^{13}$C NMR (100 MHz, CDCl$_3$, TMS): δ 164.0, 134.3, 133.2, 132.4, 127.5; IR (KBr pellets) $v_{max}$: 3156 cm$^{-1}$ (OH), 1729 cm$^{-1}$ (CO); m/z (LC-MS) 127.99 [M$^+$].

**Furan-2-carboxylic acid (Table 4, entry 18)**
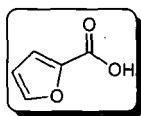


Light yellow solid; $R_f$= 0.39 (20% AcOEt:hexane); mp 126.1-129.3 °C; $^1$H NMR (400 MHz, CD$_3$OD, TMS): δ 7.85-7.45 (m, 3H, Ar-H), 4.94 (br, s, 1H, OH); $^{13}$C NMR (100 MHz, CDCl$_3$, TMS): δ 164.8, 134.7, 133.6, 132.7, 127.6; IR (KBr pellets) $v_{max}$: 3160 cm$^{-1}$ (OH), 1735 cm$^{-1}$ (CO); m/z (LC-MS) 112.02 [M$^+$].

**Acetic acid (Table 4, entry 19)**
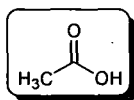


Colorless liquid; $R_f$ = 0.41 (20% AcOEt:hexane); $^1$H NMR (400 MHz, CDCl$_3$, TMS): δ 5.52 (br, s, 1H, OH), 2.04 (s, 3H, CH$_3$); $^{13}$C NMR (100 MHz, CDCl$_3$, TMS): δ 170.8, 23.1; IR (KBr pellets) $v_{max}$: 2957 cm$^{-1}$ (OH), 1711 cm$^{-1}$ (CO); m/z (LC-MS) 60.02 [M$^+$].

**Propionic acid (Table 4, entry 20)**
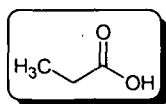
Colorless oil; $R_f$ = 0.43 (20% AcOEt:hexane); $^1$H NMR (400 MHz, CDCl$_3$,

TMS): δ 11.25 (br, s, 1H, OH), 2.48-2.41 (m, 2H, CH$_2$), 1.17 (t, $J$ = 5.6 Hz, 3H,

CH$_3$); $^{13}$C NMR (100 MHz, CDCl$_3$, TMS): δ 178.6, 27.8, 9.1; IR (KBr pellets)

$\nu_{max}$: 2971 cm$^{-1}$ (OH), 1738 cm$^{-1}$ (CO); m/z (LC-MS) 74.04 [M$^+$].

**Butyric acid (Table 4, entry 21)**
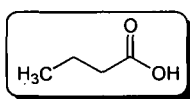


Colorless oil; $R_f$ = 0.39 (20% AcOEt:hexane); $^1$H NMR (400 MHz, CDCl$_3$,

TMS): δ 11.61 (br, s, 1H, OH), 2.32 (t, $J$ = 6.7 Hz, 2H, CH$_2$); 1.71 (m, 2H, CH$_2$),

1.05 (t, $J$ = 6.7 Hz, 3H, CH$_3$); $^{13}$C NMR (100 MHz, CDCl$_3$, TMS): δ 179.8, 37.6,

18.9, 13.5; IR (KBr pellets) $\nu_{max}$: 2978 cm$^{-1}$ (OH), 1741 cm$^{-1}$ (CO); m/z (LC-MS)

88.05 [M$^+$].

**Pentanoic acid (Table 4, entry 22)**
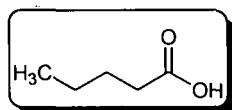


Colorless oil; $R_f$ = 0.36 (20% AcOEt:hexane); $^1$H NMR (400 MHz, CDCl$_3$,

TMS): δ 11.70 (br, s, 1H, OH), 2.30 (t, $J$ = 7.3 Hz, 2H, CH$_2$), 1.68-1.64 (m, 2H,

CH$_2$), 1.39-1.34 (m, 2H, CH$_2$), 0.94 (t, $J$ = 7.3 Hz, 3H, CH$_3$); $^{13}$C NMR (100

MHz, CDCl$_3$, TMS): δ 180.2, 34.4, 27.9, 22.5, 14.6; IR (KBr pellets) $\nu_{max}$: 3012

cm$^{-1}$ (OH), 1743 cm$^{-1}$ (CO); m/z (LC-MS) 102.07 [M$^+$].

**Formic acid (Table 4, entry 23)**
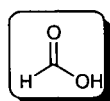
Colorless liquid; $R_f = 0.47$ (20% AcOEt:hexane); $^1$H NMR (400 MHz, CD$_3$OD,

TMS): δ 8.05 (s, 1H, CH), 5.39 (br, s, 1H, OH); $^{13}$C NMR (100 MHz, CDCl$_3$,

TMS): δ 174.2; IR (KBr pellets) $v_{max}$: 2949 cm$^{-1}$ (OH), 1718 cm$^{-1}$ (CO); m/z (LC-

MS) 46.01 [M$^+$].

**Cyclohexanecarboxylic acid (Table 4, entry 24)**
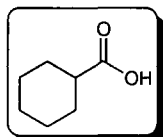


Pale yellow solid; $R_f = 0.42$ (20% AcOEt:hexane); mp 30.0-32.8 °C; $^1$H NMR

(400 MHz, CDCl$_3$, TMS): δ 11.75 (br, s, 1H, OH), 2.37-2.31 (m, 1H, CH), 1.84-

1.82 (m, 2H, CH$_2$), 1.62-1.54 (m, 2H, CH$_2$), 1.36-1.29 (m, 2H, CH$_2$), 1.14-1.07

(m, 2H, CH$_2$), 1.04-0.98 (m, 2H, CH$_2$); $^{13}$C NMR (100 MHz, CDCl$_3$, TMS): δ

182.1, 43.4, 28.3, 25.3, 24.3; IR (KBr pellets) $v_{max}$: 3119 cm$^{-1}$ (OH), 1729 cm$^{-1}$

(CO); m/z (LC-MS) 128.08 [M$^+$].

**Phenyl-acetic acid (Table 4, entry 25)**
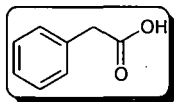


Off white solid; $R_f = 0.46$ (20% AcOEt:hexane); mp 76.1-77.3 °C; $^1$H NMR (400

MHz, CDCl$_3$, TMS): δ 11.05 (br, s, 1H, OH), 7.86-7.77 (m, 5H, Ar-H), 3.49 (s,

2H, CH$_2$); $^{13}$C NMR (100 MHz, CDCl$_3$, TMS): δ 178.8, 135.1, 132.4, 130.0,

128.5, 48.9 ; IR (KBr pellets) $v_{max}$: 3180 cm$^{-1}$ (OH), 1748 cm$^{-1}$ (CO); m/z (LC-

MS) 136.05 [M$^+$].

# References:

1. Xu, Z.P., et al. *Chem. Eng. Sci.* **61**, 1027--1040, 2006.

2. Huber, D.L. *Small* **1**, 482--501, 2005.

3. (a) Huh, Y.M., et al. *J. Am. Chem. Soc.* **127**, 12387--12391, 2005; (b) Song, H.T., et al. *J. Am. Chem. Soc.* **127**, 9992--9993, 2005.

4. (a) Daniel, M.-C., & Astruc, D. *Chem. Rev.* **104**, 293--346, 2004; (b) Schmid, G., et al. *Chem. Soc. Rev.* **28**, 179--185, 1999.

5. (a) Khlebtsov, N.G., et al. *Opt. Spectrosk.* **98**, 77--83, 2005; (b) Mulvaney, P. *MRS Bull.* **26**, 1009--1014, 2001; (c) Mock, J.J., et al. *Nano. Lett.* **3**, 485--491, 2003.

6. Astruc, D., et al. *Angew. Chem., Int. Ed. Eng.* **44**, 7852--7872, 2005.

7. (a) Shimizu, K., et al. *Angew. Chem., Int. Ed.* **48**, 3982--3986, 2009; (b) Murugadoss, A., et al. *J. Mol. Catal. A* **304**, 153--158, 2009; (c) Witham, C.A., et al. *Nature Chem.* **2**, 36--41, 2009.

8. (a) Clark, J.H., & Rhodes, C.N. *Clean synthesis using porous inorganic solid catalysts and supported reagents*, 1st Ed., Royal Society of Chemistry, UK, 2000; (b) Salehi, P., et al. *Curr. Org. Chem.* **10**, 2171--2189, 2006; (c) Hasaninejad, A., et al. *Can. J. Chem.* **85**, 416--420, 2007.

9. Laurent, S., et al. *Chem. Rev.* **108**, 2064--2110, 2008.

10. (a) Gupta, A.K., & Gupta, M. *Biomaterials* **26**, 3995--4021, 2005; (b) Mornet, S., et al. *J. Mater. Chem.* **14**, 2161--2175, 2004.

11. (a) Thomas, C.R., et al. *J. Am. Chem. Soc.* **132**, 10623--10625, 2010; (b) Yoza, B., et al. *J. Biotechnol.* **94**, 217--224, 2002; (c) White, B.R., et al. *J. Hazard. Mater.* **161**, 848--853, 2009.

12. Engh, K.R. in: M. Howe-Grant (Ed.) *Kirk-Othmer Encyclopaedia of Chemical Technology*, 4th ed. vol. 8, Wiley, New York, 1993.

13. Lemonas, J.F. *Am. Ceram. Soc. Bull.* **76**, 92--95, 1997.

14. El-Shafey, E.I., et al. *Sci. Technol.* **39**, 3237--3261, 2004.

15. Ai-Ghouti, M.A., et al. *J. Environ. Manage.* **69**, 229--238, 2003.

16. Christensen, A.N., et al. *J. Am. Ceram. Soc.* **84**, 878--880, 2001.

17. Alvarez, E., et al. *Catal. Today* **53**, 557--563, 1999.

18. Korunic, Z. *J. Stored Prod. Res.* **34**, 87--97, 1998.

19. (a) Perez-Cabero, M., et al. *Carbon* **46**, 297--304, 2008; (b) Cai, X., et al. *J. Inorg. Chem.* **46**, 3641--3645, 2006.

20. Ogliaruso, M.A., & Volfe, J.F. In *Synthesis of Carboxylic Acids Esters and Their Derivatives,* (Eds: S. Patai, Z. Rappoport), Wiley, Chichester, 1991.

21. Grigoropoulou, G., et al. *Green Chem.* **5**, 1--7, 2003.

22. Birkinshaw, J.H., et al. *J. Biochem.* **5**, 610--628, 1952.

23. (a) Heaney, H., & Newbold, A.J. *Tetrahedron Lett.* **42**, 6607--6609, 2001; (b) Travis, B.R., et al. *Org. Lett.* **5**, 1031--1034, 2003; (c) Bernini, R., et al. *Tetrahedron* **61**, 1821--1825, 2005; (d) Chakraborty, D., et al. *Tetrahedron Lett.* **50**, 6553--6556, 2009; (e) Mannam, S., & Sekar, G. *Tetrahedron Lett.* **49**, 1083--1086, 2008; (f) Tian, Q., et al. *Molecules* **13**, 948--957, 2008; (g) Hajimohammadi, M., et al. *Tetrahedron Lett.* **51**, 4061--4065, 2010.

24. (a) Sato, K., et al. *Tetrahedron Lett.* **41**, 1439--1442, 2000; (b) Dalcanale, E. *J. Org. Chem.* **51**, 567--569, 1986; (c) Shapiro, N., et al. *Green Chem.* **12**, 582--584, 2010; (d) Wittcoff, H.A., Reuben, B.G., & Plotkin, J.S. *Industrial organic chemicals*, 2nd Ed., John Wiley & Sons, Inc., Hoboken, New Jersey,

2004; (e) Shapiro, N., & Vigalok, A. *Angew. Chem. Int. Ed.* **47**, 2849--2852, 2008

25. Talukdar, D., et al. *Synlett.* **24**, 963--966, 2013.

26. (a) Das, V.K., et al. *Green Chem.* **14**, 847--854, 2012; (b) Das, V.K., et al. *Appl. Catal. A: Gen.* **456**, 118--125, 2013; (c) Das, V.K., et al. *J. Org. Chem.* **78**, 3361--3366, 2013; (d) Das, V.K., & Thakur, A.J. *Tetrahedron Lett.* **54**, 4164--4166, 2013; (f) Das, V.K., & Thakur, A.J. *ISRN Organic Chemistry* 1--6, 2013.

27. Deb, P., et al. *Phil. Mag. Lett.* **86**, 491--499, 2006.

28. Zhang, Z., & Wang, Z. *J. Org. Chem.* **71**, 7485--7487, 2006.

29. Cornell, R.M., & Schwertmann, V. *The Iron Oxides: Structure, Properties, Reactivity, Occurrences and Uses*, VCH, Tokyo, 1996.

30. (a) Tsai, W-T., et al. *J. Colloid and Interface Science* **297**, 749--754, 2006; (b) Falaras, P., et al. *Clay Miner.* **34**, 221--232, 1999.

31. Tsuchida, T. *Solid State Ionics* **63**, 464--470, 1993.

32. (a) Brzaszcz, M., et al. *Synth. Commun.* **30**, 4425--4434, 2000; (b) Travis, B.R., et al. *Org. Lett.* **5**, 1031--1034, 2003; (c) Malik, P., & Chakraborty, D. *Tetrahedron Lett.* **51**, 3521--3523, 2010; (d) Kiumars, B., et al. *Chin. J. Chem.* **26**, 1119--1121, 2008.

# Chapter 4

Sections I & II

# Section I

# Recyclable, highly efficient and low cost nano-MgO for amide synthesis under SFRC: A convenient and greener 'NOSE' approach
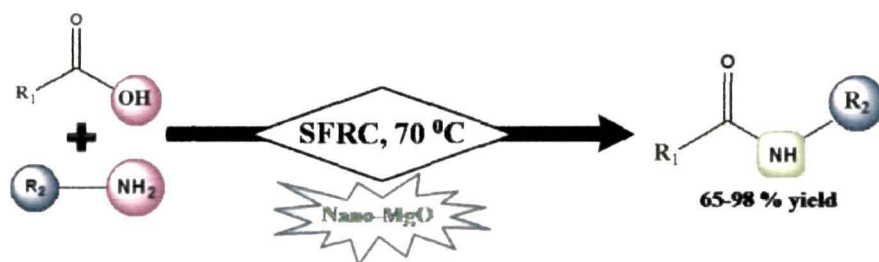
# Section I

## Recyclable, highly efficient and low cost nano-MgO for amide synthesis under SFRC: A convenient and greener 'NOSE' approach

### *4.I.1. Introduction*

Recently, in the domain of catalysis, nano magnesium oxide (MgO) has gained a respectable status as catalyst.[1] MgO has a basic property which is exploited in the high-yield synthesis of important molecules.[2] Its adsorptive properties[3] can be used in toxic waste remediation.[4] It has a high activity against bacteria, spores and viruses because of its large surface area.[5]

The widespread importance of amide moiety as one of the most versatile functionalities in chemistry and biology has been acknowledged.[6] Several catalysts and reagents[7] have been reported to effect the amidation reaction. The drawbacks inherited with these reagents and catalysts are their instability, sensitivity to moisture, harsh reaction condition, prolonged reaction time, modest yield, toxic/corrosive by-products and costly waste streams. More recently, hydroxyapatite-supported silver NPs has been used for the synthesis of amides via selective hydration of nitriles in water.[7] Kobayashi et al reported gold or gold/iron NPs catalyzed amide synthesis.[8] Mizuno and coworkers synthesized amides by hydration of nitriles promoted by amorphous MgO using reduced amounts of water.[9] Mizuno et al also reported the synthesis of amides by MgO promoted liquid-phase aerobic oxidation of methylarenes using ammonia surrogates.[10] In the recent work,[11] amide synthesis was achieved by water-soluble Gold/DNA Catalyst. However, main difficulties associated with

these cited works were very high reaction temperature, longer reaction time and application of expensive catalysts. Therefore, the synthesis of amide eliminating these drawbacks is still a demanding and challenging work for the chemists. Our group recently reported the synthesis of $N$-methylamides catalyzed by water tolerant zirconyl chloride under MWI.[12] Reddy and his co-workers have reported an acknowledgeable work on nano-MgO catalyzed $N$-formylation of aryl/alkyl amines using formic acid under MWI.[13] As a part of our ongoing research program for the development of the 'NOSE' [14] (Nanoparticles-catalyzed Organic Synthesis Enhancement) chemistry in our laboratory, we herein report recyclable nano-MgO for the synthesis of amides 3 in good to excellent yields under SFRC by reacting carboxylic acids 1 with amines 2 (scheme 1).
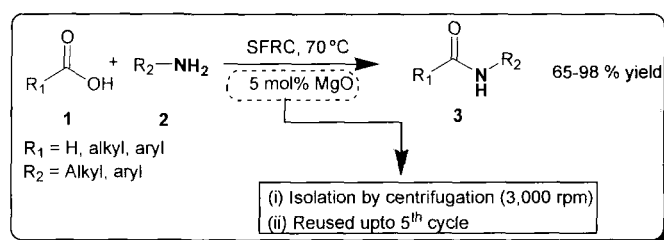


Scheme 1: General representative scheme for the synthesis of amides

### 4.1.2. Results and Discussion

### 4.1.2.1 Characterization of the nano-MgO

To characterize nano-MgO (procured from Sigma Aldrich), at first EDX analyses (figure 1) were performed to determine the elemental constituents of it.
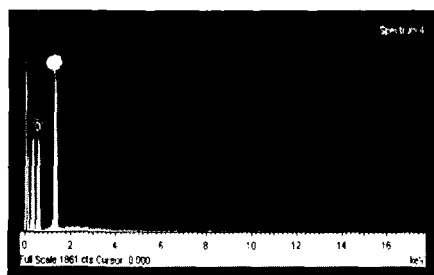


Figure 1. EDX analysis of pure nano-MgO

It shows that weight% of Mg and O are 57.29 and 42.71 and atomic% are 50.12 and 50.88 respectively. Thus, the EDX suggests the presence of only Mg and O in the nano-MgO sample.

For the identification of functional groups, bonding information, study of strength and fraction of hydrogen bonding, the FT-IR spectrum (figure 2) was recorded. It is revealed from figure 2 that there are two types of OH bonding exist in these spectra. First, is the O-H stretching and bending bonded with Mg and secondly, O-H stretching and bending attached at the surface of the samples. The O-H stretching bonded with Mg appeared as a sharp peak at 3703 cm$^{-1}$, bending bond at 1443 cm$^{-1}$. For the second, O-H stretching appeared as a broad band at 3430 cm$^{-1}$ while the bending at 1630 cm$^{-1}$. These bands had been previously characterized by several researchers.[15]
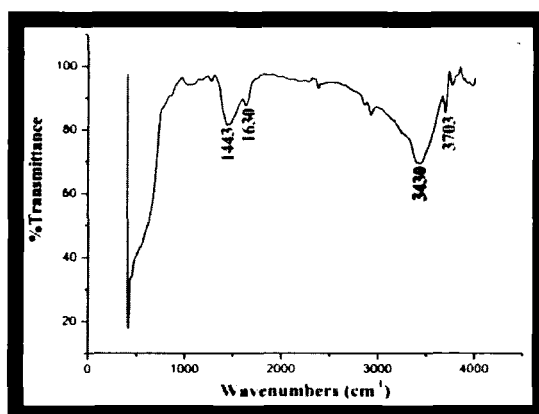


Figure 2. FTIR spectrum of nano-MgO

The result from X-ray diffractogram (figure 3) presented the peaks corresponding to (2 1 1), (2 2 0), (3 1 1), (4 1 1) and (3 3 1) planes that gave a clear indication of the existence of cubic primitive MgO with a lattice constant a, of 0.4839 nm and the peaks can be assigned to the pure phase of MgO (JCPDS PDF # 76-1363). The crystalline sizes were determined by using Scherrer equation by considering the two intense peaks (2 2 0) and (3 1 1) from XRD

pattern. The crystalline sizes were found to lie between 17.4 and 16.4 nm calculated from the X-ray line broadening by applying full width half maximum (FWHM) of characteristic peaks (2 2 0) and (3 1 1) to the Scherrer equation.
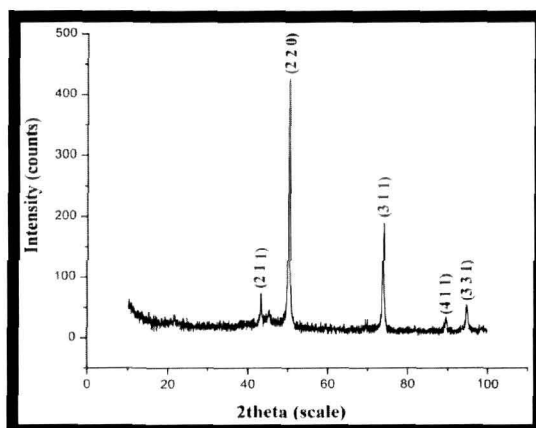


Figure 3. XRD pattern of MgO nanoparticles

The theoretical particle size was also calculated from the surface area assuming particles to be spherical in shape and the average particle diameter calculated was 18.12 nm ($S_{BET}$ =92.4 $m^2g^{-1}$ and $\rho$ =3.58 $gcm^{-3}$). The total pore volume of MgO nanopowder was found to be 0.4313 $mLg^{-1}$.

The surface morphology of nano-MgO was studied using scanning electron microscope [figures 4(A) and 4(B)]. It is evident from figures 4(A) and 4(B) that the MgO NPs has an irregular shape and poor microstructure resulting from agglomeration of MgO particles.
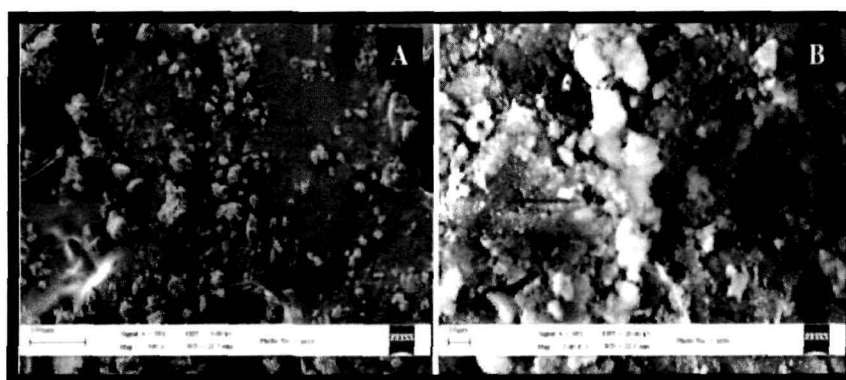


Figure 4. SEM images of nano-MgO at (A) lower and (B) higher resolution

Particle size and external morphology of nano-MgO particles were observed on a Transmission Electron Microscope (figure 5). Figure 5(A) shows isolated particles with an average diameter of 45±2 nm as well as a network of connected particles. The particles with an average diameter of 15±2 nm and 6±2 nm can be evident from figures 5(B) and 5(C). It can also be seen that some agglomeration was present and this was attributed to the large surface area of nano-MgO.
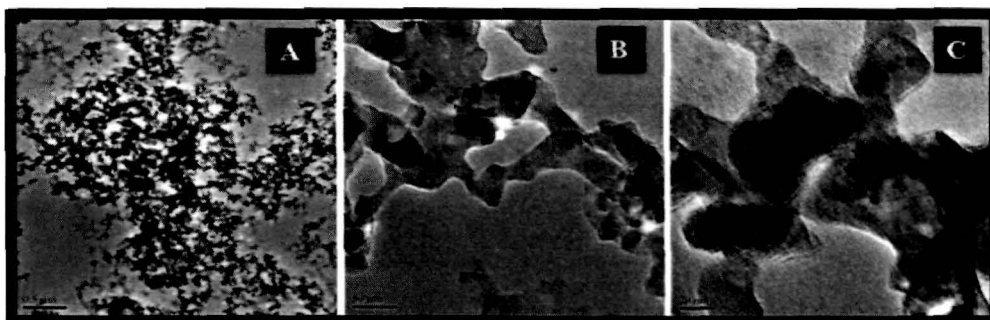


Figure 5. TEM images of nano-MgO at (A) 0.5μm, (B) 50 nm and (C) 20 nm

The TGA curve measures the compositional changes associated with the calcinations processes and is shown in figure 6. The two step pattern of weight loss has been indicated in figure 6 in the temperature range of around 110 °C and 345 °C.
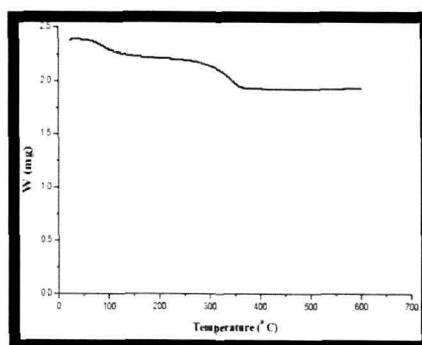


Figure 6. TGA curve of nano-MgO

### 4.1.2.2 Optimization of the reaction condition for amide synthesis

To optimize the reaction condition (Table 1), a model reaction (scheme 2)

between benzoic acid **1a** (1 mmol, 122 mg) and aniline **2a** (1 mmol, 0.09 mL) was considered. The reaction progress was monitored initially at room temperature and then by heating on a preheated oil bath up to 120 °C. Under this condition the reaction did not proceed and the starting materials remained intact (Table 1, entry 1). Then we increased the temperature up to 150 °C maintaining the same reaction condition but it also failed to yield the product (Table 1, entry 2). Observing these negative results, the importance of catalyst was realized. With this notion in mind, we started the reaction with 10 mol% of nano-MgO at 120 °C that provided 32% yield (Table 1, entry 3). Next, we carried out the same reaction at 70 °C expecting a better outcome with shorter rate. To our delight, a yield of 70% was obtained (Table 1, entry 4). For further improvement in the yield of amide and to understand the role of nano-MgO, the model reaction was performed at low catalyst loading. Significant increase in product formation was observed using 5 mol% of nano-MgO which gave 96% yield in 10 mins (Table 1, entry 6). Increasing the catalyst loading to more than 5 mol% might have reduced the surface area due to the aggregation of the particles which in turn decreased the yield of the desired products. The results of catalyst loading (Table 1, entries 4-8) indicate that catalytic activity of nano-MgO increases from 1 to 3 mol%, attains the maximum activity at 5 mol% and after that it starts decreasing. Increasing the catalyst loading to more than 5 mol% might have reduced the surface area due to the aggregation of the particles which in turn decreased the yield of the desired products. It is important to note that when the model reaction was performed at different mol% (other than 5 mol%) of nano-MgO by keeping the scavenging time constant (10 min), poor yields (5-19%) were obtained.

**Table 1.** Catalyst screening and optimization[a]
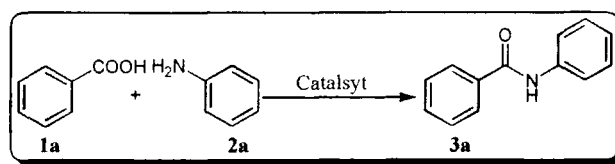


Scheme 2: Model reaction

| Entry | Catalyst | Solvent | Temp. (°C) | Time (h) | Yield (%)[b] | TON |
|---|---|---|---|---|---|---|
| 1 | None | SFRC | 120 | 9 | NR[c] | 0 |
| 2 | None | SFRC | 150 | 9 | NR[c] | 0 |
| 3[d] | Nano-MgO[i] | SFRC | 120 | 2 | 32 | 12.8 |
| 4[d] | Nano-MgO[i] | SFRC | 70 | 1 | 70 | 28 |
| 5[e] | Nano-MgO[i] | SFRC | 70 | 50 min | 74 | 29.6 |
| 6[f] | Nano-MgO[i] | SFRC | 70 | 10 min | 96 | 38.4 |
| 7[g] | Nano-MgO[i] | SFRC | 70 | 1.5 | 64 | 25.6 |
| 8[h] | Nano-MgO[i] | SFRC | 70 | 3 | 30 | 12 |
| 9[f] | Et₃N | SFRC | 70 | 7 | 5 | 2 |
| 10[f] | Imidazole | SFRC | 70 | 7 | 12 | 4.8 |
| 11[f] | Pyridine | SFRC | 70 | 7 | 5 | 2 |
| 12[f] | PPh₃ | SFRC | 70 | 7 | trace | 0 |
| 13 | K₂CO₃ | SFRC | 70 | 7 | trace | 0 |
| 14 | Nano-MgO[i] | CH₃CN | 70 | 3 | 35 | 14 |
| 15 | Nano-MgO[i] | H₂O | 70 | 5 | 30 | 12 |
| 16 | Nano-MgO[i] | CH₃OH | 70 | 5 | >27 | 10.8 |
| 17 | Nano-MgO[i] | THF | 70 | 4 | 40 | 16 |
| 18 | Nano-MgO[i] | Toluene | 70 | 6 | 44 | 17.6 |
| 19 | Nano-MgO[i] | DMSO | 70 | 2 | 20 | 8 |
| 20 | Nano-MgO[i] | Xylene | 70 | 5 | 60 | 24 |
| 21 | Nano-MgO[i] | DMF | 70 | 8 | 64 | 25.6 |
| 22[f] | Bulk-MgO | SFRC | 70 | 8 | 23 | 9.2 |

[a] Reaction condition: 2a (0.2 mL, 3 mmol), 1a (366 mg, 3 mmol), SFRC or solvent (5 mL). [b] Isolated yields. [c] No reaction. [d] 10 mol% catalyst was used. [e] 7 mol% catalyst was used. [f] 5 mol% catalyst was used. [g] 3 mol% catalyst was used. [h] 1 mol% catalyst was used. [i] Particles size (17.4-16.4 nm).

As nano-MgO is basic in nature, therefore, we compared the catalytic activity of nano-MgO with several base catalysts (Table 1). It is evident from the table 1 that nano-MgO showed the best performance amongst all as some of the catalysts decomposed at 70 °C (Table 1, entry 9). In some cases, catalyst isolation was noticeably tedious (Table 1, entries 10 and 11) and a few of them provided trace yield (Table 1, entry 12). We have also checked the effect of

**Page | 118**

solvent on the yield and the rate of the amide formation. However, application of solvent could not dramatically enhance both the rate and yield of amide at 70 °C using 5 mol% of nano-MgO (Table 1, entries 14-21). When bulk MgO was introduced in the model reaction for comparing its activity with the nano-MgO, it was observed that bulk MgO could catalyze the reaction by giving poor yield and longer reaction time (table 1, entry 22). The crucial breakthrough was observed under SFRC (Table 1, entry 6).
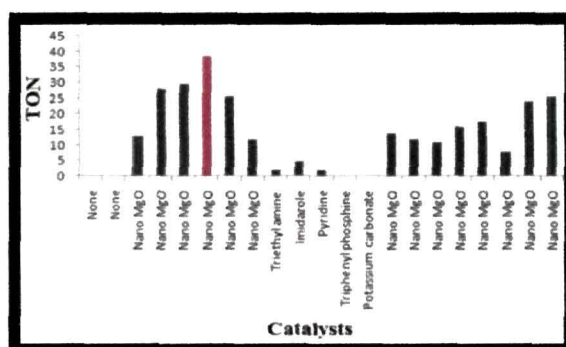


Figure 7. TON of various catalysts form Table 1

The turn over number (TON) was also calculated for each catalyst and the graph is shown in the figure 7. From the graph it is seen that the TON was the highest under SFRC at 70 °C. These outcomes provoked us to continue the reaction under SFRC using our 'NOSE' approach.

### 4.1.2.3 Basicity measurement of nano-MgO

The basicity of nano-MgO was determined using Hammett indicator and benzoic acid titration method.[16] The following Hammett indicators with their base strength (H_) were used for the basicity determination: Bromothymol Blue (H_=7.2), phenolphthalein (H_=9.8), 2,4-dinitroaniline (H_=15.0) and 4-nitroaniline (H_=18.4). With all these indicators except for 4-nitroaniline a change in color was observed. Thus, the strength of basicity of nano-MgO used in this study is in the range 9.8<H_<15.0. The basic strength and total basicity

of various loading of nano-MgO is presented in table 2. Nano-MgO has the

stronger base strength and a higher amount of basicity at 5 mol% loading (Table

2, entry 3) than the mentioned ones (Table 2, entries 1,2,4 and 5).

**Table 2.** Basicity and yield of amide using different amount of loading of nano-MgO

| Entry | Catalyst loading (mol%) | Basicity (mmol/g) | | | Total basicity (mmol/g) | Yield (%)[a] |
|---|---|---|---|---|---|---|
| | | $7.2 < H_- < 9.8$ | $9.8 < H_- < 15.0$ | $15.0 < H_- < 18.4$ | | |
| 1 | 1 | 0.83 | 2.5 | 3.3 | 6.6 | 30 |
| 2 | 3 | 1.6 | 3.8 | 5.2 | 10.6 | 64 |
| 3 | 5 | 2.2 | 5.3 | 7.1 | 14.6 | 96 |
| 4 | 7 | 1.9 | 4.1 | 5.7 | 11.7 | 74 |
| 5 | 10 | 1.7 | 3.3 | 4.7 | 9.7 | 70 |

[a] Isolated yield.

As suggested by the results in table 2, strong base sites are difficult to

generate with low loading of nano-MgO (Table 2, entries 1 and 2). When the

loading of nano-MgO was increased to 7 mol% and 10 mol%, the base strength

also got decreased which might be attributed to the aggregation of particles

reducing the active sites and surface area. Hence, nano-MgO attained the

maximum basicity at 5 mol% loading for synthesizing amide in excellent yield

(96%).

**Table 3.** Optimization of model reaction (scheme 2) with nanocatalysts[a]

| Entry | Nanocatalysts (size) | Temp. (°C) | Time (min) | Yield (%)[b] |
|---|---|---|---|---|
| 1 | $\alpha$-Fe$_2$O$_3$ (19 nm) | 70 | 180 | 44 |
| 2 | $\gamma$-Fe$_2$O$_3$ (8 nm) | 70 | 100 | 35 |
| 3 | Fe$_2$O$_3$ (12 nm) | 70 | 90 | 40 |
| 4 | Fe$_3$O$_4$ (<50 nm) | 70 | 60 | 55 |
| 5 | FeO(OH) (20-40 nm) | 70 | 80 | 36 |
| 6 | TiO$_2$ (<80 nm) | 70 | 300 | Trace |
| 7 | MgO (17.4-16.4 nm) | 70 | 10 | 96 |
| 8 | Basic Al$_2$O$_3$ (37.4-39.7 nm) | 70 | 60 | 15 |

[a] 5 mol% of catalyst was used. [b] Isolated yield.

With this encouraging catalysis by nano-MgO in the amidation reaction, we

then extended our 'NOSE' approach to other nanocatalysts considering the

same model reaction (Scheme 2) to investigate the efficiency of the different nanocatalysts in the amide synthesis. The results summarised in table 3 evident that at 5 mol% catalyst loading, only nano-MgO showed the best catalytic performance at 70 °C (Table 3, entry 7). But, the other mentioned nanocatalysts provided comparatively poorer yield at 70 °C with longer reaction time.

### 4.I.2.4 Nano-MgO catalyzed synthesis of amide derivatives

Prompted by this convenient experimental reaction condition, we next approached to assess the generality of various aromatic, heterocyclic and aliphatic amines with carboxylic acids under the standardized condition and the outcomes are summarized in table 4. It can be seen from table 4 that nano-MgO exhibits outstanding activity in the amide synthesis for both electron rich and electron poor anilines and benzoic acids (Table 4, entries 1-15).

However, anilines substituted with electron withdrawing groups gave slightly lower yields (Table 4, entries 4, 5 and 8-10) than those substituted with electron donating moieties (Table 4, entries 11-15). Benzoic acid having electron donating groups produced higher yield (Table 4, entry 3) than those with electron pulling motifs (Table 4, entries 2, 6 and 7). Benzylamine also reacted with several aromatic acids providing good to excellent yields (Table 4, entries 16-18). Aliphatic amines under the present reaction condition when treated with benzoic acid gave excellent yields (Table 4, entries 19 and 20). 2,6-Dimethyl-4-nitro-phenylamine having both electron pulling and pushing groups on the benzene ring also provided high yield (Table 4, entry 21). Benzylamine underwent reaction readily with phenylacetic acid producing good yield (Table 4, entry 22). We also studied the reaction of acetic acid with aniline substituted with both electron donating and electron withdrawing groups and we obtained

**Table 4.** Nano-MgO catalyzed synthesis of amides **3**

| Entry | R$_1$ | R$_2$ | Time (min) | Yield (%)$^{a,b}$ | Melting point (°C) |
|---|---|---|---|---|---|
| 1 | C$_6$H$_5$ | C$_6$H$_5$ | 10 | 96 | 162.5-163.5 |
| 2 | 4-ClC$_6$H$_4$ | C$_6$H$_5$ | 18 | 92 | 200.3-201.3 |
| 3 | 2-OHC$_6$H$_4$ | C$_6$H$_5$ | 15 | 94 | 137.2-138.3 |
| 4 | C$_6$H$_5$ | 3-ClC$_6$H$_4$ | 15 | 90 | 172.2-173.4 |
| 5 | C$_6$H$_5$ | 4-ClC$_6$H$_4$ | 17 | 90 | 177.0-178.7 |
| 6 | 3-NO$_2$C$_6$H$_4$ | C$_6$H$_5$ | 20 | 92 | 93.1-94.6 |
| 7 | 4-NO$_2$C$_6$H$_4$ | C$_6$H$_5$ | 22 | 92 | 98.0-100.4 |
| 8 | C$_6$H$_5$ | 2-NO$_2$C$_6$H$_4$ | 20 | 90 | 95.4-96.8 |
| 9 | C$_6$H$_5$ | 3-NO$_2$C$_6$H$_4$ | 19 | 90 | 156.2-157.2 |
| 10 | C$_6$H$_5$ | 4-NO$_2$C$_6$H$_4$ | 25 | 90 | 196.8-198.5 |
| 11 | C$_6$H$_5$ | 2-OCH$_3$C$_6$H$_4$ | 10 | 96 | 58.1-59.8 |
| 12 | C$_6$H$_5$ | 3-OCH$_3$C$_6$H$_4$ | 10 | 96 | 104.1-105.3 |
| 13 | C$_6$H$_5$ | 4-OCH$_3$C$_6$H$_4$ | 10 | 96 | 155.3-156.3 |
| 14 | C$_6$H$_5$ | 2-CH$_3$C$_6$H$_4$ | 10 | 95 | 144.5-145.5 |
| 15 | C$_6$H$_5$ | 4-CH$_3$C$_6$H$_4$ | 10 | 95 | 156.5-157.2 |
| 16 | C$_6$H$_5$ | C$_6$H$_5$CH$_2$ | 12 | 98 | 106.6-107.5 |
| 17 | 4-OCH$_3$C$_6$H$_4$ | C$_6$H$_5$CH$_2$ | 16 | 91 | $^c$ |
| 18 | ⬠ | C$_6$H$_5$CH$_2$ | 27 | 88 | $^d$ |
| 19 | C$_6$H$_5$ | CH$_3$ | 10 | 98 | 76.1-78.1 |
| 20 | C$_6$H$_5$ | C$_6$H$_{11}$ | 30 | 92 | 144.7-145.2 |
| 21 | C$_6$H$_5$ | 2,6-(CH$_3$)$_2$-4-NO$_2$C$_6$H$_2$ | 22 | 90 | 195.1-197.1 |
| 22 | C$_6$H$_5$CH$_2$ | C$_6$H$_5$CH$_2$ | 33 | 90 | 118.1-119.5 |
| 23 | CH$_3$ | C$_6$H$_5$ | 10 | 98 | 111.0-112.8 |
| 24 | CH$_3$ | 2-ClC$_6$H$_4$ | 20 | 96 | 88.7-89.1 |
| 25 | CH$_3$ | 3-ClC$_6$H$_4$ | 17 | 92 | 179.3-180.9 |
| 26 | CH$_3$ | 2-NO$_2$C$_6$H$_4$ | 20 | 90 | 93.3-94.2 |
| 27 | CH$_3$ | 3-NO$_2$C$_6$H$_4$ | 30 | 90 | 156.6-158.0 |
| 28 | CH$_3$ | 4-NO$_2$C$_6$H$_4$ | 33 | 88 | 208.4-209.8 |
| 29 | CH$_3$ | 4-OCH$_3$C$_6$H$_4$ | 15 | 97 | 137.7-138.4 |
| 30 | CH$_3$ | 4-CH$_3$C$_6$H$_4$ | 15 | 97 | 154.0-155.0 |
| 31 | CH$_3$ | 4-OHC$_6$H$_4$ | 10 | 93 | 170.5-171.8 |
| 32 | CH$_3$ | 4-COOHC$_6$H$_4$ | 35 | 91 | 259.3-261.9 |
| 33 | CH$_3$ | C$_6$H$_5$CH$_2$ | 25 | 95 | 60.5-62.0 |
| 34$^{e,f}$ | CH$_3$ | 2-NH$_2$C$_6$H$_4$ | 30 | 94 | 175.6-177.1 |
| 35 | CH$_3$ | CH$_3$ | 60 | 98 | 26.1-27.5 |
| 36 | CH$_3$ | C$_6$H$_{11}$ | 80 | 96 | 101.0-103.3 |
| 37 | CH$_3$CH$_2$ | C$_6$H$_5$CH$_2$ | 90 | 89 | 128.3-129.1 |
| 38 | CH$_3$CH$_2$CH$_2$ | C$_6$H$_5$ | 120 | 90 | 93.6-94.8 |
| 39 | CH$_3$CH$_2$ | CH$_3$ | 85 | 92 | $^d$ |
| 40 | C$_6$H$_{11}$ | C$_6$H$_5$ | 30 | 90 | 148.2-149.5 |

$^a$ Yields refer to the isolated pure products. $^b$ Products were characterised by IR and NMR ($^1$H and $^{13}$C) spectroscopy, MS and also by comparing their melting points with the authentic ones. $^c$ Colourless oil. $^d$ Liquid compound. $^e$ 2 equivalent of acetic acid was used. $^f$ 2-methylbenzimidazole was formed.

acetamide derivatives in good to excellent yields (Table 4, entries 23-33). It is interesting to note that when *o*-phenylenediamine was treated with acetic acid

instead of amide bond formation, cyclization occurred giving 2-methyl benzimidazole in excellent yield (Table 4, entry 34). Aliphatic amines also reacted with acetic acid to furnish the products in excellent yields (Table 4, entries 35 and 36). The reaction of propanoic acid and butanoic acid with aryl amines also afforded the expected products in elevated yields (Table 4, entries 37 and 38). The reaction of methylamine with propanoic acid, and aniline with cyclohexanoic acid also proceeded efficiently giving the corresponding products in good yields (Table 4, entries 39 and 40). The attempts of producing amides using cyanoacetic acid and trifluoroacetic acid failed under the current methodology. It might be due to the fast decarboxylation under the reaction condition and rapidly formed carboxylate salts of aniline decomposed kinetically before condensation with amines. However, dicarboxylic acids (such as adipic and malonic acid) and the long chain monocarboxylic acids (such as lauric and behenic acid) remained unreactive with aniline even after stirring at 80-100 °C for more than 24 h. The tolerability of different electron withdrawing and electron donating groups in the amines established the compatibility of those moieties towards the reaction condition.

### 4.1.2.5 Probable mechanism for the synthesis of amides

In the plausible mechanism, it has been hypothesized that nano-MgO activates the aryl/alkyl carboxylic acid on its surface throughout the formation
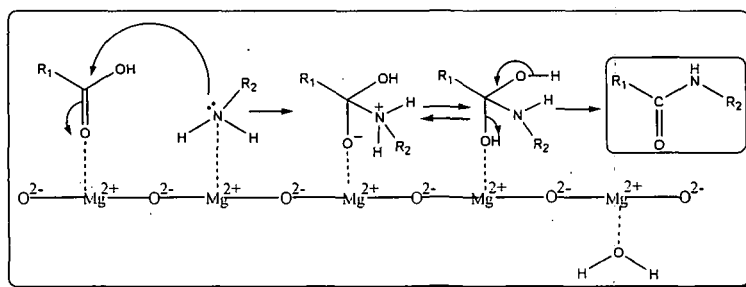


Scheme 3: Tentative mechanism for the synthesis of amides

of amides (scheme 3). A mechanism akin to this has been reported previously.[13]

### 4.1.2.6 Investigation on recycling potential of nano-MgO

The recyclability of a catalyst is a key point in the framework of green chemistry. The recycling experiment for nano-MgO was carried out by considering the model reaction under the standardized condition (Scheme 2).

**Table 5.** Reusability of nano-MgO on the yield of $N$-phenylbenzamide

| No. of cycles[a] | Fresh | 1$^{st}$ run | 2$^{nd}$ run | 3$^{rd}$ run | 4$^{th}$ run | 5$^{th}$ run | 6$^{th}$ run | 7$^{th}$ run |
|---|---|---|---|---|---|---|---|---|
| Yield [%][b] | 96 | 96 | 96 | 96 | 96 | 96 | 88 | 80 |
| Time [min] | 10 | 10 | 10 | 10 | 10 | 10 | 30 | 60 |
| TON | 38.4 | 38.4 | 38.4 | 38.4 | 38.4 | 38.4 | 35.2 | 32 |

[a] Reaction condition: 5 mmol aniline, 5 mmol benzoic acid, 0.25 mmol (5 mol%) nano basic MgO, 70 °C. [b] Yields refer to the isolated pure $N$-phenylbenzamide.

After the reaction, ethyl acetate was poured into the reaction mixture and then ultra centrifuged (3,500 r.p.m.) to pellet out the nano-MgO. The separated particles were washed with hot ethanol (5x10 mL) to remove all the organic impurities. Finally, it was decanted and dried in an oven at 100 °C for 7 h. Then the catalyst was reused in the next run in the reaction as shown in scheme 4. It is demonstrated in the table 5 that nano-MgO maintained its catalytic activity up to the 5$^{th}$ cycle and after that yield of $N$-phenylbenzamide went down markedly.

In the present work, we also conducted a comparative study on FTIR spectra of fresh and reused nano-MgO (after 5$^{th}$ run). It is found that there are shifts in the values of stretching frequencies as depicted in figure 8(a) which may be the reason for lower yield of $N$-phenylbenzamide (scheme 4) after 5$^{th}$ run. Moreover, there is an appearance of a new peak at 1121 cm$^{-1}$ which might be due to the presence of impurity after 5$^{th}$ run. The scanning electron micrograph of recycled nano-MgO after 5$^{th}$ run [figure 8(b)] was also recorded. The

recovered nano-MgO after 5th cycle showed a clear picture of highly agglomerated particles whose omnipresence in the reaction system might play a key role in reducing the yield of the product and in increasing time.
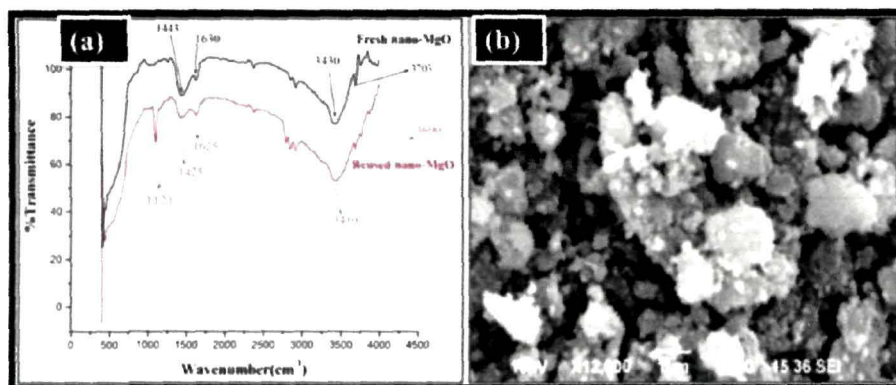


Figure 8. (a) Comparison of FTIR spectrum of fresh nano-MgO with the recycled one after 5th run, (b) SEM micrograph of reused nano-MgO after 5th run

The TEM image of reused nano-MgO after 5th run [figure 9(a)] manifested the rupture in the network of connected particles which might have taken part in the marginal loss of its activity. The network structure of nano-MgO may have tailored its high catalytic activity. The XRD pattern of fresh nano-MgO was also compared with reused one (after 5th run) and is shown in figure 9(b). It showed some important changes.
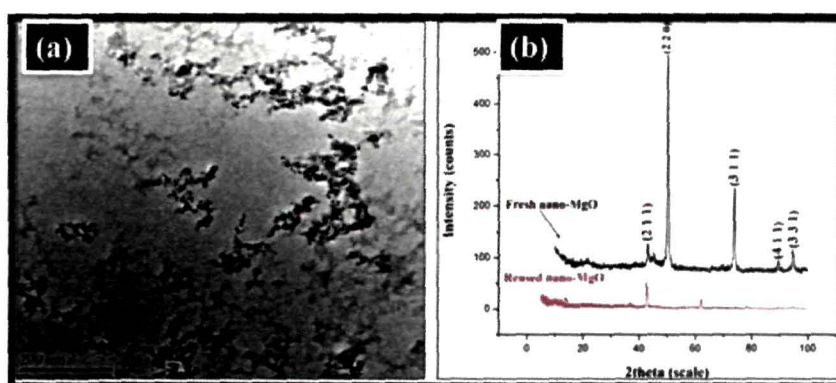


Figure 9. (a) TEM image of reused nano-MgO after 5th run, (b) Comparison of XRD pattern of fresh nano-MgO with the reused one after 5th run

Thus, it is evident [figure 9(b)] that the intensity of the highest peak (2 2 0) in fresh nano-MgO is decreased completely in the recycled one.

Apart from this, the intensities of the peaks (3 1 1), (4 1 1) and (3 3 1) also diminished in the reused nano-MgO. It may be due to either the leaching of $Mg^{2+}$ from MgO or blockage of the active pores which in turn perhaps reduced the yield of $N$-phenylbenzamide after $5^{th}$ run (scheme 4). Moreover, there is an appearance of a new peak at about 62° which might be referred to the impurity stuck into the catalyst during the consecutive cycles.

### 4.1.2.7 Leaching study of nano-MgO

To verify the amount of $Mg^{2+}$ lost from nano-MgO during its recycling (after $5^{th}$ cycle) which caused decrease in the yield of amidation product, the leaching study was performed on a UV visible spectrophotometer (figure 10). The reused nano-MgO experienced 34.7% $Mg^{2+}$ leaching from its surface which might have reduced its catalytic activity after $5^{th}$ run (scheme 2).
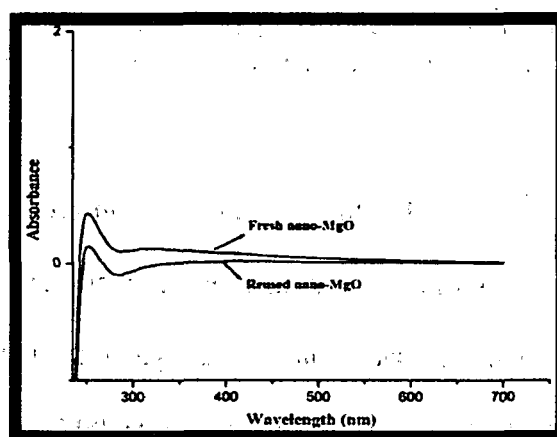


Figure 10. UV-Visible spectra of fresh and reused nano-MgO

### 4.1.2.8 Measurement of "green-ness" by using green metrics

The "green-ness" of the present methodology was evaluated by making use of different parameters of green chemistry (table 6), that shows the superiority

of nano-MgO over other catalysts. The waste produced during the course of the reaction is the least in our protocol compared to the other methodologies.[22-26] Moreover, the issues like solvent reusability and catalyst recyclability are omitted by $E$-factor which absolutely raises the accuracy.

**Table 6.** A comparison of "green-ness" among the catalysts/reagents in the synthesis of $N$-benzylbenzamide (scheme 4)
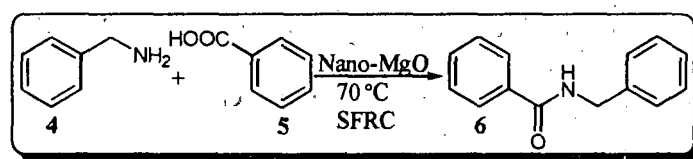


Scheme 4: Measurement of green metrics

| Catalysts/reagents | $E$-factor[a] | Mass intensity | Atom economy (%) | Yield (%)[b] |
|---|---|---|---|---|
| IBA[c] | 251.7 | 397.3 | 92.13 | 50[17] |
| CDI[d] | 31.8 | 32.9 | 53.9 | 92[18] |
| DCC | 22.6 | 67 | 48.5 | 82[19] |
| SOCl₂ | .17 | 25 | 85.3 | 72[20] |
| Sulfated tungstate | 9.3 | 26.3 | 92.13 | 81[21] |
| Nano-MgO | 1.07 | 1.09 | 92.13 | 98[our work] |

[a] $E$-factor shown does not account for the waste produced in the synthesis of reagents/catalysts. [b] Yield refers to the isolated pure $N$-benzylbenzamide. [c] Ortho-$N$,$N$-diisopropylbenzylaminoboronic acid catalyst, [d] $N$,$N$-carbonyldiimidazole.

### 4.1.3 Conclusion

In conclusion, we have developed a practical and greener 'NOSE' protocol for the clean synthesis of both aliphatic and aromatic amides utilizing nano-MgO as an efficient, reusable and cheap catalyst under SFRC. Simple experimental condition, varied substrate compatibility, high yields of the products, chemo selectivity, non-hygroscopic nature of catalyst make our protocol a more potent benign alternative over conventional ones for amide synthesis.

### 4.1.4 Experimental

#### 4.1.4.1 General Experimental Methods

Nano-MgO (The average particle diameter 18.12 nm, $S_{BET}$ =92.4 $m^2g^{-1}$, pore volume 0.4 $mLg^{-1}$ and $\rho$ =3.58 $gcm^{-3}$, purity: 99.99%) was purchased from Sigma-Aldrich and used as received. The chemicals and reagents were purchased from Sigma-Aldrich, Merck, M/S S. D. Fine Chemicals Pvt. Ltd. and Loba chemical, and used without further purification. Transmission electron microscopy was performed in (TEM) [CM12, PHILIPS] with energy dispersive spectroscopy (EDS) [OXFORD] and sample preparation facility. The surface morphology and EDX were studied using JEOL scanning electron microscope (model JSM-6390LV SEM). The XRD pattern was recorded with a Rigaku X-ray diffractometer. Melting points were determined in a Büchi 504 apparatus and are uncorrected. The leaching study was performed on a UV visible spectrophotometer (Hitachi, U-2001, Tokyo, Japan). IR spectra were recorded as KBr pellets in a Nicolet (Impact 410) FT-IR spectrophotometer. $^1H$ and $^{13}C$ NMR spectra were recorded in a 400 MHz NMR spectrophotometer (JEOL, JNM ECS) using tetramethylsilane (TMS) as the internal standard and coupling constants are expressed in Hertz. Elemental analyses were carried out in a Perkin–Elmer CHN analyser (2400 series II). Mass spectra were recorded with a Waters Q-TOF Premier and Aquity UPLC spectrometer. The thermal analysis, TGA was done on a Shimadzu, USA thermal analyzer, TG50, with a nitrogen flow rate of 30 mL/min at heating rate of 10 °C/min. Visualization was accomplished with UV lamp or $I_2$ stain. Reactions were monitored by thin-layer chromatography using aluminium sheets with silica gel 60 $F_{254}$ (Merck).

### 4.1.4.2 General procedure for the synthesis of amides

In an oven dried round bottomed flask (50 mL) nano-MgO (5.0 mol%) were added and then alky/aryl amines (5.0 mmol) and aromatic/aliphatic acid (5.0

mmol) was added. After that it was allowed to stir on a pre heated oil bath at

70 °C under aerobic condition till the required time (the progress of the reaction

was judged by TLC). After the completion, the reaction mixture was brought to

room temperature and ethyl acetate (3x10 mL) was added to it and then

centrifuged at 3,500 r.p.m. to recover the nano catalyst. Having done this, the

reaction mixture was washed with water and brine, dried over anhydrous

$Na_2SO_4$, concentrated in a rotary evaporator and finally the crude product was

charged to column chromatography [ethylacetate: hexane (3:7) as an eluent] for

purification and wherever necessary the products were recrystallized from hot

ethanol.

### 4.I.4.3 Calculation of TON for scheme 2

| Entry | Input | mmol |
|-------|-------|------|
| 1 | Benzoic acid | 3 |
| 2 | Aniline | 3 |
| 3 | Nano-MgO | 0.15 (5 mol%) |

$$TON = \frac{(3+3)}{(0.15)} \times (0.96) = 38.4$$

### 4.I.4.4 Calculation of TON for scheme 4

| Entry | Input | mmol |
|-------|-------|------|
| 1 | Benzoic acid | 5 |
| 2 | Benzylamine | 5 |
| 3 | Nano-MgO | 0.25 (5 mol%) |

$$TON = \frac{(5+5)}{(0.25)} \times (0.98) = 39$$

### 4.I.4.5 Calculations of green metrics for the synthesis of N-benzylbenzamide using nano-MgO (scheme 4)

| Entry | Input | | Output | |
|-------|-------|------|--------|------|
| 1 | Benzoic acid | 122 mg | N-benzylbenzamide | 211 mg |
| 2 | Benzylamine | 107 mg | Nano-MgO | 2 mg |
| | Total | 229 mg | Total | 213 mg |

$$E - \text{Factor} = \frac{(229 - 2)}{(211)} = 1.07$$

$$\text{Mass intensity} = \frac{(107 + 122 + 2)}{(211)} = 1.09$$

$$\text{Atom economy} = \frac{(211)}{(107 + 122)} \times 100 = 92.1$$

### 4.1.4.6 Physical and spectroscopic data of selected compounds

**N-Phenylbenzamide (Table 3, entry 1)**
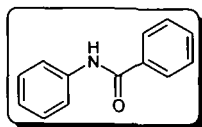


White solid; $R_f = 0.32$ [AcOEt:hexane (3:7)]; mp 150.6-153.4 °C; $^1$H NMR (400 MHz, CDCl$_3$, TMS): δ 7.92-7.46 (m, 10H, Ar-H), 6.87 (br, s, 1H, NH); $^{13}$C NMR (100 MHz, CDCl$_3$, TMS): δ 165.2, 146.5, 137.4, 135.3, 131.2, 129.7, 129.3, 129.0, 128.3, 126.4, 125.4, 121.4, 119.5, 116.7; IR (KBr pellets) $\nu_{max}$: 3410 cm$^{-1}$ (NH), 1682 cm$^{-1}$ (CO); m/z (LC-MS) 197.08 [M$^+$]; Anal. Calcd (%) for C$_{13}$H$_{11}$NO: C, 79.16; H, 5.62; N, 7.10; Found C, 79.17, H, 5.60, N, 7.09.

**4-Chloro-N-phenylbenzamide (Table 3, entry 2)**
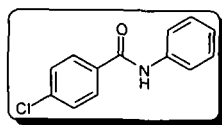


White solid; $R_f = 0.35$ [AcOEt:hexane (3:7)]; mp 200.3-201.3 °C; $^1$H NMR (400 MHz, CDCl$_3$, TMS): δ 8.02-7.66 (m, 9H, Ar-H), 6.82 (br, s, 1H, NH); $^{13}$C NMR (100 MHz, CDCl$_3$, TMS): δ 164.6, 140.5, 138.3, 137.4, 133.5, 131.5, 129.9, 129.1, 128.8, 128.4, 124.7, 120.2; IR (KBr pellets) $\nu_{max}$: 3417 cm$^{-1}$ (NH), 1708

cm$^{-1}$ (CO); m/z (LC-MS) 231.05 [M$^+$]; Anal. Calcd (%) for C$_{13}$H$_{10}$ClNO: C,

67.39; H, 4.35; N, 6.05; Found C, 67.43, H, 4.34, N, 6.09.

**2-Hydroxy-*N*-phenylbenzamide**$^{our\ work}$ (Table 3, entry 3)
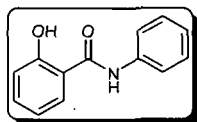


Milky white solid; R$_f$ = 0.33 [AcOEt:hexane (3:7)]; mp137.2-138.3 °C; $^1$H

NMR (400 MHz, CDCl$_3$, TMS): δ 10.14 (br, 1H, OH), 7.85-7.31 (m, 9H, Ar-

H), 6.77 (br, s, 1H, NH); $^{13}$C NMR (100 MHz, CDCl$_3$, TMS): δ 167.3, 141.2,

139.1, 138.3, 134.2, 132.3, 130.3, 129.8, 129.5, 128.8, 125.2, 120.8; IR (KBr

pellets) ν$_{max}$: 3420 cm$^{-1}$ (NH), 1712 cm$^{-1}$ (CO); m/z (LC-MS) 213.08 [M$^+$];

Anal. Calcd (%) for C$_{13}$H$_{11}$NO$_2$: C, 73.23; H, 5.20; N, 6.57; Found C, 73.23, H,

5.24, N, 6.54.

**N-(3-Chlorophenyl)benzamide (Table 3, entry 4)**
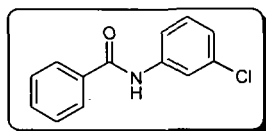


Pale yellow solid; R$_f$= 0.30 [AcOEt:hexane (3:7)]; mp172.2-173.4 °C; $^1$H NMR

(400 MHz, CDCl$_3$, TMS): δ 7.82-7.61 (m, 9H, Ar-H), 7.10 (br, s, 1H, NH); $^{13}$C

NMR (100 MHz, CDCl$_3$, TMS): δ 162.4, 140.2, 138.6, 134.4, 133.3, 131.8,

129.4, 129.3, 128.5, 126.1, 122.2; IR (KBr pellets) ν$_{max}$: 3420 cm$^{-1}$ (NH), 1717

cm$^{-1}$ (CO); m/z (LC-MS) 231.05 [M$^+$]; Anal. Calcd (%) for C$_{13}$H$_{10}$ClNO: C,

67.39; H, 4.35; N, 6.05; Found C, 67.42, H, 4.39, N, 6.02.

**N-(4-Chlorophenyl)benzamide (Table 3, entry 5)**
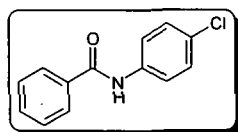
Slightly pale yellow solid; $R_f$= 0.31 [AcOEt:hexane (3:7)]; mp 177.0-178.7 °C;

$^1$H NMR (400 MHz, CDCl$_3$, TMS): δ 7.86-7.54 (m, 9H, Ar-H), 7.02 (br, s, 1H,

NH); $^{13}$C NMR (100 MHz, CDCl$_3$, TMS): δ 162.7, 140.3, 138.5, 134.7, 133.2,

131.6, 129.7, 129.0, 128.1, 126.3, 122.3; IR (KBr pellets) $v_{max}$: 3418 cm$^{-1}$ (NH),

1720 cm$^{-1}$ (CO); m/z (LC-MS) 231.05 [M$^+$]; Anal. Calcd (%) for C$_{13}$H$_{10}$ClNO:

C, 67.39; H, 4.35; N, 6.05; Found C, 67.37, H, 4.38, N, 6.04.

### 3-Nitro-$N$-phenylbenzamide (Table 3, entry 6)
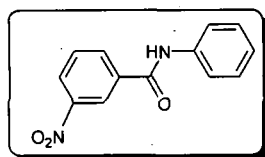


Off white solid; $R_f$ = 0.46 [AcOEt:hexane (3:7)]; mp 93.1-94.6 °C; $^1$H NMR

(400 MHz, CDCl$_3$, TMS): δ 8.41 (br, s, 1H, NH), 8.04-7.12 (m, 9H, Ar-H); $^{13}$C

NMR (100 MHz, CDCl$_3$, TMS): δ 163.2, 158.3, 141.3, 137.9, 133.1, 129.4,

127.8, 127.3, 123.3, 121.6, 119.6; IR (KBr pellets) $v_{max}$: 3382 cm$^{-1}$ (NH), 1650

cm$^{-1}$ (CO); m/z (LC-MS) 242.07 [M$^+$]; Anal. Calcd (%) for C$_{13}$H$_{10}$N$_2$O$_3$: C,

64.46; H, 4.16; N, 11.56; Found C, 64.48, H, 4.19, N, 11.52.

### 4-Nitro-$N$-phenylbenzamide (Table 3, entry 7)
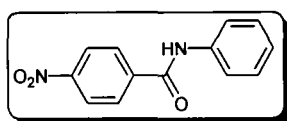


Off white solid; $R_f$ = 0.48 [AcOEt:hexane (3:7)]; mp 98.0-100.4 °C; $^1$H NMR

(400 MHz, CDCl$_3$, TMS): δ 8.47 (br, s, 1H, NH), 8.07-7.37 (m, 9H, Ar-H); $^{13}$C

NMR (100 MHz, CDCl$_3$, TMS): δ 164.3, 159.2, 142.4, 139.2, 135.6, 130.2,

128.3, 128.8, 124.5, 121.8, 119.8; IR (KBr pellets) $v_{max}$: 3380 cm$^{-1}$ (NH), 1648

cm$^{-1}$ (CO); m/z (LC-MS) 242.07 [M$^+$]; Anal. Calcd (%) for C$_{13}$H$_{10}$N$_2$O$_3$: C,

64.46; H, 4.16; N, 11.56; Found C, 64.44, H, 4.14, N, 11.56.

## *N*-(2-Nitrophenyl)benzamide (Table 3, entry 8)
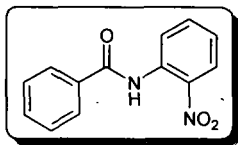


Light yellow solid; $R_f$= 0.47 [AcOEt:hexane (3:7)]; mp 95.4-96.8 °C; $^1$H NMR

(400 MHz, CDCl$_3$, TMS): δ 8.40 (br, s, 1H, NH), 7.78-7.33 (m, 9H, Ar-H); $^{13}$C

NMR (100 MHz, CDCl$_3$, TMS): δ 167.8, 140.7, 138.9, 134.5, 132.8, 130.7,

129.7, 128.7, 127.6, 125.7, 120.7; IR (KBr pellets) $v_{max}$: 3384 cm$^{-1}$ (NH), 1648

cm$^{-1}$ (CO); m/z (LC-MS) 242.07 [M$^+$]; Anal. Calcd (%) for C$_{13}$H$_{10}$N$_2$O$_3$: C,

64.46; H, 4.16; N, 11.56; Found C, 64.47, H, 4.20, N, 11.54.

## *N*-(3-Nitrophenyl)benzamide (Table 3, entry 9)
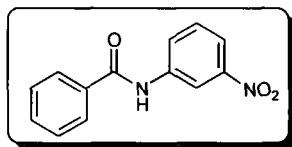


Pale yellow solid; $R_f$ = 0.44 [AcOEt:hexane (3:7)]; mp 156.2-157.2 °C; $^1$H

NMR (400 MHz, CDCl$_3$, TMS): δ 8.37 (br, s, 1H, NH), 8.04-7.41 (m, 9H, Ar-

H); $^{13}$C NMR (100 MHz, CDCl$_3$, TMS): δ 167.2, 140.6, 138.5, 134.3, 132.1,

130.0, 129.6, 128.2, 127.3, 125.5, 120.1; IR (KBr pellets) $v_{max}$: 3391 cm$^{-1}$ (NH),

1654 cm$^{-1}$ (CO); m/z (LC-MS) 242.07 [M$^+$]; Anal. Calcd (%) for C$_{13}$H$_{10}$N$_2$O$_3$:

C, 64.46; H, 4.16; N, 11.56; Found C, 64.50, H, 4.12, N, 11.59.

## *N*-(4-Nitrophenyl)benzamide (Table 3, entry 10)
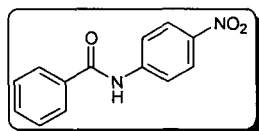


Yellow solid; $R_f$ = 0.41 [AcOEt:hexane (3:7)]; mp 196.8-198.5 °C; $^1$H NMR

(400 MHz, CDCl$_3$, TMS): δ 8.01 (br, s, 1H, NH), 7.75-7.31 (m, 9H, Ar-H); $^{13}$C

NMR (100 MHz, CDCl₃, TMS): δ 168.2, 141.8, 139.1, 135.3, 133.9, 131.8, 130.3, 129.8, 128.7, 126.6, 121.8; IR (KBr pellets) $v_{max}$: 3394 cm⁻¹ (NH), 1658 cm⁻¹ (CO); m/z (LC-MS) 242.07 [M⁺]; Anal. Calcd (%) for C₁₃H₁₀N₂O₃: C, 64.46; H, 4.16; N, 11.56; Found C, 64.44, H, 4.18, N, 11.56.

**N-(2-Methoxyphenyl)benzamide (Table 3, entry 11)**
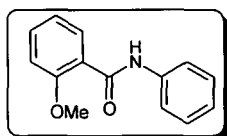


Light brown solid; R_f= 0.45 [AcOEt:hexane (3:7)]; mp 58.1-59.8 °C; ¹H NMR (400 MHz, CDCl₃, TMS): δ 8.01-7.41 (m, 9H, Ar-H), 7.33 (br, s, 1H, NH), 3.64 (s, 3H, OCH₃); ¹³C NMR (100 MHz, CDCl₃, TMS): δ 163.3, 154.5, 134.7, 131.6, 130.6, 128.7, 127.5, 121.4, 113.2, 55.3; IR (KBr pellets) $v_{max}$: 3363 cm⁻¹ (NH), 1668 cm⁻¹ (CO); m/z (LC-MS) 227.09 [M⁺]; Anal. Calcd (%) for C₁₄H₁₃NO₂: C, 73.99; H, 5.77; N, 6.16; Found C, 73.96, H, 5.73, N, 6.13.

**N-(3-Methoxyphenyl)benzamide (Table 3, entry 12)**
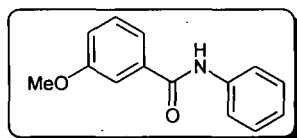


Pale brown solid; R_f= 0.43 [AcOEt:hexane (3:7)]; mp 104.1-105.3 °C; ¹H NMR (400 MHz, CDCl₃, TMS): δ 8.05-7.43 (m, 9H, Ar-H), 7.38 (br, s, 1H, NH), 3.73 (s, 3H, OCH₃); ¹³C NMR (100 MHz, CDCl₃, TMS): δ 164.5, 156.6, 136.8, 133.8, 132.7, 130.9, 129.7, 123.6, 115.4, 57.1; IR (KBr pellets) $v_{max}$: 3368 cm⁻¹ (NH), 1671 cm⁻¹ (CO); m/z (LC-MS) 227.09 [M⁺]; Anal. Calcd (%) for C₁₄H₁₃NO₂: C, 73.99; H, 5.77; N, 6.16; Found C, 73.96, H, 5.76, N, 6.19.

**N-(4-Methoxyphenyl)benzamide (Table 3, entry 13)**
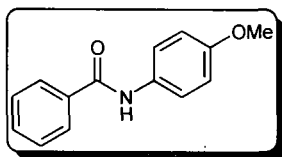
Yellowish white solid; $R_f$= 0.42 [AcOEt:hexane (3:7)]; mp 155.3-156.3 °C; $^1$H

NMR (400 MHz, CDCl$_3$, TMS): δ 8.27-7.45 (m, 9H, Ar-H), 7.32 (br, s, 1H,

NH), 3.78 (s, 3H, OCH$_3$); $^{13}$C NMR (100 MHz, CDCl$_3$, TMS): δ 165.2, 155.4,

135.6, 132.5, 131.5, 128.4, 127.6, 122.3, 114.1, 56.2; IR (KBr pellets) $v_{max}$:

3365 cm$^{-1}$ (NH), 1670 cm$^{-1}$ (CO); m/z (LC-MS) 227.09 [M$^+$]; Anal. Calcd (%)

for C$_{14}$H$_{13}$NO$_2$: C, 73.99; H, 5.77; N, 6.16; Found C, 73.98, H, 5.75, N, 6.15.

## N-o-Tolylbenzamide (Table 3, entry 14)
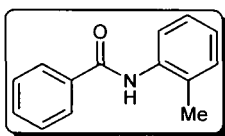


Milky white solid; $R_f$ = 0.50 [AcOEt:hexane (3:7)]; mp 144.5-145.5 °C; $^1$H

NMR (400 MHz, CDCl$_3$, TMS): δ 8.08-7.69 (m, 9H, Ar-H), 7.36 (br, s, 1H,

NH), 2.10 (s, 3H, CH$_3$); $^{13}$C NMR (100 MHz, CDCl$_3$, TMS): δ 164.6, 134.7,

134.3, 133.3, 130.8, 128.7, 127.6, 126.3, 119.3, 19.5; IR (KBr pellets) $v_{max}$:

3426 cm$^{-1}$ (NH), 1670 cm$^{-1}$ (CO); m/z (LC-MS) 211.10 [M$^+$]; Anal. Calcd (%)

for C$_{14}$H$_{13}$NO: C, 79.59; H, 6.20; N, 6.63; Found C, 79.58, H, 6.24, N, 6.65.

## N-p-Tolylbenzamide (Table 3, entry 15)
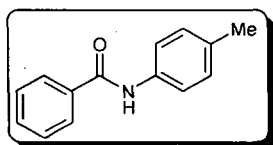


Off white solid; $R_f$= 0.47 [AcOEt:hexane (3:7)]; mp 156.5-157.2 °C; $^1$H NMR

(400 MHz, CDCl$_3$, TMS): δ 8.19-7.73 (m, 9H, Ar-H), 7.44 (br, s, 1H, NH), 2.12

(s, 3H, CH$_3$); $^{13}$C NMR (100 MHz, CDCl$_3$, TMS): δ 165.7, 135.8, 135.1, 134.4,

131.9, 129.8, 128.7, 127.4, 120.4, 20.6; IR (KBr pellets) $v_{max}$: 3423 cm$^{-1}$ (NH),

1667 cm$^{-1}$ (CO); m/z (LC-MS) 211.10 [M$^+$]; Anal. Calcd (%) for $C_{14}H_{13}NO$: C,

79.59; H, 6.20; N, 6.63; Found C, 79.62, H, 6.23, N, 6.64.

**N-Benzylbenzamide (Table 3, entry 16)**
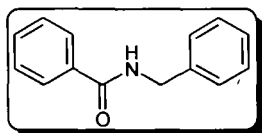


White solid; $R_f$ = 0.28 [AcOEt:hexane (3:7)]; mp 106.6-107.5 °C; $^1$H NMR (400

MHz, CDCl$_3$, TMS): δ 8.05-7.23 (m, 10H, Ar-H), 6.84 (br, s, 1H, NH), 4.01 (s,

2H, CH$_2$); $^{13}$C NMR (100 MHz, CDCl$_3$, TMS): δ 168.4, 142.4, 133.5, 131.2,

128.6, 128.3, 127.5, 127.1, 126.5, 49.3; IR (KBr pellets) $v_{max}$: 3443 cm$^{-1}$ (NH),

1675 cm$^{-1}$ (CO); m/z (LC-MS) 211.10 [M$^+$]; Anal. Calcd (%) for $C_{14}H_{13}NO$: C,

79.59; H, 6.20; N, 6.63; Found C, 79.56, H, 6.19, N, 6.67.

**N-Benzyl-4-methoxybenzamide (Table 3, entry 17)**
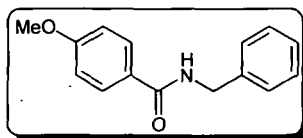


Colourless oil, $R_f$ = 0.23 [AcOEt:hexane (3:7)]; $^1$H NMR (400 MHz, CDCl$_3$,

TMS): δ 7.46 (d, $J$ = 8.27 Hz, 2H, Ar-H), 7.35-7.30 (m, 4H, Ar-H), 7.18-7.25

(m, 3H, Ar-H), 6.78 (br, s, 1H, NH), 4.02 (s, 2H, CH$_2$); $^{13}$C NMR (100 MHz,

CDCl$_3$, TMS): δ 170.2, 164.2, 144.5, 131.1, 129.7, 127.6, 127.4, 126.1, 113.1,

55.1, 50.2; IR (KBr pellets) $v_{max}$: 3389 cm$^{-1}$ (NH), 1685 cm$^{-1}$ (CO); m/z (LC-

MS) 241.11 [M$^+$]; Anal. Calcd (%) for $C_{15}H_{15}NO_2$: C, 74.67; H, 6.27; N, 5.81;

Found C, 74.63, H, 6.25, N, 5.82.

**Furan-2-carboxylic acid benzylamide (Table 3, entry 18)**
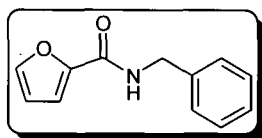
Liquid compound, $R_f$ = 0.19 [AcOEt:hexane (3:7)]; $^1$H NMR (400 MHz, CDCl$_3$,

TMS): δ 8.08 (br, s, 1H, NH), 7.95-6.52 (m, 8H, Ar-H), 4.02 (s, 2H, CH$_2$); $^{13}$C

NMR (100 MHz, CDCl$_3$, TMS): δ 164.9, 148.7, 144.4, 137.6, 129.3, 124.5,

119.8, 115.3, 112.5, 54.8; IR (KBr pellets) $v_{max}$: 3470 cm$^{-1}$ (NH), 1730 cm$^{-1}$

(CO); m/z (LC-MS) 201.08 [M$^+$]; Anal. Calcd (%) for C$_{12}$H$_{11}$NO$_2$: C, 71.63; H,

5.51; N, 6.96; Found C, 71.65, H, 5.50, N, 6.97.

*N*-Methylbenzamide$^{our\ work}$ (Table 3, entry 19)
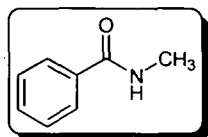


Pale yellow solid; $R_f$ = 0.64 [AcOEt:hexane (3:7)]; mp 76.1-78.1 °C; $^1$H NMR

(400 MHz, CDCl$_3$, TMS): δ 7.88-7.11 (m, 5H, Ar-H), 6.92 (br, s, 1H, NH), 2.52

(s, 3H, CH$_3$); $^{13}$C NMR (100 MHz, CDCl$_3$, TMS): δ 168.2, 140.3, 135.2, 130.4,

128.6, 127.2, 126.8, 44.8; IR (KBr pellets) $v_{max}$: 3451 cm$^{-1}$ (NH), 1668 cm$^{-1}$

(CO); m/z (LC-MS) 135.07 [M$^+$]; Anal. Calcd (%) for C$_8$H$_9$NO: C, 71.09; H,

6.71; N, 10.36; Found C, 71.11, H, 6.72, N, 10.32.

*N*-Cyclohexylbenzamide (Table 3, entry 20)
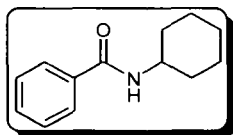


Yellow powder; $R_f$ = 0.39 [AcOEt:hexane (3:7)]; mp 144.7-145.2 °C; $^1$H NMR

(400 MHz, CDCl$_3$, TMS): δ 7.85-7.73 (m, 2H, Ar-H), 7.52-7.48 (m, 3H, Ar-H),

5.27 (br, s, 1H, NH), 3.54 (m, 1H, CH), 1.84-1.82 (m, 2H, CH$_2$), 1.62-1.54 (m,

2H, CH$_2$), 1.36-1.29 (m, 2H, CH$_2$), 1.14-1.07 (m, 2H, CH$_2$), 1.04-0.98 (m, 2H,

CH$_2$); $^{13}$C NMR (100 MHz, CDCl$_3$, TMS): δ 170.0, 138.2, 133.4, 129.4, 128.9, 127.2, 48.2, 41.3, 32.9, 25.5, 24.7; IR (KBr pellets) v$_{max}$: 3454 cm$^{-1}$ (NH), 1661 cm$^{-1}$ (CO); m/z (LC-MS) 203.13 [M$^+$]; Anal. Calcd (%) for C$_{13}$H$_{17}$NO: C, 76.81; H, 8.43; N, 6.89; Found C, 76.80, H, 8.41, N, 6.91.

*N*-(2,6-Dimethyl-4-nitrophenyl)benzamide$^{our\ work}$ (Table 3, entry 21)
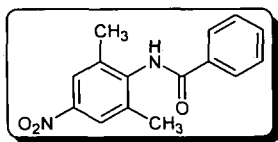


Pale yellow solid; R$_f$ = 0.21 [AcOEt:hexane (3:7)]; mp 195.1-197.1 °C; $^1$H NMR (400 MHz, CDCl$_3$, TMS): δ 7.95-7.44 (m, 7H, Ar-H), 7.13 (br, s, 1H, NH), 2.35 (s, 3H, CH$_3$), 2.15 (s, 3H, CH$_3$); $^{13}$C NMR (100 MHz, CDCl$_3$, TMS): δ 163.2, 148.7, 147.8, 143.8, 137.3, 133.6, 131.8, 130.6, 128.6, 127.5, 121.8, 18.5, 20.7; IR (KBr pellets) v$_{max}$: 3445 cm$^{-1}$ (NH), 1725 cm$^{-1}$ (CO); m/z (LC-MS) 270.10 [M$^+$]; Anal. Calcd (%) for C$_{15}$H$_{14}$N$_2$O$_3$: C, 66.66; H, 5.22; N, 10.36; Found C, 66.64, H, 5.26, N, 10.35.

*N*-Benzyl-2-phenylacetamide (Table 3, entry 22)
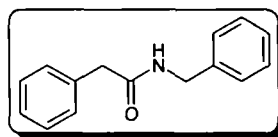


White solid; R$_f$ = 0.48 [AcOEt:hexane (3:7)]; mp 118.1-119.5 °C; $^1$H NMR (400 MHz, CDCl$_3$, TMS): δ 8.61 (br, s, 1H, NH), 7.71-7.27 (m, 10H, Ar-H), 4.43 (s, 2H, CH$_2$), 3.45 (s, 2H, CH$_2$); $^{13}$C NMR (100 MHz, CDCl$_3$, TMS): δ 170.6, 148.3, 141.3, 138.4, 135.1, 132.6, 129.7, 127.5, 121.8, 54.2, 41.7; IR (KBr pellets) v$_{max}$: 3451 cm$^{-1}$ (NH), 1669 cm$^{-1}$ (CO); m/z (LC-MS) 225.12 [M$^+$]; Anal. Calcd (%) for C$_{15}$H$_{15}$NO: C, 79.97; H, 6.71; N, 6.22; Found C, 79.94, H, 6.69, N, 6.20.

*N*-Phenylacetamide (Table 3, entry 23)
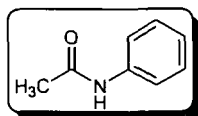


White solid; $R_f$ = 0.28 [AcOEt:hexane (3:7)]; mp 111.0-112.8 °C; $^1$H NMR (400 MHz, CDCl$_3$, TMS): δ 7.41-7.38 (m, 2H, Ar-H), 7.22-7.12 (m, 3H, Ar-H), 5.34 (br, s, 1H, NH), 2.07 (s, 3H, CH$_3$); $^{13}$C NMR (100 MHz, CDCl$_3$, TMS): δ 168.7, 140.8, 129.1, 124.4, 120.4, 19.6; IR (KBr pellets) $v_{max}$: 3410 cm$^{-1}$ (NH), 1706 cm$^{-1}$ (CO); m/z (LC-MS) 135.07 [M$^+$]; Anal. Calcd (%) for C$_8$H$_9$NO: C, 71.09; H, 6.71; N, 10.36. Found C, 71.06, H, 6.72, N, 10.34.

*N*-(2-Chlorophenyl)acetamide (Table 3, entry 24)
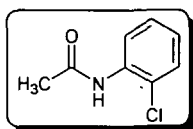


Colourless solid; $R_f$ = 0.22 [AcOEt:hexane (3:7)]; mp 88.7-89.1 °C; $^1$H NMR (400 MHz, CDCl$_3$, TMS): δ 7.91-7.32 (m, 4H, Ar-H), 7.08 (br, s, 1H, NH), 2.03 (s, 3H, CH$_3$); $^{13}$C NMR (100 MHz, CDCl$_3$, TMS): δ 169.2, 142.1, 134.1, 128.7, 124.2, 121.5, 18.4; IR (KBr pellets) $v_{max}$: 3415 cm$^{-1}$ (NH), 1711 cm$^{-1}$ (CO); m/z (LC-MS) 169.03 [M$^+$]; Anal. Calcd (%) for C$_8$H$_8$ClNO: C, 56.65; H, 4.75; N, 8.26. Found C, 56.65, H, 4.72, N, 8.22.

*N*-(3-Chlorophenyl)acetamide (Table 3, entry 25)
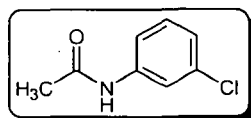


Off white crystalline needle; $R_f$ = 0.26 [AcOEt:hexane (3:7)]; mp 179.3-180.9 °C; $^1$H NMR (400 MHz, CDCl$_3$, TMS): 7.45 (br, s, 1H), δ 7.34 (s, 1H, Ar-H), 7.27-7.19 (m, 3H, Ar-H), 2.17 (s, 3H); $^{13}$C NMR (100 MHz, CDCl$_3$, TMS): δ

168.4, 136.4, 129.3, 129.0, 121.1, 29.7, 24.6; IR (KBr pellets) $v_{max}$: 3406 cm$^{-1}$

(NH), 1702 cm$^{-1}$ (CO); m/z (LC-MS) 169.03 [M$^+$]; Anal. Calcd (%) for

$C_8H_8ClNO$: C, 56.65; H, 4.75; N, 8.26. Found C, 56.62, H, 4.79, N, 8.25.

**N-(2-Nitrophenyl)acetamide (Table 3, entry 26)**
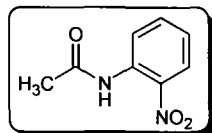


Milky white solid; $R_f$= 0.23 [AcOEt:hexane (3:7)]; mp 93.3-94.2 °C; $^1$H NMR

(400 MHz, CDCl$_3$, TMS): δ 7.93-7.41 (m, 4H, Ar-H), 7.19 (br, s, 1H, NH), 2.08

(s, 3H, CH$_3$); $^{13}$C NMR (100 MHz, CDCl$_3$, TMS): δ 167.1, 141.0, 133.0, 127.6,

123.1, 120.4, 17.6; IR (KBr pellets) $v_{max}$: 3435 cm$^{-1}$ (NH), 1725 cm$^{-1}$ (CO); m/z

(LC-MS) 180.05 [M$^+$]; Anal. Calcd (%) for $C_8H_8N_2O_3$: C, 53.33; H, 4.48; N,

15.55. Found C, 53.34, H, 4.50, N, 15.52.

**N-(3-Nitrophenyl)acetamide (Table 3, entry 27)**
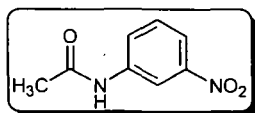


Light yellow solid; $R_f$ = 0.25 [AcOEt:hexane (3:7)]; mp 156.6-158.0 °C; $^1$H

NMR (400 MHz, CDCl$_3$, TMS): δ 7.90-7.38 (m, 4H, Ar-H), 7.17 (br, s, 1H,

NH), 2.10 (s, 3H, CH$_3$); $^{13}$C NMR (100 MHz, CDCl$_3$, TMS): δ 167.6, 141.5,

133.7, 128.1, 123.6, 120.9, 18.1; IR (KBr pellets) $v_{max}$: 3440 cm$^{-1}$ (NH), 1730

cm$^{-1}$ (CO); m/z (LC-MS) 180.05 [M$^+$]; Anal. Calcd (%) for $C_8H_8N_2O_3$: C,

53.33; H, 4.48; N, 15.55. Found C, 53.31, H, 4.48, N, 15.52.

**N-(4-Nitrophenyl)acetamide (Table 3, entry 28)**
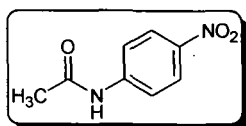
Pale yellow solid; $R_f$ = 0.29 [AcOEt:hexane (3:7)]; mp 208.4-209.8 °C; $^1$H

NMR (400 MHz, CDCl$_3$, TMS): δ 7.67 (d, $J$ = 6.78 Hz, 2H, Ar-H), 7.41 (d, $J$ =

6.78 Hz, 2H, Ar-H), 6.87 (br, s, 1H, NH), 2.34 (s, 3H, CH$_3$); $^{13}$C NMR (100

MHz, CDCl$_3$, TMS): δ 169.5, 142.4, 134.6, 129.0, 124.5, 121.8, 19.0; IR (KBr

pellets) $v_{max}$: 3443 cm$^{-1}$ (NH), 1733 cm$^{-1}$ (CO); m/z (LC-MS) 180.05 [M$^+$];

Anal. Calcd (%) for C$_8$H$_8$N$_2$O$_3$: C, 53.33; H, 4.48; N, 15.55. Found C, 53.35, H,

4.46, N, 15.58.

### *N*-(4-Methoxyphenyl)acetamide (Table 3, entry 29)
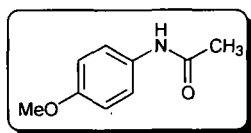


Light purple powder; $R_f$ = 0.32 [AcOEt:hexane (3:7)]; mp 137.7-138.4 °C; $^1$H

NMR (400 MHz, CDCl$_3$, TMS): δ 7.67 (br, s, 1H, NH), 7.36 (d, $J$ = 7.80 Hz,

2H, Ar-H), 7.09 (d, $J$ = 7.76 Hz, 2H), 2.29 (s, 3H, OCH$_3$), 2.12 (s, 3H, CH$_3$);

$^{13}$C NMR (100 MHz, CDCl$_3$, TMS): δ 168.5, 135.4, 133.9, 129.4, 120.1, 24.4,

20.8; IR (KBr pellets) $v_{max}$: 3378 cm$^{-1}$ (NH), 1674 cm$^{-1}$ (CO); m/z (LC-MS)

165.08 [M$^+$]; Anal. Calcd (%) for C$_9$H$_{11}$NO$_2$: C, 65.44; H, 6.71; N, 8.48. Found

C, 65.44, H, 6.74, N, 8.44.

### *N*-*p*-Tolylacetamide (Table 3, entry 30)
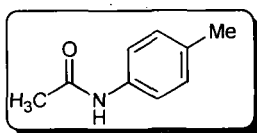


Off white solid; $R_f$ = 0.36 [AcOEt:hexane (3:7)]; mp 154.0-155.0 °C; $^1$H NMR

(400 MHz, CDCl$_3$, TMS): δ 8.51 (br, s, 1H, NH), 7.82 (d, $J$ = 5.92 Hz, 2H, Ar-

H), 7.64 (d, $J$ = 5.92 Hz, 2H, Ar-H), 2.38 (s, 3H, CH$_3$), 2.16 (s, 3H, CH$_3$); $^{13}$C

NMR (100 MHz, CDCl$_3$, TMS): δ 168.8, 137.3, 133.4, 129.8, 129.3, 120.4,

120.1, 21.9, 19.3; IR (KBr pellets) $v_{max}$: 3389 cm$^{-1}$ (NH), 1673 cm$^{-1}$ (CO); m/z

(LC-MS) 149.08 [M$^+$]; Anal. Calcd (%) for $C_9H_{11}NO$: C, 72.46; H, 7.43; N,

9.39. Found C, 72.45, H, 7.48, N, 9.37.

**$N$-(4-Hydroxyphenyl)acetamide (Table 3, entry 31)**
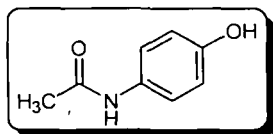


Light reddish solid; $R_f$ = 0.16 [AcOEt:hexane (3:7)]; mp 170.5-171.8 °C; $^1$H

NMR (400 MHz, CDCl$_3$, TMS): δ 10.22 (br, s, 1H, OH), 8.33 (br, s, 1H, NH),

7.80-7.47 (m, 4H, Ar-H), 2.10 (s, 3H, CH$_3$); $^{13}$C NMR (100 MHz, CDCl$_3$,

TMS): δ 170.1, 152.9, 134.3, 127.2, 127.9, 120.8, 119.8, 17.6; IR (KBr pellets)

$v_{max}$: 3396 cm$^{-1}$ (NH), 1679 cm$^{-1}$ (CO); m/z (LC-MS) 151.06 [M$^+$]; Anal. Calcd

(%) for $C_8H_9NO_2$: C, 63.56; H, 6.00; N, 9.27. Found C, 63.52, H, 6.01, N, 9.30.

**4-Acetylaminobenzoic acid (Table 3, entry 32)**
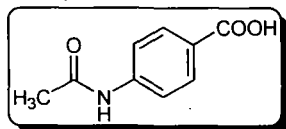


White solid; $R_f$ = 0.61 [AcOEt:hexane (3:7)]; mp 259.3-261.9 °C; $^1$H NMR (400

MHz, CDCl$_3$, TMS): δ 11.02 (br, s, 1H, OH), 8.98 (br, s, 1H, NH), 8.11 (d, $J$ =

7.68 Hz, 2H, Ar-H), 7.85 (d, $J$ = 7.68 Hz, 2H, Ar-H), 2.21 (s, 3H, CH$_3$); $^{13}$C

NMR (100 MHz, CDCl$_3$, TMS): δ 173.0, 169.3, 150.2, 139.6, 132.2, 123.3,

21.7; IR (KBr pellets) $v_{max}$: 3408 cm$^{-1}$ (NH), 1666 cm$^{-1}$ (CO); m/z (LC-MS)

179.06 [M$^+$]; Anal. Calcd (%) for $C_9H_9NO_3$: C, 60.33; H, 5.06; N, 7.82. Found

C, 60.30, H, 5.09, N, 7.84.

**$N$-Benzylacetamide (Table 3, entry 33)**
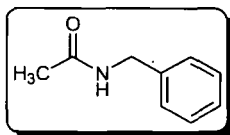
Yellow solid; $R_f$= 0.25 [AcOEt:hexane (3:7)]; mp 60.5-62.0 °C; $^1$H NMR (400 MHz, CDCl$_3$, TMS): δ 7.36-7.28 (m, 5H, Ar-H), 6.19 (br, s, 1H, NH), 4.09 (s, 2H, CH$_2$), 1.89 (s, 3H, CH$_3$); $^{13}$C NMR (100 MHz, CDCl$_3$, TMS): δ 170.9, 135.1, 129.4, 129.0, 127.3, 47.9, 13.7; IR (KBr pellets) $v_{max}$: 3416 cm$^{-1}$ (NH), 1671 cm$^{-1}$ (CO); m/z (LC-MS) 149.08 [M$^+$]; Anal. Calcd (%) for C$_9$H$_{11}$NO: C, 72.46; H, 7.43; N, 9.39. Found C, 72.44, H, 7.42, N, 9.42.

**2-Methyl-1$H$-benzimidazole (Table 3, entry 34)**
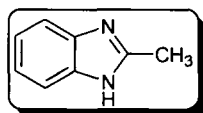


White solid; $R_f$= 0.31 [AcOEt:hexane (3:7)]; mp 175.6-177.1 °C; $^1$H NMR (400 MHz, CDCl$_3$, TMS): δ 7.50 (d, $J$ = 6.69 Hz, 2H, Ar-H), 7.41 (d, 2H, $J$ = 6.69 Hz, 2H, Ar-H), 5.42 (br, s, 1H, NH), 3.12 (s, 3H, CH$_3$); $^{13}$C NMR (100 MHz, CDCl$_3$, TMS): δ 150.2, 134.3, 132.7, 130.0, 126.5, 125.5, 122.9, 19.5; IR (KBr pellets) $v_{max}$: 3610 (NH), 2988 (CH), 1558 (CN); m/z (LC-MS) 132.07 [M$^+$]; Anal. Calcd (%) for C$_8$H$_8$N$_2$: C, 72.70; H, 6.10; N, 21.20. Found C, 72.74, H, 6.15, N, 21.24.

**$N$-Methylacetamide (Table 3, entry 35)**
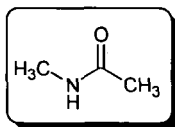


Colourless solid; $R_f$= 0.38 [AcOEt:hexane (3:7)]; mp 26.1-27.5 °C; $^1$H NMR (400 MHz, CDCl$_3$, TMS): δ 5.52 (br, s, 1H, NH), 2.82 (s, 3H, CH$_3$), 2.04 (s, 3H, CH$_3$); $^{13}$C NMR (100 MHz, CDCl$_3$, TMS): δ 170.8, 26.4, 23.1; IR (KBr pellets)

$v_{max}$: 3332 cm$^{-1}$ (NH), 1690 cm$^{-1}$ (CO); m/z (LC-MS) 73.05 [M$^+$]; Anal. Calcd

(%) for C$_3$H$_7$NO: C, 49.30; H, 9.65; N, 19.16. Found C, 49.34, H, 9.63, N,

19.15.

## *N*-Cyclohexylacetamide (Table 3, entry 36)
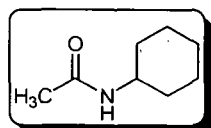


Yellow solid; R$_f$ = 0.32 [AcOEt:hexane (3:7)]; mp 101.0-103.3 °C; $^1$H NMR

(400 MHz, CDCl$_3$ TMS): δ 5.29 (br, s, 1H, NH), 4.05 (m, 1H, CH), 2.54 (s, 3H,

CH$_3$), 1.95-1.23 (m, 10H, CH$_2$), $^{13}$C NMR (100 MHz, CDCl$_3$, TMS): δ 172.5,

51.6, 43.9, 43.2, 33.0, 32.2, 23.6, 22.3; IR (KBr pellets) $v_{max}$: 3334 cm$^{-1}$ (NH),

1691 cm$^{-1}$ (CO); m/z (LC-MS) 141.12 [M$^+$]; Anal. Calcd (%) for C$_8$H$_{15}$NO: C,

68.04; H, 10.71; N, 9.92. Found C, 68.03, H, 10.69, N, 9.95.

## *N*-Benzylpropionamide (Table 3, entry 37)
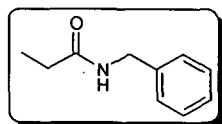


White solid; R$_f$ = 0.53 [AcOEt:hexane (3:7)]; mp 128.3-129.1 °C; $^1$H NMR (400

MHz, CDCl$_3$, TMS): δ 8.27 (br, s, 1H, NH), 7.87-7.36 (m, 5H, Ar-H), 2.17 (q,

2H, $J$ = 7.5 Hz, CH$_2$), 1.83 (t, $J$ = 7.5 Hz, 3H, CH$_3$), 1.23 (s, 3H, CH$_3$); $^{13}$C

NMR (100 MHz, CDCl$_3$, TMS): δ 170.2, 140.6, 129.8, 126.4, 122.3, 52.8, 28.1,

11.5; IR (KBr pellets) $v_{max}$: 3432 cm$^{-1}$ (NH), 1713 cm$^{-1}$ (CO); m/z (LC-MS)

163.10 [M$^+$]; Anal. Calcd (%) for C$_{10}$H$_{13}$NO: C, 73.59; H, 8.03; N, 8.58. Found

C, 73.55, H, 8.06, N, 8.62.

## *N*-Phenylbutyramide (Table 3, entry 38)
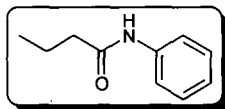
White solid; R$_f$= 0.57 [AcOEt:hexane (3:7)]; mp 93.6-94.8 °C; $^1$H NMR (400

MHz, CDCl$_3$, TMS): δ 8.53 (br, s, 1H, NH), 7.93-7.44 (m, 5H, Ar-H), 2.28 (t, $J$

= 7.6 Hz, 2H, CH$_2$), 1.68 (sextet, $J$ = 7.6 Hz, 2H, CH$_2$), 0.97 (t, $J$ = 7.6 Hz, 2H,

CH$_3$); $^{13}$C NMR (100 MHz, CDCl$_3$, TMS): δ 172.2, 138.5, 129.3, 123.5, 120.0,

118.2, 114.4, 39.3, 18.3, 13.9; IR (KBr pellets) ν$_{max}$: 3434 cm$^{-1}$ (NH), 1720 cm$^{-1}$

(CO); m/z (LC-MS) 163.10 [M$^+$]; Anal. Calcd (%) for C$_{10}$H$_{13}$NO: C, 73.59; H,

8.03; N, 8.58. Found C, 73.57, H, 8.62, N, 8.57.

*N*-Methylpropionamide$^{our\ work}$ (Table 3, entry 39)
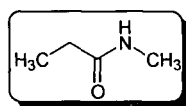


Colourless liquid; R$_f$= 0.27 [AcOEt:hexane (3:7)]; $^1$H NMR (400 MHz, CDCl$_3$,

TMS): δ 8.76 (s, 1H, NH), 2.74 (q, $J$ = 5.77 Hz, 2H, CH$_2$), 2.21 (t, $J$ = 5.77 Hz,

3H, CH$_3$), 1.15 (s, 3H, CH$_3$); $^{13}$C NMR (100 MHz, CDCl$_3$, TMS): δ 175.7, 27.6,

26.4, 12.8; IR (KBr pellets) ν$_{max}$: 3443 cm$^{-1}$ (NH), 1737 cm$^{-1}$ (CO); m/z (LC-

MS) 87.07 [M$^+$]; Anal. Calcd (%) for C$_4$H$_9$NO: C, 55.15; H, 10.41; N, 16.08.

Found C, 55.14, H, 10.44, N, 16.07.

**Cyclohexanecarboxylic acid phenylamide (Table 3, entry 40)**
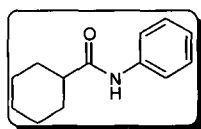


Yellow solid; R$_f$ = 0.31 [AcOEt:hexane (3:7)]; mp 148.2-149.5 °C; $^1$H NMR

(400 MHz, CDCl$_3$, TMS): δ 7.61-7.41 (m, 5H, Ar-H), 5.33 (br, s, 1H, NH), 3.58

(m, 1H, CH), 1.87-1.84 (m, 2H, CH$_2$), 1.72-1.69 (m, 2H, CH$_2$), 1.38-1.31 (m,

2H, CH$_2$), 1.17-1.03 (m, 4H, CH$_2$); $^{13}$C NMR (100 MHz, CDCl$_3$, TMS): δ

172.3, 139.4, 134.5, 130.2, 129.4, 128.3, 47.9, 42.4, 33.2, 26.4, 24.0; IR (KBr pellets) $v_{max}$: 3459 cm$^{-1}$ (NH), 1665 cm$^{-1}$ (CO); m/z (LC-MS) 203.13 [M$^+$]; Anal. Calcd (%) for $C_{13}H_{17}NO$: C, 76.81; H, 8.43; N, 6.89; Found C, 76.80, H, 8.43, N, 6.87.

**References:**

1. (a) Safari, J., et al. *Monatsh. Chem.* **141**, 1339--1345, 2010; (b) Choudary, M.B., et al. *J. Am. Chem. Soc.* **127**, 13167--13171, 2005.

2. Hattori, H. *Chem. Rev.* **95**, 537--550, 1995.

3. Pacchioni, G., et al. *Surf. Sci.* **275**, 450--458, 1992.

4. Sawai, J., et al. *World J. Microbiol. Biotechnol.* **16**, 187--194, 2000.

5. Peter, K.S. et al. *Langmuir* **18**, 6679--6686, 2002.

6. Greenberg, A., Breneman, C.M., & Liebman J.F. *The Amide Linkage: Selected Structural Aspects in Chemistry, Biochemistry, and Materials Science, (Eds.),* Wiley-Interscience, New York, 2000.

7. (a) Shaabani, A., et al. *Tetrahedron Lett.* **48**, 6137--6142, 2007; (b) Muthaiah, S., et al. *J. Org. Chem.* **75**, 3002--3006, 2010; (c) Mitsudome, T., et al. *Chem. Commun.* **14**, 3258--3260, 2009.

8. Soule, J-F., et al. *J. Am. Chem. Soc.* **133**, 18550--18553, 2011.

9. Yamaguchi, K., et al. *Chem. Lett.* **41**, 574--576, 2012.

10. Wang, Y., et al. *Angew. Chem. Int. Ed.* **51**, 7250--7253, 2012.

11. Wang, Y., et al. *Angew. Chem. Int. Ed.* **50**, 8917--8921, 2011.

12. Talukdar, D., et al. *Synlett.* **11**, 1597--1601, 2011.

13. Reddy, M.B.M., et al. *Catal. Lett.* **138**, 82--87, 2010.

14. (a) Das, V.K., et al. *Green Chem.* **14**, 847--854, 2012; (b) Das, V.K., et al. *Appl. Catal. A: Gen.* **456**, 118--125, 2013; (c) Das, V.K., et al. *J. Org. Chem.* **78**, 3361--3366, 2013; (d) Das, V.K., & Thakur, A.J. *Tetrahedron Lett.* **54**, 4164--4166, 2013; (f) Das, V.K., & Thakur, A.J. *ISRN Organic Chemistry* 1--6, 2013.

15. (a) Yacob, A.R., et al. *Eng. Technol.* **56**, 408--412, 2009; (b) Jung, H.S., et

   al. *J. Colloid Interface Sci.* **259**, 127--132, 2003.

16. (a) Xie, W.L., et al. *Appl. Catal. A* **300**, 67--74, 2006; (b) Forni, L. *Catal.*

   *Rev.* **8**, 65--115, 1974.

17. Arnold, K., et al. *Green Chem.* **10**, 124--134, 2008.

18. Herz, J.E., & Mantecon, R.E. *Org. Prep. Proc. Int.* **4**, 129--134, 1972.

19. Sheehan, J.C., & Hess, P.G. *J. Am. Chem. Soc.* **77**, 1067--1068, 1955.

20. Pearson, A.J., & Roush, W.R. *Handbook of Reagents for Organic Synthesis:*

   *Activating Agents and Protecting Groups*, Wiley, New York, 1999.

21. Chaudhari, P.S., et al. *Green Chem.* **12**, 1707--1710, 2010.

# Section II

# Highly active nano-MgO catalyzed, mild and efficient synthesis of amidines via electrophilic activation of amides

# Section II

## Highly active nano-MgO catalyzed, mild and efficient synthesis of amidines via electrophilic activation of amides

### 4.II.1 Introduction

More recently, nano magnesium oxide (MgO) has been utilized extensively because of its potential applications as catalyst.[1] In the domain of catalysis, MgO has a potent basic property which is exploited in various organic transformations[2] and also allows the high-yield synthesis of the significant molecules.[3] Synchronizing with the theme of green chemistry,[4] syntheses of N-bonded compounds under solvent-free condition have received much attention.[5]

Amidines are significant intermediates in the synthesis of many biologically active compounds[6] and there are many strategies reported in the literature for its synthesis.[7] They also serve as important synthons for the preparation of azacyclic compounds.[8] Thus, the synthesis of amidines is still a topic of immense scope. Here we disclose a practical, convenient and greener procedure for the synthesis of amidines under solvent-free condition at 70 °C catalyzed by nano-MgO (Scheme 1).



Scheme 1: Synthesis of amidine

Ogata *et al.*,[9] reported the synthesis of amidines in the presence of polyphosphoric acid trimethylsilyl ester by treating amine and amide in equimolar ratio at 160 °C under nitrogen atmosphere. But lower yield of the products, high reaction temperature, application of corrosive reagent and its non

reusability, and tiresome reaction condition made the methodology less advantageous. To the best of our knowledge, there is no report on nano-MgO catalyzed synthesis of amidines.

### 4.II.2 Result and discussion

#### 4.II.2.1 Optimization of the reaction condition for amidine synthesis

The study was initiated by the model reaction (Scheme 2) between **4** (5 mmol, 680 mg) and **5** (5 mmol, 0.45 mL) to give **6** without using any catalyst/solvent at 120 °C (Table 1). Under this condition, a mixture of unknown compounds was detected (Table 1, entry 1). Utilizing 5 mL of solvents (Table 1, entries 2-7) and conducting the reaction at lower temperature could not lead to product formation. As indicated in Table 1, when pyridine (10 mol%) was used as catalyst at 70 °C for this transformation then **6** was isolated in 7% yield (Table 1, entry 8). This observation prompted us to opt for the best base catalyst for the synthesis of **6**. Several base catalysts were tested under the current condition but the reaction could not be improved both in terms of yields and time (Table 1, entries 9-14). When fully characterized nano-MgO[10] was used under the present conditions, it increased the yield to a reasonable extent (Table 1, entry 15). To obtain better yield of **6**, the catalyst loading was optimized (Table 1, entries 15-18) and it was found that nano-MgO worked efficiently at 5 mol% (Table 1, entry 17). When the catalyst was changed to nano-$Al_2O_3$ and bulk MgO at 5 mol% loading under the similar conditions, low yields were recorded and were found to be inferior to nano-MgO (Table 1, entries 19 and 20). Bulk MgO having larger particles with smaller surface area was found to be less reactive than nano-MgO under the present reaction conditions. Overall, the reaction with nano-MgO was found to be very clean and no side product/by product (s) was formed.

**Table 1.** Optimization of reaction condition[a]
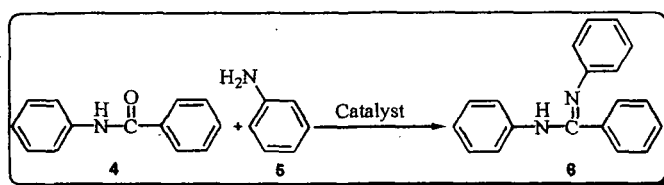


Scheme 2: Model reaction

| Entry | Catalyst | Solvent | Temp. (°C) | Time (h) | Yield (%)[b] |
|-------|----------|---------|-----------|----------|-----------|
| 1 | None | None | 120 | 20 | [c] |
| 2 | None | EtOH | 70 | 23 | NR[d] |
| 3 | None | MeOH | 70 | 18 | NR[d] |
| 4 | None | CH₃CN | 80 | 20 | NR[d] |
| 5 | None | THF | 70 | 22 | NR[d] |
| 6 | None | H₂O | 80 | 24 | NR[d] |
| 7 | None | DMSO | 100 | 16 | NR[d] |
| 8[e] | Pyridine | SFRC | 70 | 12 | 7 |
| 9[e] | K₂CO₃ | SFRC | 70 | 15 | 5 |
| 10[e] | NaOH | SFRC | 70 | 19 | 15 |
| 11[e] | KOH | SFRC | 70 | 24 | 10 |
| 12[e] | Et₃N | SFRC | 70 | 13 | Trace |
| 13[e] | PPh₃ | SFRC | 70 | 17 | [c] |
| 14[e] | Imidazole | SFRC | 70 | 17 | [c] |
| 15[e] | Nano-MgO[i] | SFRC | 70 | 7 | 80 |
| 16[f] | Nano-MgO[i] | SFRC | 70 | 5 | 85 |
| 17[g] | Nano-MgO[i] | SFRC | 70 | 3 | 94 |
| 18[h] | Nano-MgO[i] | SFRC | 70 | 9 | 80 |
| 19[g] | Bulk MgO | SFRC | 70 | 12 | 68 |
| 20[g] | Nano-Al₂O₃[j] | SFRC | 70 | 7 | 70 |

[a] Reaction condition: **4** (5 mmol, 680 mg) and **5** (5 mmol, 0.45 mL), SFRC or solvent (5 mL), stirring [b] Isolated yields, [c] Mixture of unknown compounds, [d] No reaction, [e] 10 mol% catalyst was used, [f] 7 mol% catalyst was used, [g] 5 mol% catalyst was used, [h] 3 mol% catalyst was used, [i] Particles size (17.4-16.4 nm), [j] Particle size (37.4–39.7 nm).

### 4.II.2.2 Nano-MgO catalyzed synthesis of amidine derivatives

With this efficient system in hand, we next extended the scope of the substrate to various alkyl/aryl amines (Table 2). We found that the reaction was applicable to a broad range of derivatives. However, a careful analysis of the results from the Table 2 indicate that amines with electron donating moiety reacted smoothly requiring less time (Table 2, entries 1-3), but amines substituted with electron-withdrawing functionality required more time to react (Table 2, entries 4 and 5) providing comparable yields. However, under the present conditions, in

comparision to aryl amines, cyclohexylamine furnished the desired amidine in good yield (Table 2, entry 6). In our studies, aniline was used to accomplish the corresponding amidine derivatives. when treated with N-phenylacetamide and cyclohexanecarboxylic acid phenylamide under the current reaction conditions (Table 2, entries 7 and 8). When electron withdrawing groups were present in the amide structure, the reaction took longer time for the formation of product (Table 2, entries 9 and 10). This might be due to the steric hindrance provided by the substituted phenyl groups in amide to the incoming nucleophile. When the reaction was performed involving both $R^1$ and $R^2$ as a methyl group, it furnished very poor yield (7%).

**Table 2.** Nano-MgO catalyzed synthesis of amidine derivatives [a] vide Scheme 1

| Entry | $R^1$ | $R^2$ | Time (h) | Yield (%)[b,c] | Melting point (°C)[9] |
|-------|-------|-------|----------|----------------|------------------------|
| 1 | $C_6H_5$ | $C_6H_5$ | 3 | 94 | 142.8-144.8 |
| 2 | $C_6H_5$ | $4-OCH_3C_6H_4$ | 3 | 94 | 108.1-109.6 |
| 3 | $C_6H_5$ | $4-CH_3C_6H_4$ | 3 | 93 | 130.8-131.2 |
| 4 | $C_6H_5$ | $4-NO_2C_6H_4$ | 5 | 90 | 182.7-183.5 |
| 5 | $C_6H_5$ | $4-ClC_6H_4$ | 6 | 91 | 140.1-141.3 |
| 6 | $C_6H_5$ | $C_6H_{11}$ | 5 | 85 | 142.0-142.8 |
| 7 | $CH_3$ | $C_6H_5$ | 5 | 92 | 126.3-127.8 |
| 8 | $C_6H_{11}$ | $C_6H_5$ | 6 | 88 | 110.0-111.7 |
| 9 | $4-NO_2C_6H_4$ | $C_6H_5$ | 5 | 89 | 150.6-153.4 |
| 10 | $4-ClC_6H_4$ | $C_6H_5$ | 5 | 88 | 149.1-149.3 |

[a] Reaction condition: 1 (1 mmol) and 2 (1 mmol), Nano-MgO (5 mol%), SFRC, stirring, [b] Yields refer to the isolated pure products, [c] Products were characterized by IR and NMR ($^1H$ and $^{13}C$) spectroscopy, MS and also by comparing their melting points with the authentic ones.

### 4.II.2.3 Possible mechanism for the synthesis of amidine

A tentative mechanism has been proposed for the synthesis of amidine derivatives (Scheme 3). It is hypothesized that the non-bonded pair of electron on oxygen atom of carbonyl moiety in amide possibly co-ordinates to the vacant $3p$ orbital of $Mg^{2+}$ of nano-MgO facilitating the electrophilic activation of amide (I). Now (II) can attack as a nucleophilic to form an intermediate (III). Finally the

elimination of water from (IV) gave rise to the formation of amidine (V). The

activation of the substrate by nano-MgO has been reported previously.[10]
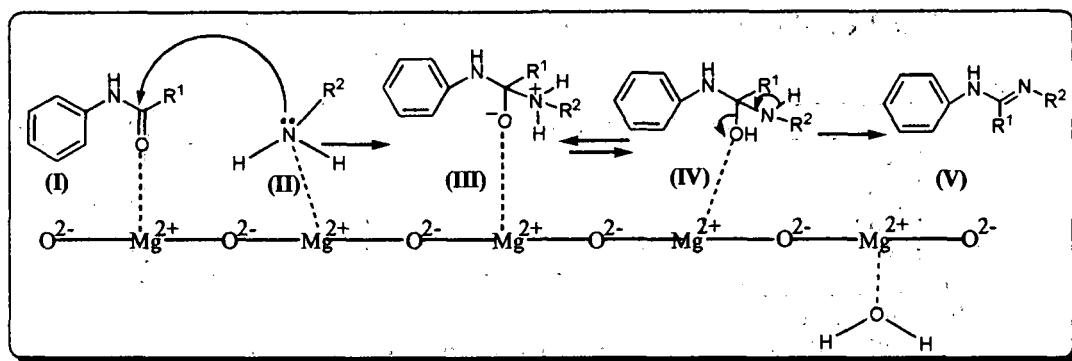


Scheme 3: Tentative mechanism for the synthesis of amidine

### 4.II.2.4 Investigation on recycling potential of nano-MgO

In this heterogeneous process, the catalyst was recyclable with a slight loss in

its activity (Table 3). After completion of the reaction (Scheme 2), the catalyst

was recovered from the reaction mixture by adding ethyl acetate (10 mL) under

centrifugation (3,500 r.p.m.). The extracted catalyst in this way was decanted and

finally dried in an oven at 100 °C for 7 h. It was then reused for the fresh reaction

(Figure 1). A slight decrease in catalytic activity was observed with recyclization

(Table 3).
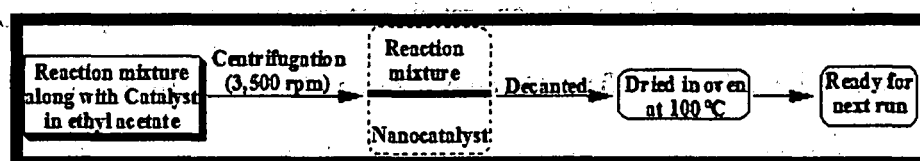


Figure 1. Flow sheet representation of catalyst isolation

In addition, the powder X-ray diffraction analysis exhibited identical peaks for

both the fresh and recovered nano-MgO [Figure 2(b)]. However, the intensity of

the peaks (2 2 0), (3 1 1), (4 1 1) and (3 3 1) diminished slightly which might be

due to loss during centrifugation and subsequent removal of the supernatant

liquid. The loss (15.4%) of the catalyst[10] [Figure 2(a)] was determined by UV

visible spectroscopy. This might be the reason for slight decrease in catalytic

activity of the catalyst.

**Table 3.** Recyclability[a] of nano-MgO

| Entry | Catalyst recovery (%) | Time (h) | Yield (%)[b] |
|---|---|---|---|
| 1st run[c] | 99 | 3 | 94 |
| 2nd run[c] | 96 | 4 | 94 |
| 3rd run[c] | 90 | 6 | 91 |
| 4th run[c] | 84 | 7 | 88 |

[a] Reaction condition: Nano-MgO (5 mol%), 4 (5 mmol, 680 mg), 5 (5 mmol, 0.45 mL), SFRC, [b] Yields refer to the isolated 6, [c] The recovered catalyst was used under identical reaction conditions to those for the 1st run.
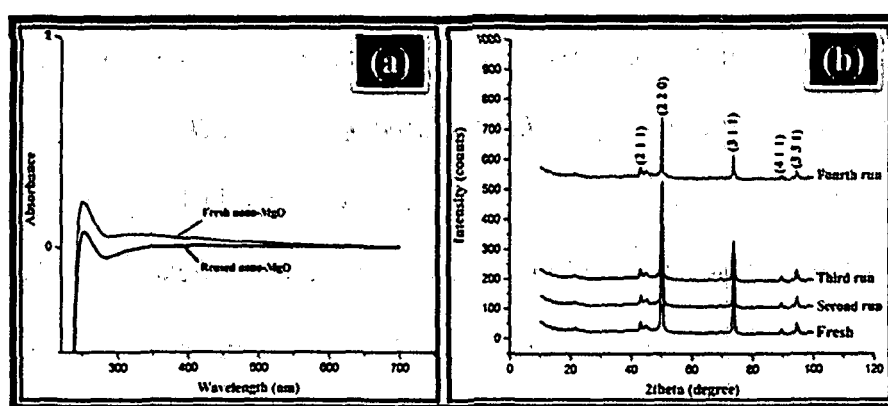


Figure 2. (a) UV-Visible spectra and (b) Powder XRD pattern of fresh and reused

nano-MgO

### 4.II.3 Conclusion

In conclusion, we have demonstrated that nano-MgO is highly active in

catalyzing the mild and efficient synthesis of amidine derivatives under solvent-

free condition at 70 °C. The method offers several advantages including excellent

yields of the products, safe handling, experimental simplicity, catalyst

recyclability and cost effectiveness which make it useful.

### 4.II.4 Experimental

#### 4.II.4.1 General Experimental Methods

Nano-MgO (The average particle diameter 18.12 nm, $S_{BET}$ =92.4 $m^2g^{-1}$ and 0.4

$mLg^{-1}$ and $\rho$ =3.58 $gcm^{-3}$, purity: 99.99%) was purchased from Sigma Aldrich

and used as received. The chemicals and reagents were purchased from Sigma-Aldrich, Merck, M/S S. D. Fine Chemicals Pvt. Ltd. and Loba chemical, and used without further purification. The XRD pattern was recorded with a Rigaku X-ray diffractometer. Melting points were determined in a Büchi 504 apparatus and are uncorrected. The leaching study was performed on UV visible spectrophotometer, Hitachi (U-2001, Tokyo, Japan). IR spectra were recorded as KBr pellets in a Nicolet (Impact 410) FT-IR spectrophotometer. $^1H$ and $^{13}C$ NMR spectra were recorded in a 400 MHz NMR spectrophotometer (JEOL, JNM ECS) using tetramethylsilane (TMS) as the internal standard and coupling constants are expressed in Hertz. Elemental analyses were carried out in a Perkin–Elmer CHN analyser (2400 series II). Mass spectra were recorded with a Waters Q-TOF Premier and Aquity UPLC spectrometer. The thermal analysis, TGA was done on a Shimadzu, USA thermal analyzer, TG50, with a nitrogen flow rate of 30 mL/min at heating rate of 10 °C/min. Reactions were monitored by thin-layer chromatography using aluminium sheets with silica gel 60 $F_{254}$ (Merck). Visualization was accomplished with UV lamp or $I_2$ stain.

### 4.II.4.2 Representative Procedure for the synthesis of N,N'-Diphenyl-benzamidine

To a two necked round bottomed flask (50 mL), nano-MgO (5.0 mol%, 2.0 mg) was added along with the addition of N-phenylbenzamide (1.0 mmol, 197 mg) and stirred (30 min) on a preset oil bath at 70 °C. After that aniline (1 mmol, 0.91 mL) was added, stirring was continued till the required time (the progress of the reaction was judged by TLC). The reaction mixture was brought to room temperature and ethyl acetate (3x10 mL) was added and centrifuged at 3500 rpm to pellet out the nanocatalyst. It was then washed with hot ethanol (5x10 mL) to

remove all the organic impurities. Finally, it was decanted and dried in an oven at 100 °C for 7 h. Then the catalyst was reused in the next run in the reaction. Having done this, the reaction mixture (in ethyl acetate) was washed with water and brine, dried over anhydrous $Na_2SO_4$, concentrated in a rotary evaporator and finally the crude product was purified by column chromatography (30% ethyl acetate: hexane as the eluent). All the products listed in Table 2 are known compounds and have been characterized by comparing with those reported ones.[10]

### 4.II.5 Physical and Spectroscopic data of selected compounds

**N,N'-Diphenyl-benzamidine (Table 2, entry 1)**
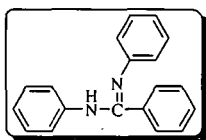


Off white solid; $R_f = 0.35$ (30% AcOEt: hexane); mp 142.8-144.8 °C; ^{1}H NMR (400 MHz, $CDCl_3$, TMS): δ 8.45 (br, 1H, NH), 7.46-7.52 (m, 15H, Ar-H); ^{13}C NMR (100 MHz, $CDCl_3$, TMS): δ 163.7, 153.4, 146.1, 132.5, 131.8, 130.2, 129.3, 128.1, 127.3, 125.0, 122.3, 118.4, 115.7; IR (KBr pellets) $v_{max}$: 3356 cm^{-1} (NH), 1618 cm^{-1} (CN); m/z (GC-MS) 272.13 [M[+]]; Anal. Calcd (%) for $C_{19}H_{16}N_2$: C, 83.79; H, 5.92; N, 10.29%. Found C, 83.73, H, 5.87, N, 10.26%.

**N,N-Diphenyl-formamidine (Table 2, entry 2)**
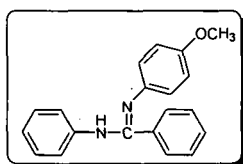


Pale yellow solid; $R_f = 0.37$ (30% AcOEt:hexane); mp 108.1-109.6 °C; ^{1}H NMR (400 MHz, $CDCl_3$, TMS): δ 8.78 (br, 1H, NH), 3.46 (s, 3H, $CH_3$), 7.40-7.58 (m,

14H, Ar-H); $^{13}$C NMR (100 MHz, CDCl$_3$, TMS): δ 163.3, 153.1, 146.4, 132.1, 131.2, 130.0, 129.2, 128.7, 127.5, 125.3, 122.6, 118.2, 115.3, 56.7; IR (KBr pellets) $v_{max}$: 3360 cm$^{-1}$ (NH), 1621 cm$^{-1}$ (CN); m/z (GC-MS) 302.14 [M$^+$]; Anal. Calcd (%) for C$_{20}$H$_{18}$N$_2$O: C, 79.44; H, 6.00; N, 9.26; Found C, 79.31, H, 5.81, N, 8.94.

*N*-Phenyl-*N'*-p-tolyl-benzamidine (Table 2, entry 3)
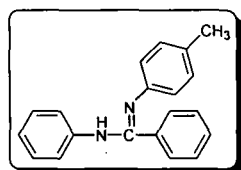


Light brown solid; R$_f$= 0.45 (30% AcOEt:hexane); mp 130.8-131.2 °C; $^1$H NMR (400 MHz, CDCl$_3$, TMS): δ 8.70 (br, 1H, NH), 2.46 (s, 3H, CH$_3$), 6.58-7.25 (m, 14H, Ar-H); $^{13}$C NMR (100 MHz, CDCl$_3$, TMS): δ 163.8, 154.1, 146.6, 133.2, 132.5, 131.4, 130.3, 129.6, 127.7, 125.8, 122.7, 118.8, 115.7, 21.3; IR (KBr pellets) $v_{max}$: 3343 cm$^{-1}$ (NH), 1627 cm$^{-1}$ (CN); m/z (GC-MS) 286.15 [M$^+$]; Anal. Calcd (%) for C$_{20}$H$_{18}$N$_2$: C, 83.88; H, 6.34; N, 9.78. Found C, 83.53; H, 6.27; N, 9.45.

4-Nitro-*N*,*N'*-diphenyl-benzamidine (Table 2, entry 9)
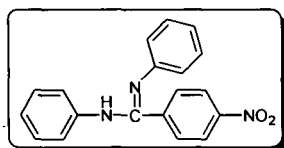


Off white solid; R$_f$= 0.67 (30% AcOEt:hexane); mp 150.6-153.4 °C, $^1$H NMR (400 MHz, CDCl$_3$, TMS): δ 8.03 (br, 1H, NH), 7.70-7.98 (m, 14H, Ar-H); $^{13}$C NMR (100 MHz, CDCl$_3$, TMS): δ 164.2, 153.5, 149.7, 146.2, 139.4, 129.6, 127.1, 126.6, 123.4, 122.2, 118.1, 115.1, 114.3; IR (KBr pellets) $v_{max}$: 3420 cm$^{-1}$ (NH), 1538 (NO), 1642 cm$^{-1}$ (CN); m/z (GC-MS) 317.12 [M$^+$]; Anal. Calcd (%) for C$_{19}$H$_{15}$N$_3$O$_2$: C, 71.91; H, 4.76; N, 13.24. Found C, 71.69, H, 4.45, N, 12.93.

**4-Chloro-*N*,*N'*-diphenyl-benzamidine (Table 2, entry 10)**
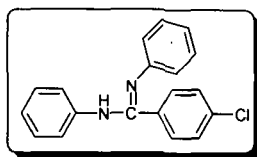


Light yellowish brown solid, $R_f$= 0.76 (30% AcOEt:hexane); mp 149.1-149.3 °C;

$^1$H NMR (400 MHz, CDCl$_3$, TMS): δ 9.3 (br, 1H, NH), 7.39-7.89 (m, 14H, Ar-

H); $^{13}$C NMR (100 MHz, CDCl$_3$, TMS): δ 164.4, 153.6, 149.8, 146.5, 136.5,

129.7, 127.3, 126.8, 123.6, 122.4, 118.3, 115.4, 114.7; IR (KBr pellets) $v_{max}$:

3388 cm$^{-1}$ (NH), 1626 (CN); m/z (GC-MS) 306.09 [M$^+$]; Anal. Calcd (%) for

C$_{19}$H$_{15}$ClN$_2$: C, 74.38; H, 4.93; N, 9.13. Found C, 74.16, H, 4.66, N, 8.87.

# References:

1. (a) Climent, M.J., et al. *J. Catal.* **247**, 223--230, 2007; (b) Liang, S.H.C., & Gay, I.D. *J. Catal.* **101**, 293--300, 1986; (c) Tsuji, H., et al. *J. Catal.* **148**, 759--770, 1994; (d) Sadjadi, S., et al. *Monatsh. Chem.* **140**, 1343--1347, 2009; (e) Safari, J., et al. *Monatsh. Chem.* **141**, 1339--1345, 2010; (f) Choudary, B.M., et al. *J. Am. Chem. Soc.* **127**, 13167--13171, 2005; (g) Kumar, D., et al. *Tetrahedron* **63**, 3093--3097, 2007.

2. Hattori, H. *Chem. Rev.* **95**, 537--558, 1995.

3. Lamb, H.H., et al. *J. Am. Chem. Soc.* **111**, 8367--8373, 1989.

4. Anastas, P.T., & Warner, J.C. in *Green Chemistry: Theory and Practice*, Oxford University Press: New York, 1998.

5. (a) Martins, M.A.P., et al. *Chem. Rev.* **109**, 4140--4182, 2009; (b) Walsh, P.J., et al. *Chem. Rev.* **107**, 2503--2545, 2007; (c) Tanaka, K., & Toda, F. *Chem. Rev.* **100**, 1025--1074, 2000; (d) Nagendrappa, G. *Resonance* **7**, 59--68, 2002; (e) Tanaka, K. *Solvent-free Organic Synthesis*; Wiley-VCH: Weinheim, 2009.

6. (a) Gautier, J.A., Miocque, M., & Farnoux, C.C. in *The Chemistry of Amidines and Imidates*; Patai, S., Ed.; John Wiley & Sons: New York, Sydney, Toronto, 1975; (b) Granik, V. G. *Russ. Chem. Rev.* **52**, 377--393, 1983.

7. (a) Katritzky, A.R., Meth-Cohn, O., & Rees, C.W. *Comprehensive Organic Functional Group Transformations*, eds., Pergamon Press, Oxford, 1995; (b) Shriner, R.L., et al. *Chem. Rev.* **35**, 351--425, 1944; (c) Santos, M.S., et al. *Quim. Nova* **29**, 1301--1306, 2006; (d) Kishore, K. et al. *Tetrahedron Lett.* **45**, 6991--6994, 2004; (e) Gupta, S., et al. *Tetrahedron Lett.* **51**, 1887--1890, 2010.

8. Usui, H., et al. *J. Heterocycl. Chem.* **30**, 551--552, 1993.

9. Ogata, S.-I., et al. *Bull. Chem. Soc. Jpn.* **59**, 2171--2177, 1986.

10. Das, V.K., et al. *Appl. Catal. A: Gen.* **456**, 118--125, 2013.

# Chapter 5

# Chapter 5

## Piper-Betle-Shaped Nano-S Catalyzed Synthesis of 1-Amidoalkyl-2-naphthols under Solvent-Free Reaction Condition: A Greener "Nanoparticle-Catalyzed Organic Synthesis Enhancement" Approach
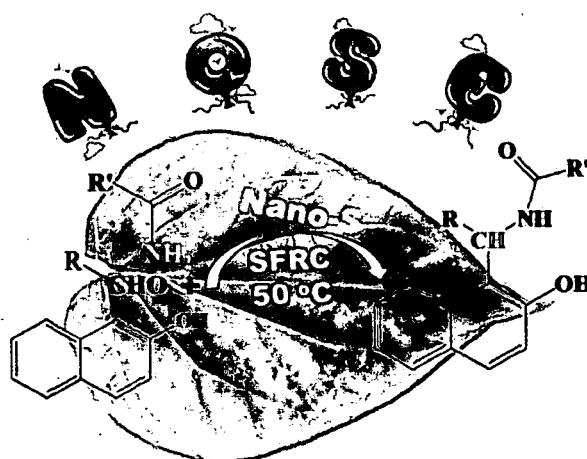
# Piper-Betle-Shaped Nano-S Catalyzed Synthesis of 1-Amidoalkyl-2-naphthols under Solvent-Free Reaction Condition: A Greener "Nanoparticle-Catalyzed Organic Synthesis Enhancement" Approach

## *5.1 Introduction*

In the modern theme of investigation of science, nanotechnology is mastering intricacies for the synthesis and application of interesting nanomaterials.[1] In the field of nanotechnology, nanoparticles has been traced the tremendous awareness as nanocatalysis [2] which can be modeled as the frontiers between the homogeneous and heterogeneous catalysis.[3] Hence, nanocatalysis should proffer the prospects for the synthesis of biologically important and synthetically challenging compounds.[4]

Over the past few years synthesis and application of sulfur in bulk or micro or nano form has been persisting significance due to its remarkable applications in phosphatic fertilizers, plastics, enamels, antimicrobial agents, gun powders, petroleum refining, ore leaching processes, pulp and paper industries, and in agrochemical industries.[5] Its nanostructures are valuable for the synthesis of sulfur nanocomposites for lithium batteries, [6] modification of carbon nanostructures,[7] in the synthesis of sulfur nanowires with carbon to form hybrid materials with useful properties for gas sensor and catalytic applications.[8] There are some reports on the preparation and properties of sulfur nanoparticles.[9]

The multi component reactions (MCRs) are promising as a constructive source for devising small drug-like molecules with several levels of structural diversity owing to the fact that these involve three or more compounds reacting in a single event, but in a row to form new products.[10] These reactions are also being greeted

in terms of practical considerations and economic viability.[11] In the premise of

green chemistry,[12] MCRs under solvent free reaction condition (SFRC)[13a-d] are

fascinating since it involves the best reaction medium with 'no medium'.[13e]

In the current hours of interest, the synthesis of 1-amidoalkyl-2-naphthol

derivatives[14] have been continued under hot topic of research on account of

bearing 1,3-amino-oxygenated functional groups which are ubiquitous to a

variety of biologically important natural products and potent drugs, including a

number of nucleoside antibiotics and HIV protease inhibitors, such as ritonavir

and lipinavir.[15] Additionally, $\alpha$-amidomethyl-$\beta$-naphthol also exhibit depressor[16a]

and bradycardia effects in humans,[16b] as a ligand in asymmetric synthesis[16c] and

as a catalyst.[16d] Thus, the synthesis of $\alpha$-amidomethyl-$\beta$-naphthol is still in

demand.

There are numerous approaches described in the literature for the synthesis of 1-

amidoalkyl-2-naphthols. These protocols[17] suffer from shortcomings such as

large waste production, higher reaction temperature, prolonged reaction time, low

yields, harsh conditions, undesirable byproducts, toxicity, low recovery, and

reusability of the catalyst. Therefore, to overcome those drawbacks and in our

continual interest in the growth of "NOSE" (Nanoparticle-catalyzed Organic

Synthesis Enhancement) chemistry,[18] we herein repot a convenient protocol for

novel sulfur nanoparticle-catalyzed synthesis of 1-amidoalkyl-2-naphthols under

SFRC at 50 °C (Scheme 1). To the best of our knowledge, nano-S-catalyzed
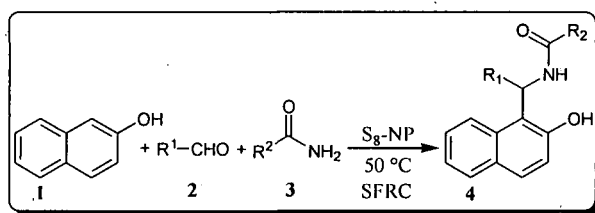


Scheme 1: Synthesis of 1-amidoalkyl-2-naphthols

synthesis of 1-amidoalkyl-2-naphthols is not yet reported.

## 5.2 Results and discussion

### 5.2.1 Characterization of nano-S₈

The preparation of nano-S was accomplished by annealing of elemental sulfur which in turn was achieved by catalytic conversion of $H_2S$.[19] To characterize the sulfur nanoparticles synthesized at 120 °C and 180 °C, the EDX analysis was performed to find the elemental composition. EDX confirmed the presence of sulfur element only [figure 1(a)]. Both atomic and weight percent for pure nano-S was found 100%. SEM image [figure 1(b)] of pure nano-S explored its sheet like structure that might be due to the stronger intermolecular forces of attraction amongst the sulfur molecules. The TGA curve [figure 1(c)] indicated the thermal stability having two step pattern of weight loss within 180-290 °C. The first weight loss (<180 °C) is attributed to the evaporation of physically absorbed water and the second weight loss at 290 °C is accompanied by the active liberation of $H_2S$ [figure 1(c)].
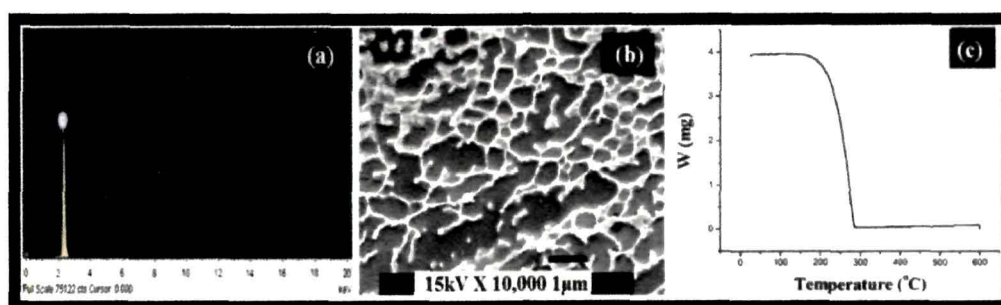


Figure 1. a) EDX analysis, b) SEM image, and c) TGA curve of pure nano-S

The X-ray diffraction patterns (figure 2) for (a) bulk-S, (b) nano-S₈ synthesized at 120 °C and (c) at 180 °C revealed that the samples (a), (b) and (c) showed peaks corresponding to (2 2 2), (0 2 6), (1 1 7), (3 1 3), (0 4 4), (0 6 2), (0 6 6), (3 5 7) and (5 5 1) planes indicating the presence of cubic orthorhombic face centered S₈ (i.e. α-form) with face centred lattice sites (JCPDS PDF # 78-1889).

The sharp XRD peaks of bulk sulfur (figure 2a) got broadened on annealing to 120 °C and 180 °C [fig. 2(b) and 2(c)] which confirmed the transformation into the nano form. The crystallite sizes were found to lie between 13.8-25.6 nm in (b) and 7.3-5.4 nm in (c) calculated from the X-ray line broadening by applying full width half maximum (FWHM) of characteristic peaks (2 2 2) and (1 1 7) to the Scherrer equation. These sizes are consistent with those measured from the TEM images, indicating the single crystal structure of nanoparticles.
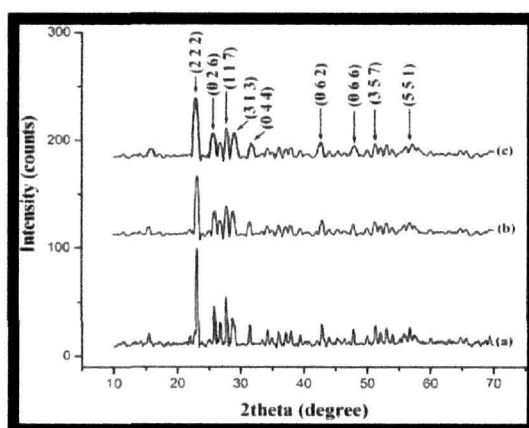


Figure 2. XRD pattern of (a) pure bulk sulfur, (b) nano sulfur annealed at 120 °C and (c) nano sulfur annealed at 180 °C

High-resolution TEM (figure 3) showed that the majority of isolated particles were having piper betle shape and a very few were of spherical structure with an average diameter of 5.2 nm [Figure 3(a)] and 18.3 nm [figure 3(b)] respectively.
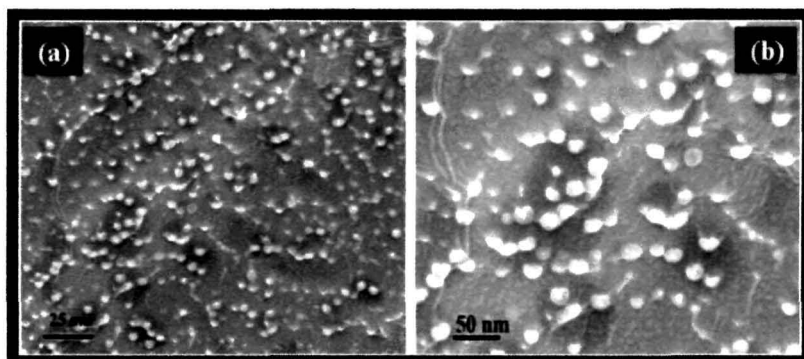


Figure 3. TEM micrographs of nano-S at a) 25 nm and b) 50 nm scale

## 5.2.2 Optimization of the reaction conditions

With the idea of developing a green procedure with almost no waste produced for the synthesis of amidoalkyl-naphthol derivatives, the optimization of the reaction condition (Table 1) was performed by considering the model reaction (scheme 2) among 2-naphthol **5**, urea **6** and benzaldehyde **7** at room temperature under neat condition by grinding with mortar and pestle but the reaction did not proceed (Table 1, entry 1). Stirring the reaction mixture at 50 °C/ 70 °C/ 120 °C aerobically (16 h) also could not form any product (Table 1, entries 2-4). These negative results sensed the necessity of a catalyst.

**Table 1.** Optimization of reaction condition[a]
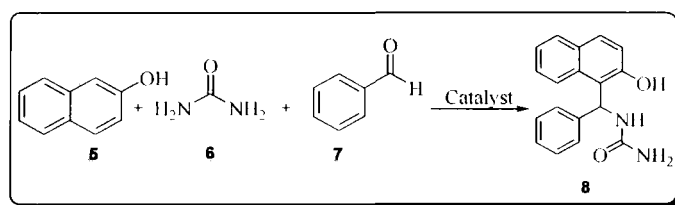


Scheme 2: Model reaction

| Entry | Catalyst | Solvent | T (°C) | T (h) | Yield (%)[b] |
|-------|----------|---------|--------|-------|--------------|
| 1 | None | SFRC | rt[h] | 3 | NR[c] |
| 2 | None | SFRC | 50 | 16 | NR[c] |
| 3 | None | SFRC | 70 | 16 | NR[c] |
| 4 | None | SFRC | 120 | 16 | NR[c] |
| 5 | [d]Nano-MgO | SFRC | 50 | 5 | 32 |
| 6 | [e]Nano-Al$_2$O$_3$ | SFRC | 50 | 5 | 25 |
| 7 | [f]Nano-TiO$_2$ | SFRC | 50 | 6 | [j] |
| 8 | [g]Nano-S$_8$ | SFRC | 50 | 30[k] | 98 |
| 9 | [g]Nano-S$_8$ | SFRC | 60[i] | 30[k] | 52 |
| 10 | [g]Nano-S$_8$ | EtOAc | 50 | 6 | 48 |
| 11 | [g]Nano-S$_8$ | MeOH | 50 | 7 | 24 |
| 12 | [g]Nano-S$_8$ | EtOH | 50 | 7 | 26 |
| 13 | [g]Nano-S$_8$ | THF | 50 | 9 | 44 |
| 14 | [g]Nano-S$_8$ | Toluene | 50 | 5 | [j] |
| 15 | [g]Nano-S$_8$ | H$_2$O | 50 | 12 | 12 |
| 16 | Pyridine | SFRC | 50 | 8 | 17 |
| 17 | Imidazole | SFRC | 50 | 8 | 17 |
| 18 | Et$_3$N | SFRC | 50 | 8 | 15 |
| 19 | PPh$_3$ | SFRC | 50 | 8 | 17 |

[a] Reaction condition: Benzaldehyde (0.3 mL, 3mmol), urea (0.180 g, 3mmol), naphthol (0.432 g, 3mmol), SFRC or solvent (5mL). [b] Isolated yields. [c] No reaction was observed, 3.5 mol% catalyst was used. Particles sizes: [d] (17.4-16.4nm), [e] (37.4-39.7nm), [f] (<80 nm), [g] (5.2-18.3 nm). [h] Grinded. [i] Ultrasound. [j] Trace. [k] Minute.

Next, we investigated the reaction by using nanocatalysts (3.5 mol%) under SFRC at 50 °C (Table 1, entries 5-9). To our surprise, the mentioned nanocatalysts furnished the products in trace to poor yields but nano sized $S_8$ showed outstanding activity in the formation of desired product **8** (Table 1, entry **8**) in excellent yields within much shorter time. The reaction was very clean with no side product formation. In order to check the effect of solvents (if any) in the reaction, several solvents were screened. The reactions were sluggish, gave poor yield with longer reaction time and tiresome catalyst isolation in the presence of solvents (Table 1, entries 10-15). This may be attributed to the aggregation of sulfur nanoparticles which might reduce its surface area and blocked the active sites. Notably, the bulk basic catalysts were not effective in the reaction (Table 1, entries 16-19).

We also examined the influence of catalyst loading in the model reaction (scheme 2). The results are summarised in the table 2 and graphically in figure 4 which indicated that the catalytic efficiency of nano-$S_8$ increased from 1 to 3 mol% and showed the maximum efficiency at 3.5 mol% loading.

**Table 2.** Optimization of catalyst loading[a]

| Entry | Catalyst loading (mol%) | Time (h) | Yield (%)[b] |
|-------|------------------------|----------|--------------|
| 1 | 1 | 5 | 44 |
| 2 | 2 | 3 | 58 |
| 3 | 3 | 2 | 70 |
| 4 | 3.5 | 30 min | 98 |
| 5 | 4 | 50 min | 80 |
| 6 | 5 | 1 | 74 |
| 7 | 7 | 2 | 60 |
| 8 | 2 | 30 min | 17 |
| 9 | 4 | 30 min | 22 |
| 10 | 6 | 30 min | 38 |
| 11 | 7 | 30 min | 40 |
| 12 | 8 | 30 min | 43 |

[a] Reaction was performed at 50 °C under SFRC and aerobic conditions using nano-$S_8$. [b] Isolated yield.

Increasing catalyst loading keeping the reaction time constant (30 min), did

not improve the yield (Table 2, entries 8-12).
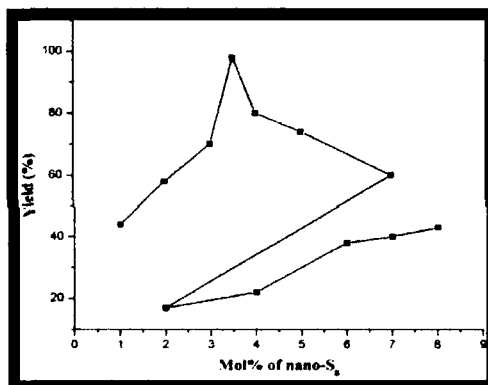


Figure 4. Graph of isolated yield of 8 versus mol% of nano-S$_8$

### 5.2.3 Nano-S catalyzed synthesis of 1-amidoalkyl-2-naphthol derivatives

To generalise the reaction, various benzaldehyde derivatives were tested with

naphthol and urea/acetamide under the standardized condition and the outcomes

were summarized in table 3. Vaghei et. al reported the synthesis of (4-

Hydroxyphenyl)-(2-hydroxynaphthalen-1-yl)methyl using catalytic amount of

TBBDA.[17e] Since then and before there was no report involving 4-hydroxy

benzaldehyde as a starting material but using nano-S it reacted efficiently with

urea/acetamide/benzamide and naphthol furnishing the desired product in

excellent yields (Table 3, entries 5, 15 and 20). No by-products were formed.

Overall, the aldehydes which were in the liquid state favoured the product

formation efficiently due to best the possible mixing although the reactions were

conducted under SFRC. The transformation of benzaldehydes carrying different

electron withdrawing and electron donating moieties into the corresponding

amidoalkyl naphthol products proceeded smoothly under the present reaction

condition that demonstrated the compatibility of those moieties towards the

reaction condition.

**Table 3.** Nano-S catalyzed synthesis of amidoalkyl naphthols

| Entry | $R^1$ | $R^2$ | Time (min) | Yield (%)[a,b] |
|-------|-------|-------|------------|---------------|
| 1 | $C_6H_5$ | $NH_2$ | 30 | 98 |
| 2 | $4\text{-}ClC_6H_4$ | $NH_2$ | 15 | 94 |
| 3 | $3\text{-}NO_2C_6H_4$ | $NH_2$ | 15 | 94 |
| 4 | $4\text{-}OCH_3C_6H_4$ | $NH_2$ | 35 | 92 |
| 5 | $4\text{-}OHC_6H_4$ | $NH_2$ | 45 | 92 |
| 6 | $trans\text{-}C_6H_4CHCH$ | $NH_2$ | 30 | 92 |
| 7 | 2-Furyl | $NH_2$ | 30 | 94 |
| 8 | 2-Thienyl | $NH_2$ | 30 | 95 |
| 9 | $2\text{-}CH_3C_6H_4$ | $CH_3$ | 30 | 91 |
| 10 | $CH_3CH_2$ | $CH_3$ | 60 | 84 |
| 11 | $CH_3CH_2CH_2$ | $CH_3$ | 60 | 85 |
| 12 | $3\text{-}NO_2C_6H_4$ | $CH_3$ | 10 | 90 |
| 13 | $2\text{-}ClC_6H_4$ | $CH_3$ | 25 | 91 |
| 14 | $C_6H_5$ | $CH_3$ | 30 | 95 |
| 15 | $4\text{-}OHC_6H_4$ | $CH_3$ | 25 | 90 |
| 16 | $trans\text{-}C_6H_4CHCH$ | $CH_3$ | 45 | 90 |
| 17 | $C_6H_5$ | $C_6H_5$ | 30 | 95 |
| 18 | $4\text{-}CH_3C_6H_4$ | $C_6H_5$ | 30 | 95 |
| 19 | $4\text{-}ClC_6H_4$ | $C_6H_5$ | 30 | 95 |
| 20 | $4\text{-}OHC_6H_4$ | $C_6H_5$ | 25 | 95 |
| 21 | $CH_3CH_2CH_2$ | $C_6H_5$ | 40 | 90 |

[a] Yields refer to the isolated pure products. [b] Products were characterized by IR and NMR ($^1H$ and $^{13}C$ spectroscopy, MS and also by comparing their melting points with the authentic ones. [c] Mixture of unknown products.

### 5.2.4 Possible mechanism for the formation of 1-amisoalkyl-2-naphthol derivatives
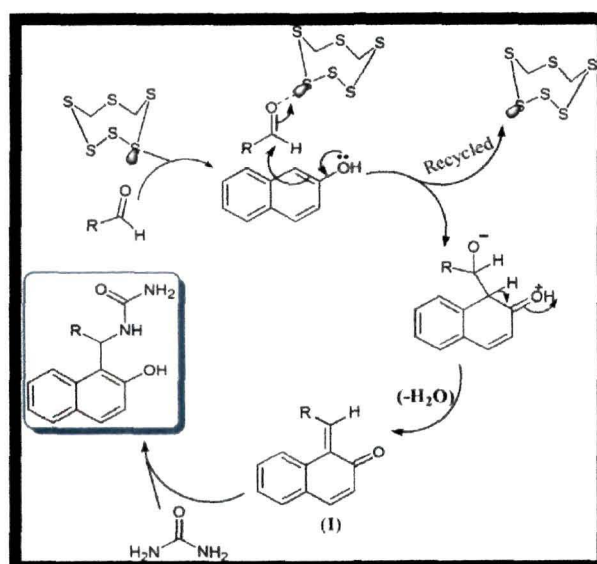


Figure 5. Plausible mechanism for nano-S catalyzed synthesis of 1-amidoalkyl-2-naphthol

A plausible mechanism explaining the sequence of the events is tailored in figure 5. We presumed that the reaction proceeded via *ortho*-quinone methides(*o*-QMs)[20] (I) formed by the nucleophilic addition of 2-naphthol to an aldehyde which was activated by nano-S. Finally, (I) reacted with amides/urea via Michael addition to produce amidoalkyl naphthols. The activation of the aldehydes akin to it, have been previously reported with the sulphur containing catalysts.[17d, 21]

### 5.2.5 Investigation of recycling potential of nano-$S_8$

The data assembled from the catalyst recyclability test (Table 4) delineated that the nano-S was equally active in the synthesis of **8** (scheme 2) from fresh up to the 5th cycle and after that its yield slightly decreased with a bit longer reaction time. The TONs (turn over numbers) were also maintained from fresh up to the 5th cycle and then dropped off to some extent.

**Table 4.** Catalyst recyclability test

| Entry | Number of cycles[a] | Time (min) | Yield (%)[b] | TONs |
|-------|---------------------|------------|--------------|------|
| 1 | Fresh | 30 | 98 | 84.0 |
| 2 | 1st cycle | 30 | 98 | 84.0 |
| 3 | 2nd cycle | 30 | 98 | 84.0 |
| 4 | 3rd cycle | 30 | 98 | 84.0 |
| 5 | 4th cycle | 30 | 98 | 84.0 |
| 6 | 5th cycle | 45 | 98 | 84.0 |
| 7 | 6th cycle | 60 | 90 | 77.1 |
| 8 | 7th cycle | 90 | 85 | 72.8 |

[a] Reaction condition: Benzaldehyde (1.02 mL, 10 mmol), urea (0.6 g, 10 mmol), naphthol (1.44 g, 10 mmol), SFRC. [b] Isolated yields.

The XRD pattern of the reused nano-S after 3rd and 5th run were compared with the fresh one [figure 6 (a)]. The reused nano-S after 3rd run demonstrated unchanged morphology but after 5th run showed a slight diminution in the intensity of the highest peak (2 2 2) and an increase in the intensity of (5 5 1) peak. It might be due to the dislocation in the crystal planes[18] during the consecutive cycles. The TEM micrograph [figure 6 (b)] after 5th run portrayed the

aggregation of the particles that might have reduced the activity of nano-S affording poorer yield.
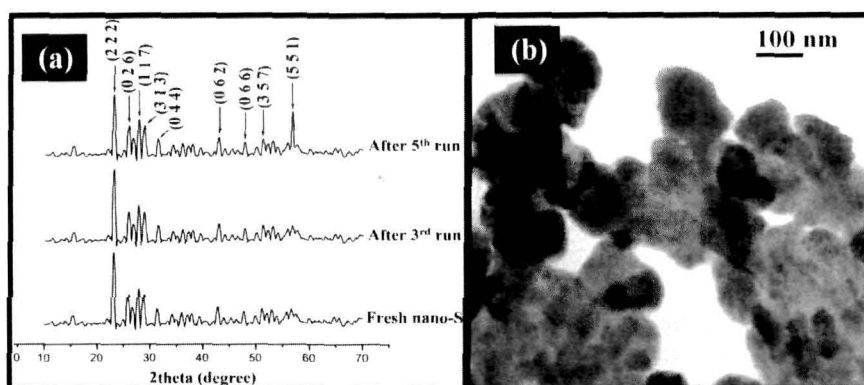


Figure 6. a) XRD pattern of reused nano-S after 3rd and 5th run and b) TEM micrograph of reused nano-S after 5th run

### 5.2.5.1 Regeneration of activity of reused nano-$S_8$

The recycled catalyst could not be used directly because some organic matter may get adsorbed on its surface. Therefore, the regeneration of the activity of nano-S after 5th run was accomplished. To verify the decomposition of catalyst after 5th run (if any), EDX analysis was performed. Interestingly, nano-S after 5th run confirmed the existence of sulfur only [figure 7 (a)]. With this pleased observation the recycled catalyst was first washed with hot deionized water to acquit most organic adsorbates and impurities. Calcination was then performed at 60 °C under sonication (45 min) by putting in distilled THF to reactivate the catalyst by collapsing the agglomeration.

The XRD pattern [figure 7 (b)] of reactivated nano-S after calcination under sonication revealed the enhancement in the intensity and broadening of the peaks (0 2 6), (1 1 7), (3 1 3), (0 4 4), (0 6 2), (0 6 6) and (3 5 7) while a slight decrease in the intensity of (2 2 2) and (5 5 1) planes.
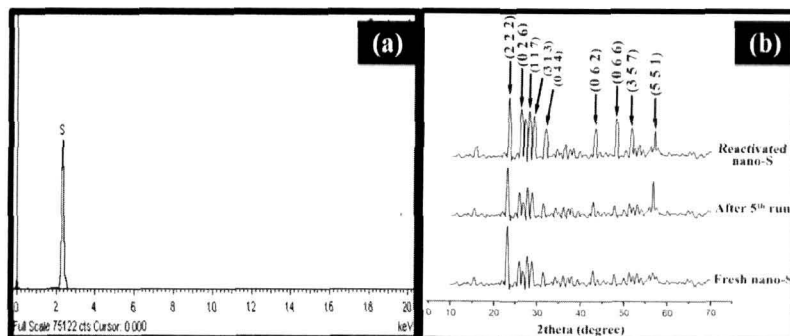
Figure 7. a) EDX analysis of reused nano-S after 5$^{th}$ reused and b) XRD pattern

of regenerated nano-S after 5$^{th}$ run

The TEM image (figure 8) of reactivated nano-S explored the spherical particles with an average diameter of 37 nm. The reusability test of reactivated nano-S was performed from the model reaction (scheme 2) and the consequences are shown in the table 5.
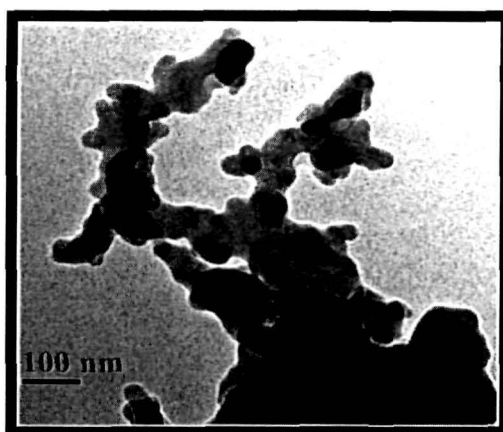


Figure 8. TEM image of reactivated nano-S after 5$^{th}$ reused

**Table 5.** Reusability test[a] of reactivated nano-S

| Entry | Number of cycles[a] | Time (min) | Yield (%)[b] |
|-------|--------------------|-----------|--------------|
| 1 | Reactivated | 30 | 96 |
| 2 | 1$^{st}$ run | 30 | 91 |
| 3 | 2$^{nd}$ run | 40 | 90 |
| 4 | 3$^{rd}$ run | 50 | 90 |
| 5 | 4$^{th}$ run | 90 | 86 |
| 6 | 5$^{th}$ run | 120 | 72 |

[a] Reaction condition: Benzaldehyde (1.02 mL, 10 mmol), urea (0.6 g, 10 mmol), naphthol (1.44 g, 10 mmol), SFRC. [b] Isolated yields.

Our data (collected in table 5) showed that the reactivated nano-S could be reused up to the 3$^{rd}$ consecutive runs without significant loss in its activity and after that its action slowed down.

The "green-ness" of the present methodology was evaluated by different parameters of green chemistry (Table 6) by considering scheme 2 that established the supremacy of nano-S over other catalysts. The waste produced during the course of the reaction is the least in our protocol compared to the other methodologies. Moreover, the issues like solvent reusability and catalyst recyclability are omitted by E-factor which absolutely raises the accuracy.

**Table 6.** A comparison of "green-ness" among the catalysts/reagents in the synthesis of [(2-Hydroxynaphthalen-1-yl)-phenylmethyl]urea 8

| Catalysts | E-factor[a] | Mass Intensity | Atom Efficiency (%) | Yield (%)[b] |
|---|---|---|---|---|
| Cu$_{1.5}$PMo$_{12}$O$_{40}$ | 0.93 | 2.62 | 89.48 | 95[22] |
| [TEBSA$^c$][HSO$_4$] | 0.43 | 1.58 | 68.75 | 73[17(g)] |
| Sulfamic acid | 0.24 | 1.66 | 75.35 | 80[17(a)] |
| KHSO$_4$ | 0.12 | 1.28 | 84.77 | 90[23] |
| TBBDA$^d$ | 0.20 | 1.24 | 84.77 | 90[17(e)] |
| [bmim]HSO$_4$ | 0.13 | 1.22 | 86.65 | 92[17(b)] |
| I$_2$ | 2.68 | 3.78 | 85.71 | 91[20(a)] |
| ZrOCl$_2$·8H$_2$O | 1.26 | 2.53 | 78.17 | 83[10(a)] |
| Dual acidic IL @SiO$_2$$^e$ | 0.32 | 1.49 | 76.29 | 81[14(a)] |
| Nano-S | 0.05 | 1.11 | 92.31 | 98[our work] |

$^a$ E-factor shown does not account for the waste produced in the synthesis of catalysts. $^b$ Isolated pure yield. $^c$ N-(4-sulfonic acid)butyltriethyl ammonium hydrogen sulfate. $^d$ N,N,N',N'-tetrabromobenzene-1,3-disulfonamide. $^e$ 3-sulfobutyl-1-(3-propyltriethoxysilane) Imidazolium hydrogen sulfate onto silica gel.

## 5.3 Conclusion

In conclusion, we have introduced a potent, benign, highly active and reusable nano-S for the one pot synthesis of 1-amidoalkyl-naphthols under 'SFRC' using our 'NOSE' approach. The method for the synthesis of nano-S is cheaper and its utilization in industry will leave almost zero waste production along with easy

isolation and regeneration of its activity. The chemistry of nano-S as a catalyst is not explored yet in organic synthesis, therefore, we believe, this protocol is going to be a breakthrough on its catalytic application.

## 5.4 Experimental

### 5.4.1 General Experimental Methods

The chemicals and reagents were purchased from Sigma-Aldrich, Merck, M/S S. D. Fine Chemicals Pvt. Ltd. and Loba chemical, and used without further purification. Transmission electron microscopy was performed by (TEM) [CM12, PHILIPS] with energy dispersive spectroscopy (EDS) [OXFORD] and sample preparation facility. The surface morphology and EDX were studied using JEOL scanning electron microscope (model JSM-6390LV SEM). The XRD pattern was recorded with Rigaku X-ray diffractometer. Melting points were determined in a Büchi 504 apparatus. IR spectra were recorded as KBr pallets in a Nicolet (Impact 410) FT-IR spectrophotometer. $^{1}H$ and $^{13}C$ NMR spectra were recorded in a 400 MHz NMR spectrophotometer (JEOL, JNM ECS) using tetramethylsilane (TMS) as the internal standard and coupling constants are expressed in Hertz. Elemental analyses were carried out in a Perkin–Elmer CHN analyser (2400 series II). Mass spectra were recorded with a Waters Q-TOF Premier and Aquity UPLC spectrometer. Visualization was accomplished with UV lamp or $I_2$ stain. Reactions were monitored by thin-layer chromatography using aluminium sheets with silica gel 60 $F_{254}$ (Merck).

### 5.4.2 Typical Procedure for the Synthesis of Nano-S

Elemental sulfur (1 g) was taken in a silica crucible and heated in an oven preset at 120 °C for 25 min. The melted substance was brought down to room temperature and then placed over an ice bath. Finally, it was grinded with mortar

and pestle. This process was repeated thrice. After that, it was washed with double distilled water (3×15 mL) and dried in oven at 100 °C. The synthesis of nano-S at 180 °C was accomplished akin to the above.

### 5.4.3 Representative Procedure for Synthesis of Amidoalkyl Naphthols (Table 3, entry 1)

A 1:1:1 mixture of 2-naphthol (0.144 g, 1 mmol), benzaldehyde (0.102 mL, 1 mmol), urea (0.060 g, 1 mmol), and nano-S ($S_8$-NP) (0.00896 g, 3.5 mol%) was taken in a mortar and grinded with a pestle. The grinded mixture was transferred in a round-bottom flask (50 mL) and placed in a preheated oil bath at 50 °C under SFRC by stirring under aerobic condition for the required time. The progress of the reaction was monitored by TLC. After completion (confirmed by TLC), the reaction mixture was brought down to room temperature and ethyl acetate (5 mL) was added to it. It was then ultracentrifuged (3,500 r.p.m.) to pellet out the nano-S. The separated catalyst was washed with hot ethanol (3×10 mL), decanted, and finally dried in an oven at 100 °C. The reaction mixture containing the desired product was purified either by column chromatography or TLC preparative or in few cases by recrystallization from hot ethanol. The analytical data of this product (0.28616 g, 98% yield) are in good accord with the reported data. This procedure was followed for all of the products listed in Table 3.

### 5.4.4 Recycling potential of nano-S

After carrying out the experiment, dry methanol was poured into the reaction mixture and centrifuged (3,000 r.p.m.) to pellet out the nano-S. The separated particles were washed with hot distilled ethanol (5x10 mL) to remove organic impurities. Then the ethanol was evaporated and the catalyst was dried in an oven at 100 °C for 3 h. The catalyst was recycled in the next run.

### 5.4.5 Turn Over Number (TON) for nano-S (Table 5)

| Entry | Input | mmol |
|-------|-------|------|
| 1 | Naphthol | 10 |
| 2 | Urea | 10 |
| 3 | benzaldehyde | 10 |
| 4 | Nano-S | 3.5 mol% (0.35 mmol) |

$$\text{TONs for entries 1 to 6} = \frac{(10 + 10 + 10)}{(0.35)} \times (0.98) = 84.0$$

$$\text{TONs for entry 7} = \frac{(10 + 10 + 10)}{(0.35)} \times (0.90) = 77.1$$

$$\text{TONs for entry 8} = \frac{(10 + 10 + 10)}{(0.35)} \times (0.85) = 72.8$$

### 5.4.6 Calculation of Green metrics

#### 5.4.6.1 Calculation of green metrics for $Cu_{1.5}PMo_{12}O_{40}$ catalyzed synthesis of [(2-Hydroxy-naphthalen-1-yl)phenylmethyl]urea[21]



Scheme 3: $Cu_{1.5}PMo_{12}O_{40}$ catalyzed synthesis of **8**

| Entry | Input | | Output | |
|-------|-------|------|--------|------|
| 1 | Naphthol | 1440 mg | **8** | 2774 mg |
| 2 | Urea | 600 mg | $Cu_{1.5}PMo_{12}O_{40}$ | 959 mg |
| 3 | Benzaldehyde | 1060 mg | | |
| 4 | Bu₄NBr | 3220 mg | | |
| | Total | 6320 mg | Total | 3733 mg |

$$E - \text{Factor} = \frac{(6320 - 3733)}{(2774)} = 0.93$$

$$\text{Mass intensity} = \frac{(6320 + 959)}{(2774)} = 2.62$$

$$\text{Atom economy} = \frac{(292)}{(106 + 60 + 144)} \times 100 = 94.19\%$$

$$\text{Atom efficiency} = 94.19\% \times 95\% = 89.41\%$$

### 5.4.6.2 Calculation of green metrics for [TEBSA][HSO₄] catalyzed synthesis of

*[(2-Hydroxy-naphthalen-1-yl)phenylmethyl]urea*[7g]



Scheme 4: [TEBSA][HSO₄] catalyzed synthesis of **8**

| Entry | Input | | Output | |
|---|---|---|---|---|
| 1 | Naphthol | 1440 mg | **8** | 2132 mg |
| 2 | Urea | 720 mg | [TEBSA][HSO₄] | 168 mg |
| 3 | Benzaldehyde | 1060 mg | | |
| | Total | 3220 mg | Total | 2300 mg |

$$E - \text{Factor} = \frac{(3220 - 2300)}{(2132)} = 0.43$$

$$\text{Mass intensity} = \frac{(3220 + 168)}{(2132)} = 1.58$$

$$\text{Atom economy} = \frac{(292)}{(106 + 60 + 144)} \times 100 = 94.19\%$$

$$\text{Atom efficiency} = 94.19\% \times 73\% = 68.75\%$$

### 5.4.6.3 Calculation of green metrics for sulfamic acid catalyzed synthesis of

*[(2-Hydroxynaphthalen-1-yl)phenylmethyl]urea*[7a]



Scheme 5: Sulfamic acid catalyzed synthesis of **8**

| Entry | Input | | Output | |
|---|---|---|---|---|
| 1 | Naphthol | 1440 mg | **8** | 2336 mg |
| 2 | Urea | 900 mg | Sulfamic acid | 485 mg |
| 3 | Benzaldehyde | 1060 mg | | |
| | Total | 3400 mg | Total | 2821 mg |

$$E - \text{Factor} = \frac{(3400 - 2821)}{(2336)} = 0.24$$

$$\text{Mass intensity} = \frac{(3400 + 485)}{(2336)} = 1.66$$

$$\text{Atom economy} = \frac{(292)}{(106 + 60 + 144)} \times 100 = 94.19\%$$

$$\text{Atom efficiency} = 94.19\% \times 80\% = 75.35\%$$

**5.4.6.4 Calculation of green metrics for KHSO$_4$ catalyzed synthesis of [(2-Hydroxynaphthalen-1-yl)phenylmethyl]urea[22]**



Scheme 6: KHSO$_4$ catalyzed synthesis of **8**

| Entry | Input | | Output | |
|---|---|---|---|---|
| 1 | Naphthol | 1440 mg | **8** | 2628 mg |
| 2 | Urea | 660 mg | KHSO$_4$ | 204 mg |
| 3 | Benzaldehyde | 1060 mg | | |
| | Total | 3160 mg | Total | 2832 mg |

$$E - \text{Factor} = \frac{(3160 - 2832)}{(2628)} = 0.12$$

$$\text{Mass intensity} = \frac{(3160 + 204)}{(2628)} = 1.28$$

$$\text{Atom economy} = \frac{(292)}{(106 + 60 + 144)} \times 100 = 94.19\%$$

Atom efficiency = 94.19% × 90% = 84.77%

## 5.4.6.5 Calculation of green metrics for TBBDA catalyzed synthesis of [(2-Hydroxy-naphthalen-1-yl)phenylmethyl]urea[17e]



Scheme 7: TBBDA catalyzed synthesis of 8

| Entry | Input | | Output | |
|-------|-------|------|--------|--------|
| 1 | Naphthol | 1440 mg | **8** | 2628 mg |
| 2 | Urea | 720 mg | TBBDA | 55.2 mg |
| 3 | Benzaldehyde | 1060 mg | | |
| | Total | 3220 mg | Total | 2683.2 mg |

$$E - \text{Factor} = \frac{(3220 - 2683.2)}{(2628)} = 0.20$$

$$\text{Mass intensity} = \frac{(3220 + 55.2)}{(2628)} = 1.24$$

$$\text{Atom economy} = \frac{(292)}{(106 + 60 + 144)} \times 100 = 94.19\%$$

Atom efficiency = 94.19% × 90% = 84.77%

## 5.4.6.6 Calculation of green metrics for [bmim]HSO₄ catalyzed synthesis of [(2-Hydroxynaphthalen-1-yl)phenylmethyl]urea[17b]



Scheme 8: [bmim]HSO₄ catalyzed synthesis of 8

| Entry | Input | | Output | |
|---|---|---|---|---|
| 1 | Naphthol | 1440 mg | **8** | 2686 mg |
| 2 | Urea | 660 mg | [bmim]HSO$_4$ | 118 mg |
| 3 | Benzaldehyde | 1060 mg | | |
| | Total | 3160 mg | Total | 2804 mg |

$$E - \text{Factor} = \frac{(3160 - 2804)}{(2686)} = 0.13$$

$$\text{Mass intensity} = \frac{(3160 + 118)}{(2686)} = 1.22$$

$$\text{Atom economy} = \frac{(292)}{(106 + 60 + 144)} \times 100 = 94.19\%$$

$$\text{Atom efficiency} = 94.19\% \times 92\% = 86.65\%$$

### 5.4.6.7 Calculation of green metrics for dual acidic IL @SiO$_2$ catalyzed synthesis of [(2-Hydroxynaphthalen-1-yl)phenylmethyl]urea[14a]



Scheme 9: Dual acidic IL @SiO$_2$catalyzed synthesis of **8**

| Entry | Input | | Output | |
|---|---|---|---|---|
| 1 | Naphthol | 1440 mg | **8** | 2365 mg |
| 2 | Urea | 840 mg | Catalyst | 200 mg |
| 3 | Benzaldehyde | 1060 mg | | |
| | Total | 3340 mg | Total | 2565 mg |

$$E - \text{Factor} = \frac{(3340 - 2565)}{(2365)} = 0.32$$

$$\text{Mass intensity} = \frac{(3340 + 200)}{(2365)} = 1.49$$

$$\text{Atom economy} = \frac{(292)}{(106 + 60 + 144)} \times 100 = 94.19\%$$

$$\text{Atom efficiency} = 94.19\% \times 81\% = 76.29\%$$

### 5.4.6.8 Calculation of green metrics for $I_2$ catalyzed synthesis of [(2-Hydroxynaphthalen-1-yl)phenylmethyl]urea[20a]



Scheme 10: $I_2$ catalyzed synthesis of 8

| Entry | Input | | Output | |
|---|---|---|---|---|
| 1 | Naphthol | 1440 mg | 8 | 2657 mg |
| 2 | Urea | 780 mg | $I_2$ | 127 mg |
| 3 | Benzaldehyde | 1060 mg | | |
| 4 | DCM | 6650 mg | | |
| | Total | 9930 mg | Total | 2784 mg |

$$E - \text{Factor} = \frac{(9300 - 2784)}{(2657)} = 2.68$$

$$\text{Mass intensity} = \frac{(9930 + 127)}{(2657)} = 3.78$$

$$\text{Atom economy} = \frac{(292)}{(106 + 60 + 144)} \times 100 = 94.19\%$$

$$\text{Atom efficiency} = 94.19\% \times 91\% = 85.71\%$$

### 5.4.6.9 Calculation of green metrics for $ZrOCl_2 \cdot 8H_2O$ catalyzed synthesis of [(2-Hydroxynaphthalen-1-yl)phenylmethyl]urea[10a]



Scheme 11: $ZrOCl_2 \cdot 8H_2O$ catalyzed synthesis of 8

| Entry | Input | | Output | |
|---|---|---|---|---|
| 1 | Naphthol | 1440 mg | **8** | 2424 mg |
| 2 | Urea | 660 mg | [bmim]HSO$_4$ | 322 mg |
| 3 | Benzaldehyde | 1060 mg | | |
| 4 | DCM | 2660 mg | | |
| | Total | 5820 mg | Total | 2746 mg |

$$E - \text{Factor} = \frac{(5820 - 2746)}{(2424)} = 1.26$$

$$\text{Mass intensity} = \frac{(5820 + 127)}{(2424)} = 2.53$$

$$\text{Atom economy} = \frac{(292)}{(106 + 60 + 144)} \times 100 = 94.19\%$$

$$\text{Atom efficiency} = 94.19\% \times 83\% = 78.1\%$$

**5.4.6.10 Calculation of green metrics for nano-S catalyzed synthesis of [(2-Hydroxynaphthalen-1-yl)phenylmethyl]urea$^{our\ work}$**



Scheme 12: Nano-S catalyzed synthesis of **8**

| Entry | Input | | Output | |
|---|---|---|---|---|
| 1 | Naphthol | 1440 mg | **8** | 2862 mg |
| 2 | Urea | 6000 mg | Nano-S | 90 mg |
| 3 | Benzaldehyde | 1060 mg | | |
| | Total | 3100 mg | Total | 2952 mg |

$$E - \text{Factor} = \frac{(3100 - 2952)}{(2862)} = 0.05$$

$$\text{Mass intensity} = \frac{(3100 + 90)}{(2862)} = 1.11$$

$$\text{Atom economy} = \frac{(292)}{(106 + 60 + 144)} \times 100 = 94.19\%$$
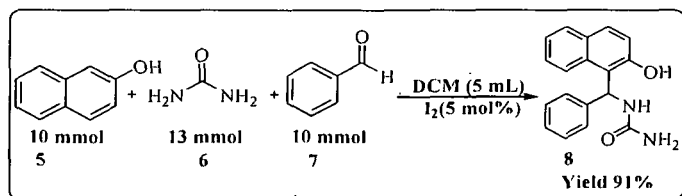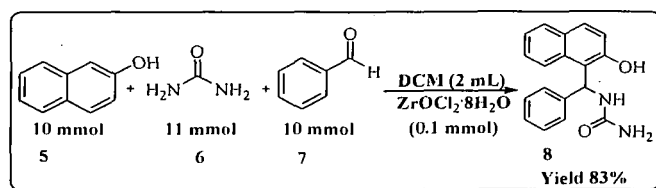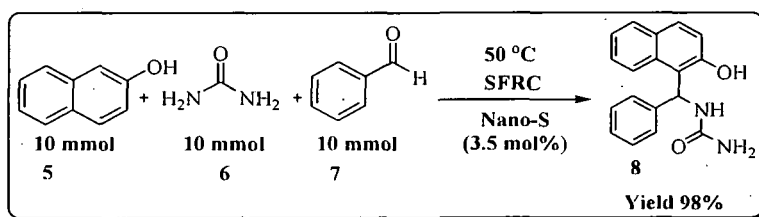
Atom efficiency = 94.19% × 98% = 92.31%

## 5.5 Physical and spectroscopic data for all products

**[(2-Hydroxynaphthalen-1-yl)phenylmethyl]urea (Table 2, entry 1)**
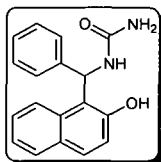


White solid; $R_f$= 0.37 (50% AcOEt: hexane); mp 171.2-173.5 °C; $^1$H NMR (400 MHz, DMSO-$d_6$, TMS): δ 9.99 (br, s, 1H, OH), 7.75-7.70 (m, Ar-H), 7.35 (br, s, 1H, NH), 7.17-7.13 (m, Ar-H), 6.90 (s, 1H, CH), 5.79 (s, 2H, NH$_2$); $^{13}$C NMR (100 MHz, DMSO-$d_6$, TMS): δ 159.1, 153.3, 144.7, 132.5, 131.1, 129.5, 129.1, 128.3, 126.4, 126.2, 122.9, 121.2,119.7, 48.6; IR (KBr pellets) $v_{max}$ (cm$^{-1}$): 3453 (NH), 3382 (OH), 3231 (NH$_2$), 2956 (CH), 1661 (CO); m/z (GC-MS) 292.12 [M$^+$]; Anal. Calcd (%) for C$_{18}$H$_{16}$N$_2$O$_2$: C, 73.95; H, 5.52; N, 9.58; Found C, 74.04; H, 5.22; N, 9.64.

**[(4-Chlorophenyl)-(2-hydroxynaphthalen-1-yl)methyl]urea (Table 2, entry 2)**
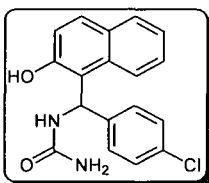


White solid; $R_f$= 0.35 (50% AcOEt: hexane); mp 210.6-212.7 °C; $^1$H NMR (400 MHz, DMSO-$d_6$, TMS): δ 9.96 (br, s, 1H, OH), 7.79-7.71 (m, Ar-H, 6H), 7.36 (br, s, 1H, NH), 7.24-7.10 (m, Ar-H, 4H), 6.86 (s, 1H, CH), 5.80 (s, 2H, NH$_2$); $^{13}$C NMR (100 MHz, DMSO-$d_6$, TMS): δ 159.0, 153.4, 144.0, 132.5, 130.8, 129.7, 129.1, 128.3, 128.1, 127.1, 123.0, 118.9, 49.9; IR (KBr pellets) $v_{max}$ (cm$^{-1}$): 3485 (NH), 3390 (OH), 3192 (NH$_2$), 2955(CH), 1650 (CO); m/z (GC-MS) 326.08 [M$^+$]; Anal. Calcd (%) for C$_{18}$H$_{15}$ClN$_2$O$_2$: C, 66.16; H, 4.63; N, 8.57;

Found C, 66.08; H, 4.43; N, 8.67.

## [(2-Hydroxynaphthalen-1-yl)-(3-nitrophenyl)methyl]urea (Table 2, entry 3)
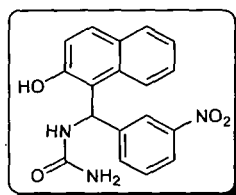


Light yellow powder; $R_f = 0.31$ (50% AcOEt:hexane); mp 186.6-188.1 °C; $^1$H

NMR (400 MHz, DMSO-$d_6$, TMS): δ 9.91 (br, s, 1H, OH), 8.11-8.07 (m, 6H, Ar-

H), 7.91-7.85 (m, 4H, Ar-H), 7.34 (br, s, 1H, NH), 6.84 (s, 1H, CH), 5.82 (s, 2H,

NH$_2$); $^{13}$C NMR (100 MHz, DMSO-$d_6$, TMS): δ 161.7, 153.4, 147.3, 145.0,

133.4, 132.1, 130.2, 129.2, 128.9, 128.6, 128.1, 127.3, 123.3, 119.1, 49.4; IR

(KBr pellets) $v_{max}$ (cm$^{-1}$): 3484 (NH), 3374 (OH), 3260 (NH$_2$), 2971 (CH), 1632

(C=O); m/z (GC-MS) 337.11 [M$^+$]; Anal. Calcd for $C_{18}H_{15}N_3O_4$: C, 64.09; H,

4.48; N, 12.46. Found: C, 64.14; H, 4.49; N, 12.66.

## [(2-Hydroxynaphthalen-1-yl)-(4-methoxyphenyl)methyl]urea (Table 2, entry 4)
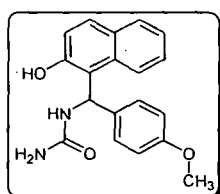


White solid; $R_f = 0.38$ (50% AcOEt: hexane); mp 182.3-184.7 °C; $^1$H NMR (400

MHz, DMSO-$d_6$, TMS): δ 10.03 (br, s, 1H, OH), 7.95-7.89 (m, 6H, Ar-H), 7.44

(br, s, 1H, NH), 7.28-7.23 (m, 4H, Ar-H), 6.88 (s, 1H, CH), 5.79 (s, 2H, NH$_2$),

3.57 (s, 3H, CH$_3$); $^{13}$C NMR (100 MHz, DMSO-$d_6$, TMS): δ 162.2, 153.4, 142.5,

135.5, 133.6, 129.5, 128.9, 128.2, 126.1, 123.5, 122.1, 118.6, 56.1, 50.1; IR (KBr

pellets) $v_{max}$ (cm$^{-1}$): 3481 (NH), 3370 (OH), 3265 (NH$_2$), 2977 (CH), 1637 (CO);

m/z (GC-MS) 322.13 [M$^+$]; Anal. Calcd for $C_{19}H_{18}N_2O_3$: C, 70.79; H, 5.63; N,

8.69. Found: C, 70.73; H, 5.33; N, 8.61.

**[(2-Hydroxynaphthalen-1-yl)-(4-hydroxyphenyl)methyl]urea (Table 2, entry 5)**
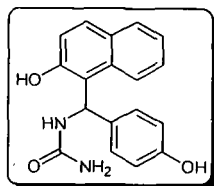


White solid; $R_f$= 0.31 (50% AcOEt: hexane); mp 146.7-148.6 °C; $^1$H NMR (400 MHz, DMSO-$d_6$, TMS): δ 10.51 (br, s, 1H, OH), 8.13-7.95 (m, 6H, Ar-H), 7.57 (br, s, 1H, NH), 7.20-6.98 (m, 4H, Ar-H), 6.69 (s, 1H, CH), 5.79 (s, 2H, NH$_2$); $^{13}$C NMR (100 MHz, DMSO-$d_6$, TMS): δ 160.7, 150.5, 143.5, 132.5, 129.0, 129.6, 128.1, 127.8, 127.3, 125.6, 124.8, 122.6, 122.1, 119.8, 47.5; IR (KBr pellets) $v_{max}$ (cm$^{-1}$) 3458 (NH), 3340 (OH), 3287 (NH$_2$), 2965 (CH), 1656 (C=O); m/z (GC-MS) 308.12 [M$^+$]; Anal. Calcd for C$_{18}$H$_{16}$N$_2$O$_3$: C, 70.12; H, 5.23; N, 9.09. Found: C, 70.19; H, 4.93; N, 9.03.

**[1-(2-Hydroxynaphthalen-1-yl)-3-phenylallyl]urea**$^{our\ work}$ **(Table 2, entry 6)**
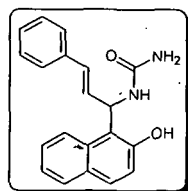


Pale yellow solid; $R_f$= 0.25 (50% AcOEt: hexane); mp 169.7-173.2 °C; $^1$H NMR (400 MHz, DMSO-$d_6$, TMS): δ 10.54 (br, s, 1H, OH), 8.11 (d, $J$ = 7.5Hz, 1H), 8.35 (d, $J$ = 7.5 Hz, 1H), 7.75-7.71 (m, 6H, Ar-H), 7.55 (br, s, 1H, NH), 6.91 (s, 1H, CH), 5.82 (s, 2H, NH$_2$); $^{13}$C NMR (100 MHz, DMSO-$d_6$, TMS): δ 168.6, 153.3, 150.6, 144.8, 136.3, 132.3, 129.3, 128.6, 128.0, 127.5, 127.1, 126.6, 126.1, 123.5, 122.1, 118.9, 118.1, 49.8; IR (KBr pellets) $v_{max}$ (cm$^{-1}$): 3418 (NH), 3353

(OH), 3278 (NH$_2$), 2970 (CH), 1653 (CO); m/z (GC-MS) 318.14 [M$^+$]; Anal.

Calcd for C$_{20}$H$_{18}$N$_2$O$_2$: C, 75.45; H, 5.70; N, 8.80. Found: C, 75.30; H, 5.96; N,

8.89.

## [Furan-2-yl-(2-hydroxynaphthalen-1-yl)methyl]urea (Table 2, entry 7)
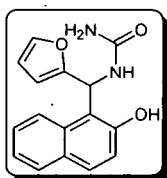


Off white solid; R$_f$= 0.35 (50% AcOEt: hexane); mp 162.3-163.7 °C; $^1$H NMR

(400 MHz, DMSO-$d_6$, TMS): δ 9.97 (s, 1H, OH), 7.75-7.69 (m, 6H, Ar-H), 7.39

(s, 1H, NH), 6.86-6.88 (m, 3H, Ar-H), 6.02 (s, 1H, CH), 5.76 (s, 2H, NH$_2$); $^{13}$C

NMR (100 MHz, DMSO-$d_6$, TMS): δ 159.6, 156.8, 153.7, 141.8, 132.8, 129.7,

129.0, 128.7, 126.9, 122.9, 119.0, 118.2, 110.8, 105.6, 50.2; IR (KBr pellets) v$_{max}$

(cm$^{-1}$): 3471 (NH), 3392 (OH), 3254 (NH$_2$), 2987 (CH), 1669 (CO); m/z (GC-

MS) 282.10 [M$^+$]; Anal. Calcd (%) for C$_{16}$H$_{14}$N$_2$O$_3$: C, 68.07; H, 5.00; N, 9.92;

Found C, 68.45; H, 4.93; N, 10.12.

## [(2-Hydroxynaphthalen-1-yl)-thiophen-2-yl-methyl]urea (Table 2, entry 8)
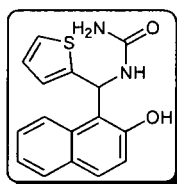


Light yellow solid; R$_f$= 0.36 (50% AcOEt:hexane); mp 159.2-161.7 °C; $^1$H NMR

(400 MHz, DMSO-$d_6$, TMS): δ 9.95 (s, 1H, OH), 7.77-7.71 (m, 6H, Ar-H), 7.33

(s, 1H, NH), 6.83-6.88 (m, 3H, Ar-H), 6.22 (s, 1H, CH), 5.80 (s, 2H, NH$_2$); $^{13}$C

NMR (100 MHz, DMSO-$d_6$, TMS): δ 160.1, 157.3, 154.4, 141.9, 133.4, 129.8,

129.2, 128.8, 126.2, 122.7, 119.2, 118.5, 110.3, 105.9, 49.8; IR (KBr pellets) v$_{max}$

(cm$^{-1}$): 3474 (NH), 3398 (OH), 3258 (NH$_2$), 2982 (CH), 1672 (CO); m/z (GC-

MS) 298.08 [M$^+$]; Anal. Calcd (%) for C$_{16}$H$_{14}$N$_2$O$_2$S: C, 64.41; H, 4.73; N, 9.39; Found C, 64.58; H, 4.99; N, 9.43.

*N*-[(2-Hydroxynaphthalen-1-yl)-*o*-tolylmethyl]acetamide (Table 2, entry 9)
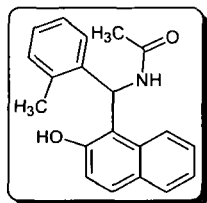


Off white solid; R$_f$= 0.38 (50% AcOEt: hexane); mp 200.3-202.7 °C; $^1$H NMR (400 MHz, DMSO-$d_6$, TMS): δ 9.98 (br, s, 1H, OH), 8.04-7.89 (m, 6H, Ar-H), 7.30-7.21 (m, 4H, Ar-H), 6.65 (br, s, 1H, NH), 5.77 (s, 1H, CH), 2.27 (s, 3H, CH$_3$), 1.89 (s, 3H, CH$_3$); $^{13}$C NMR (100 MHz, DMSO-$d_6$, TMS): δ 167.5, 152.7, 143.5, 139.5, 134.3, 132.4, 129.2, 128.6, 128.1, 126.3, 125.4, 123.4, 122.0, 118.3, 50.1, 22.7, 19.4; IR (KBr pellets) ν$_{max}$ (cm$^{-1}$): 3422 (NH), 3322 (OH), 2993 (CH), 1625 (CO); m/z (GC-MS) 305.14 [M$^+$]; Anal. Calcd (%) for C$_{20}$H$_{19}$NO$_2$: C, 78.66; H, 6.27; N, 4.59; Found C, 78.60; H, 6.57; N, 4.64.

*N*-[1-(2-Hydroxy-naphthalen-1-yl)-propyl]-acetamide (Table 2, entry 10)
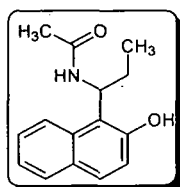


White solid; R$_f$= 0.42 (50% AcOEt: hexane); mp 172.9-174.4 °C; $^1$H NMR (400 MHz, DMSO-$d_6$, TMS): δ 10.05 (br, s, 1H, OH), 8.64 (br, s, 1H, NH), 7.82-7.75 (m, 6H, Ar-H), 6.24 (t, 1H, $J$ = 7.3 Hz, CH), 2.17 (s, 3H, CH$_3$), 1.91-1.97 (m, 1H, CH2), 0.93 (t, 3H, $J$ = 7.3 Hz, CH$_3$); $^{13}$C NMR (100 MHz, DMSO-$d_6$, TMS): δ 166.4, 152.3, 134.6, 132.0, 131.3, 128.6, 128.1, 127.7, 127.2, 126.8, 126.1, 122.6, 119.4, 118.0, 48.6, 36.2, 19.8, 13.7; IR (KBr pellets) ν$_{max}$ (cm$^{-1}$): 3418 (NH), 3228 (OH), 3004 (CH), 1636 (CO); m/z (GC-MS) 243.13 [M$^+$]; Anal. Calcd (%)

for $C_{15}H_{17}NO_2$: C, 74.05; H, 7.04; N, 5.76; Found C, 74.12; H, 7.37; N, 5.56.

*N*-[1-(2-Hydroxynaphthalen-1-yl)butyl]acetamide (Table 2, entry 11)
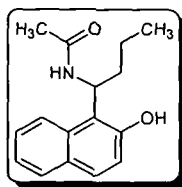


White solid; $R_f$= 0.40 (50% AcOEt: hexane); mp 221.3-223.8 °C; $^1$H NMR (400 MHz, DMSO-$d_6$, TMS): δ 10.15 (br, s, 1H, OH), 8.60 (br, s, 1H, NH), 7.80-7.73 (m, 6H, Ar-H), 6.04 (t, 1H, $J$ = 7.7 Hz, CH), 2.12 (s, 3H, CH$_3$), 1.81-1.73 (m, 1H, CH$_2$), 1.36-1.29 (m, 1H, CH$_2$), 0.96 (t, 3H, $J$ = 7.7 Hz, CH$_3$); $^{13}$C NMR (100 MHz, DMSO-$d_6$, TMS): δ 163.4, 152.1, 134.6, 132.4, 131.3, 129.1, 128.7, 128.2, 127.3, 126.7, 126.1, 122.0, 119.1, 118.3, 47.9, 36.6, 19.8, 13.7; IR (KBr pellets) $v_{max}$ (cm$^{-1}$): 3451 (NH), 3234 (OH), 3041 (CH), 1636 (CO); m/z (GC-MS) 257.14 [M$^+$]; Anal. Calcd (%) for $C_{16}H_{19}NO_2$: C, 74.68; H, 7.44; N, 5.44; Found C, 74.93; H, 7.62; N, 5.74.

*N*-[(2-Hydroxynaphthalen-1-yl)-(3-nitrophenyl)methyl]acetamide (Table 2, entry 12)
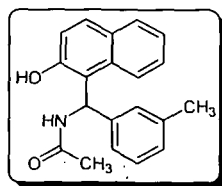


Pale yellow solid; mp 240.2-241.6 °C; $R_f$= 0.36 (50% AcOEt: hexane); $^1$H NMR (400 MHz, DMSO-$d_6$, TMS): δ 10.03 (br, s, 1H, OH), 8.03-7.73 (m, 6H, Ar-H), 7.51 (br, s, 1H, NH), 7.11-7.02 (m, 4H, Ar-H), 6.10 (s, 1H, CH), 1.95 (s, 3H, CH$_3$); $^{13}$C NMR (100 MHz, DMSO-$d_6$, TMS) δ: 162.3, 154.2, 132.5, 130.1, 129.4, 128.8, 128.1, 127.3, 126.4, 123.3, 122.9, 122.1, 118.3, 117.0, 115.3, 114.1,

43.9, 22.3; IR (KBr pellets) $v_{max}$ (cm$^{-1}$): 3436 (NH), 3258 (OH), 2997 (CH), 1644

(CO); m/z (GC-MS) 336.11 [M$^+$]; Anal. Calcd (%) for $C_{19}H_{16}N_2O_4$: C, 67.85; H,

4.79; N, 8.33; Found C, 67.49; H, 4.86; N, 8.40.

**N-[(2-Chlorophenyl)-(2-hydroxynaphthalen-1-yl)methyl]acetamide (Table 2, entry 13)**
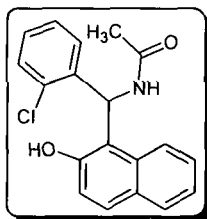


Off white solid; $R_f$ = 0.38 (50% AcOEt: hexane); mp 212.8-214.5 °C; $^1$H NMR

(400 MHz, DMSO-$d_6$, TMS): δ 9.98 (br, s, 1H, OH), 7.94-7.88 (m, 6H, Ar-H),

7.47 (br, s, 1H, NH), 7.29-7.36 (m, 4H, Ar-H), 6.03 (s, 1H, CH), 1.91 (s, 3H,

CH$_3$); $^{13}$C NMR (100 MHz, DMSO-$d_6$, TMS): δ 165.6, 154.1, 140.4, 133.5,

133.4, 132.8, 132.1, 130.3, 129.8, 129.1, 128.7, 127.6, 127.0, 123.1, 123.6, 119.2,

117.4, 48.6, 23.5; IR (KBr pellets) $v_{max}$ (cm$^{-1}$): 3440 (NH), 3251 (OH), 2990

(CH), 1645 (CO); m/z (GC-MS) 325.09 [M$^+$]; Anal. Calcd (%) for $C_{19}H_{16}ClNO_2$:

C, 70.05; H, 4.95; N, 4.30; Found C, 69.96; H, 4.55; N, 4.45.

**N-[(2-Hydroxynaphthalen-1-yl)-phenylmethyl]acetamide (Table 2, entry 14)**
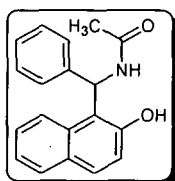


White solid; $R_f$ = 0.46 (50% AcOEt: hexane); mp: 228.3-229.5 °C; $^1$H NMR (400

(br, s, 1H, CH), 7.21-7.07 (m, 5H, Ar-H), 2.01 (s, 3H, CH$_3$); $^{13}$C (100 MHz,

DMSO-$d_6$, TMS): δ 167.6, 152.7, 144.7, 134.6, 128.9, 128.7, 128.1, 127.8, 127.1,

125.5, 124.7, 123.6, 122.3, 122.1, 118.2, 43.6, 21.7; IR (KBr pellets) $v_{max}$ (cm$^{-1}$):

3459 (NH), 3388 (OH), 3007 (CH), 1660 (CO); m/z (GC-MS) 291.13 [M$^+$];

Anal. Calcd (%) for C$_{19}$H$_{17}$NO$_2$: C, 78.33; H, 5.88; N, 4.81; Found C, 78.70; H,

5.93; N, 4.91.

*N*-[(2-Hydroxynaphthalen-1-yl)-(4-hydroxyphenyl)methyl]acetamide$^{our}$  $^{work}$

(Table 2, entry 15)
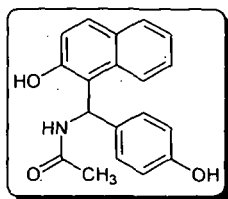


A light crimson solid; R$_f$ = 0.29 (50% AcOEt:hexane); mp 185.8-189.6 °C; $^1$H

NMR (400 MHz, DMSO-$d_6$, TMS): δ 10.07 (br, s, 1H, OH), 7.71-7.68 (m, 6H,

Ar-H), 7.44 (br, s, 1H, NH), 7.22-7.17 (m, 4H,, Ar-H), 6.41 (s, 1H, CH), 1.97 (s,

3H, CH$_3$); $^{13}$C NMR (100 MHz, DMSO-$d_6$, TMS): δ 167.2, 148.1, 140.3, 130.4,

129.7, 129.1, 128.4, 127.7, 127.2, 125.6, 124.1, 122.7, 122.1, 120.5, 119.0, 49.3

22.1; IR (KBr pellets) v$_{max}$ (cm$^{-1}$): 3480 (NH), 3365 (OH), 2992 (CH), 1675

(CO); m/z (GC-MS) 307.12 [M$^+$]; Anal. Calcd (%) for C$_{19}$H$_{17}$NO$_3$: C, 74.25; H,

5.58; N, 4.56; Found C, 74.33; H, 5.52; N, 4.26.

*N*-[1-(2-Hydroxynaphthalen-1-yl)-3-phenylallyl]acetamide (Table 2, entry

16)
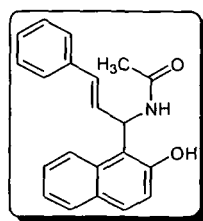


Off white solid; R$_f$ = 0.28 (50% AcOEt:hexane); mp 174.5-176.0 °C; $^1$H NMR $^1$H

NMR (400 MHz, DMSO-$d_6$, TMS): δ 11.03 (br, s, 1H, OH), 8.29 (d, $J$ = 6.9 Hz,

1H), 8.17 (d, $J$ = 6.9 Hz, 1H), 7.80-7.74 (m, 6H, Ar-H), 7.51 (br, s, 1H, NH), 6.23

(s, 1H, CH), 2.05 (s, 3H, CH$_3$); $^{13}$C NMR (100 MHz, DMSO-$d_6$, TMS): δ 169.1, 155.2, 151.4, 145.2, 134.4, 133.0, 130.2, 129.1, 128.7, 128.0, 127.5, 126.7, 126.2, 123.4, 122.3, 118.7, 118.2, 48.7, 21.3; IR (KBr pellets) $v_{max}$ (cm$^{-1}$): 3411 (NH), 3350 (OH), 2989 (CH), 1659 (CO); m/z (GC-MS) 317.14 [M$^+$]; Anal. Calcd for C$_{21}$H$_{19}$NO$_2$: C, 79.47; H, 6.03; N, 4.41. Found: C, 79.51; H, 6.09; N, 4.77.

*N*-[(2-Hydroxynaphthalen-1-yl)-phenylmethyl]benzamide (Table 2, entry 17)
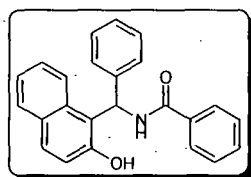


White solid; R$_f$= 0.25 (50% AcOEt: hexane); mp 235.1-237.5 °C; $^1$H NMR (400 MHz, DMSO-$d_6$, TMS): δ 10.34 (br, s, 1H, OH), 8.17-8.11 (m, 6H, Ar-H), 7.92-7.87 (m, 5H, Ar-H), 7.40 (br, s, 1H, NH), 7.20-7.14 (m, 5H, Ar-H), 6.07 (s, 1H, CH); $^{13}$C NMR (100 MHz, DMSO $d_6$, TMS): δ 169.5, 153.4, 148.2, 145.2, 134.8, 133.4, 132.8, 132.2, 130.8, 130.3, 129.7, 128.4, 128.1, 127.7, 127.1, 123.8, 122.6, 122.6, 121.0, 119.3, 118.1, 49.7; IR (KBr pellets) $v_{max}$ (cm$^{-1}$): 3475 (N-H), 3361 (OH), 2984 (CH), 1656 (CO); m/z (GC-MS) 353.14 [M$^+$]; Anal. Calcd for C$_{24}$H$_{19}$NO$_2$: C, 81.56; H, 5.42; N, 3.96. Found: C, 81.73; H, 5.51; N, 3.90.

*N*-[(2-Hydroxynaphthalen-1-yl)-*p*-tolylmethyl]benzamide (Table 2, entry 18)
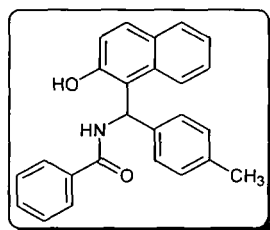


Light yellow solid; R$_f$= 0.27 (50% AcOEt:hexane); mp 207.5-209.8 °C; $^1$H NMR (400 MHz, DMSO-$d_6$, TMS): δ 9.91 (br, s, 1H, OH), 8.04-7.98 (m, 6H, Ar-H), 7.63 (br, s, 1H, NH), 7.23-7.14 (m, 9H, Ar-H), 6.07 (s, 1H, CH), 1.91 (s, 3H,

CH$_3$); $^{13}$C NMR (100 MHz, DMSO-$d_6$, TMS): δ 167.8, 153.1, 143.3, 139.5, 134.7, 132.9, 129.1, 128.8, 128.2, 126.3, 125.5, 123.4, 122.6, 119.4, 118.1, 48.7, 20.3; IR (KBr pellets) $v_{max}$ (cm$^{-1}$): 3419 (NH), 3317 (OH), 3071 (CH), 1623 (CO); m/z (GC-MS) 367.16 [M$^+$]; Anal. Calcd for C$_{25}$H$_{21}$NO$_2$: C, 81.72; H, 5.76; N, 3.81. Found: C, 81.53; H, 6.11; N, 3.87.

**N-[(4-Chlorophenyl)-(2-hydroxynaphthalen-1-yl)methyl]benzamide** (Table 2, entry 19)
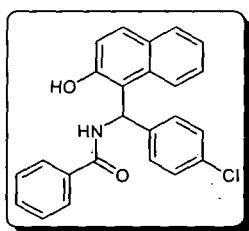


Off white solid; R$_f$= 0.24 (50% AcOEt: hexane); mp 179.0-181.6 °C; $^1$H NMR (400 MHz, DMSO-$d_6$, TMS): δ 10.06 (br, s, 1H, OH), 8.06-7.97 (m, 6H, Ar-H), 7.43 (br, s, 1H, NH), 7.28-7.23 (m, 4H, Ar-H), 7.07-7.01 (m, 5H, Ar-H), 6.12 (s, 1H, CH); $^{13}$C NMR (100 MHz, DMSO-$d_6$, TMS): δ 165.0, 153.3, 138.7, 134.1, 132.5, 132.1, 131.2, 130.6, 129.7, 128.4, 128.2, 128.0, 127.8, 127.3, 126.7, 126.2, 122.9, 122.4, 118.7, 116.6, 48.9; IR (KBr pellets) $v_{max}$ (cm$^{-1}$): 3440 (NH), 3325 (OH), 3070 (CH), 1644 (CO); m/z (GC-MS) 387.10 [M$^+$]; Anal. Calcd for C$_{24}$H$_{18}$ClNO$_2$: C, 74.32; H, 4.68; N, 3.61. Found: C, 74.26; H, 4.60; N, 3.86.

**N-[(2-Hydroxynaphthalen-1-yl)-(4-hydroxyphenyl)methyl]benzamide**[our work] (Table 2, entry 20)
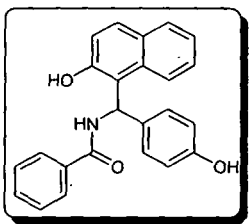


Light brown solid; R$_f$= 0.21 (50% AcOEt :hexane); mp 191.3-193.3 °C; $^1$H NMR

(400 MHz, DMSO-$d_6$, TMS): δ 11.24 (br, s, 1H, OH), 8.94 (br, s, 1H, NH), 8.11-

8.05 (m, 6H, Ar-H), 7.81-7.76 (m, 4H, Ar-H), 7.21-7.15 (m, 5H, Ar-H), 6.79 (s,

1H, CH); $^{13}$C NMR (100 MHz, DMSO-$d_6$, TMS): δ 169.6, 156.4, 152.4, 149.2,

144.7, 139.2, 134.5, 132.5, 132.1, 130.0, 129.6, 129.2, 128.8, 128.1, 127.9, 127.1,

125.2, 124.4, 122.9, 122.2, 120.8, 119.3, 50.3 ; IR (KBr pellets) $v_{max}$ (cm$^{-1}$): 3488

(NH), 3366 (OH), 2955 (CH), 1655 (CO); m/z (GC-MS) 369.14 [M$^+$]; Anal.

Calcd for C$_{24}$H$_{19}$NO$_3$: C, 78.03; H, 5.18; N, 3.79. Found: C, 77.67; H, 5.22; N,

4.08.

### N-[1-(2-Hydroxynaphthalen-1-yl)butyl]benzamide (Table 2, entry 21)
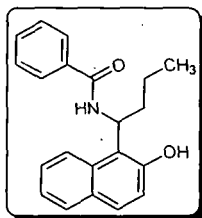


White solid; R$_f$= 0.33 (50% AcOEt: hexane); mp 240.1-242.7 °C; $^1$H NMR (400

MHz, DMSO-$d_6$, TMS): δ 10.08 (br, s, 1H, OH), 8.11-8.05 (m, 6H, Ar-H), 7.83-

7.79 (m, 5H, Ar-H), 7.31 (br, s, 1H, NH), 6.34 (t, 1H, J = 6.5 Hz, CH), 2.15 (s,

3H, CH$_3$), 1.84-1.78 (m, 1H, CH$_2$), 1.39-1.33 (m, 1H, CH$_2$), 0.97 (t, 3H, J = 6.5

Hz, CH$_3$); $^{13}$C NMR (100 MHz, DMSO-$d_6$, TMS): δ 162.7, 155.3, 148.1, 144.6,

139.7, 139.2, 135.1, 133.7, 132.4, 129.3, 128.8, 128.3, 127.7, 126.2, 125.3, 122.8,

119.6, 118.4, 48.7, 36.3, 19.4, 13.3; IR (KBr pellets) $v_{max}$ (cm$^{-1}$): 3469 (NH),

3239 (OH), 3010 (CH), 1659 (CO); m/z (GC-MS) 319.16 [M$^+$]; Anal. Calcd (%)

for C$_{21}$H$_{21}$NO$_2$: C, 78.97; H, 6.63; N, 4.39; Found C, 79.11; H, 6.92; N, 4.45.

# References:

1. (a) Pinheiro, A.V., et al. *Nat. Nanotechnol.* **6**, 763--772, 2011; (b) Mahmoudi, M. et al. *Chem. Rev.* **111**, 5610--5637, 2011.

2. Grunes, J., & Somorjai, G.A. *Chem. Commun.* **18**, 2257--2260, 2003.

3. Astruc, D., et al. *Angew. Chem., Int. Ed.* **44**, 7852--7872, 2005.

4. (a) Shimizu, K., et al. *Angew. Chem., Int. Ed.* **48**, 3982--3986, 2009; (b) Witham, C.A., et al. *Nat. Chem.* **2**, 36--41, 2010.

5. Ober, J.A. *Materials Flow of Sulfur: US Geological Survey Open File* Report **02-298**, 4--52, 2003. <http://pubs.usgs.gov/of/2002/of 02-298/>.

6. (a) Yu, X., et al. *J. Power Sources* **132**, 181--186, 2004; (b) Zheng, W., et al. *Electrochim. Acta* **51**, 1330--1335, 2006.

7. Barkauskas, J., et al. *Mater. Res. Bull.* **42**, 1732--1739, 2007.

8. Santiago, P., et al. *Microsc. Microanal.* **12**, 690--701, 2007.

9. (a) Deshpande, A.S., et al. *Nanoscale Res. Lett.* **3**, 221--229, 2008; (b) Ghanemi, K., et al. *Talanta* **85**, 763--769, 2011; (c) Chaudhuri, R.G., & Paria, S. *J. Colloid Interface Sci.* **343**, 439--446, 2010.

10. (a) Nagawade, R.R., & Shinde, D.B. *Acta. Chim. Slov.* **54**, 642--646, 2007; (b) Zhu, J., & Bienayme, H. *Multicomponent Reactions*, Wiley-VCH: Weinheim, Germany, 2005; (c) Thomson, L.A., & Ellman, J.A. *Chem. Rev.* **96**, 555--600, 1996.

11. Weber, L., et al. *Synlett.* **3**, 366--374, 1999.

12. Anastas, P.T., & Warner, J.C. *Green Chemistry: Theory and Practice*, Oxford, New York, 1998.

13. (a) Martins, M.A.P., et al *Chem. Rev.* **109**, 4140--4182, 2009; (b) Walsh, P.J., et al. *Chem. Rev.* **107**, 2503--2545, 2007; (c) Tanaka, K., & Toda, F. *Chem.*

*Rev.* **100**, 1025--1074, 2000; (d) Nagendrappa, G. *Resonance* **7**, 59--68, 2002;

(e) Tanaka, K. in *Solvent-free Organic Synthesis*, Wiley-VCH, Weinheim, 2009.

14. (a) Zhang, Q., et al. *Green Chem.* **12**, 2246--2254, 2010; (b) Hajipour, A.R., et al. *Tetrahedron Lett.* **50**, 5649--5651, 2009.

15. Dingermann, T., & Steinhilber, D. Folkers, G. In *Molecular Biology in Medicinal Chemistry*; Wiley-VCH: Weinheim, 2003.

16. (a) Szatmari, I., & Fuloop, F. *Curr. Org. Synth.* **1**, 155--165, 2004; (b) Shen, A.Y., et al. *Eur. J. Med. Chem.* **34**, 877--882, 1999; (c) Hulst, R., et al. *Tetrahedron Asymm.* **7**, 1373--1384, 1996; (d) Li, X., et al. *Tetrahedron Asymm.* **10**, 759--763, 1999.

.17. (a) Patil, S.B., et al. *Ultrason. Sonochem.* **14**, 515--518, 2007; (b) Sapkal, S.B., et al. *Bull. Korean Chem. Soc.* **30**, 2887--2889, 2009; (c) Jiang, W.-Q., et al. *Chin. J. Chem.* **26**, 1697--1701, 2008; (d) Shaterian, H.R., et al. *Synth. Commun.* **38**, 3375--3389, 2008; (e) Ghorbani-Vaghei, R., & Malaekehpour, S.M. *Cent. Eur. J. Chem.* **8**, 1086--1089, 2010; (f) Shaterian, H.R., & Yarahmadi, H. *Tetrahedron Lett.* **49**, 1297--1300, 2008; (g) Hajipour, A.R., et al. *Tetrahedron Lett.* **50**, 5649--5651, 2009.

18. Das, V.K., et al. *Green Chem.* **14**, 847--854, 2012.

19. Nagal, G. *Chem. Eng.* **104**, 125--128, 1997.

20. (a) Das, B., et al. *J. Mol. Catal. A: Chem.* **261**, 180--183, 2007; (b) Khodaei, M.M., et al. *Synlett.* **6**, 916--920, 2006.

21. Wang, M., & Liang, Y. *Monatsh. Chem.* **142**, 153--157, 2011.

22. Supale, A.R., & Gokavi, G.S. *J. Chem. Sci.* **122**, 189--192, 2010.

23. Cai, X-H., et al. *Int. J. Chem.* **3**, 119--122, 2011.

# Chapter 6

# Chapter 6

# A convenient 'NOSE' approach for the synthesis of 6-Amino-1,3-dimethyl-5-indolyl-1*H*-pyrimidine-2,4-dione derivatives catalyzed by nano-Ag
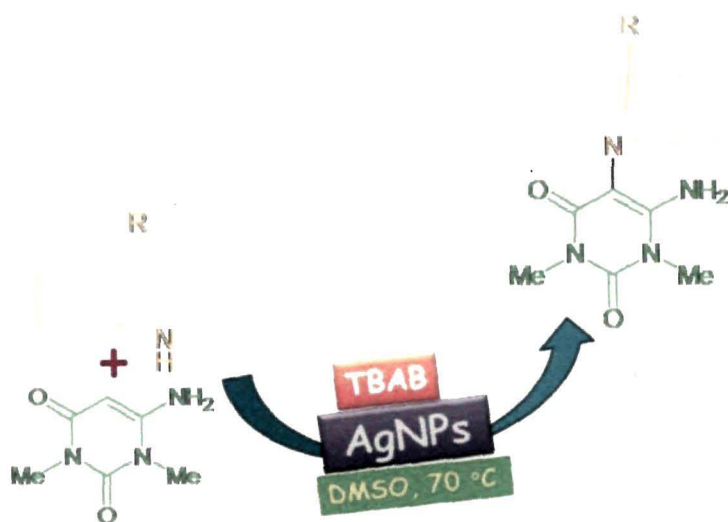
# A convenient 'NOSE' approach for the synthesis of 6-Amino-1,3-dimethyl-5-indolyl-1H-pyrimidine-2,4-dione derivatives catalyzed by nano-Ag

## 6.1 Introduction

Apart from its multifarious involvements [1] in the field of science and technology, nanoparticles have been sparking an explosive growth as nanocatalysis[2] in consequence of the frontiers between the homogeneous and heterogeneous catalysis.[3] Recently, the distinguished catalytic actions[4] of Ag NPs have been investigated for several organic transformations. Nano sized Ag has also been broadly used as antimicrobial agent as well as retarding the growth of mold, harmful spores and germ.[5] Silver nonmaterial are seriously engaged in the manufacture of consumer commodities involving mobile phones, refrigerators, and clothes to medical devices like catheters, implant surfaces, and plasters.[6] Ag NPs have also occupied place in imaging and immune detection.[7] In the recent years, synthesis of Ag NPs by employing benign bio-surfactants as potential greener stabilizers[8] have been under the hot topic of research due to their unique structural diversity, high specificity, higher biodegradability, biocompatibility and digestibility, ecofriendly, reusability, stability over the different extreme conditions such as high temperature, pH and salinity, less toxicity, widespread applicability and production from the renewable sources, mainly from wastes.[9] Uracil analogues and its derivatives have magnetized the organic chemists due to their interesting biological and chemotherapeutic importances. [10] The vital synthesis of uracil derivatives can be worked out at its nucleophilic C-5 position[11] and the presence of amino group at C-6 position enhances its nucleophilicity

dramatically.[12]

In our research program for the advancement of 'NOSE' (Nanoparticles-catalyzed Organic Synthesis Enhancement)[13] chemistry in our laboratory, we herein account the synthesis of uracil based compounds (6-Amino-1,3-dimethyl-5-indolyl-1$H$-pyrimidine-2,4-dione derivatives) in one pot having 6-Amino-1,3-dimethyl-uracil and indole derivatives catalyzed by biosurfactant capped Ag NPs at 70 °C in DMSO (scheme 1). Recently, our group reported the synthesis of uracil based compounds.[14]
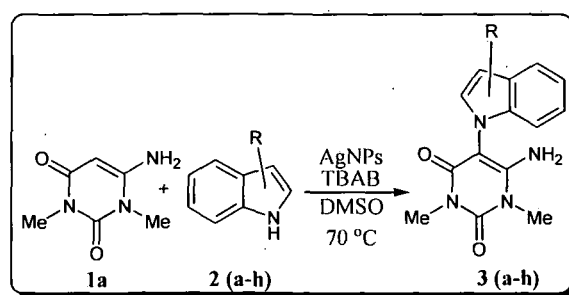


Scheme 1: Synthesis of uracil based compound

## 6.2 Results and discussion

### 6.2.1 Characterization of nano-Ag

In our attempt for the synthesis of uracil based compounds, we first prepared AgNPs using biosurfactant under mild condition[15] and characterized it. The thermal decomposition was studied by thermo-gravimetric analysis [figure 1(a)]. The plot showed that the two steps thermal degradation began at 160 °C and completed above 310 °C. The first weight loss above 160 °C was attributed to the evaporation of physically absorbed water in the air and the second weight loss at 310 °C may be due to the decomposition of precursor which was completed at this temperature. Figure 1(b) represented the X-ray diffraction pattern of AgNPs. The sample produced peaks corresponding to (0 0 4), (1 0 0), (1 0 1), (1 0 3), (0 0 6), (1 1 0) and (1 1 2) planes. AgNPs exhibited hexagonal primitive lattice

structure (JCPDS data card no 87-0598). The crystalline sizes of AgNPs were determined by Scherer equation considering the two highest peaks (0 0 4) and (1 0 1), and were found to lie between 11 and 16 nm respectively.
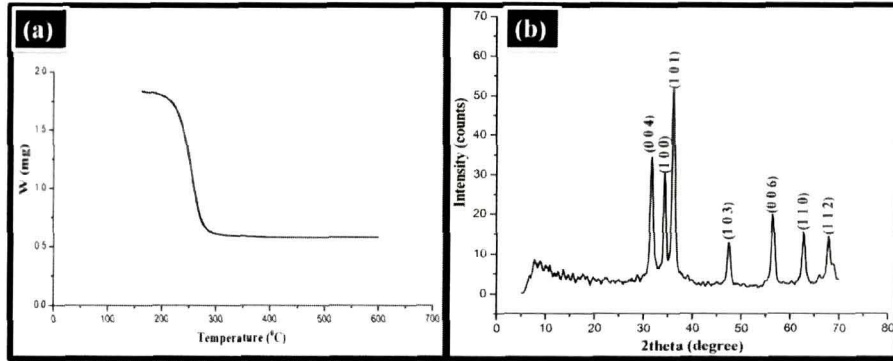


Figure 1. (a) TGA curve of AgNPs and (b) XRD pattern of AgNPs

The external morphology studied by SEM (figure 2) presented an overview of spherical shaped AgNPs in the network of each other. In addition the material has uniform morphology and particle size distribution.
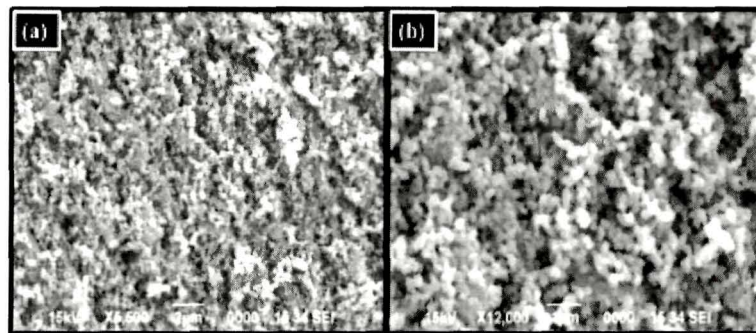


Figure 2. SEM image of AgNPs (a) at 2μm scale and (b) at 1 μm scale

TEM investigations of nano-Ag disclosed that the particles were spherical in shapes (figure 3). The average particle sizes from the TEM images were calculated manually. Figure 3a revealed the presence of both smaller and larger size particles with an average diameter of 1.67 nm and 11.11 nm respectively. The particles having average diameter of 22.51 nm could be seen in figure 3b with a bit of agglomerations. The single and magnified particles were observed in

figure 3c and 3d at 10 nm scale. The SAED pattern (embedded in figure 3b) presented an overview of crystallinity of nano-Ag.
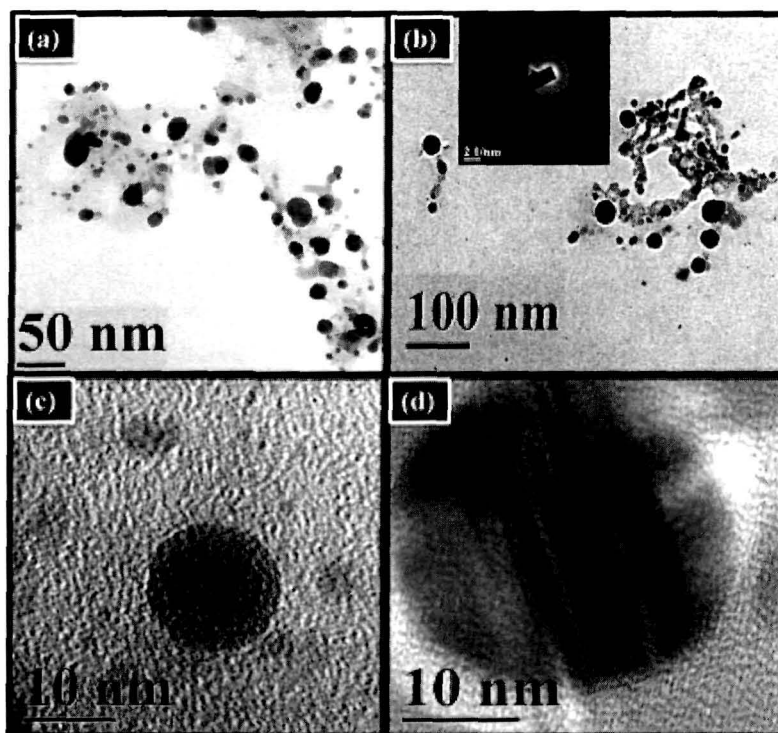


Figure 3. TEM images of nano-Ag at (a) 50 nm, (b) 100 nm, (c) 10 nm and (d) 10 nm scale

### 6.2.2 Optimization for the reaction condition for the synthesis of uracil based compound

With an idea of synthesizing uracil based compounds, we considered a model reaction between $N,N$-dimethyl-6-amino uracil **1** and indole **2** in the presence of $K_2CO_3$ to form **3** (not yet reported) and optimized the reaction condition (Table 1). Performing the reaction in neat using **1**, **2** and $K_2CO_3$ by grinding with mortar and pestle, stirring in water at room temperature/70 °C could not yield **3** (Table 1, entries 1-3). Varying the solvents (Table 1, entries 4-10) at 70 °C to check the effect on formation of **3** in neat, provided the formation of unknown mixtures in DMSO (Table 1, entry 6) and THF (Table 1, entry 10). These results indicated the requirement of a catalyst for the maximum conversion of **1** and **2** into **3**.

**Page | 198**

**Table 1.** Catalyst screening and optimization[a]



Scheme 2: Model reaction
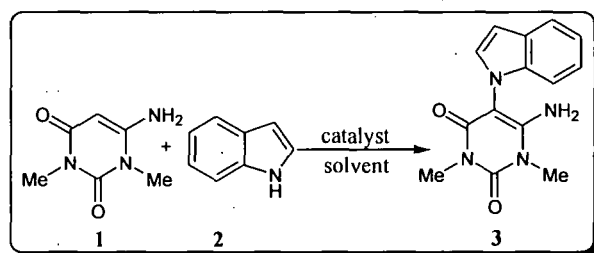
| Entry | Conditions[a] | Yield (%)[b] |
|---|---|---|
| 1 | No catalyst, $K_2CO_3$, no solvent, room temperature, grinded, 3h | c |
| 2 | No catalyst, $K_2CO_3$, no solvent, room temperature, 19h | c |
| 3 | No catalyst, $K_2CO_3$, $H_2O$, room temperature/70 °C, 19h | c |
| 4 | No catalyst, $K_2CO_3$, MeOH, 70 °C, 12h | c |
| 5 | No catalyst, $K_2CO_3$, EtOH, 70 °C, 12h | c |
| 6 | No catalyst, $K_2CO_3$, DMSO, 70 °C, 16h | d |
| 7 | No catalyst, $K_2CO_3$, DMF, 70 °C, 16h | c |
| 8 | No catalyst, $K_2CO_3$, MeCN, 70 °C, 16h | c |
| 9 | No catalyst, $K_2CO_3$, Toluene, 70 °C, 16h | c |
| 10 | No catalyst, $K_2CO_3$, THF, 16h | d |
| 11[e] | Nano-Ag, $K_2CO_3$, DMSO, 70 °C, 10h | 57 |
| 12[f] | Nano-Ag, $K_2CO_3$, DMSO, 70 °C, 7h | 47 |
| 13[g] | Nano-Ag, $K_2CO_3$, DMSO, 70 °C, 9h | 42 |
| 14[h] | Nano-Ag, $K_2CO_3$, DMSO, 70 °C, 6h | 68 |
| 15[h] | Nano-Ag, TBAB (5 mmol), $K_2CO_3$, DMSO, 70 °C, 6h | 75 |
| 16[h] | Nano-Ag, TBAB (30 mol%), $K_2CO_3$, DMSO, 70 °C, 6h | 80 |
| 17[h] | Nano-Ag, TBAB (20 mol%), $K_2CO_3$, DMSO, 70 °C, 6h | 83 |
| 18[h] | Nano-Ag, TBAB (10 mol%), $K_2CO_3$, DMSO, 70 °C, 6h | 85 |
| 19[h] | Nano-Ag, TBAB (7 mol%), $K_2CO_3$, DMSO, 70 °C, 4h | 90 |
| 20[h] | Nano-Ag, TBAB (5 mol%), $K_2CO_3$, DMSO, 70 °C, 6h | 80 |
| 21[i] | Nano-Ag, TBAB (5 mol%), $K_2CO_3$, DMSO, 70 °C, 8h | 76 |
| 22[j] | Nano-Ag, TBAB (3 mol%), $K_2CO_3$, DMSO, 70 °C, 10h | 58 |
| 23 | No catalyst, TBAB (7 mol%), $K_2CO_3$, DMSO, 70 °C, 8h | c |
| 24[h] | Nano-Ag, TBAB (7 mol%), $Na_2CO_3$, DMSO, 70 °C, 4h | 88 |
| 25[h] | Nano-Ag, TBAB (7 mol%), NaOH, DMSO, 70 °C, 4h | 85 |
| 26[h] | Bulk-$AgNO_3$, TBAB (7 mol%), $K_2CO_3$, DMSO, 70 °C, 4h | 44 |
| 27[h] | Nano-MgO, TBAB (7 mol%), $K_2CO_3$, DMSO, 70 °C, 4h | 7 |
| 28[h] | Nano-S, TBAB (7 mol%), $K_2CO_3$, DMSO, 70 °C, 4h | Trace |
| 29[h] | Nano-$Al_2O_3$, TBAB (7 mol%), $K_2CO_3$, DMSO, 70 °C, 4h | 5 |
| 30[h] | Nano-Ag, TBAB (7 mol%), $K_2CO_3$, DMSO, 120 °C, 4h | 78 |

[a] Reaction condition: **1** (5 mmol, 775 mg), **2** (5 mmol, 586 mg), $K_2CO_3$/$Na_2CO_3$/ NaOH (5 mmol, 690/530/200 mg), solvent (5 mL), [b] Isolated yield, [c] No reaction, [d] Unknown mixture, [e] 10 mol% catalyst, [f] 15 mol% catalyst, [g] 20 mol% catalyst, [h] 7 mol% catalyst, [i] 5 mol% catalyst, [j] 3mol% catalyst.

When nano-Ag (10 mol%) was used, only 57% of **3** was obtained (Table 1,

entry 11). Extension of catalyst loading to 15 and 20 mol% decreased the yield of

**3** (Table 1, entries 12, 13) due to the aggregation of AgNPs which might have reduced the surface area by blocking the active sites. When the catalyst loading was minimized to 7 mol%, better yield (Table 1, entry 14) was noticed. When tetrabutylammonium bromide (TBAB) was used in same equivalent with respect to **1, 2** and $K_2CO_3$, yield of **3** was further slightly enhanced (Table 1, entry 15). When the loading of TBAB was decreased to 30 mol% the yield of **3** was again increased (Table 1, entry 16) and the best result was obtained while it was used in 7 mol% akin to Ag nanoparticles (Table 1, entries 17-19). It is noteworthy to mention that keeping nano-Ag loading constant (7 mol%) and reducing the amount of TBAB (5 mol%) could not further improve the yield of **3** (Table 1, entry 20). Declining the loading of both nano-Ag and TBAB in an equal mol% (1:1) also could not raise the yield of **3** (Table 1, entries 21, 22). It was also observed that TBAB alone could not catalyze the formation of **3** (Table 1, entry 23). Thus, it was deduced that TBAB enhanced the catalytic activity of nano-Ag for the maximum conversion of **1** and **2** into **3** when 7 mol% of both of them were utilized but below that optimum level the yield of **3** was found lower which might be attributed to the decrease in number of active sites on the surface of the catalyst. Next, the action of $Na_2CO_3$ and NaOH were not preferable on the rate of the reaction and yield of **3** (Table 1, entries 24, 25). To verify the formation of **3** the model reaction was performed in the presence of $AgNO_3$ but it could not furnish **3** in high yield as done by nano-Ag (Table 1, entry 26) confirming its omni requirement. Testing the formation of **3** with other nanocatalysts expressed the trace to poor yield in DMSO at 70 °C (Table 1, entries 27-29). Finally, performing the reaction in the presence of nano-Ag at 120 °C bestowed **3** in lower yield (Table 1, entry 30). Overall, the reaction was observed clean using

7 mol% nano-Ag in DMSO at 70 °C and no side product formation took place.

## 6.2.3 Nano-Ag catalyzed synthesis of uracil based compounds

Incited with these outcomes, we next generalized the reaction considering a panel of different indole derivatives and the consequences are summarized in table 2. It is apparent that both electron donating and withdrawing groups participated in promoting good yields for the synthesis of uracil based compounds. Indole, 2-methyl indole and 3-methyl indole underwent reaction with 1 to produce the desire products in good yields (table 2, entries 1-3).

**Table 2.** Nano-Ag catalyzed synthesis of uracil based compounds

| Entry | Indole derivatives | Products | Time (h) | Yield (%)$^{a,b}$ |
|-------|--------------------|----------|----------|---------------------|
| 1 | Indole (2a) | 3a | 4 | 84 |
| 2 | 2-methyl indole (2b) | 3b | 7 | 80 |
| 3 | 3-methyl indole (2c) | 3c | 7 | 80 |
| 4$^{c}$ | Indole-3-carboxylic acid (2d) | 3d | 10 | 70 |
| 5$^{c}$ | Indol-3-propanoic acid (2e) | 3e | 10 | 64 |
| 6$^{c}$ | Indol-3-butanoic acid (2f) | 3f | 10 | 62 |
| 7$^{d}$ | Indol-3-acetonitrile (2g) | 3g | 8 | 78 |
| 8 | 5-bromo indole (2h) | 3h | 5 | 81 |
| 9 | Indol-3-ol(2i) | 3i | 11 | 56 |
| 10 | Indol-4-ol (2j) | 3j | 11 | 55 |

$^{a}$ Isolated yield, $^{b}$ Products were characterized by IR and NMR ($^{1}$H and $^{13}$C) spectroscopy, MS, and also by comparing their melting points with the authentic ones, $^{c}$ 10 mol% (nano-Ag and TBAB) was used, $^{d}$ Brownish yellow viscous oil.

Indole-3-carboxylic acid, Indole-3-propanoic and indole-3-butyric acid when treated with 7 mol%.nano-Ag and TBAB, 26%, 30% and 34% yields of the compounds were recorded under the present reaction condition which was not satisfactory, therefore, loading of both of them were increased to 10 mol% that enhanced the yields (table 2, entries 4-6). The possible cause for this outcome might be the presence of bulky groups in the substrate. Indole-3-acetonitrile also smoothly underwent reaction with 1 furnishing the product (table 2, entry 7). 5-Bromo indole bestowed the preferred product in good yield when it was treated

**Page | 201**

with **1** (table 2, entry 8). Indol-3-ol and Indol-4-ol when treated with **1** bequeathed the desire compounds in slightly lower yields (table 2, entries 9, 10).

### 6.2.4 Plausible mechanism for the formation of 3a

The mechanism of the reaction is not clear, however, a plausible mechanism has been proposed (scheme 3). It is hypothesized that nano-Ag has activated (**I**), first, for the abstraction of proton by base and further, for the nucleophilic attack by (**IV**) to form the intermediate (**III**). It is thought that DMSO has played a dramatic role by solvating (**III**) but not (**IV**) thereby separating them. This leaves a relatively free (**IV**) which would be expected to be more reactive nucleophile.[16] Finally, deprotonation by TBAB afforded the desired product.
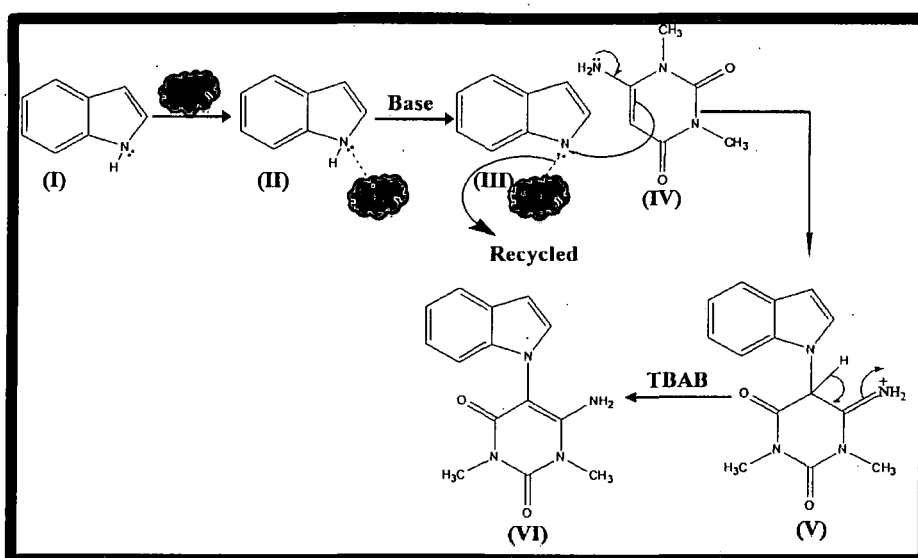


Scheme 3: Tentative mechanism for the formation of **3a**

### 6.2.5 Investigation on recycling potential of nano-Ag

Next, we focused on investigating the reusability of nano-Ag by considering the model reaction (scheme 2). As indicated in table 3, the nano-Ag was found to be active from fresh up to the $3^{rd}$ run and after that its activity slightly declined. The TONs also remained constant up to the $3^{rd}$ run and after that it lowered. To detect the cause for poorer yield of the product and deactivation of the catalyst,

**Table 3.** Catalyst reusability test

| No. of cycles[a] | Fresh | Run 1 | Run 2 | Run 3 | Run 4 | Run 5 | Run 6 |
|---|---|---|---|---|---|---|---|
| Yield (%)[b] | 90 | 90 | 90 | 90 | 88 | 84 | 80 |
| Time (h) | 4 | 4 | 4 | 4 | 7 | 10 | 14 |
| TON | 25.7 | 25.7 | 25.7 | 25.7 | 25.1 | 24.0 | 22.8 |
| TOF (h$^{-1}$) | 6.42 | 6.42 | 6.42 | 6.42 | 3.58 | 2.40 | 1.62 |

[a] Reaction conditions: **1** (10 mmol, 1550 mg), **2** (10 mmol, 1170 mg), $K_2CO_3$ (10 mmol, 1380 mg), DMSO (10 mL), TBAB (7 mol%, 225 mg), nano-Ag (7 mol%, 76 mg), 70 °C. [b] Yields refer to the isolated pure products.

the TEM images of nano-Ag after 3$^{rd}$ and 6$^{th}$ runs were recorded. It could be observed from figures 4 (a) and 4 (b) that nano-Ag started aggregating giving larger particles which might have reduced the surface area and blocked the active sites and hence deactivated the catalyst.
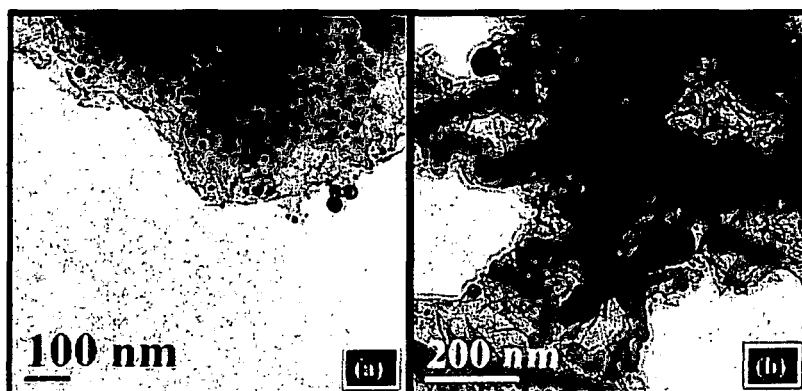


Figure 4. TEM images of nano-Ag after (a) 3$^{rd}$ run and (b) 6$^{th}$ run

## 6.3 Conclusion

In conclusion, we have developed an efficient protocol for the synthesis of uracil based compounds at 70 °C in DMSO catalyzed by heterogeneous, recyclable and moisture stable nano-Ag as catalyst. The reaction was optimized with respect to various parameters and could be employed for the synthesis of aminoindolyl dimethyl pyrimidindione derivatives. We consider that this work would find broad applications for new chemical transformations including the synthesis of challenging bioactive compounds and complex natural products.

## 6.4 Experimental

### 6.4.1 General experimental methods

The chemicals and reagents were purchased from Sigma-Aldrich, Merck, M/S S. D. Fine Chemicals Pvt. Ltd. and Loba chemical, and used without further purification. Transmission electron microscopy was performed by (TEM) [CM12, PHILIPS] with energy dispersive spectroscopy (EDS) [OXFORD] and sample preparation facility. The surface morphology and EDX were studied using JEOL scanning electron microscope (model JSM-6390LV SEM). The XRD pattern was recorded with Rigaku X-ray diffractometer. Melting points were determined in a Büchi 504 apparatus. IR spectra were recorded as KBr pallets in a Nicolet (Impact 410) FT-IR spectrophotometer. $^1$H and $^{13}$C NMR spectra were recorded in a 400 MHz NMR spectrophotometer (JEOL, JNM ECS) using tetramethylsilane (TMS) as the internal standard and coupling constants are expressed in Hertz. Elemental analyses were carried out in a Perkin–Elmer CHN analyser (2400 series II). Mass spectra were recorded with a Waters Q-TOF Premier and Aquity UPLC spectrometer. Visualization was accomplished with UV lamp or $I_2$ stain. Reactions were monitored by thin-layer chromatography using aluminium sheets with silica gel 60 $F_{254}$ (Merck).

### 6.4.2 Representative procedure for the synthesis of 3a

A 1:1 mixture of 1,3-dimethyl-6-amino uracil 1a (0.155 g, 1 mmol), indole 2a (0.117 g, 1 mmol), TBAB (0.023 g, 7 mol%), and nano-Ag (0.0074 g, 7 mol %) was taken in a mortar where DMSO (5 mL) was added and grinded with a pestle to ensure proper mixing. The grinded mixture was transferred in a round-bottom flask (50 mL) and placed in a preheated oil bath at 70 °C under SFRC by stirring under aerobic condition for the required time. The progress of the reaction was monitored by TLC. After completion (confirmed by TLC), the reaction mixture

was brought down to room temperature and DMSO was removed in vacuo. Then ethyl acetate (5 mL) was added to it. It was then ultracentrifuged (3,500 rpm) to pellet out the nano-Ag. The separated catalyst was washed with hot ethanol (3 × 10 mL), decanted, and finally dried in an oven at 100 °C. The reaction mixture containing the desired product was purified either by column chromatography or TLC. This procedure was followed for all of the products listed in Table 2.

### 6.5 Physical and spectroscopic data for the compounds

**6-Amino-5-indol-1-yl-1,3-dimethyl-1$H$-pyrimidine-2,4-dione (Table 2, entry 1)**
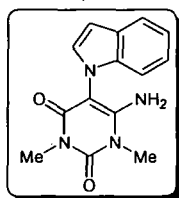


White solid; R$_f$= 0.44 (30% AcOEt:hexane); mp 98.3-101.8 °C; $^1$H NMR (400 MHz, CDCl$_3$ TMS): δ 7.63-7.07 (m, 5H, Ar-H), 6.52 (d, $J$ = 1.2 Hz, 1H, Ar-H), 6.32 (br, 2H, NH$_2$), 2.97 (s, 3H, N-CH$_3$), 2.77 (s, 3H, N-CH$_3$); $^{13}$C NMR (100 MHz, CDCl$_3$, TMS): δ 164.5, 161.0, 152.1, 141.1, 135.7, 127.7, 124.1, 121.9, 120.6, 119.7, 110.0, 102.4, 81.4, 28.7, 28.1; m/z (GC-MS) 270.11 [M$^+$]; Anal. Calcd (%) for C$_{14}$H$_{14}$N$_4$O$_2$: C, 62.21; H, 5.22; N, 20.73. Found C, 62.24., H, 5.27, N, 20.71.

**6-Amino-1,3-dimethyl-5-(2-methyl-indol-1-yl)-1$H$-pyrimidine-2,4-dione (Table 2, entry 2)**
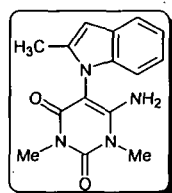
Off white solid; R$_f$ = 0.48 (30% AcOEt:hexane); mp 114.2-118.6 °C; $^1$H NMR

(400 MHz, CDCl$_3$ TMS): δ 7.51 (d, $J$ = 8.23 Hz, 1H, Ar-H), 7.16-7.08 (m, 3H,

Ar-H), 6.52 (br, 2H, NH$_2$), 6.13 (s, 1H, Ar-H), 3.18 (s, 3H, N-CH$_3$), 3.01 (s, 3H,

N-CH$_3$), 2.33 (s, 3H, CH$_3$); $^{13}$C NMR (100 MHz, CDCl$_3$, TMS): δ 162.0, 160.4,

152.2, 142.5, 136.1, 135.3, 129.1, 121.0, 119.7, 116.2, 110.4, 100.4, 81.3, 29.7,

27.5, 13.9; m/z (GC-MS) 284.13 [M$^+$]; Anal. Calcd (%) for C$_{15}$H$_{16}$N$_4$O$_2$: C,

63.37; H, 5.67; N, 19.71. Found C, 63.40, H, 5.70, N, 19.75.

**6-Amino-1,3-dimethyl-5-(3-methyl-indol-1-yl)-1$H$-pyrimidine-2,4-dione**

**(Table 2, entry 3)**
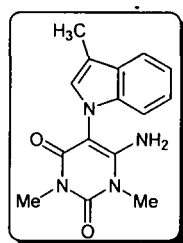


Off white solid; R$_f$ = 0.47 (30% AcOEt:hexane); mp 150.4-153.0 °C; $^1$H NMR

(400 MHz, CDCl$_3$ TMS): δ 7.58-7.13 (m, 4H, Ar-H), 6.96 (s, 1H, Ar-H), 6.54

(br, 2H, NH$_2$), 2.89 (s, 3H, N-CH$_3$), 2.70 (s, 3H, N-CH$_3$), 2.35 (s, 3H, CH$_3$); $^{13}$C

NMR (100 MHz, CDCl$_3$, TMS): δ 165.4, 162.1, 152.2, 142.7, 136.1, 135.3,

129.2, 121.2, 119.6, 116.3, 110.3, 100.5, 82.6, 29.8, 27.6, 13.7; m/z (GC-MS)

284.13 [M$^+$]; Anal. Calcd (%) for C$_{15}$H$_{16}$N$_4$O$_2$: C, 63.37; H, 5.67; N, 19.71.

Found C, 63.39, H, 5.69, N, 19.74.

**1-(6-Amino-1,3-dimethyl-2,4-dioxo-1,2,3,4-tetrahydro-pyrimidin-5-yl)-1$H$-**

**indole-3-carboxylic acid (Table 2, entry 4)**
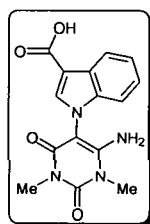
White solid; $R_f$ = 0.41 (30% AcOEt:hexane); mp 222.4-225.3 °C; $^1$H NMR (400

MHz, CDCl$_3$ TMS): δ 8.12 (br, 1H, OH), 7.41-7.38 (m, 4H, Ar-H), 6.87 (s, 1H,

Ar-H), 6.39 (br, 2H, NH$_2$), 3.41 (s, 3H, N-CH$_3$), 3.39 (s, 3H, N-CH$_3$); $^{13}$C NMR

(100 MHz, CDCl$_3$, TMS): δ 173.4, 164.6, 161.3, 152.7, 136.4, 123.3, 122.7,

119.3, 118.4, 111.3, 107.7, 82.1, 29.8, 28.6; m/z (GC-MS) 314.10 [M$^+$]; Anal.

Calcd (%) for C$_{14}$H$_{14}$N$_4$O$_2$: C, 57.32; H, 4.49; N, 17.83. Found C, 57.11, H, 4.35,

N, 17.54.

**[1-(6-Amino-1,3-dimethyl-2,4-dioxo-1,2,3,4-tetrahydro-pyrimidin-5-yl)-1H-**

**indol-3-yl]-acetic acid (Table 2, entry 5)**
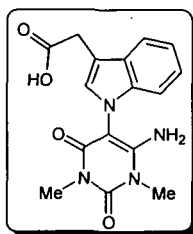


Pale yellow solid; $R_f$ = 0.39 (30% AcOEt:hexane); mp 210.3-214.5 °C; $^1$H NMR

(400 MHz, CDCl$_3$ TMS): δ 8.07 (br, 1H, OH), 7.34-7.13 (m, 4H, Ar-H), 6.75 (s,

1H, Ar-H), 6.45 (br, 2H, NH$_2$), 3.80 (s, 2H, CH$_2$), 3.57 (s, 3H, N-CH$_3$), 3.33 (s,

3H, N-CH$_3$); $^{13}$C NMR (100 MHz, CDCl$_3$, TMS): δ 176.3, 164.4, 160.0, 152.3,

136.1, 123.2, 122.4, 119.9, 118.8, 111.2, 107.9, 81.7, 35.8, 29.2, 28.7; m/z (GC-

MS) 328.12 [M$^+$]; Anal. Calcd (%) for C$_{16}$H$_{16}$N$_4$O$_4$: C, 58.53; H, 4.91; N, 17.06.

Found C, 58.14, H, 4.55, N, 10.73.

**4-[1-(4-Amino-1,3-dimethyl-2,6-dioxo-hexahydro-pyrimidin-5-yl)-1H-indol-**

**3-yl]-butyric acid (Table 2, entry 6)**
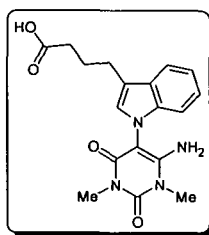
Yellow solid; $R_f$ = 0.37 (30% AcOEt:hexane); mp 186.6-189.8 °C; $^1$H NMR (400 MHz, CDCl$_3$ TMS): δ 8.09 (br, 1H, OH), 7.60-7.11 (m, 4H, Ar-H), 6.96 (s, 1H, Ar-H), 6.40 (br, 2H, NH$_2$), 3.18 (s, 3H, N-CH$_3$), 3.08 (s, 3H, N-CH$_3$), 2.82 (t, $J$ = 7.32 Hz, 2H, CH$_2$), 2.42 (t, $J$ = 7.32 Hz, 2H, CH$_2$), 2.07-2.03 (m, 2H, CH$_2$); $^{13}$C NMR (100 MHz, CDCl$_3$, TMS): δ 180.0, 165.1, 163.0, 152.9, 136.4, 127.4, 122.0, 121.6, 119.3, 118.9, 115.4, 111.2, 81.8, 33.6, 29.4, 28.6, 25.1, 24.4; m/z (GC-MS) 328.12 [M$^+$]; Anal. Calcd (%) for C$_{18}$H$_{20}$N$_4$O$_4$: C, 60.66; H, 5.66; N, 15.72. Found C, 60.32, H, 5.41, N, 15.58.

**1-(6-Amino-1,3-dimethyl-2,4-dioxo-1,2,3,4-tetrahydro-pyrimidin-5-yl)-1$H$-indole-3-carbonitrile (Table 2, entry 7)**
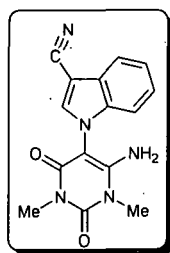


Brownish yellow viscous oil; $R_f$ = 0.51 (30% AcOEt:hexane); $^1$H NMR (400 MHz, CDCl$_3$ TMS): δ 7.49 (d, $J$ = 7.8 Hz, 1H, Ar-H), 7.24-7.11 (m, H, Ar-H), 6.92 (s, 1H, Ar-H), 6.57 (br, 2H, NH$_2$), 2.99 (s, 3H, N-CH$_3$), 2.69 (s, 3H, N-CH$_3$); $^{13}$C NMR (100 MHz, CDCl$_3$, TMS): δ 164.8, 162.3, 151.0, 136.6, 126.3, 123.5, 123.1, 120.4, 119.1, 118.6, 118.4, 118.0, 112.1, 111.8, 104.4, 84.2, 34.5, 31.1; m/z (GC-MS) 295.11 [M$^+$]; Anal. Calcd (%) for C$_{15}$H$_{13}$N$_5$O$_2$: C, 61.01; H, 4.44; N, 23.72. Found C, 60.70, H, 4.12, N, 23.41.

**6-Amino-5-(5-bromo-indol-1-yl)-1,3-dimethyl-1$H$-pyrimidine-2,4-dione (Table 2, entry 8)**
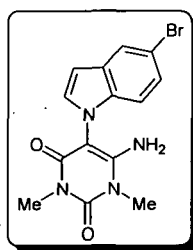
Yellow solid; $R_f$ = 0.38 (30% AcOEt:hexane); mp 106.0-109.7 °C; $^1$H NMR (400 MHz, CDCl$_3$ TMS): δ 7.80 (d, $J$ = 6.4 Hz, 1H, Ar-H), 7.29-7.22 (m, 3H, Ar-H), 6.08 (br, 2H, NH$_2$), 2.80 (s, 3H, N-CH$_3$), 2.70 (s, 3H, N-CH$_3$); $^{13}$C NMR (100 MHz, CDCl$_3$, TMS): δ 164.1, 162.5, 152.7, 142.1, 134.4, 129.7, 125.4, 124.9, 123.2, 113.1, 112.5, 102.3, 84.2, 29.5, 27.3; m/z (GC-MS) 348.02 [M$^+$]; Anal. Calcd (%) for C$_{14}$H$_{13}$BrN$_4$O$_2$: C, 48.16; H, 3.75; N, 16.05. Found C, 47.77, H, 3.48, N, 15.71.

**6-Amino-5-(3-hydroxy-indol-1-yl)-1,3-dimethyl-1$H$-pyrimidine-2,4-dione (Table 2, entry 9)**
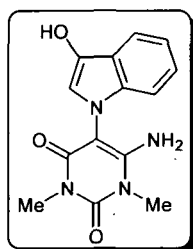


Pale yellow solid; $R_f$ = 0.51 (30% AcOEt:hexane); mp 171.2-175.6 °C; $^1$H NMR (400 MHz, CDCl$_3$ TMS): δ 9.52 (br, 1H, OH), 7.45 (d, $J$ = 7.8 Hz, 1H, Ar-H), 7.28-7.14 (m, H, Ar-H), 6.93 (s, 1H, Ar-H), 6.52 (br, 2H, NH$_2$), 3.11 (s, 3H, N-CH$_3$), 2.95 (s, 3H, N-CH$_3$); $^{13}$C NMR (100 MHz, CDCl$_3$, TMS): δ 164.6, 162.4, 152.2, 142.4, 130.5, 128.4, 125.7, 111.6, 104.8, 100.4, 84.2, 33.5, 31.7; m/z (GC-MS) 286.11 [M$^+$]; Anal. Calcd (%) for C$_{14}$H$_{14}$N$_4$O$_3$: C, 58.73, H, 4.93, N, 19.57. Found C, 58.61, H, 4.88, N, 19.41.

**6-Amino-5-(4-hydroxy-indol-1-yl)-1,3-dimethyl-1$H$-pyrimidine-2,4-dione**

(Table 2, entry 10)
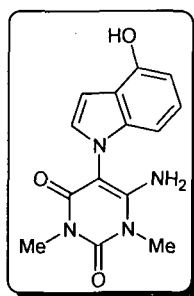


Faint yellow solid; R$_f$= 0.54 (30% AcOEt:hexane); mp 120.4-123.4 °C; $^1$H NMR (400 MHz, CDCl$_3$ TMS): δ 9.49 (br, 1H, OH), 8.14-8.04 (m, 1H, Ar-H), 7.18-6.74 (m, 3H, Ar-H), 6.32 (d, $J$ = 6.4 Hz, 1H, Ar-H), 5.84 (br, 2H, NH$_2$), 3.01 (s, 3H, N-CH$_3$), 2.79 (s, 3H, N-CH$_3$); $^{13}$C NMR (100 MHz, CDCl$_3$, TMS): δ 164.0, 162.0, 150.4, 142.2, 130.7, 128.5, 125.0, 111.7, 11.6, 104.5, 100.9, 84.0, 33.7, 31.5; m/z (GC-MS) 286.11 [M$^+$]; Anal. Calcd (%) for C$_{14}$H$_{14}$N$_4$O$_3$: C, 58.73; H, 4.93; N, 19.57. Found C, 58.42, H, 4.67, N, 19.25.

# References:

1. (a) Horie, M., et al. *Chem. Res. Toxicol.* **25**, 605--619, 2012; (b) Tan, A., et al. *Nanomedicine* **6**, 1101--1114, 2011.

2. Narayanan, R., & El-Sayed, M.A. *J. Phys. Chem. B* **108**, 8572--8580, 2004.

3. Astruc, D., et al. *Angew. Chem., Int. Ed.* **44**, 7852--7872, 2005.

4. (a) Mikami, Y., et al. *Tetrahedron Lett.* **51**, 5466--5468, 2010; (b) Mitsudome, T., et al. *Angew. Chem., Int. Ed.* **47**, 138--141, 2008; (c) Mitsudome, T., et al. *Chem. Commun.* **22**, 3258--3260, 2009; (d) Gholap, A.R., et al. *J. Mol. Catal. A;Chem.* **245**, 37--46, 2006.

5. Chen, X., & Schluesener, H.J. *Toxicol. Lett.* **176**, 1--12, 2008.

6. (a) Russell, A.D., & Hugo, W.B. *Progr. Med. Chem.* **31**, 351--370, 1994; (b) Liau, S.Y., et al. *Lett. Appl. Microbiol.* **25**, 279--283, 1997; (c) Brett, D.W. *Ostomy/Wound Manage.* **52**, 4--51, 2006.

7. (a) Kneipp, J., et al. *Nanomedicine: Nanotechnology, Biology, and Medicine* **6**, 214--226, 2010; (b) Yang, Y., et al. *J. Phys. Chem. C* **111**, 9095--9104, 2007.

8. (a) Kiran, G.S., et al. *Journal of Biotechnology* **148**, 221--225, 2010; (b) Kasture, M.B., et al. *J. Chem. Sci.* **120**, 515--520, 2008.

9. (a) Bharali, P., et al. *Int. Biodeter. Biodeg.* **65**, 682--690, 2011; (b) Benincasa, M., et al. *Antonie Van Leeuwenhoek* **85**, 1--8, 2004; (c) Banat, I.M., et al. *Applied Microbiol. Biotechnol.* **53**, 495--508, 2000.

10. (a) Manta, S., et al. *Bioorg. Chem.* **38**, 48--55, 2010; (b) Herman, B.D., et al. *The J. Biologic. Chem.* **285**, 12101--12108, 2010; (c) Plant, A., et al. *J. Org. Chem.* **74**, 4870--4873, 2009.

11. (a) Das, S., et al. *Acta Cryst. Sec. E* **65**, 2416--2417, 2009; (b) Dabiri, M., et al. *Tetrahedron* **64**, 7307--7311, 2008; (c) Zamora, F., et al. *Inorg. Chem.* **35**,

4858--4864, 1996.

12. Lam, B.L., & Pridgen, L.N. *J. Org. Chem.* 51, 2592--2594, 1986.

13. (a) Das, V.K., et al. *Green Chem.* **14**, 847--854, 2012; (b) Das, V.K., et al. *Appl. Catal. A: Gen.* **456**, 118--125, 2013; (c) Das, V.K., et al. *J. Org. Chem.* **78**, 3361--3366, 2013; (d) Das, V.K., & Thakur, A.J. *Tetrahedron Lett.* **54**, 4164--4166, 2013; (f) Das, V.K., & Thakur, A.J. *ISRN Organic Chemistry* 1--6, 2013.

14. (a) Das, S., et al. *RSC Advances* **3**, 3407--3413, 2013; (b) Das, S., & Thakur, A.J. *Eur. J. Org. Chem.* **12**, 2301--2308, 2011.

15. Saikia, J.P., et al. *Colloids and Surfaces B: Biointerfaces* **104**, 330--332, 2013.

16. (a) Zuagg, H.E., et al. *J. Org. Chem.* **26**, 644--651, 1961; (b) Parker, A.J. *Quart. Rev. Chem. Soc. Lond.* **16**, 163--187, 1962; (c) Goto, M., et al. *Tetrahedron Lett.* **40**, 8129--8132, 1999.

# Chapter 7

## Conclusion & Future Scope

## 7.1 Overall Conclusion

### 7.1.1 Conclusion from chapter 2 (sections I & II)

We have shown that the $N$-formylation of amines and $N,N$-diformylation of bis-uracil derivatives occur under solvent free conditions using nano rod-shaped basic $Al_2O_3$ as an efficient catalyst in 'NOSE' approach.

The advantages offered by these methods include:

(a) Simple experimental procedure and reaction setup only at 40 °C/70 °C.

(b) Does not require any specialized equipment.

(c) High yields of desired products.

(d) Proceeds under ambient conditions with diverse substrate compatibility.

(e) Moisture stability of the catalyst.

(f) Suitable recyclability.

(g) Cost effectiveness.

(h) Environmentally benign along the line of green chemistry.

### 7.1.2 Conclusion from chapter 3

The following findings can be drawn from chapter 3:

(a) A convenient 'NOSE' chemistry approach involving a novel $Fe_2O_3NPs@DE$ catalyst for the greener oxidation of aldehydes.

(b) DE acts as a smart support for $Fe_2O_3NPs$ and enhances its oxidative catalytic action. $Fe_2O_3$ NP having particle size 12 nm completely fitted into its pores and due to which a strong interaction took place between them and the active sites on the surface of $Fe_2O_3$ NP get exposed for catalysis.

(c) The method offers several advantages including excellent yields of the products, safe handling, and experimental simplicity.

(d) The measurement of 'green-ness' of the protocol using green metrics make it

a useful, attractive and benign alternative over the existing methodologies.

### 7.1.3 Conclusion from chapter 4

Chapter 4 (sections I & II) summarizes:

(a) We have developed a practical and greener 'NOSE' protocol for the clean synthesis of both aliphatic and aromatic amides as well as amidines utilizing nano-MgO as an efficient, reusable and cheap catalyst under SFRC at 70 °C.

(b) Simple experimental condition, varied substrate compatibility, high yields of the products, chemo selectivity.

(c) Non-hygroscopic nature of catalyst makes our protocol a more potent benign alternative over conventional ones for amide synthesis.

(d) The 'green-ness' of this protocol makes it a benign alternative for the large scale synthesis. Hence, we believe that nano-MgO would find increasing applications for those which enable the synthesis of complex natural products and derivatives.

### 7.1.4 Conclusion from chapter 5

Chapter 5 derives the following outcomes;

(a) We have introduced a potent, benign, highly active and reusable nano-S for the one pot synthesis of 1-amidoalkyl-naphthols under SFRC using our 'NOSE' approach.

(b) The method for the synthesis of nano-S is cheaper and its utilization in industry will leave almost zero waste production along with easy isolation and regeneration of its activity.

(c) The chemistry of nano-S as a catalyst is not explored yet in organic synthesis, therefore, we believe, this protocol is going to be a breakthrough on its catalytic application.

### 7.1.5 Conclusion from chapter 6

Chapter 6 enlightens:

(a) We have developed an efficient protocol for the synthesis of uracil based compounds at 70 °C in DMSO catalyzed by heterogeneous, recyclable and moisture stable nano-Ag as catalyst.

(b) The reaction was optimized with respect to various parameters and could be employed for the synthesis of aminoindolyldimethyl pyrimidindione derivatives.

(c) We consider that this work would find broad applications for new chemical transformations including the synthesis of challenging bioactive compounds and complex natural products.

### 7.2 Future Scopes

The following future scopes can be drawn from the current investigation:

1. To search for new synthetic methods which will eliminate the associated drawbacks of previously reported reaction schemes with added advantages.

2. Application of the newly discovered catalysts for sulfide oxidation reaction.

3. To synthesize hydrophilic nanoparticles and its application as catalyst in water for the synthesis of organic compounds.

4. Further development of 'NOSE' chemistry approach for the synthesis of useful nanomaterials (carbon dots) from the available useless biomass and its application as catalyst for the production of green fuel.

# Appendix 1

## List of publication

1. **Vijay Kumar Das, Ashim Jyoti Thakur**; Greener oxidation of aldehydes over bio-silica supported $Fe_2O_3$ nanoparticles: A convenient 'NOSE' approach *Applied Catalysis A: General,* **2014,** 470, 97-103.

2. **Vijay Kumar Das**, Madhurjya Borah, and Ashim Jyoti Thakur; "Synthesis of 1-amidoalkyl-2-naphthols with $S_8$-NPs"; *Synfacts,* **2013,** 9, 794

3. **Vijay Kumar Das** and Ashim Jyoti Thakur; **"Nano rod shaped basic $Al_2O_3$ catalyzed *N,N*-diformylation of bis-uracil Derivatives: A greener 'NOSE' approach"**; *ISRN Organic Chemistry,* **2013,** 1-6

4. **Vijay Kumar Das** and Ashim Jyoti Thakur; "Highly active nano-MgO catalyzed mild and efficient synthesis of amidines via the electrophilic activation of amides"; *Tetrahedron Letters,* 2013, **54,** 4164-4166

5. **Vijay Kumar Das**, Madhurjya Borah, and Ashim Jyoti Thakur; "Piper-Betle-Shaped Nano-S-Catalyzed Synthesis of 1-Amidoalkyl-2-naphthols under Solvent-Free Reaction Condition: A Greener Nanoparticle-Catalyzed Organic Synthesis Enhancement Approach"; *Journal of Organic Chemistry,* **2013,** *78,* 3361-3366

6. **Vijay Kumar Das**, Rashmi Rekha Devi, and Ashim Jyoti Thakur; "Recyclable, highly efficient and low cost nano-MgO for amide synthesis under SFRC: A convenient and greener 'NOSE' approach"; *Applied Catalysis A: General,* **2013,** *456,* 118-125

7. **Vijay Kumar Das**, Rashmi Rekha Devi, Prasanta Kumar Raul and Ashim Jyoti Thakur; "Nano rod-shaped and reusable basic $Al_2O_3$ catalyst for *N*-formylation of amines under solvent-free conditions: A novel, practical and convenient 'NOSE' approach"; *Green Chemistry,* **2012,** *14,* 847-854

8. **Vijay Kumar Das**, Subrata Das, and Ashim Jyoti Thakur; "Protection and deprotection chemistry catalyzed by zirconium oxychloride octahydrate $(ZrOCl_2 \cdot 8H_2O)$"; *Green Chemistry Letters and Reviews,* **2012,** *5,* 577-586

9. **Vijay Kumar Das**, "Danishefsky's Diene"; *Synlett,* **2011,** *3,* 0430-0431

10. Subrata Das, **Vijay Kumar Das**, Lakhinath Saikia, and Ashim Jyoti Thakur, "Environment-friendly and solvent-free synthesis of symmetrical bis-imines

under microwave irradiation"; *Green Chemistry Letters and Reviews*, **2012**, *5*, 457-474

11. Manshi Das Purkayastha, Dipankar Kalita, **Vijay Kumar Das**, Charu Lata Mahanta, Ashim Jyoti Thakur, and Mihir Kanti Chaudhuri; "Effects of L-ascorbic acid addition on micro-filtered coconut water: Preliminary quality prediction study using 1H-NMR, FTIR and GC-MS"; *Innovative Food Science and Emerging Technologies*, **2012**, *13*, 184-199

12. **Vijay Kumar Das** and Ashim Jyoti Thakur; "A convenient 'NOSE' approach for the synthesis of 6-Amino-1,3-dimethyl-5-indolyl-1H-pyrimidine-2,4-dione derivatives catalyzed by nano-Ag"; (To be communicated)

## Seminar / Workshop / Symposium / Summer School Etc. Attended/ Presented

1. Indo-Finish Symposium on "Role of catalysts on production of green fuel" (01 Feb-2013)

2. Finland-India-Sweden seminar encompassing various aspects of "Green Chemistry" (22 March-2012)

3. Workshop on Integrated Arsenic and Iron Removal from Groundwater:Arsiron Nilogon, organized by Tezpur University, India. (25 June-2011)

4. National conference on smart nanostructure (18-20 Jan 2011)

5. One day workshop on Intellectual Property Rights Sensitization: IPRSW-2010 organized by Tezpur University, India. (23 Dec-2010)

6. Frontier Lecture Series at Tezpur University organized by Jawaharlal Nehru Centre for Advanced Scientific Research, Bangalore in collaboration with the Department of Chemical Sciences, Tezpur University, India. (20-22 Nov-2009)

7. National Seminar on Catalysis, organized by Department of Chemical Sciences,Tezpur University, Assam, India, (Dec-2009)

8. Summer School on Green Chemistry, organized by Department of Chemical Sciences, Tezpur University, India. (2-22 June 2009)

9. National Seminar on Recent Advances in Chemical Sciences in Dibrugarh University, Assam, (26-27 March 2009)

# Greener oxidation of aldehydes over bio-silica supported Fe₂O₃ nanoparticles: A convenient 'NOSE' approach

CrossMark

Vijay Kumar Das, Ashim Jyoti Thakur*

*Department of Chemical Sciences, Tezpur University, Napaam 784028, India*

ARTICLE INFO

ABSTRACT

A recyclable, robust and highly active Fe₂O₃ nanoparticles supported over bio-silica, i.e. diatomaceous earth (Fe₂O₃NPs@DE) catalyzed oxidation of aryl/alkyl/heteroaryl aldehydes at room temperature has been developed. The DE enhanced the catalytic activity of Fe₂O₃ NPs dramatically by serving itself as a smart support. Fe₂O₃NPs@DE could be efficiently reused with a slight loss in its catalytic activity. The novel supported catalyst is air stable and hence all the reactions can be conducted under aerobic condition. By the measurement of the "green-ness" our protocol emerges as a benign alternative over the existing methodologies.

© 2013 Elsevier B.V. All rights reserved.

## 1. Introduction

In the recent period, metal oxide nanoparticles have attracted increasing interests for their applications such as cellular delivery carriers [1], magnetic storage media [2] and MRI contrast agents [3,4]. The nanoparticles show features contradictory to the bulk metal due to quantum size effects, including novel electronic, optical and chemical behaviour [5,6]. The tuning in the properties may be achieved via control of shape, size, inter-particle spacing and dielectric environment, and methods to vary these parameters have been developed [7–9]. The metal oxide nanocatalysis is considered as a bridge between homogeneous and heterogeneous catalysis because of their growing interest on the catalytic properties [10]. Hence, the field of metal oxide nanocatalysis should recommend prospects for mining new chemical reactions [11–13]. Consequently, it is noteworthy that the combination of safe supported-catalysis with the use of solvent-free technique represents a suitable way towards the so-called ideal synthesis [14–16]. Over the past few years, Fe₂O₃ NPs have found tremendous attentions due to their high magnetic moment, low toxicity and ease of synthesis [17]. Fe₂O₃ NPs have also been applied in drug and gene delivery systems, separation and purification technology, magnetic resonance imaging and hyperthermia [18,19]. They have also found significant importance in the extraction of heavy metal

ions and in the treatment of cancer cells through the application of external magnetic fields [20–22].

Diatomaceous earth (DE) or diatomite also called bio-silica, typically consists of 87%–91% SiO₂, with significant quantities of Al₂O₃ and Fe₂O₃ [23]. Due to its porous structure, high silica content, low density, low conductivity coefficient, etc. [24], it has widely been applied as filter aid [25], adsorbent [26], insulating material [27], catalyst support or carrier [28] and natural insecticide or grain protectant [29]. It is noted that diatomaceous earth has excellent absorption power because of its macroporous structure [30,31].

Oxidation of aldehydes to the corresponding carboxylic acid using oxidizing agent is a fundamental reaction in organic synthesis [32]. Classically, this has been accomplished with the help of oxidants such as KMnO₄ [33], Jone's reagent [34], bromine [35], HNO₃ [36] etc., which are not acceptable in present day's scenario. Hence, from the ecological sight, using clean, cheap and less toxic oxidant such as hydrogen peroxide [37] towards green oxidations of aldehydes [38] is of great significance. H₂O₂ is an ideal waste-avoiding oxidant, since water is the only by-product, and is very attractive as an oxidant for liquid-phase reactions because of its solubility in water and many organic solvents. In the recent years, a range of methodologies using H₂O₂ as an oxidant under harsh basic conditions [39] or in combination with other reagents and transition metals have been stated in the literature [40–46]. A few of the pioneering works in the green oxidation of aldehydes to carboxylic acid have been explored in the literature [47–52]. Very recently, our group also reported the oxidation of aldehydes into the corresponding carboxylic acid in the presence of aqueous H₂O₂ catalyzed by VO(acac)₂ [53]. Despite the existing tactics, most of them endure

---

* Corresponding author. Tel.: +91 3712 275059, fax: +91 3712 267005/6.
*E-mail address:* ashim@tezu.ernet.in (A.J. Thakur).

*Research Article*

# Nanorod-Shaped Basic Al$_2$O$_3$ Catalyzed *N,N*-Diformylation of Bisuracil Derivatives: A Greener "NOSE" Approach

## Vijay K. Das and Ashim J. Thakur

*Department of Chemical Sciences, Tezpur University (A Central University), Napaam, Assam 784028, India*

Correspondence should be addressed to Ashim J. Thakur; ajt.tezu03@gmail.com

A feasible "NOSE" (nanoparticles-catalyzed organic synthesis enhancement) protocol has been developed for *N,N*-diformylation of bisuracil derivatives using nano-Al$_2$O$_3$ rods as an efficient, inexpensive, and recyclable catalyst under solvent-free reaction condition at 40°C. The catalyst was reused up to the 4th cycle without affecting the rate and yield of the *N,N*-diformylation products appreciably.

## 1. Introduction

The exercise of metal/metal oxide nanoparticles as a frontier between the homogeneous catalysis and heterogeneous catalysis [1] in organic synthesis has invoked tremendous interests [2] in the recent times. The interesting features inherited with these small particle sizes are their large surface area along with more edges and corners and distinct electronic, optical, magnetic, thermal, and chemical properties [3–5]. The crucial role of nanoparticles in organic transformations is their excellent catalytic activity, straightforward recoverability, better selectivity, criteria of evolution, and their versatile role in green chemistry [6–10]. Thus, the domain of metal nanoparticle catalysis [11–13] should offer opportunities for mining new chemical reactions [14–16] which include the synthesis of biologically important and synthetically challenging natural products. In the context of green chemistry [17], organic synthesis in solvent-free reaction condition [18–21] has occupied a significant position in the recent years since solvent-free reaction condition involves the best reaction medium with "no medium" [22].

One of the key motifs present in the biopolymer RNA [23–26] is uracil, a nucleobase of the pyrimidine family which participates in various functions in our life processes [27]. Uracil derivatives also have several potent medicinal properties such as bronchodilators and anticancer [28, 29], antiallergic [30, 31], antiviral [32, 33], antihypertensive, and adenosine receptor antagonists [34, 35]. Recently, our research group

reported a greener protocol for the synthesis of bisuracil derivatives [36]. Bisuracil and their analogues have also been isolated from marine sea hare *Dolabella auricularia* [37]. Some of the *N*-substituted bisuracil analogues have been screened for bioactivities against several diseases [38].

To explore the possible applications of the metal/metal oxide nanoparticles in organic synthesis, we have been focusing on the advancement of a protocol termed "NOSE" (nanoparticles-catalyzed organic synthesis enhancement) [39–41] chemistry in our laboratory. To the best of our knowledge, there has been no report on nano-rod-shaped Al$_2$O$_3$ catalyzed *N,N*-diformylation of bisuracil derivatives. Recently, we reported *N*-formylation of amines catalyzed by nano-Al$_2$O$_3$ under solvent-free reaction condition [39]. This work inspired us to focus on nano-Al$_2$O$_3$ catalysis for the *N,N*-diformylation of bisuracil analogous. Therefore, in this paper, we wish to account for the same (Scheme 1).

Nano-Al$_2$O$_3$ draws our attention due to its crystalline size and shape, abrasive and insulating properties, less toxicity, large surface area, basic surface characteristics, high resistant towards bases and acids and excellent wear resistance [40–44].

## 2. Materials and Methods

*2.1. General Experimental Methods.* Rod-shaped nano-Al$_2$O$_3$ (the average particle diameter is 8.12 nm and average length

# Piper-Betle-Shaped Nano-S-Catalyzed Synthesis of 1-Amidoalkyl-2-naphthols under Solvent-Free Reaction Condition: A Greener "Nanoparticle-Catalyzed Organic Synthesis Enhancement" Approach

Vijay K. Das, Madhurjya Borah, and Ashim J. Thakur*

Department of Chemical Sciences, Tezpur University, Napaam, Tezpur, Assam, India

**S** *Supporting Information*

**ABSTRACT:** Nano-S prepared by an annealing process showed excellent catalytic activity for the synthesis of 1-amidoalkyl-2-naphthols under solvent-free reaction condition at 50 °C. The catalyst could be reused up to the fifth cycle without loss in its action. The green-ness of the present protocol was also measured using green metrics drawing its superiority.
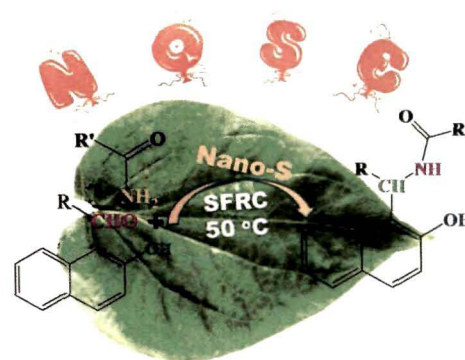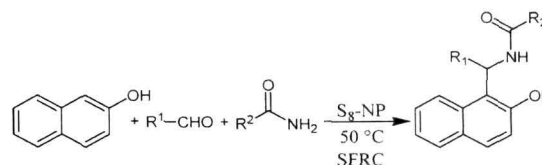
Recently, nanotechnology is mastering intricacies for the synthesis and application of interesting nanomaterials.[1] Nanoparticles have evoked tremendous awareness as nano-catalysts,[2] bridging the homogeneous and heterogeneous catalysis.[3] Hence, nanocatalysis should proffer the prospects for the synthesis of challenging compounds.[4]

The synthesis of sulfur in bulk or micro- or nanoform has been pursued significantly due to its remarkable applications[5] in sulfur nanocomposites,[6] modified carbon nanostructures,[7] and sulfur nanowires,[8] etc. There are some reports for the preparation and properties of sulfur nanoparticles.[9]

The multicomponent reactions[10] (MCRs) are promising constructive sources for devising large molecules with economic viability.[11] In the premise of green chemistry,[12] MCR under solvent-free reaction condition (SFRC)[13a,b] are fascinating since it involves the best reaction medium with "no medium".[13c] The synthesis of amidoalkyl naphthols[14] is important as the 1,3-amino-oxygenated moiety is ubiquitous to a variety of biologically significant compounds.[15]

There are numerous approaches described in the literature for the synthesis of 1-amidoalkyl-2-naphthols. These protocols[16] suffer from shortcomings such as large waste production, higher reaction temperature, prolonged reaction time, low yields, harsh conditions, undesirable byproducts, toxicity, low recovery, and reusability of the catalyst. Therefore, to overcome those drawbacks and in our continual interest in the growth of "NOSE" (nanoparticle-catalyzed organic synthesis enhancement) chemistry,[17] we herein report a convenient protocol for novel sulfur nanoparticle-catalyzed synthesis of 1-amidoalkyl-2-naphthols under SFRC at 50 °C (Scheme 1). To the best of our knowledge, nano-S-catalyzed synthesis of 1-amidoalkyl-2-naphthols is not yet reported.

**Scheme 1. Synthesis of 1-Amidoalkyl-2-naphthols**



The preparation of nano-S was accomplished by annealing elemental sulfur, which in turn was achieved by catalytic conversion of $H_2S$.[18] To characterize the sulfur nanoparticles synthesized at 120 and 180 °C, the EDX analysis was performed to find the elemental composition. EDX confirmed the presence of sulfur element only (Figure 1a). Both atomic and weight percent for pure nano-S was found to be 100%. SEM image (Figure 1b) of pure nano-S explored its sheet-like structure that might be due to the stronger intermolecular forces of attraction among the sulfur molecules.

The TGA curve (Figure 1c) indicated the thermal stability having a two-step pattern of weight loss within 180−290 °C. The first weight loss (<180 °C) is attributed to the evaporation of physically absorbed water, and the second weight loss at 290 °C is accompanied by the active liberation of $H_2S$ (Figure 1c).

The X-ray diffraction patterns (Figure 2) for (a) bulk-S, (b) nano-$S_8$ synthesized at 120 °C and (c) at 180 °C revealed that the samples (a), (b), and (c) showed peaks corresponding to (222), (026), (117), (313), (044), (062), (066), (357), and (551) planes, indicating the presence of cubic orthorhombic

V. K. DAS, M. BORAH, A. J. THAKUR* (TEZPUR UNIVERSITY, INDIA)

# Synthesis of 1-Amidoalkyl-2-Naphthols with $S_8$-NPs
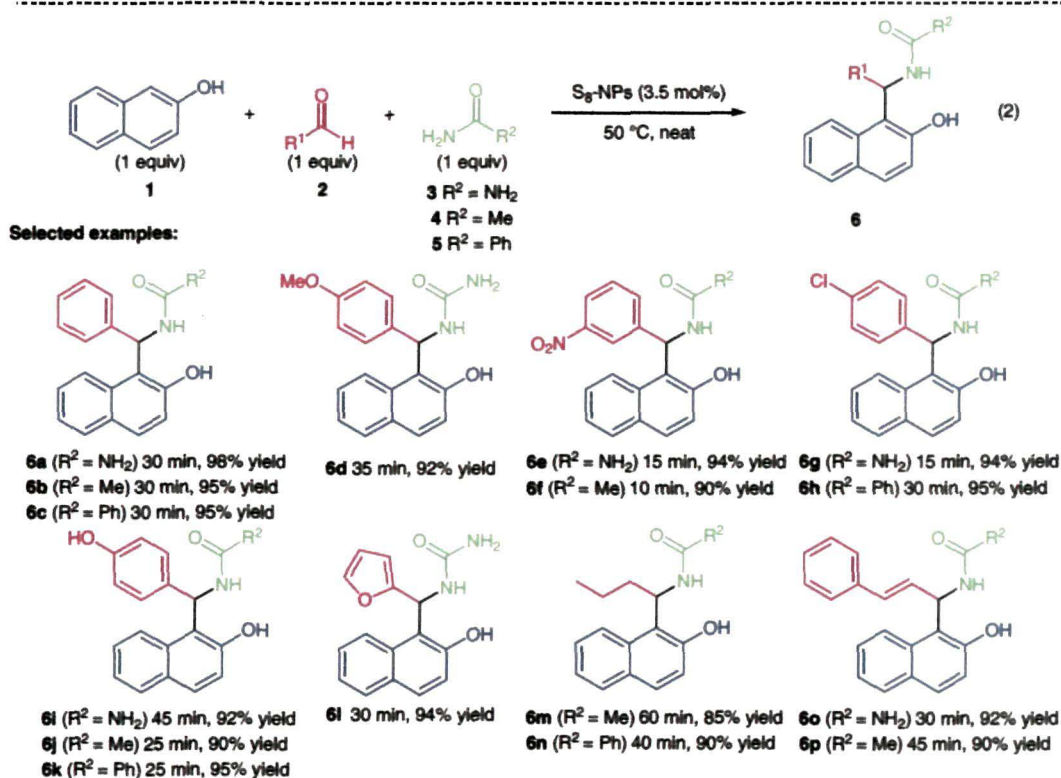


Significance: Sulfur nanoparticles ($S_8$-NPs) were prepared by annealing of elemental sulfur at 120 °C (eq. 1). $S_8$-NPs catalyzed the three-component reaction of 2-naphthol (**1**), aldehydes **2**, and amides (**3–5**) at 50 °C under solvent-free conditions to give the corresponding 1-amidoalkyl-2-naphthols **6** in up to 98% yield (21 examples, eq. 2). In the formation of **6a**, the catalyst was recovered by centrifugation and reused seven times (1$^{st}$ reuse: 98% yield, 5$^{th}$ reuse: 98% yield, 6$^{th}$ reuse: 90% yield, 7$^{th}$ reuse: 85% yield).

Comment: In the recycling experiments, the catalytic activity of $S_8$-NPs was slightly decreased at the 6$^{th}$ reuse run. Reactivation of the recovered catalyst was performed by washing with hot deionized water followed by sonication in THF at 60 °C. The reactivated catalyst was recycled five times in the formation of **6a** (1$^{st}$ cycle: 96% yield, 2$^{nd}$ cycle: 91% yield, 3$^{rd}$ cycle: 90% yield, 4$^{th}$ cycle: 90% yield, 5$^{th}$ cycle: 86% yield, 6$^{th}$ cycle: 72% yield). The catalytic activity of $S_8$-NPs was superior to that of metal oxide nanoparticles (MgO-NPs, $Al_2O_3$-NPs, and $TiO_2$-NPs) and organic bases (pyridine, imidazole, $Et_3N$, and $Ph_3P$).

# Highly active nano-MgO catalyzed, mild, and efficient synthesis of amidines via electrophilic activation of amides

CrossMark

Vijay Kumar Das, Ashim Jyoti Thakur *

*Department of Chemical Sciences, Tezpur University (A Central University), Tezpur, Napaam 784 028, Assam, India*

ABSTRACT

Nano-MgO catalyzed synthesis of amidine derivatives is developed under solvent-free reaction condition at 70 °C. Reusability of the catalyst and shorter reaction time as well as high yields are the advantages of this procedure.

© 2013 Elsevier Ltd. All rights reserved.

More recently, nano magnesium oxide (MgO) has been utilized extensively because of its potential applications as catalyst.[1] In the domain of catalysis, MgO has a potent basic property which is exploited in various organic transformations[2] and also allows the high-yield synthesis of the significant molecules.[3] Synchronizing with the theme of green chemistry,[4] syntheses of *N*-bonded compounds under solvent-free conditions have received much attention.[5]

Amidines are significant intermediates in the synthesis of many biologically active compounds[6] and there are many strategies reported in the literature for their synthesis.[7] They also serve as important synthons for the preparation of azacyclic compounds.[8] Thus, the synthesis of amidines is still a topic of immense scope. Here we disclose a practical, convenient, and greener procedure for the synthesis of amidines under solvent-free conditions at 70 °C catalyzed by nano-MgO (Scheme 1). Ogata et al.[9] reported the synthesis of amidines in the presence of polyphosphoric acid trimethylsilyl ester by treating amine and amide in equimolar ratio at 160 °C under nitrogen atmosphere. But lower yield of the products, high reaction temperature, application of corrosive reagent and its non reusability, and tiresome reaction condition made the methodology less advantageous. To the best of our knowledge, there is no report on nano-MgO catalyzed synthesis of amidines.

The study was initiated by the model reaction (Scheme 2) between **4** (5 mmol, 680 mg) and **5** (5 mmol, 0.45 mL) to give **6** without using any catalyst/solvent at 120 °C (Table 1). Under this

condition, a mixture of unknown compounds was detected (Table 1, entry 1). Utilizing 5 mL of solvents (Table 1, entries 2–7) and conducting the reaction at lower temperature did not lead to product formation. As indicated in Table 1, when pyridine (10 mol %) was used as catalyst at 70 °C for this transformation then **6** was isolated in 7% yield (Table 1, entry 8). This observation prompted us to opt for the best base catalyst for the synthesis of **6**. Several base catalysts were tested under the current condition but the reaction could not be improved both in terms of yields and time (Table 1, entries 9–14). When fully characterized nano-MgO[9] was used under the present conditions, it increased the yield to a reasonable extent (Table 1, entry 15). To obtain better yield of **6**, the catalyst loading was optimized (Table 1, entry 15–18) and it was found that nano-MgO worked efficiently at 5 mol % (Table 1,

$R^1$ = Aryl, methyl, cyclohexyl and $R^2$ = Aryl, cyclohexyl
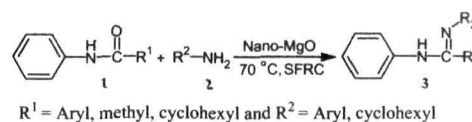
**Scheme 1.** Synthesis of amidine.
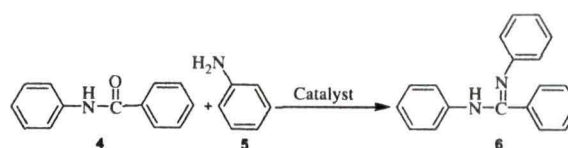
**Scheme 2.** Model reaction.

* Corresponding author. Tel.: +91 267008x5059; fax: +91 (3712) 267005/6.
  *E-mail address:* ashim@tezu.ernet.in (A.J. Thakur).

# Recyclable, highly efficient and low cost nano-MgO for amide synthesis under SFRC: A convenient and greener 'NOSE' approach

CrossMark

Vijay Kumar Das[a], Rashmi Rekha Devi[b,1], Ashim Jyoti Thakur[a,*]

[a] Department of Chemical Sciences, Tezpur University, Napaam 784028, India[2]
[b] Defence Research Laboratory, Post Bag No. 2, Tezpur 784001, India

ARTICLE INFO

ABSTRACT

A clean synthesis of amide derivatives has successfully been accomplished utilizing reusable nano-MgO under 'SFRC' (solvent free reaction condition). The 'green-ness' of this protocol makes it a benign alternative for the large scale synthesis.

© 2013 Elsevier B.V. All rights reserved.

## 1. Introduction

Recently, in the domain of catalysis, nano magnesium oxide (MgO) has gained a respectable status as catalyst [1,2]. MgO has a basic property which is exploited in the high-yield synthesis of important molecules [3]. Its adsorptive properties [4] can be used in toxic waste remediation [5]. It has a high activity against bacteria, spores and viruses because of its large surface area [6].

The widespread importance of amide moiety as one of the most versatile functionalities in chemistry and biology has been acknowledged [7]. Several catalysts and reagents [8–10] have been reported to effect the amidation reaction. The drawbacks inherited with these reagents and catalysts are their instability, sensitivity to moisture, harsh reaction condition, prolonged reaction time, modest yield, toxic/corrosive by-products and costly waste streams. More recently, hydroxyapatite-supported silver NPs have been used for the synthesis of amides via selective hydration of nitriles in water [10]. Kobayashi et al. reported gold or gold/iron NPs catalyzed amide synthesis [11]. Mizuno and coworkers synthesized amides by hydration of nitriles promoted by amorphous MgO using reduced amounts of water [12]. Mizuno et al. also reported the synthesis of amides by MgO promoted liquid-phase aerobic oxidation

of methylarenes using ammonia surrogates [13]. In the recent work [14], amide synthesis was achieved by water-soluble Gold/DNA catalyst. However, main difficulties associated with these cited works were very high reaction temperature, longer reaction time and application of expensive catalysts. Therefore, the synthesis of amide eliminating these drawbacks is still a demanding and challenging work for the chemists. Our group recently reported the synthesis of N-methylamide catalyzed by water tolerant zirconyl chloride under MWI [15]. Reddy et al. have reported an acknowledgeable work on nano-MgO catalyzed N-formylation of aryl/alkyl amines using formic acid under MWI [16]. As a part of our ongoing research program for the development of the 'NOSE' (Nanoparticles-catalyzed Organic Synthesis Enhancement) [17] chemistry in our laboratory, we herein report recyclable nano-MgO for the synthesis of amides 3 in good to excellent yields under SFRC by reacting carboxylic acids 1 with amines 2 (Scheme 1).

## 2. Experimental

### 2.1. General procedure for the synthesis of amides

In an oven dried round bottomed flask (50 mL) nano-MgO (5.0 mol%) were added and then alky/aryl amines (5.0 mmol) and aromatic/aliphatic acid (5.0 mmol) was added. After that it was allowed to stir on a pre heated oil bath at 70 °C under aerobic condition till the required time (the progress of the reaction was judged by TLC). After the completion, the reaction mixture was brought to room temperature and ethyl acetate (3 × 10 mL) was added to

* Corresponding author.
E-mail address: ashim@tezu.ernet.in (A.J. Thakur).
[1] Tel.: +91 3712 258508; fax: +91 3712 258534.
[2] Tel.: +91 3712 275059; fax: +91 3712 267005/6.

# Green Chemistry

Dynamic Article Links

**PAPER**

# Nano rod-shaped and reusable basic Al₂O₃ catalyst for N-formylation of amines under solvent-free conditions: A novel, practical and convenient 'NOSE' approach†

Vijay Kumar Das,[a] Rashmi Rekha Devi,[b] Prasanta Kumar Raul[b] and Ashim Jyoti Thakur*[a]

An expeditious, simple, highly efficient, practical and green protocol for the N-formylation of alkyl/aryl amines and indole derivatives catalyzed by novel nano rod-shaped basic Al₂O₃ under solvent-free conditions has been developed. The catalyst is efficiently recycled up to the 5th run, an important point in the domain of green chemistry. The methodology provides cleaner conversion, shorter reaction times and high selectivity which makes the protocol attractive.

## Introduction

In the wake of increasing awareness in environmentally benign techniques during the past few years, organic synthesis under solvent-free conditions has gained much popularity.[1] In this regard, the synthesis of N-bonded compounds has received considerable attention from the sight of green chemistry.[2] There is a growing appreciation for N-formylation of primary or secondary amines into formamides which is a common methodology in synthetic organic chemistry. The reaction product, formamides serve either as a polar solvent or as an important intermediate in several organic transformations since their skeletons exist in pharmaceutically valuable compounds such as fluoroquinolines,[3] imidazoles,[4] 1,2-dihydro quinolines,[5] nitrogen-bridged heterocycles,[6] oxazolidinones[7] and cancer chemotherapeutic agents.[8] They have also found significant applications as Lewis base catalysts in various organic transformations,[9–14] synthesis of formamidines,[15] isocyanides[16] and as N-formylating agents in histone proteins as a secondary modification arising from oxidative DNA damage.[17]

The literature is enumerated with several strategies[18–28] prescribed for N-formylation of amines. Regardless of the existing methodologies, most of them suffer from different drawbacks such as thermal instability, sensitivity to moisture, application of toxic and expensive formylating agents and catalysts, poor atom economy, high temperatures, prolonged reaction times, harsh

reaction conditions, formation of undesirable by-products, low yields, while also leading to diformylation and/or lack of regioselectivity and tedious work up. Therefore, the synthesis of formamides still remains an active research area in terms of operational simplicity and economic viability. In the recent years, formic acid[29–33] has been continually accepted as a potent formylating agent owing to its lower toxicity, inexpensivity and easy practical applicability.

With the nanotechnology now available to the scientists, of late, Somorjai et al. emphasizes that catalysis by transition metal nanoparticles is the central field of nanoscience and nanotechnology,[34] which are the frontiers between homogeneous and heterogeneous catalysis.[35] The growing interest on the catalytic properties of transition metal nanoparticles is due to their large surface area, distinct electronic, optical, magnetic, thermal and chemical properties.[36] The ultimate goal to work with nanoparticles is their high catalytic activity, recoverability, improved selectivity, criteria of evolution and role in green chemistry.[37] Hence, organic synthesis catalyzed by metal/metal oxide nanoparticles[38] has received tremendous importance in recent decades.

To cater the burgeoning needs and aspirations, we have been focussing on the development of a protocol named 'NOSE'[39] (nanoparticles-catalyzed organic synthesis enhancement) chemistry in our laboratory. Nanoscale supports to create catalysts with larger surface areas along with more edges and corners, which can lead to higher performance of the catalyst. Other parameters (e.g. oxygen mobility, etc.) might also play key role for enhancing catalytic activity. There are few reports that describe N-formylation of amines using nanoparticles. Preedasuriyachai and co-workers[40] have presented nanogold catalyzed N-formylation of amines under aerobic conditions with MeOH or formalin. However, in terms of disadvantage, nanogold itself is very expensive. To the best of our knowledge, N-formylation of amine catalyzed by basic nano crystalline Al₂O₃ has not been reported. Very recently, a research group has reported the nanocrystalline Al₂O₃ catalyzed one-pot synthesis of poly-substituted

ᵃDepartment of Chemical Sciences, Tezpur University, Napaam, 784028, India. E-mail: ashim@tezu.ernet.in; Fax: +91(3712)267005/6; Tel: +91(3712)267008 ext. 5059
ᵇDefence Research Laboratory, Post Bag No. 2, Tezpur, 784001, India. Fax: +91(3712)258534; Tel: +91(3712)258508

# RESEARCH LETTER

## Protection and deprotection chemistry catalyzed by zirconium oxychloride octahydrate (ZrOCl₂·8H₂O)

Vijay K. Das, Subrata Das and Ashim J. Thakur*

*Department of Chemical Sciences, Tezpur University (A Central University), Tezpur, Napaam 784028, Assam, India*

*(Received 14 September 2010; final version received 14 March 2012)*

An efficient, chemoselective, convenient, and straightforward methodology has been developed for the protection of C=O group of aldehydes/ketones as C=N moiety of hydrazones catalyzed by ZrOCl₂·8H₂O (10 mol%) in acetonitrile and the same catalyst in methanol oxidatively cleaves C=N moiety of hydrazones to provide parent carbonyl compounds in high yields. The reactions have been performed in aerobic condition. The catalyst is inexpensive, readily available, easy to handle, insensitive to air and moisture, easily recoverable and can be reused and importantly less toxic.

**Keywords:** protection; deprotection; catalyst; hydrazone; zirconium oxychloride octahydrate

## Introduction

As far as the synthesis of complex target molecules is concerned, protection–deprotection is essential (*1*) and hence serves as a central theme in organic chemistry (*2*). Hydrazone is regarded as one of the important protective moieties for carbonyl compound in multi-step synthesis of many target molecules (*3*). Apart from carbonyl protection they also serve as carbanion equivalents in C–C bond forming reactions (*4,5*). Accordingly, lots of efforts have been exercised for the development of a mild and efficient methodology for masking carbonyl moiety of aldehydes/ketones in the form of hydrazone and the subsequent oxidative cleavage of hydrazones to regenerate the parent carbonyl compounds. But, some of the reported methods (*6–21*) have one or the other limitations such as requirement of strongly oxidizing or reducing acidic or basic reagents, use of reagents in stoichiometric amounts or more, tedious work up procedure, low yield, longer reaction time, harsh reaction condition, lack of selectivity, associated with environmental hazard and importantly, tolerability to other functional groups. It is also likely that by product formed in the reaction may block the active sites of the catalyst thereby reducing its activity. Importantly, presence of sensitive structural features in molecules restricts the choice of reagents. Hence, there has been considerable interest in this area and still scope is there for further development.

The application of ZrOCl₂·8H₂O as a catalyst in organic synthesis has attracted our attention as it is relatively cheaper, readily available, easy to handle, insensitive to air and moisture (*22*) and importantly less toxic (*23*). This octahydrate of Zirconium oxychloride is a mild Lewis acid having some distinct differences (*24,25*) from other metal hydrates. An account by Zhang et al. recently reviewed effectiveness of Zirconium-based compounds in many organic transformations, for example addition reaction, rearrangement reaction, protection of common functional groups such as carbonyl, carboxylic acid, amino and hydroxy groups (*26*) and their subsequent deprotection. Zolfigol et al. described the application of zirconium compounds in deprotection, oxidation, C–C, C–N, and C–O bond forming reactions (*27*). Catalytic activity of ZrOCl₂·8H₂O has been described for the oxidation of alcohols (*28*); acylation of alcohols, phenols, amines, and thiols (*29*); esterification of long chain carboxylic acids and alcohols (*30*); enaminones and enamino ester synthesis (*31*); chemoselective synthesis of 2-aryloxazolines and bis-oxazolines (*32*); and synthesis of benzoxazoles, benzothiazoles, benzimidazoles, and oxazolo[4,5-*b*]-pyridines (*33*).

## Results and discussion

In continuation to our interest in protection and deprotection (*34*) and zirconium chemistry (*35*), we want to divulge herein a new and convenient protocol

## SYNLETT
# Spotlight 343

This feature focuses on a reagent chosen by a postgraduate, highlighting the uses and preparation of the reagent in current research

## Danishefsky's Diene

Compiled by Vijay Kumar Das

Vijay Kumar Das was born in 1984 in Nagaon, Assam, India. He received his B.Sc. degree in chemistry from the Gauhati University, India in 2005, and his M.Sc. degree in Applied Chemistry from the Tezpur University, India in 2008. Currently, he is working towards his Ph.D. degree under the supervision of Dr. A. J. Thakur, Associate Professor, at the same university. His current research interests focus on the application of nanoparticles in organic synthesis.

Department of Chemical Sciences, Tezpur University, Napaam, Tezpur 784028, Assam, India
E-mail: vijay@tezu.ernet.in

### Introduction

The Danishefsky's diene, *trans*-1-methoxy-3-trimethylsiloxy-1,3-butadiene (also known as Kitahara diene), was first introduced by Danishefsky and Kitahara in 1974.[1] Since the diene is very electron-rich it is used as a very reactive reagent in Diels–Alder reactions. The methoxy group accounts for the regiospecificity observed in the Diels–Alder reaction, since the electrophilic carbon to which it is attached will react preferentially with the most nucleophilic atom of the dienophile. The electron-donating nature of this diene confers high reactivity and orientational specificity in its reaction with unsymmetrical dienophiles.

The high reactivity coupled with the easy availability makes 1-methoxy-3-trimethylsiloxy-1,3-butadiene a potentially very important reagent in organic synthesis. Its first synthesis was reported by Danishefsky and Kithara starting from 4-methoxy-3-buten-2-one in the presence of trimethylsilyl chloride and zinc chloride (Scheme 1).[2]
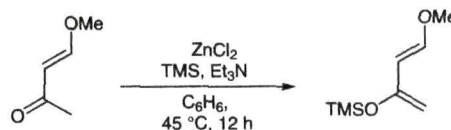


**Scheme 1**

### Abstracts

(A) The enantioselective hetero-Diels–Alder reaction of Danishefsky's diene with benzaldehyde has been achieved both experimentally and theoretically, incorporating a series of α,α,α',α'-tetraaryl-1,3-dioxolane-4,5-dimethanol (TADDOL) derivatives as catalysts, affording 2-phenyl-2,3-dihydro-4*H*-pyran-4-one (1).[3]
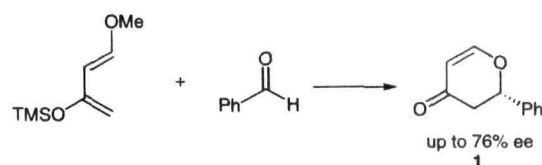


(B) After acetylation, condensation between Danishefsky's diene and benzoquinone afforded a stable methoxytriacetoxydihydronaphthalene intermediate 2, which was subsequently transformed into the regiospecific 7-naphthylboronic acid 3 by the Snieckus DOM protocol.[4]
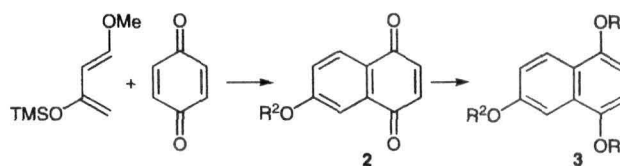


(C) Mandai and co-workers delineated the reaction of Danishefsky's diene with aryl-/alkyl-substituted aldimine catalyzed by silver in the presence of a ligand leading to the formation of pyridinone 4.[5]

Taylor & Francis
Taylor & Francis Group
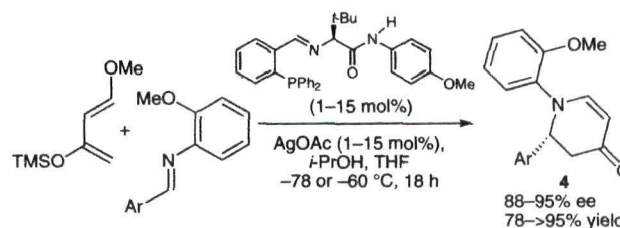
# RESEARCH LETTER

## Environment-friendly and solvent-free synthesis of symmetrical bis-imines under microwave irradiation

Subrata Das, Vijay K. Das, Lakhinath Saikia and Ashim Jyoti Thakur*

*Department of Chemical Sciences, Tezpur University, Tezpur, Napaam Tezpur 784 028, India*

A short library of symmetrical bis-imines has been constructed efficiently from the reaction between dialdehydes and mono amines or diamines and mono aldehydes under microwave irradiation catalyzed by *p*-toluenesulphonic acid. The methodology is associated with shorter reaction time, good yields and simple workup.

**Keywords:** condensation; imines; aldehydes; amines; green chemistry; microwave

## Introduction

Imines are valuable functional groups or chemical compounds containing a carbon nitrogen double (C=N) bond. Condensation reaction of aldehydes and primary amines resulting imines, commonly called Schiff bases (first discovered by Schiff in 1864) or azomethines are well known in organic synthesis. In inorganic chemistry, these versatile Schiff bases are used as chelate for metal ion complexation (1–6). Some of these metal complexes are used as catalysts in various organic reactions (7,8). Biologically, imines show anti-convulsant, anti-depressant, analgesic, anti-inflammatory, antiplatelet, antimalarial, antimicrobial, antimycobacterial, and antiviral activity (9–11). Similar to imines, bis-imines (bis-Schiff bases) also finds use as analytical, medicinal, polymer, and liquid crystalline materials (12–14). Most of the biologically active nitrogen containing heterocyclic compounds and biologically active inorganic metal complexes are synthesized using bis-imines as starting materials and as synthetic intermediates (15–19).

The C=N bond in imines often suffers exchange reaction (20) as well as hydrolysis. Such reversible C=N bond formation (21,22) is very useful to synthesize the most thermodynamically stable macrocyclic (23–27) and interlocked compounds (28,29). Also, literatures are available on the heterocyclic substituted bis-imines and some of these fused bis-imines showed bio-activity (30), for example, bis-imines of isatin and their derivatives are known to possess a wide spectrum of pharmacological proper-

ties including antibacterial, antifungal, anti-HIV, and antiviral activity (31–39).

Different types of bis-imines were required in one of our ongoing programs. The conventional synthesis of such compounds involves longer reaction time using volatile organic solvents followed by extensive separation and/or purification (40–49). Moreover, the methods are not general. As a part of our green chemistry program and practice (50–52), in embracing the principles of green chemistry (53–55), herein we want to divulge a simple and general approach for the synthesis of bis-imines 3 and 6, by using 5 mol% *p*-toluenesulphonic acid (TSA) as a cheap catalyst under microwave irradiation (MWI) without using any solvent (Scheme 1), thereby paving the way for an environmentally benign condition. As shown in Scheme 1, synthesis of bis-imines involves the reaction between either diamine and mono aldehydes or dialdehyde and mono amines.

Use of Microwave energy for the enhancement of organic reactions, that is Microwave Organic Reactions Enhancement provides greener reaction condition coupled with clean product, increase yield and better time economy (56–63). The present investigation is aimed at looking alternative conditions for the synthesis of bis-imines with the following objectives: (1) search for milder reaction condition, (2) to reduce the reaction time, (3) to increase the yield, (4) to promote economical and environmental friendly experimental (green procedures) by performing the reaction under microwave and solvent-less/free condition, (5) to use cost-effective, mild, and economical catalysts.

---

*Corresponding author. Email: ashim@tezu.ernet.in

# Effects of L-ascorbic acid addition on micro-filtered coconut water: Preliminary quality prediction study using $^1$H-NMR, FTIR and GC-MS ☆

M. Das Purkayastha [a], Dipankar Kalita [a], Vijay K. Das [b], Charu Lata Mahanta [a],
Ashim J. Thakur [b], Mihir K. Chaudhuri [c],*

[a] Department of Food Engineering and Technology, School of Engineering, Tezpur University, Assam, India
[b] Department of Chemical Sciences, School of Science & Technology, Tezpur University, Assam, India
[c] Tezpur University, Assam, India

## ARTICLE INFO

## ABSTRACT

Coconut water was processed through 2-stage microfiltration system and L-ascorbic acid (25 mg/100 ml) was added to it, and then stored at 4 °C. Micro-filtered coconut water, with (AS) or without (US) added ascorbic acid was analyzed on 0 and 21 days of storage, using $^1$H-NMR, FTIR and GC-MS. The spectral analyses revealed that the addition of L-ascorbic acid to micro-filtered coconut water was able to retain methyl-α-D-rhamnopyranoside (prime glycoside detected in micro-filtered coconut water) better in AS than US, and also controlled the formation of free fatty acids and delayed rancidity in AS. Good correlation was found between these spectral results. PCA for both FTIR and $^1$H-NMR data sets presented the separation of fresh and stored micro-filtered coconut water samples. While still in the early stages of investigation, this work showed the potentiality of $^1$H-NMR, FTIR and GC-MS tools for monitoring the changes in micro-filtered coconut water.
*Industrial relevance:* Recently, microfiltration of coconut water has been found to be an alternative to thermal sterilization. A preliminary study was undertaken to study the effect of addition of L-ascorbic acid on the quality of micro-filtered coconut water, by using $^1$H NMR, FTIR and GC-MS, mainly to detect the tentative chemical changes occurring in it during low temperature storage (4 °C for 21 days). High correlation was found between the results of these instrumental methods, the use of which can be used as key determinants for assessing the quality of such processed coconut water during routine inspection and also in further in-depth research.

© 2011 Elsevier Ltd. All rights reserved.

## 1. Introduction

Water of green coconut is largely consumed worldwide, not only as a refreshing drink but also because of its various therapeutic qualities (Loki & Rajamohan, 2003). Preservation process is necessary to increase its shelf-life to enable commercialization. The water when taken out from the nut spoils within a day because of external contamination by microorganisms (Reddy, Das, & Das, 2005). The commercial production of canned coconut water has employed a high-temperature/short-time preservation process, which results in elimination of not only microbes, but also almost the entire delicate flavor. This severely limits the marketability of the product (Jayanti, Rai, Dasgupta, & De, 2010). Selecting technological processes to preserve the natural wholesome properties of the drink still remains a challenge. Recently, microfiltration has been found to be an alternative to thermal sterilization, to obtain processed coconut water, which can be as good as fresh coconut water (Anonymous, 2007;

Barrett, Somogyi, & Ramaswamy, 2004; Reddy, Das, & Das, 2007). As such, micro-filtered coconut water was taken as the base material for our present study.

Coconut water contains a considerable amount of fats and oils, which depends upon the cultivar and maturation stage of the coconut (Campos, Souza, Coelho, & Gloria, 1996; Fonseca et al., 2009; Jackson, Gordon, Wizzard, McCook, & Rolle, 2004; Reddy et al., 2007). These fats and oil, with increasing storage duration of coconut water, results in free fatty acid formation (Rolle, 2007). The increase in free fatty acid content affects the aroma and thereby the quality of either fresh or processed product. Reddy et al. (2007) observed that microfiltration technique is not sufficient to completely filter lipids from the processed coconut water. This necessitates the addition of antioxidants into the processed coconut water. Even if the coconut water is extracted aseptically, its exposure to air initiates some reactions such as oxidation promoted by enzymes polyphenol oxidase (PPO) and peroxidase (POD), which are naturally present in the coconut water (Duarte, Coelho, & Liete, 2002). Also coconut water is rich in minerals and electrolytes (Jackson et al., 2004; Reddy et al., 2007) which catalyzes lipid oxidation and formation of volatile compounds. These reactions have a negative effect on sensorial and nutritional qualities of the coconut water (Campos et al., 1996; Duarte et al., 2002). In order to reduce these problems, Rolle (2007) recommended that the